Rheological Analysis of Mud

Towards an Implementation of the Nautical Bottom Concept in the Port of Hamburg

Shakeel, A.

DOI
10.4233/uuid:6b3693c8-0764-4b72-8091-b082a7227d44

Publication date
2022

Document Version
Final published version

Citation (APA)
Shakeel, A. (2022). *Rheological Analysis of Mud: Towards an Implementation of the Nautical Bottom Concept in the Port of Hamburg*. [Dissertation (TU Delft), Delft University of Technology]. https://doi.org/10.4233/uuid:6b3693c8-0764-4b72-8091-b082a7227d44

Important note
To cite this publication, please use the final published version (if applicable).
Please check the document version above.

RHEOLOGICAL ANALYSIS OF MUD

TOWARDS AN IMPLEMENTATION OF THE NAUTICAL BOTTOM CONCEPT IN THE PORT OF HAMBURG

RHEOLOGICAL ANALYSIS OF MUD

TOWARDS AN IMPLEMENTATION OF THE NAUTICAL BOTTOM CONCEPT IN THE PORT OF HAMBURG

Dissertation

for the purpose of obtaining the degree of doctor
at Delft University of Technology
by the authority of the Rector Magnificus prof.dr.ir. T.H.J.J. van der Hagen
chair of the Board for Doctorates
to be defended publicly on
Monday 27 June 2022 at 17:30 o'clock

by

Ahmad SHAKEEL

Erasmus Mundus European Masters in Engineering Rheology,
KU Leuven, Belgium; University of Minho, Portugal; University of Calabria, Italy,

born in Lahore, Pakistan.

This dissertation has been approved by the promotors.

Composition of the doctoral committee:

Rector Magnificus,	chairperson
Prof. dr. J. Pietrzak,	Delft University of Technology, promotor
Dr. C. Chassagne,	Delft University of Technology, promotor
Dr. O. Kirichek,	Delft University of Technology, copromotor

Independent members:

Prof. dr. A.J. Manning,	University of Plymouth
Prof. dr. P. Coussot,	École des Ponts ParisTech
Prof. dr. ir. M. van Loosdrecht,	Delft University of Technology
Prof. dr. A. Benamar,	Université Le Havre Normandie
Prof. dr. ir. Z. Wang,	Delft University of Technology, reserve member

This research is funded by the Hamburg Port Authority, Germany and carried out within the framework of the MUDNET academic network.

Keywords: Mud; Rheology; Nautical bottom; Yield stress; Density; Organic matter

Printed by: Gildeprint - Enschede

Front & Back: Ahmad Shakeel

ISBN 978-94-6419-532-3

An electronic version of this dissertation is available at
http://repository.tudelft.nl/.

To my Grandfather
Muhammad Khalil Farooqi

CONTENTS

SUMMARY

The nautical bottom (the level at which contact with a ship's keel causes either damage or unacceptable effects on controllability and manoeuvrability of a ship) should be associated to a measurable physical characteristic. Bulk density is typically used as a criterion for nautical bottom by many ports worldwide. However, the rheological properties particularly the yield stress of mud would be better parameters for defining a criterion for nautical bottom due to their strong correlation with the flow properties of mud and navigability. The density-yield stress correlation depends significantly on different parameters of mud such as organic matter type and content, clay type and content, particle size distribution and salinity. Therefore, a single critical value of density cannot be chosen for the nautical bottom criterion in a port like Port of Hamburg, where the above mentioned parameters are varying from one harbour location to another. This justifies the need for a study of the rheological properties (yield stress) of mud in Port of Hamburg.

The experiments presented in this thesis are performed in the laboratory, with samples obtained from various locations and depths within the Port of Hamburg over a range of 2 - 3 years. First of all, in order to work with a suitable rheological geometry and measuring protocol, a comparative analysis of yield stresses by using different geometries and protocols is performed. Couette geometry is found to be the most suited for analysing the rheological properties of soft mud layers (defined as fluid mud and pre-consolidated mud). Vane geometry is found more appropriate to study the rheology of consolidated mud, in order to avoid the wall-slip phenomenon occurring with the Couette geometry for consolidated layers. Regarding rheological protocols, stress ramp-up test proves to be the fastest, reliable and repeatable test for measuring the two yield stresses (defined as "static" and "fluidic") associated to the structural breakdowns in the undisturbed (unremoulded) mud samples. These static and fluidic yield stresses are found to be correlated with conventional yield stresses (defined as "static" and "dynamic/Bingham" yield stresses in the literature). No extensive pre-shearing before or during the rheological protocol is used as done in other protocols, in order to obtain the yield stresses of undisturbed mud samples, which is a state typically found under in-situ conditions. The two-step yielding nature of the investigated sediment is attributed to two structural breakdown and reorganization during shearing and is visually confirmed by rheo-optical analysis.

In a second step, the depth and spatial variability in the rheological properties of mud from Port of Hamburg is investigated. The rheological properties are observed to increase as a function of density (i.e., buried depth) of mud. Mud samples having higher organic matter content (represented by Total Organic Carbon, TOC) show higher elasticity than the samples having lower organic matter content, for a given density. This variation in organic matter content along the port (i.e., higher TOC at upstream while

lower TOC at downstream) defines the spatial variability in the rheological properties of mud particularly for the density-yield stress correlation. The organic matter content is further observed to influence the flocs characteristics (size and density), which is eventually reflected by the bulk rheological properties. For samples with a same TOC content, it is found that the increase in rheological properties as a function of density is strongly dependent on the sample origin. Two types of samples are investigated: (i) samples collected in-situ as a function of depth (naturally-deposited sediment), (ii) samples prepared by diluting the consolidated mud sample of the same location (diluted samples). It is found that the yield stress of naturally-deposited sediment is higher than for diluted samples, for a same density. This difference is attributed to the breakage of organic matter bonds with clay particles during the preparation of diluted samples.

The two-step yielding nature of mud, for the entire investigated shear rate range, is modelled using the sum of two empirical expressions (one for each yield step). The switching from one expression to another is ensured by the use of a step function. The proposed model effectively captures the two-step yielding behaviour of mud within the density range of $1050 - 1200$ kg. m^{-3}. The proposed two-step yielding model has been implemented in the software of the rheological in-situ equipment of Port of Hamburg, where, in particular, the fluidic yield stress will be measured in-situ for nautical bottom application.

Structural recovery tests of mud samples are also performed as these tests enable to estimate both recovery time and recovery extent after shear. The structural recovery after extensive shearing of mud is observed to be larger for samples having low density and/or organic matter content as compared to the samples having high density and/or organic matter content. This result enables to predict that there should be a strong spatial and depth variability in structural recovery behaviour in the port as well, in addition to a spatial and depth variation in yield stresses and moduli. The characteristic time for recovery is found to be significantly affected by the pre-shear rate and organic matter content.

The influence of organic matter degradation (anaerobic and aerobic) on the rheological properties of mud is studied. The degradation of organic matter (particularly anaerobic) results in a decrease in rheological properties (yield stresses, modulus and thixotropy) of mud due to the destruction of organic bridges between mineral particles and also because of the formation of gas bubbles. Moreover, the decrease in rheological properties of mud becomes significant for mud samples having high density and/or organic matter content (which are found in upstream locations). The anaerobic degradation is further observed to significantly influence the rheological properties of mud after two different time intervals of degradation (3 days and 150 days). In contrast, the effect of aerobic degradation of organic matter on the rheological properties of mud is not clear most probably because of the interaction of metal ions with oxygen under aerobic conditions, which can lead to the formation of metal complexes.

Compiling all the results obtained in this study allowed to estimate a suitable value (50 Pa) for the fluidic yield stress as a starting point for in-situ pilot experiments. This value is currently being adopted in one of the key locations (KH) of the Port of Hamburg for pilot experiments. It is important to note that the density values vary within the range

of 1085 − 1215 kg. m^{-3} for different locations corresponding to 50 Pa fluidic yield stress. This justifies the use of yield stress as a more suitable physical characteristic than density for defining navigable fluid mud layer in Port of Hamburg. Moreover, the fluid mud layer (which meets the requirement of 50 Pa) displays a weak thixotropic behaviour, which suggests that the selected yield stress value will not be significantly influenced by the thixotropic character of mud. The results presented in this thesis will serve as a database for upcoming CFD simulations and in-situ pilot experiments.

SAMENVATTING

De nautische bodem (het niveau waarop contact met de kiel van een schip schade of onaanvaardbare effecten op de bestuurbaarheid en manoeuvreerbaarheid van een schip veroorzaakt) moet worden gekoppeld aan een meetbare fysische eigenschap. Bulkdichtheid wordt doorgaans door veel havens over de hele wereld gebruikt als criterium voor nautische bodem. De reologische eigenschappen, met name de zwichtspanning van slib, zijn echter beter geschikte parameters voor het definiëren van een criterium voor nautische bodem vanwege hun sterke correlatie met de stromingseigenschappen van slib en bevaarbaarheid. De correlatie tussen dichtheid en zwichtspanning hangt in belangrijke mate af van verschillende parameters van slib, zoals type en gehalte aan organische stof, type en gehalte aan klei, deeltjesgrootteverdeling en zoutgehalte. Daarom kan voor het nautische bodemcriterium in een haven zoals de haven van Hamburg, waar bovengenoemde parameters per locatie verschillen, geen unieke kritische dichtheidswaarde worden gekozen. Dit rechtvaardigt de noodzaak van een onderzoek naar de reologische eigenschappen (zwichtspanning) van slib in de haven van Hamburg.

Om een geschikte reologische geometrie en meetprotocol te kiezen, wordt eerst een vergelijkende analyse van zwichtspanningen uitgevoerd met behulp van verschillende geometrieën en protocollen. De Couette-geometrie blijkt het meest geschikt te zijn voor het analyseren van de reologische eigenschappen van zachte sliblagen (gedefinieerd als vloeibaar slib en voorgeconsolideerd slib). Een vin-geometrie wordt geschikter gevonden om de reologie van geconsolideerd slib te bestuderen, om wandslip die optreedt bij de Couette-geometrie voor geconsolideerde lagen te voorkomen. Met betrekking tot reologische protocollen blijkt de schuifspannings-opvoertest de snelste, meest betrouwbare en herhaalbare test te zijn voor het meten van de twee zwichtspanningen (gedefinieerd als "statisch" en "vloeibaar") die verband houden met de structuurafbraak in de ongestoorde (ongeroerde) slibmonsters. Deze statische en vloeibare zwichtspanningen blijken gecorreleerd te zijn met conventionele zwichtspanningen (in de literatuur gedefinieerd als "statische" en "dynamische/Bingham"zwichtspanningen). Er wordt geen uitgebreide voorbelasting vóór of tijdens het reologische protocol gebruikt zoals in andere protocollen, om de zwichtspanningen van ongestoorde slibmonsters te verkrijgen, d.w.z. representatief voor in-situ omstandigheden. De dubbele zwichtspanning van het onderzochte sediment wordt toegeschreven aan structuurveranderingen en -afbraak tijdens afschuiving en wordt visueel bevestigd door reo-optische analyse.

Hierna worden de ruimtelijke gradiënten in de reologische eigenschappen van slib uit de haven van Hamburg onderzocht. Er wordt waargenomen dat de zwichtspanning toeneemt als een functie van de dichtheid (d.w.z. begraven diepte) van slib. Slib met een hoger gehalte aan organische stof (weergegeven door Total Organic Carbon, TOC) is sterker dan de monsters met een lager gehalte aan organische stof, voor een gegeven dicht-

heid. Deze variatie in het gehalte aan organische stof in de haven (d.w.z. hogere TOC stroomopwaarts en lagere TOC stroomafwaarts) definieert de ruimtelijke gradiënten in de reologische eigenschappen van slib, met name wat betreft de correlatie tussen dichtheid en zwichtspanning. Verder wordt waargenomen dat het gehalte aan organische stof de eigenschappen van de vlokken (grootte en dichtheid) beïnvloedt, wat uiteindelijk wordt weerspiegeld door de reologische eigenschappen van de bulk. Voor monsters met hetzelfde TOC-gehalte blijkt dat de toename van de zwichtspanning als functie van de dichtheid sterk afhankelijk is van de oorsprong van het monster. Twee soorten monsters worden onderzocht: (i) monsters verzameld in situ als functie van de diepte (natuurlijk afgezet sediment), (ii) monsters bereid door het geconsolideerde slibmonster van dezelfde locatie te verdunnen (verdunde monsters). Het is gebleken dat de zwichtspanning van natuurlijk afgezet sediment hoger is dan voor verdunde monsters, bij dezelfde dichtheid. Dit verschil wordt toegeschreven aan het verbreken van bindingen van organisch materiaal met kleideeltjes tijdens de voorbereiding van verdunde monsters.

De tweestaps bezwijkgedrag van slib wordt voor het gehele onderzochte afschuifsnelheidsbereik gemodelleerd met behulp van de som van twee empirische uitdrukkingen (één voor elke bezwijkstap). Het overschakelen van de ene uitdrukking naar de andere wordt gerealiseerd door het gebruik van een stapfunctie. Het voorgestelde model legt het tweestaps-bezwijkgedrag van slib effectief vast binnen het dichtheidsbereik van 1050 – 1200 kg. m^{-3}. Het voorgestelde tweestaps-bezwijkmodel is geïmplementeerd in de software van de reologische in-situ-apparatuur van de haven van Hamburg, waarmee met name de vloeibare zwichtspanning in-situ zal worden gemeten voor nautische bodemtoepassing.

Structurele hersteltests van slibmonsters worden ook uitgevoerd, aangezien deze tests het mogelijk maken om zowel de hersteltijd als de herstelgraad na afschuiving in te schatten. Het structurele herstel na uitgebreide afschuiving van slib blijkt groter te zijn voor monsters met een lage dichtheid en/of organische stofgehalte in vergelijking met monsters met een hoge dichtheid en/of organische stofgehalte. Dit resultaat maakt het mogelijk om te voorspellen dat er ook een sterke ruimtelijke en dieptevariatie in structureel herstelgedrag in de haven zou moeten zijn, naast een ruimtelijke en dieptevariatie in zwichtspanningen en moduli. De karakteristieke tijd voor herstel blijkt significant te worden beïnvloed door de afschuifsnelheid voorafgaand aan de test en het gehalte aan organische stof.

De invloed van afbraak van organische stof (anaëroob en aeroob) op de reologische eigenschappen van slib wordt bestudeerd. De afbraak van organisch materiaal (in het bijzonder anaëroob) resulteert in een afname van de reologische eigenschappen (zwichtspanningen, modulus en thixotropie) van slib door het breken van organische verbindingen tussen minerale deeltjes en ook door de vorming van gasbellen. Bovendien wordt de afname van de reologische eigenschappen van slib significant voor slibmonsters met een hoge dichtheid en/of organische stofgehalte (die worden gevonden op stroomopwaartse locaties). Verder wordt waargenomen dat de anaërobe afbraak de reologische eigenschappen van slib significant beïnvloedt na twee verschillende tijdsintervallen van afbraak (3 dagen en 150 dagen). Daarentegen is het effect van aërobe afbraak van organisch materiaal op de reologische eigenschappen van slib niet eenduidig, hoogstwaar-

schijnlijk vanwege de interactie van metaalionen met zuurstof onder aërobe omstandigheden, wat kan leiden tot de vorming van metaalcomplexen.

Door alle resultaten die in deze studie zijn verkregen te combineren, kon een kritische waarde (50 Pa) worden geschat voor de vloeibare zwichtspanning voor nautische bodemimplementatie. Deze waarde wordt momenteel toegepast op een van de sleutellocaties (KH) van de haven van Hamburg voor pilot-experimenten. Het is belangrijk op te merken dat de dichtheidswaarden variëren binnen het bereik van 1085 − 1215 kg. m^{-3} voor verschillende locaties die overeenkomen met 50 Pa vloeibare zwichtspanning. Dit rechtvaardigt het gebruik van zwichtspanning als een geschikter fysiek kenmerk dan dichtheid voor het definiëren van de nautische bodem in de haven van Hamburg. Bovendien vertoont de vloeibare sliblaag (die voldoet aan de eis van 50 Pa) slechts een zwak thixotroop gedrag, wat suggereert dat het geselecteerde zwichtspanningscriterium voor nautische bodem niet significant zal worden beïnvloed door het thixotrope karakter van slib. De resultaten gepresenteerd in dit proefschrift zullen dienen als een database voor toekomstige numerieke simulaties en in-situ pilot-experimenten.

1

INTRODUCTION

In ports, frequent dredging operations are required to ensure that vessels having large drafts can safely manoeuvre. These dredging operations cost millions of euros and in order to optimize these costs the nautical bottom (i.e., the level at which contact with the ship's keel causes an effect on safe navigation) should be associated with in-situ measurable parameters. In this introduction, important concepts and definitions are introduced along with the thesis outline. In particular, it will be shown that yield stress is the required parameter to be measured. Rheological properties (i.e., yield stress, moduli and thixotropy) of mud are required to set a criterion for the yield stresses measured in-situ and hence will be the focus of the present thesis.

1

1.1. NAUTICAL BOTTOM

SAFE navigation and excellent accessibility within ports and waterways is vital for port authorities. Safe navigation is primarily controlled by the space available under the ship's keel[1], referred to as under keel clearance (UKC)[2]. There are two approaches for maintaining a sufficient UKC: (i) by restricting the maximum draft of vessels, and (ii) by controlling the desired nautical bottom with dredging operations (Kirichek et al., 2018). The nautical bottom (Fig. 1.1) is typically defined as: "*a level at which physical characteristics of the bottom reach a critical limit beyond which contact with a ship's keel causes either damage or unacceptable effects on controllability and manoeuvrability*" (PIANC, 1997).

The first approach is uneconomical because it would restrict the accessibility of the port for larger and energy efficient vessels. The second option is more favourable for port authorities, however, the environmental impact and cost of the dredging operations can limit its applicability. The nautical bottom definition provides a general viewpoint without giving a practical solution. Moreover, this definition raises a number of questions including:

1. How to define and quantify "unacceptable effects"?
2. Which physical parameter(s) are associated to the "characteristics of the bottom"?
3. How to define and estimate critical value(s) of this/these parameter(s)?

The answer to the first question depends on a number of parameters such as training and expertise level of pilots, local environmental conditions, size and speed of the vessel, quality of navigational assistance (availability of tug assistance) and economical concerns. For the other two questions, it is clear that the selected physical characteristics should directly relate to the forces exerted by the mud layer on the ship's hull upon its contact and also the effect on the ship propeller.

Two different approaches are typically used to maintain the desired nautical bottom: (i) passive approach (McAnally et al., 2016) and (ii) active approach (Wurpts and Torn, 2005). Passive approach relies on a bathymetric survey method which ultimately leads to the recommendation of a mud property beyond which it is safe/unsafe for a ship to sail. This mud property is typically the bulk density for most cases. For example, the ports of Rotterdam, Suriname, Bangkok, Bordeaux and Nantes adopted a density criterion of 1200 kg. m^{-3} (McAnally et al., 2016). But higher values (almost 1300 kg. m^{-3}) were found for other ports such as Le Havre (Benamar et al., 2015). Bottom surveying techniques such as eco-sounding are generally used to detect the mud-water level. However, the frequency dependence of eco-sounding results is the most common problem with this technique, and a proper calibration is difficult owing to the variability in mud

[1] Keel: The principal fore-and-aft structural member of a ship frame, located along the center-line of the hull bottom

[2] Under-keel clearance (UKC): The space or distance between the keel of a (usually) loaded ship and the channel bottom in a static or still-water condition; the allowable margin of safe water for which ship passages are deemed adequate by local port authorities and pilots; the difference between the loaded ship draft and the lowest safe channel depth

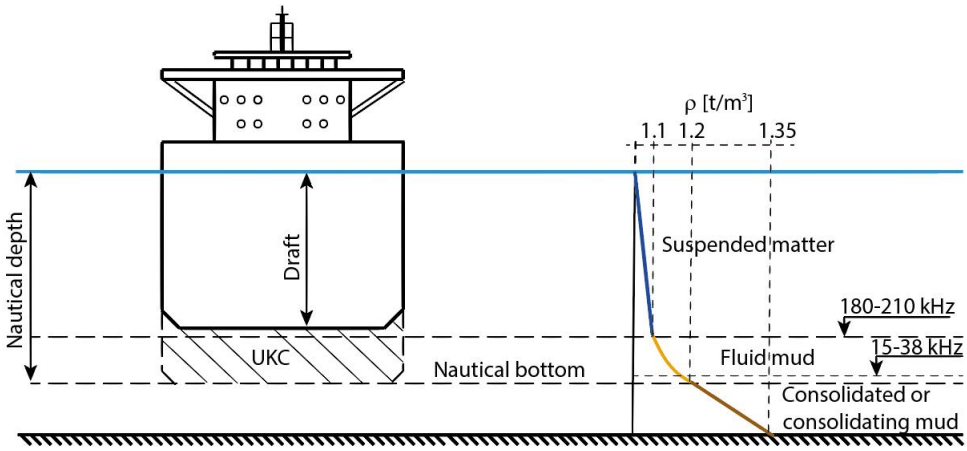

Figure 1.1: The nautical bottom defined by the density limit of 1200 kg. m^{-3} (Kirichek et al., 2018).

composition (Vantorre et al., 2006). On the other hand, active approach relies on the maintenance of navigational channels whereby the physical, biological and chemical properties of fluid mud are tuned in order to significantly influence its rheological and settling behaviour. This methodology has been adopted in the Port of Emden. The mechanical destruction of the mud's floc structure restricts the rapid consolidation of mud (McAnally et al., 2016).

As navigability is strongly linked to the flow properties of the water-mud medium, rheological properties like viscosity and yield stress (i.e., stress required to initiate the flow of mud) are better candidates to define suitable physical characteristics and can be utilized to define a suitable criterion. The reason for selecting bulk density as a criterion for nautical bottom is linked to the limitations of in-situ measurements of rheological properties and the lack of systematic investigation of rheological characteristics of mud. However, recent developments made it possible to effectively analyse the in-situ rheological properties of mud (Kirichek and Rutgers, 2020). On the other hand, German ports defined the nautical bottom on the basis of yield stress of mud (50 – 100 Pa) (Wurpts and Torn, 2005) with the corresponding density values ranging from 1100 to 1250 kg. m^{-3} (Uliczka, 2005). This variation in density values is linked to the fact that the relation between density and yield stress can be significantly influenced by several parameters including type and content of organic matter, clay type, particle size distribution and salinity. Hence, it is difficult and impractical to choose a critical value of the density for a port with varying above mentioned parameters along the port. In short, for defining the criterion for nautical bottom on the basis of rheological properties of mud, the following points need to be considered: (i) systematic analysis of the influence of different parameters (TOC content, type and state of organic matter, bulk density and salinity) on the rheology of mud, (ii) appropriate tools for in-situ measurement of rheological properties, and (iii) proper correlation between lab and in-situ measurements. In this thesis, primarily point (i) will be considered.

1

1.2. MUD

As discussed in the previous section, the properties of mud should be linked to its rheological properties (i.e., yield stress). As the composition and structure of mud is variable from one harbour location to another, it is expected that a large-scale systematic study is required to obtain a good understanding of the dependence of the rheological properties on the mud's parameters. Mud layers, typically found at the bottom of rivers, lakes and in coastal areas, belong to the category of cohesive material. These deposits consist of water, clay minerals, sand, silt and organic matter such as living microorganisms and in particular their excreted biopolymers (Mehta, 2013). These mud layers are usually exposed to a continuous wave motion and disturbances produced by ship movement (Mehta, 2013, Ross and Mehta, 1989), human actions such as dredging (Gordon, 1974), natural climatic events and bioturbation (Harrison and Wass, 1965). The water column can be divided into different layers (see Fig. 1.2). In its large upper part, where mud particles are advected by currents and diffused by turbulent motion, mud is found as suspended particulate matter (SPM). Close to the bottom, different mud layers are found with increasing density as a function of depth. These layers can be defined as fluid mud (FM), pre-consolidated sediment (PS) and consolidated sediment (CS). Besides having different densities, these mud layers are known to have significantly different compositions and rheological fingerprints.

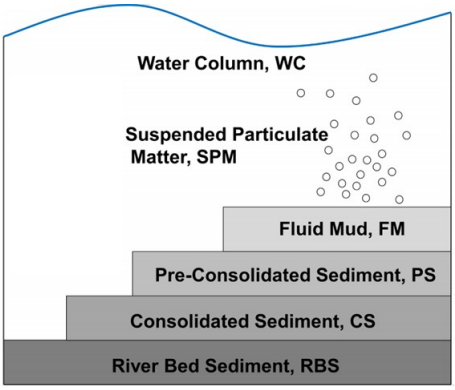

Figure 1.2: Different mud layers formed in-situ having different densities.

Fluid mud, the most important mud layer from a navigational perspective, is typically identified as a layer with a density of 1030 − 1300 kg. m^{-3} whereby hindered settling of particles plays a role due to the presence of flocs (i.e., aggregates of clay particles and organic matter) (Inglis and Allen, 1957, McAnally et al., 2007, Whitehouse et al., 2000). All mud layers, but particularly the fluid mud layer, display complex rheological behaviour, i.e., combination of thixotropy, shear-thinning, two-step yielding and viscoelasticity (Coussot, 1997, Van Kessel and Blom, 1998). The rheological/cohesive properties of mud are observed to vary as a function of solid fraction (or bulk density), type and concentration of organic matter, type of clay minerals, ionic concentration and clay content (Malarkey et al., 2015, Parsons et al., 2016, Paterson et al., 1990, Paterson and Hagerthey, 2001, Schindler et al., 2015, Shakeel, Kirichek, and Chassagne, 2019, Shakeel

et al., 2020b, Wurpts and Torn, 2005). The thorough understanding of the rheological characteristics of mud, as a function of above-mentioned parameters, needs to be performed to estimate the strength, the flow and thickness of (fluid) mud in ports and waterways for adapting the nautical bottom approach. The link between these parameters and a large-scale case study (a systematic investigation of a large port area as a function of time) still remains to be done. The quantification of the rheological properties for fluid mud also facilitates the definition of boundary conditions for sediment transport modelling, which in turn helps optimizing the dredging operations and defining the proper maintenance strategy for navigational channels (Kirichek et al., 2018, May, 1973, Parker and Kirby, 1982, Whitehouse et al., 2000). However, in order to calibrate and improve the in-situ measurement techniques, it is essential that the key rheological parameters are extensively estimated beforehand in the laboratory using suitable protocols. This raises new questions that are discussed in the next section.

1.3. RHEOLOGY

THIS section summarizes the extensive work that has been performed over the years regarding the rheological properties of mud-related systems. In particular, measurement techniques and protocols are discussed and the rheological properties of a large number of mud systems over the world are given.

1.3.1. YIELD STRESS AND ITS MEASUREMENTS

Composite slurries and suspensions can exhibit either solid-like or liquid-like properties when a stress is imposed. These materials then behave like elastic solids at small stresses whereas they tend to flow above a critical value of stress, called yield stress. There are lots of examples of such systems including cosmetic creams, toothpaste, margarine, polymeric gels, and colloidal suspensions (Bird et al., 1983, Clayton et al., 2003, Yoshimura and Prud'homme, 1988). Yield stress determination is very important for industrial processes. In the frame of this thesis, yield stress has been found to be an important parameter to define navigable fluid mud layers for ports and waterways (Kirichek et al., 2018, Møller et al., 2006, Q. Nguyen and Boger, 1992, Wurpts and Torn, 2005, Fontein and Wal, n.d.).

The term yield stress was first introduced by Bingham and co-workers for plastic yielding in metals (Barnes, 1999, Bingham, 1922). Since the last two decades, a huge interest in yield stress materials has led to the development of several experimental techniques for estimating yield stress values. However, these values can vary more than one order of magnitude depending upon the selected method and the handling procedure of sample before measurements (James et al., 1987, Q. D. Nguyen et al., 2006, Steffe, 1996, Uhlherr et al., 2005, Zhu et al., 2001). This variability in yield stress values is usually attributed to the differences in principles associated with the experimental methods, criterion of yield stress definition and the time scale of the chosen experiment (D. C. Cheng, 1986).

Conventional methods to measure yield stresses typically include steady stress/shear rate sweep, oscillatory amplitude sweep, creep and stress growth experiments (Coussot, 2014, Dinkgreve et al., 2016, Q. Nguyen and Boger, 1992). In addition to these con-

1

ventional methods, there are some rheological protocols particularly reported for mud samples. For instance, Claeys et al., 2015 proposed a protocol to analyse the rheological properties of mud in the laboratory using a vane-type rheometer. Their main objectives were to attain the equilibrium flow curves of the samples with a good repeatability and to deduce the undrained shear strength and dynamic yield stress of the mud samples. Their protocol starts with a stress growth test at a very small shear rate (1 s^{-1}) to obtain the undrained shear strength of "undisturbed" samples, followed by a pre-shearing step at a very high shear rate (1000 s^{-1}), to completely disturb the sample. The stress growth test is highly dependent on the applied shear rate and, therefore, the selection of a suitable shear rate for the samples of different consistencies (i.e., fluid mud and consolidated) is very critical (Rogers et al., 2010, Stokes and Telford, 2004, Q. Yuan et al., 2017). This protocol is therefore not appropriate to analyse the yield stress of "undisturbed" mud samples. Moreover, this protocol is based on nine cycles or more (depending upon the selected shear rates) of applying/removing shear rate and the total time of an experiment is about 15 − 20 min/sample. It can be concluded that this protocol is not suitable to measure yield stresses of a large number of samples. Apart from different rheological methods, several geometries including concentric cylinder (Couette), parallel plate, cone plate and vane type, are available to perform rheological measurements. Each geometry has its own merits and limitations, and is selected depending on the composition of the sample under investigation. In addition, an inclined blade vane geometry (Bougouin et al., 2022) can also be used to analyze the rheological properties of mud, which avoids the particle settling by mixing the suspension in two directions (radial and axial).

SINGLE-STEP VERSUS TWO-STEP YIELDING

Over the last decade, the rotational rheometers have been significantly modified allowing to conduct more sophisticated rheological analysis and understand new rheological features. For instance, it has recently been found that, instead of a single yielding response, a prominent two-step yielding behaviour was observed for different soft materials (Ahuja et al., 2020, Pham et al., 2008, Shao et al., 2013, Arief and Mukhopadhyay, 2019, Shukla et al., 2015, Sentjabrskaja et al., 2013). This two-step yielding suggested the existence of different structural levels related to different types of interactions. Experimental evidence for this interesting two-step yielding phenomenon has been found in literature for various systems including colloidal glasses (Pham et al., 2008), carbopol microgel (Shao et al., 2013), fine-grained sediments (Nie et al., 2020), colloidal gel (Chan and Mohraz, 2012), magneto-rheological systems (Segovia-Gutiérrez et al., 2012) and muscovite dispersions (Nosrati et al., 2011) using different rheological tests. The most frequently used experiment, to investigate the two-step yielding, is to perform the oscillatory amplitude sweep test by increasing either stress or strain amplitude and recording the material's response in terms of storage ($G^{'}$) and loss ($G^{''}$) moduli. The two-step yielding is typically recognized by the two distinct peaks in $G^{'}$ or $G^{''}$ response, which are usually linked with the bond and cage breaking process (Dagois-Bohy et al., 2017). It has also been reported in the literature that this two-step yielding behaviour strongly depends on the solids volume fraction, ϕ. The experiments have revealed that the second yield point becomes less significant as ϕ decreases, until the system displays only a single-step yielding behaviour at $\phi \sim 0.2$ (Koumakis and Petekidis, 2011, Kramb and Zukoski,

2010). A brief overview of the different systems showing two-step yielding, along with the possible explanation of two-step yielding response is presented in Table 1.1.

Table 1.1: A brief overview of the literature on the two-step yielding systems.

Investigated system	Experiments	Possible explanation for two-step yielding	Ref.
PMMA particles stabilized with PS dispersed in *cis*-decalin	Oscillatory amplitude sweep, stress growth, creep, flow curve	The first yielding was associated with the breaking of attractive bonds between the particles and the second yield point was linked with the cage breaking phenomenon	Pham et al., 2008
Carbopol microgel	Oscillatory amplitude sweep, oscillatory time sweep	The first yielding was attributed to the network rupture followed by the cluster formation due to strain densification. The second yield point was associated with the breakage of these clusters	Shao et al., 2013
Muscovite particles dispersed in water	Stress sweep	The first yield point was suggested to be linked with the breakdown of 3D network of particle aggregates. The second yielding was attributed to the rupture of aggregates into individual particles	Nosrati et al., 2011
CoNi nanoplatelet dispersed in castor oil	Oscillatory amplitude sweep	The first yield point was associated with the inter-cluster bond breaking followed by the densification, while the second one was linked with the cluster breaking process	Arief and Mukhopadhyay, 2019
Anionic surfactants, clay, and abrasive particles of calcite dispersed in water	Oscillatory amplitude sweep	The first yielding was attributed to the network rupture, while the second one to the collapse of aggregates	Shukla et al., 2015
Cocoa powder dispersed in the mixture of vegetable oil and water	Oscillatory amplitude sweep	The first yielding point was associated with the fragmentation of network structure into large agglomerates, while the second yield point was attributed to the breakage of agglomerates into small fragments	Ahuja and Gamonpilas, 2017
PMMA particles stabilized by PHSA chains dispersed in the mixture of cis-decalin and cycloheptyl bromide	Stress growth	Two-step yielding was linked with the existence of cages of two different sizes (i.e., two different length scales)	Sentjabrskaja et al., 2013
Mixture of PS core/PNIPAM shell microgels and PSS particles dispersed in water	Oscillatory amplitude sweep	The first yield point was attributed to the breakage of inter-connected clusters and the second one was linked with the further collapse of clusters. The incorporation of PSS particles weakens the network structure and converges the two-step yielding into a single step	Jia et al., 2015
PMMA particles stabilized by PHSA chains dispersed in *cis*-decalin	Oscillatory amplitude sweep, stress growth	In case of glasses, the first yield point was attributed to the bond breakage and the second one to the cage breaking. In case of gels: the first yield point was attributed to the bond breakage while the second one to the cluster breaking	Koumakis and Petekidis, 2011

PMMA = poly methyl methacrylate; PHSA = polyhydrostearic acid; PS = polystyrene; PNIPAM = poly(N-isopropylacrylamide); PSS = sulphonated polystyrene

An extensive rheological/yield stress analysis of natural mud samples from different parts

of the world using different methods and geometries has been reported in the literature (Babatope et al., 2008, Bai et al., 2002, Coussot, 1997, Coussot, 2007, Faas and Wartel, 2006, Huang and Aode, 2009, Jiang and Mehta, 1995, Van Kessel and Blom, 1998). Van Kessel and Blom, 1998 presented the comparison of rheological properties of natural and artificial mud samples using three different geometries: (i) Couette, (ii) double concentric and (iii) cone and plate. They found in particular that their results were dependent on the geometries used in the tests. Moreover, the results showed higher yield stress values for estuarine mud samples compared with the kaolinite clay due to the cohesive nature of the samples. J. Xu and Huhe, 2016 presented the rheological studies of natural mud at Lianyungang (China) with the help of both steady and dynamic measurements. They correlated the yield stress values with the mud volume concentration and fitted the experimental data with an exponential empirical relation. Soltanpour and Samsami, 2011 compared the rheology of kaolinite and Hendijan mud, northwest part of Persian Gulf. They linked the rheological parameters with the water content in the natural and artificial sediments using exponential relations. Similarly, the relation between Bingham yield stress and the density of the natural mud sediments was also reported in the literature using empirical exponential relations (Carneiro et al., 2017, Fonseca et al., 2019). Yang, Yu, et al., 2014 investigated the rheological characteristics of three different cohesive sediments from the Yangtze River, and shoal of the Hangzhou Bay and Yangcheng Lake (China). The results revealed three different deformation regions in the flow curves obtained from shear rate sweep tests. In literature, the yield stresses of mud are typically investigated as a function of mud density by step-by-step dilution of a high density consolidated mud (Fonseca et al., 2019, Huang and Aode, 2009, Soltanpour and Samsami, 2011). However, the in-situ mud layers can have significantly different composition, in addition to the water content. Therefore, a comparative analysis of rheological properties of natural and diluted mud layers is needed.

1.3.2. STORAGE AND LOSS MODULI

The storage modulus ($G^{'}$) and loss modulus ($G^{''}$) of a system typically represent the strength of the network formed by its components and can be estimated by performing either oscillatory amplitude sweep or oscillatory frequency sweep test. Oscillatory amplitude sweep experiments typically involve the application of a sinusoidal strain or stress at a particular frequency. The outcome of this method can be plotted in the form of $G^{'}$ and $G^{''}$ curves as a function of either stress or strain. $G^{'}$ and $G^{''}$, obtained from oscillatory experiments, are the in-phase and out-of-phase responses of the material, respectively, to the applied sinusoidal stress/strain. Several ways of determining yield stress from oscillatory experiments have been suggested in the literature such as: (1) crossover point between $G^{'}$ and $G^{''}$ (Kugge et al., 2011, Perge et al., 2014, Renou et al., 2010), (2) decline in storage modulus as a function of stress/strain, given by the point of intersection between the horizontal line representing the linear viscoelastic behaviour and a line representing the non-linear behaviour well above the yield point (De Graef et al., 2011, Rouyer et al., 2005), (3) by plotting the elastic stress as a function of stress/strain. These amplitude sweep tests, at a constant frequency, are typically performed prior to the frequency sweep experiments in order to recognize the different transition regimes for selecting suitable stress values. Three different regimes are: (i) a linear regime where

the sample displays a solid-like behaviour ($G^{'} > G^{''}$); (ii) a transition regime in which the transformation from solid-like to liquid-like state occurs; and (iii) a non-linear regime where a liquid-like behaviour is observed ($G^{''} > G^{'}$). For example, J. Xu and Huhe, 2016 presented the rheological studies of estuarine mud at Lianyungang (China) using both steady and dynamic measurements. From the oscillatory experiments, two regions were identified: elastic and viscous.

On the other hand, oscillatory frequency sweep tests are usually performed within linear viscoelastic regime, identified by amplitude sweep tests. These tests are very useful for examining the mechanical properties of the samples without altering the structure of the samples. The results are typically represented in terms of complex modulus (G^*) and phase angle (δ) as a function of frequency. The complex modulus values with weak frequency dependency and very small phase angle values (no crossover) usually represent the solid-like behaviour of the samples. A similar solid-like behaviour of natural sediments for frequency sweep tests, within the linear viscoelastic regime, has been reported in the literature (Soltanpour and Samsami, 2011, Van Kessel and Blom, 1998, J. Xu and Huhe, 2016). These mechanical properties (i.e., moduli) of natural sediments are observed to increase as a function of volume concentration of solids (Huang and Aode, 2009). Table 1.2 presents a detailed overview of the rheological properties of mud obtained from different sources.

1.3.3. THIXOTROPY AND STRUCTURAL RECOVERY

Thixotropy is a (quasi-)reversible phenomenon. It is one of the most frequently observed complex rheological behaviours of the colloidal suspensions, in which the properties of the material are both time and shear rate dependent. Therefore, a material is typically stated as thixotropic if its viscosity displays a time dependency after applying the shear on an undisturbed sample and that the material displays a progressive recovery of this property after the removal of the applied shear (Mewis, 1979). This complex behaviour is usually observed in a wide range of suspensions having dispersed particles of various shapes and sizes such as fibrous systems, foams, emulsions and polymeric materials (D. C.-H. Cheng, 1987). For instance, Yang, Tan, et al., 2014 discussed the comparative rheology of kaolinite and natural mud samples using mechanical and shear vibrational loads. They observed a typical thixotropic and shear thinning behaviour for cohesion-less sandy sediments, whereas a combination of thixotropy and anti-thixotropy, as a function of shear rate, was evident for cohesive sediments (kaolinite and mud). Moreover, the recovery time after fluidization was longer for cohesive mud and kaolinite as compared to the sandy sediments. Likewise, the transient experiments for mud showed the time-scale of few seconds for short term structural changes while for long-term structural recovery a time-scale of the order of $10^4 - 10^5$ s was observed (Van Kessel and Blom, 1998).

There are several methods to study the thixotropic behaviour of a system. Mewis and co-workers have determined the inherent drawbacks of using steady shearing methods to analyse the structural recovery of the system because in these methods the material's structure has to be disturbed in order to be probed during the recovery phase (Schoukens and Mewis, 1978). Mewis and de Bleyser, 1972 have shown that the struc-

tural recovery of a polyamide gel in linseed oil can be studied by performing oscillatory measurements (i.e., non-destructive) within the linear viscoelastic regime of the material. This linear viscoelastic method has, henceforth, been used to analyse the rate and extent of structural recovery after steady or large amplitude oscillatory shearing for a variety of materials such as polymeric solutions (Janssens et al., 2017), pickering emulsions (Whitby and Garcia, 2014), slurries (Phuoc et al., 2014), cement pastes (Roussel et al., 2012), nanocomposite systems (Mobuchon et al., 2007), emulsion gels (Sun and Zhang, 2015) and synthetic colloidal dispersions (Mobuchon et al., 2009). The rate and extent of this structural recovery can be expressed in terms of thixotropy at a given kinematical condition (Mewis and de Bleyser, 1972).

Large amplitude oscillatory shear (100% strain) was used to break the structure of ferric oxide suspensions in mineral oil followed by the evolution of structure after the release of applied strain (Kanai et al., 1992). The extent and rate of structural recovery was observed to depend on the interactions between the particles and the concentration of the suspensions. Kinloch et al., 2002 examined the structural evolution in aqueous nanotube dispersions. The highly concentrated suspension recovered its initial storage and loss moduli within 1.5 h. Similar structural recovery was also described by Derec et al., 2003 and Coussot et al., 2006 for colloidal silica suspensions and pastes within linear viscoelastic regime upon cessation of shearing. The results showed (i) that the material behaves like a solid below yield stress but with irreversible deformations over long time periods and (ii) a structural recovery phenomenon (i.e., logarithmic increase in modulus) as a function of rest time above yield stress.

The growth of floc size and viscosity as a function of pre-shearing for different synthetic flocculated systems was studied in detail (He et al., 2012, McMinn et al., 2004, W. Xu et al., 2011). He et al., 2012 reported the temporal evolution of floc size and structure as a function of shear for flocculated kaolinite suspensions using polyaluminum chloride (PACl) as a coagulant. The results showed an increase in floc size as a function of shear rate (i.e., aggregation) in the initial stage followed by a plateau at 3 s^{-1} of shear rate and then a decline in floc size at higher shear rates ($11 - 16\ s^{-1}$) due to the irreversible breakage of flocs. The effect of extracellular polymer (EPS) extraction from activated sludge on the time evolution of storage modulus was also investigated in the literature (D. Q. Yuan et al., 2014). It was observed that the extraction of loosely bound EPS from the activated sludge resulted in higher elasticity (i.e., better structure) as a function of time. Hence, it is important to understand the structural recovery behaviour of mud as a function of its composition, density, applied shear rate and also the state of organic matter (i.e., fresh or degraded).

Table 1.2: Detailed overview of the rheological properties of mud from different sources.

Study area(s)	Rheometer & geometry	Density range ($kg.m^{-3}$)	Rheological method for yield stress	Yield stress range (Pa)	Modulus range (Pa)	Viscosity range (Pa.s)	Main outcome(s)	Ref.
Debris flow (Manival, Possuet, Mount St. Helens)	Rheometer: Rheometrics RMS-800; CarriMed; Geometry: Parallel plate; Cone and plate	1512 – 1792	Herschel–Bulkley model fitting on flow curve obtained from controlled shear rate test	29 – 470	–	–	• The rheological properties (i.e., yield stress) of mud suspensions were observed to vary significantly as a function of clay type, solid content, electrolyte concentration and pH.	Coussot and Piau, 1994
Southwest Coast, India; Okeechobee Lake, Florida; Mobile Bay, Alabama	Rheometer: CarriMed	1046 – 1118	–	–	0.10 – 119	224 – 27600	• A small-strain rheological model was developed to analyse the viscoelastic properties of mud. • The viscoelastic properties were observed to significantly depend on the applied frequency, for a particular solid content. • The proposed model was semi-empirical and only applicable for stresses below the yield stress.	Jiang and Mehta, 1995
Port of Rotterdam, the Netherlands	Rheometer: Rheometrics RMS-800; CarriMed; Geometry: Couette; Double concentric; Cone and plate	1064	Toorman model fitting on steady and transient tests	1	45	0.0136	• The transient experiments for mud showed the time-scale of few seconds for short term structural changes while for long-term structural recovery a time-scale of the order of 10^4-10^5 s was observed. • The Toorman thixotropic model (Toorman, 1997) successfully captured the flow curve of mud by using both short-term and long-term structural changes. • The mud sample displayed higher yield stress values than the kaolinite clay due to its cohesive nature. • Below 0.01 strain level, the mud samples exhibited a solid-like behaviour in oscillatory experiments. • A large variability in structure and composition of mud (both in space and time) makes it difficult from practical point of view.	Van Kessel and Blom, 1998
La Penzé Estuary, Morlaix, France	Rheometer: CarriMed; Geometry: Parallel plate	1380 – 1630	Decline in viscosity in flow curve	291 – 43164	970 – 143880	$775564 - 11.5 \times 10^7$	• The flow curves of mud samples showed four different transition regimes. • An exponential relation between rheological properties and density of mud was observed.	Aubry et al., 2003
Emden Port	Rheometer: Rheologica Stresstech HTHP; Geometry: Couette	1013 – 1142	Stress ramp-up test	0.07 – 90	–	0.1 – 2	• A good correlation between the solid content and yield stress of mud was observed for samples from different locations. • A decline in viscosity or change in slope of shear rate as a function of stress was found to be a reliable method for yield stress determination, verified by creep and recovery method. • The Toorman model was modified by using the empirical correlations between the rheological properties and solid content.	Oberrecht and Wurpts, 2014, Wurpts and Torn, 2005

Eckernförde Bay, Germany; Kieier Förde Bay, Germany	Rheometer: Brookfield RVT 8-speed coaxial rotational viscometer; Geometry: Couette	1038 – 1280	Bingham model fitting on flow curve obtained from controlled shear rate test	1.07 – 20.50	–	0.111 – 0.673	• Higher yield stress values along with shear thickening behaviour was observed for mud samples having higher concentrations of silt-sized particles (silt/clay > 1). • Lower yield stresses and shear thinning behaviour was found for mud samples having abundance of clay-sized particles (silt/clay < 1). • The removal of organic matter by chemical treatment of mud resulted in lower yield stress values and enhanced shear thinning behaviour. • The influence of type and content of organic matter and type of clay on the rheological properties of mud needs to be investigated in detail.	Faas and Wartel, 2006
Weston Supermare Estuary, UK	Rheometer: CarriMed; Geometry: Vane	1032 – 1239	Stress ramp-up test	1 – 82	10 – 22000	–	• The results showed an exponential relation between the yield stress and solid content of mud. • The dynamic bulk density, viscoelastic properties and water turbidity from the mud bed was determined in response to plane shear waves at a fixed frequency in a flume.	Babatope et al., 2006
Hangzhou Bay, China	Rheometer: Rheometrics RMS-605; Geometry: Couette; Cone and plate	1145 – 1634	Worrall-Tuliani and Dual Bingham model fitting on flow curve obtained from controlled shear rate test	1.06 – 182.75	0.02 – 15	0.002 – 1.225	• The outcome of this study showed that Dual-Bingham model is much easier to implement than Worrall-Tuliani model for the flow curve of mud. • The results showed that both steady and dynamic rheological properties of mud vary exponentially as a function of volume concentration of solids, with fitting parameters dependent on clay content, organic matter content, particle size distribution and mineral composition	Huang and Aode, 2009
Cassino Beach, Patos Lagoon, Brazil	Rheometer: Brookfield RVT 8-speed coaxial rotational viscometer; Geometry: Couette	1050 – 1300	Bingham model fitting on flow curve obtained from controlled shear rate test	1.05 – 7.6	–	0.02 – 4.7	• The shear strength of remoulded samples was observed to be 2-3 orders of magnitude lower than the strength of sediment bed determined by vane or penetrometer.	Reed et al., 2009
Cassino Beach, southern Brazil; Atchafalaya mud stream, Louisiana; Neuse River Estuary, North Carolina	Rheometer: Brookfield RVT 8-speed coaxial rotational viscometer; Geometry: Couette	1132 – 1138	Bingham model fitting on flow curve obtained from controlled shear rate test	1.7 – 5.4	–	1.9 – 70	• The flow curves obtained from Brookfield with fixed shear rates (Newtonian fluid) and (Krieger and Maron, 1954) approach with variable shear rates (Non-Newtonian fluid) matched quite well. • The clay content, its surface area and its interactions with organic content can significantly influence the rheological properties of mud, which needs further investigation.	Faas and Reed, 2010
Hendijan Coast, Persian Gulf	Rheometer: Anton Paar Physica MCR 300; Geometry: Parallel plate	1417 – 1545	Bingham model fitting on flow curve obtained from controlled shear rate test	20 – 98	3122 – 24,993	3.1 – 13.7	• The steady (i.e., Bingham) rheological parameters were significantly affected by the water content. • The dynamic (i.e., viscoelastic) rheological properties were observed to by highly dependent on frequency. • The large differences in the magnitude of both steady and dynamic rheological properties between kaolinite and mud highlighted the necessity of direct measurements on natural mud samples.	Soltanpour and Samsami, 2011
German Ems; Weser estuaries	Rheometer: Anton Paar Physica MCR 301; Geometry: Parallel plate	1035 – 1065	Extrapolation (i.e., Bingham) of flow curve obtained from stress ramp-up test	1 – 13	–	0.007 – 0.01	• The dependence of apparent viscosity of mud on the solid fraction and shear rate was investigated. • The flow curve of mud was fitted with a modified Worrall–Tuliani model using parametrization of rheological properties.	Knoch and Malcherek, 2011

Suisun Bay, California	Rheometer: AR2000ex, TA Instruments; Geometry: Vane	1641	Cross over between G' and G'' in amplitude sweep test	55.7	–	–	• The results showed an exponential relation between flow-point stress (i.e., bed yield point) and the solid concentration. • A similar exponential function was used for other locations (i.e., Grizzly Bay) where the potential exists for fluid mud formation.	Samsami et al., 2012
Yangcheng Lake, China; Shoal of Hangzhou Bay, China; Mouth of Yangtze River, China	Rheometer: Rheolab-QC, Anton Paar; Geometry: Vane	1650 – 1761	1. Stress ramp-up test 2. Stress growth test at fixed shear rate using Vane 3. Herschel–Bulkley model fitting on flow curve obtained from controlled shear rate test	772 – 3960; 303 – 4950; 89.64 – 220.75	–	11.28 – 119.69	• The outcome of this study showed that all the investigated approaches produced different values of yield stress.	Yang, Yu, et al., 2014
Mouth of Yangtze River, China	Rheometer: Brookfield viscometer (DV-II); Geometry: T-bar spindles	1240	–	–	–	4.1×10^6	• The sandy sediments displayed typical thixotropic behaviour while the cohesive mud and kaolinite samples showed anti-thixotropy at lower shear rates. • The complex viscosity of mud was observed to decrease by applying oscillatory load, which even become stronger at higher oscillatory frequencies. • The recovery time after fluidization was longer for cohesive mud and kaolinite as compared to the sandy sediments.	Yang, Tan, et al., 2014
Suisun Bay, California	–	1641	1. Bingham and Casson model fitting on flow curve 2. Creep test	175 – 217	–	0.84 – 11	• The definition and implementation of nautical bottom concept in port channels requires an understanding of the biochemical effects on the rheological properties of mud and resistance against ship movement.	Mehta et al., 2014
Lianyungang, China	Rheometer: Thermo Scientific HAAKE RheoStress 6000; Geometry: Couette	1098 – 1305	Dual Herschel–Bulkley model fitting on flow curve obtained from controlled shear rate test	0.358 – 28.029	2 – 1050	0.001 – 1.483	• The outcome of this study showed that the influence of consolidation time and temperature on the rheological properties (i.e., yield stress) of mud became stronger as a function of increasing solid content. • Two regions, i.e., elastic dominant and viscous dominant, were observed in the amplitude sweep tests for mud. • The steady and dynamic rheological properties showed an exponential relation with the sediment volume concentration.	J. Xu and Huhe, 2016
Adriatic Sea Sediments, Po delta, Italy; Mediterranean Sea Sediments, Cap de Creus Canyon, France	Rheometer: Rotovisco RV-12, Thermo Haake; Geometry: Couette	1111 – 1239	Bingham and Herschel–Bulkley model fitting on flow curve obtained from controlled shear rate test	5 – 480; 0.35 – 300	–	–	• A viscous resistance term was obtained by normalizing the flow curve (i.e., by dividing the shear stress and shear rate by a reference value). • A linear correlation between the viscous resistance and strength parameters (viscosity and yield stress) of sediments was observed, which provided an easy and simple approach for approximating flow properties.	Jeong and Park, 2016
Port of Santos, Brazil	Rheometer: Rheolab-QC, Anton Paar; Geometry: Vane	1109 – 1310	Bingham model fitting on flow curve obtained from adapted Claeys et al. protocol	10.6 – 567.2	–	–	• The results showed the spatial variability in rheological properties of mud even at a reach of 3 km, which highlighted the necessity of detailed rheological analysis of mud.	Carneiro et al., 2017

Yueqing Bay, China	Rheometer: AR-G2, TA Instruments; Geometry: Parallel plate	1370	Maximum stress point in amplitude sweep test	38	2×10^{7}	–	• The oscillatory strain amplitude was observed to significantly influence the mud fluidization. • The frequency of oscillation displayed negligible effect on the viscoelastic properties of mud obtained within the linear viscoelastic (LVE) regime.	Yang and Yu, 2018
Chorfa dam, Algeria	Rheometer: Thermo Scientific HAAKE RheoStress 600; Geometry: Couette	1032 – 1254	Empirical fitting of flow curve obtained from controlled shear rate test using: 1. Power law model 2. Herschel–Bulkley model 3. Bingham model 4. Casson model	0.011 – 29.39	–	0.0002 – 0.0164	• The results showed a non-Newtonian behaviour along with the increase in viscosity by increasing the solid concentration of mud higher than the critical concentration. • The shear thinning behaviour was evident for the mud samples. • The data of mud samples was best fitted by using power law model.	Messaoudi et al., 2018
West Lake Hangzhou, China	Rheometer: Rheolab-QC, Anton Paar; Geometry: Vane	1032 – 1426	Stress ramp-up test	25 – 2570	–	8.29×10^{-7} – 4.09	• The sediments displayed non-Newtonian and shear thinning behaviour, which was described by Carreau model. • The results showed an exponential increase in zero shear viscosity and critical shear stress as a function of sediment concentration while the corresponding shear rate and critical shear rate were found to be independent of solid content.	Yang et al., 2018
Port of Santos, Brazil; Port of Rio Grande, Brazil; Port of Itajaí, Brazil; Amazon South Channel	Rheometer: Rheolab-QC, Anton Paar; Geometry: Vane	1085 – 1512	Bingham model fitting on flow curve obtained from adapted Claeys et al. protocol	5 – 379	–	–	• A correlation between viscous amplitude of tuning fork and the Bingham yield stress of mud was developed by using four mud samples having significantly different physical properties.	Fonseca et al., 2019
Lianyungang Port, China	Rheometer: Anton Paar Physica MCR 302; Geometry: Couette	1107 – 1546	1. Flow curve from shear rate ramp-up test 2. Decline in G' from strain amplitude sweep test	0.014 – 380	300	0.002 – 0.22	• The static and fluidic yield stress values showed an exponential relation with the bulk density of mud. • The frequency of oscillation showed a negligible effect on the elastic regime while the transition and viscous regimes were significantly influenced by frequency during amplitude sweep tests. • The large amplitude oscillatory tests (i.e., stress waveform and Lissajous pattern by the Fourier transformation method) showed an increase in non-linearity at the transition regime.	Nie et al., 2020
Hemipelagic marine sediment; Salton Sea mud volcano	Rheometer: Thermo Scientific HAAKE Rheoscope 1; Geometry: Cone and plate	1170 – 1340; 1670 - 1760	Bingham model fitting on the ramp-down curve of controlled shear rate test	18 – 702; 145 - 769	-	8.9 – 126.4; 9.3 – 125.1	• The mud sample showed the existence of a yield stress even at 10% of particle concentration. • The yield stress and consistency of sediments was observed to increase by increasing the particle concentration.	Knappe et al., 2020

1.4. PROBLEM DESCRIPTION AND KNOWLEDGE GAPS

IN ports, frequent maintenance dredging operations are required to guarantee the port accessibility. As these dredging operations are expensive, an economical and sustainable solution is sought by Port Authorities. A possible solution is to minimize dredging operations and to optimize the tidal window to allow ships to pass through the top mud layer, which is very weak in strength, instead of dredging it. This type of solution already exists, whereby the nautical depth is defined based on the rheological properties (i.e., yield stress) of fluid mud, and is in use in the Port of Emden. However, other ports including Port of Hamburg, Germany are still looking for solutions, adapted to the boundary conditions of their harbours and type of mud present. One of the potential solutions is the implementation of nautical bottom based on the yield stresses of mud. By keeping this solution in view, Port of Hamburg initiated an interdisciplinary project having multiple domains such as (i) investigation of detailed rheological properties of mud (this thesis), (ii) investigation of bio-geochemical properties of mud (another PhD student in parallel), (iii) CFD simulations of ship navigation through fluid mud (another PhD student in parallel) and (iv) pilot experiments and the implementation of yield stress for nautical bottom (by port authorities).

Therefore, the main aim of this study is "to investigate the rheological characteristics (i.e., yield stress, moduli and thixotropy) of mud as a function of several influencing factors including the state and content of organic matter, bulk density, and sampling locations. Moreover, this study will provide the input rheological parameters for the CFD simulations performed by another PhD student. The rheological data-set produced in this thesis for mud samples from different locations and depths of port of Hamburg will also be used to calibrate the in-situ measurement device (Rheotune). In the end, this thesis will also provide a suitable value of yield stress to the port authorities as a starting point for some preliminary pilot experiments, in order to define the nautical bottom using yield stress value.

1.5. RESEARCH QUESTIONS AND THESIS OUTLINE

SEVERAL key research questions were identified which provided the basis of different chapters of the thesis, given as:

1. **Which rheological geometry and rheological protocol are appropriate to measure the yield stresses of harbour mud?** This research question is addressed in Chapter 3 by comparing the results for different geometries and protocols. In this chapter also, the structural changes in the mud samples upon shearing is linked to the bulk rheological behaviour of mud.
2. **What is the spatial and depth variability of the rheological properties of mud?** In Chapter 4, the spatial and depth variability of the rheological properties of mud are studied. The influence of density and organic matter content on the rheology of mud are detailed. The size and density of mud flocs are estimated, and are shown to well correlate with the bulk rheological properties of mud from different locations of Port of Hamburg.
3. **How much different are the rheological properties of natural and artificially made**

mud layers? The rheological properties of naturally existing mud layers and artificially made mud layers (i.e., by diluting dense mud sample) are compared in Chapter 4.

4. **Which rheological model(s) is suited to fit the experimental data of mud?** A new empirical model is proposed in Chapter 5 to capture the rheological behaviour of mud (i.e., two-step yielding). This model is shown to work very well and will be used further in numerical simulations by colleagues to identify the main rheological parameter influencing the ship manoeuvring.
5. **How much and how fast the structure (or strength) of mud recovers itself after the disturbances (i.e., pre-shear)?** The detailed analysis of structural recovery in mud as a function of several parameters (i.e., pre-shear rate, pre-shear time and organic matter content) is given in Chapter 6.
6. **What is the effect of degradation of organic matter, present in mud, on the rheological characteristics of mud?** Chapter 7 presents the influence of organic matter degradation on the rheological properties (i.e., yield stress, moduli and thixotropy) of mud collected from different locations of Port of Hamburg.

Furthermore, Chapter 2 provides an extended material and methods description, and an overall conclusion will be given in the last chapter.

2

MATERIALS AND METHODS

This chapter has as objective to present the materials and techniques that are employed for carrying out the analysis presented in the thesis. The experiments are performed for natural mud samples. The detailed rheological analysis of mud samples collected from Port of Hamburg, Germany presented in the forthcoming chapters is performed with the help of the different rheological protocols described in this chapter.

2.1. CORE SAMPLING

IN this study, natural mud samples were collected from 12 different locations of the Port of Hamburg Germany (Table A1 and A2 in Appendix A) during 21 monitoring campaigns (Table A3) spanned over 2 – 3 years using a core sampler of 1 m length. In short, this core sampler goes inside the mud layers at the required depth, thereby filling the mud inside the core, and then the lid is closed by a mechanical action (i.e., by pulling the string attached to the lid). The mud-filled core is then carefully taken out. This core sampler is useful in collecting "undisturbed" mud samples with naturally occurring density gradient profile, in order to estimate the properties of mud as close as possible to in-situ conditions. Figure 2.1 shows the selected locations at the Port of Hamburg with the associated names and the corresponding GPS coordinates of these locations are presented in Appendix A (Table A1). The selected locations were chosen on the basis of a preliminary analysis, which highlighted that these locations showed significant sedimentation rates along with different amounts of organic matter (TOC) in mud samples. In addition to these locations, few mud samples were also taken from more upstream (river side) area of port (see Table A2 in Appendix A), in order to analyze the larger spatial variability in the rheological properties of mud. The collected core samples (Fig. 2.2a) were sub-sampled into different mud layers based on the differences in their visual consistency and consolidation stage, and named as: fluid mud (FM), fluid mud to pre-consolidated (FM/PS), pre-consolidated sediment (PS), pre-consolidated to consolidated sediment (PS/CS) and consolidated sediment (CS) (Fig. 2.2b). The samples were packed in the sealed containers and transported to the laboratory for detailed analysis.

2.2. BULK DENSITY

BEFORE analyzing the rheological properties of mud, the bulk density of each collected mud sample was determined. The dry density of the mud samples was measured using a gas pycnometer (ISO:17892-3, 2015) and found to be within the range of 2375 – 2534 kg. m^{-3}. The bulk density of the mud samples was estimated by oven drying method. The mass of each mud sample was determined before and after oven drying at 105 °C for 24 h. This gave the mass of dry solids and water content in the mud samples. By using the densities of water (1000 kg. m^{-3}) and minerals (2650 kg. m^{-3}), the corresponding volumes were then estimated. The final bulk density of mud samples was then calculated based on these masses and volumes. This bulk density was in good agreement with the bulk density measured using an Anton Paar portable density meter (DMA 35).

2.3. PARTICLE SIZE DISTRIBUTION (PSD)

THE particle size distribution of each collected mud sample was measured by static light scattering technique (Malvern Mastersizer 2000MU). There are several limitations of this instrument which need to be considered such as: (i) the conversion between raw data and PSD is based on the Mie theory which assumes that all the particles are spherical; (ii) only a certain concentration range is accessible for measurements, limited by laser obscuration; and (iii) for samples with notable sand fractions, this technique gives inaccurate average particle diameter (D_{50}) due to the smoothing of the data-set

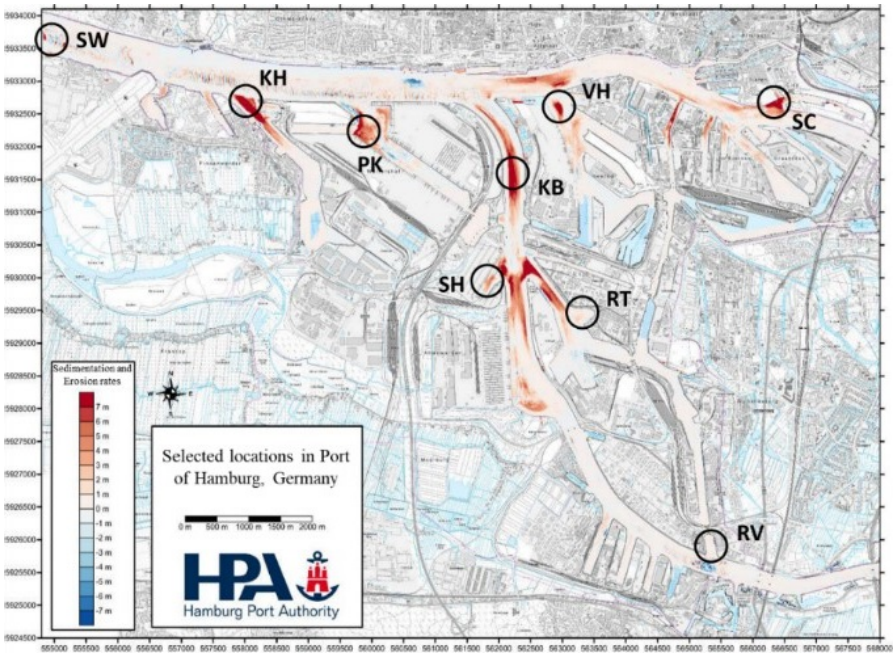

Figure 2.1: Selected locations in the Port of Hamburg, Germany for collecting mud samples. SW = Sedimentfang Wedel, KH = Köhlfleet mit Köhlfleethafen, PK = Parkhafen, KB = Köhlbrand, VH = Vorhafen, SC = Strandhafen Chicagokai, SH = Sandauhafen, RT = Rethe, RV = Reiherstieg Vorhafen. Left side of the map represents the sea side and right side of the map represents the river side (source: adapted from Hamburg Port Authority).

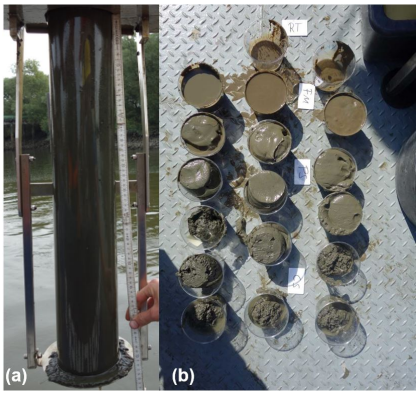

Figure 2.2: (a) Frahmlot core sampler (b) different layers of mud samples having different visual consistencies.

by the software (Ibanez Sanz, 2018). However, this technique was used in this study because it is very easy and fast to use. The mud samples were diluted, without any pretreatment, in order to achieve the required range of obscuration (i.e., from 10 to 20%) in the Malvern equipment. Figure 2.3a shows the PSD of mud samples from different loca-

tions in the Port of Hamburg. The bi-modal distribution observed for samples from SW and SC locations showed the presence of sand-sized particles in the mud sample. For other locations, the average particle size (D_{50}) was similar and lies within the range of 15 to 21 µm. The particle size distribution of mud layers having different densities was also similar (D_{50} = 14.5 – 18.6 µm), as shown in Fig. 2.3b.

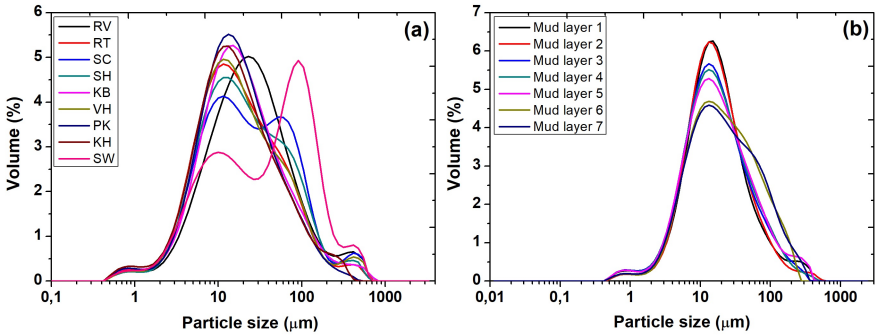

Figure 2.3: Particle size distribution of (a) mud samples from different locations of Port of Hamburg, Germany (see Fig. 2.1) and (b) different mud layers from PK location.

2.4. RHEOLOGICAL ANALYSIS

BEFORE conducting the rheological experiments, all the mud samples were homogenized by mild hand stirring, in order to avoid the effect of dewatering/consolidation on the rheological properties of mud. A HAAKE MARS I rheometer (Thermo Scientific, Germany) was used to perform the rheological characterization of mud samples. This rheometer can either be operated in stress controlled, shear rate controlled or deformation controlled mode. Four different geometries, including smooth and grooved concentric cylinder (Couette and Couette-G, CC25 DIN Ti), cone and plate (C60/2° Ti L), parallel plate (P35 Ti L), and vane (FL22) were used to perform different rheological tests. For concentric cylinder geometry, the cup inside and bob outside diameters were 27 mm and 25 mm, respectively. The distance between the bob and the bottom of the cup was 5.30 mm. Vane geometry having diameter of 22 mm, with the cup of 27 mm, was used by maintaining a distance of 1 mm between the vane and the bottom of the cup. Cone and plate geometry, having diameter of 60 mm with 2° cone angle and 0.104 mm gap between the cone and plate, was used to perform experiments. The diameter of parallel plate geometry was 35 mm. A gap of 2 mm was adjusted between the plates for the rheological experiments.

The temperature was maintained at a desired value (20 °C) during each rheological experiment using a Peltier controller system. A waiting time of 3 – 5 min was used before each experiment to eliminate the disturbances created by inserting the bob in the cup to reach its measurement position. This time was estimated by performing preliminary oscillatory time sweep experiments in the linear viscoelastic regime. After this time interval, the increase in storage modulus as a function of time was not very significant, which showed the 'complete' recovery of the disturbed sample. The repeatability of the exper-

iments was checked by performing each experiment in duplicate and the repeatability error was always less than 2%. Different rheological tests were performed to analyze different rheological properties of mud samples and are detailed underneath.

2.4.1. METHODS FOR STEADY MEASUREMENTS

CREEP

The creep test is often used to measure yield stress values (Christopoulou et al., 2009). In a typical creep test, constant stresses in a range encompassing the yield stress are imposed in successive experiments to the sample and the resultant strain is measured as a function of time. Below the yield stress, the sample behaves like a solid with small strain which reaches a constant value with time. Above the yield stress, the strain shows a sudden increase and becomes an increasing function of time. The measurement time is important in this method to analyze the correct value of yield stress. Contrary to the other methods, the creep method requires a prior knowledge of the range of yield stress, in which structural break-up (yielding) is expected. In this thesis, the applied stress values were chosen to be: (i) below first yield point, (ii) above first yield point, (iii) below second yield point and (iv) above second yield point, as determined by the stress ramp-up tests.

STRESS GROWTH

In a stress growth method, a constant shear rate is applied and the resultant shear stress is measured as a function of time. Typical stress growth curves initially display a linear regime followed by either a deviation from linearity or a stress overshoot and then finally a steady state value of stress (Barnes and Nguyen, 2001). Different yield stress values can be obtained from this method depending upon the definition of yield point such as deviation from linearity, peak stress, or steady state (equilibrium) stress value (Møller et al., 2006). In this study, different shear rates ranging from 0.01 to 10 s^{-1} were applied and the stress was recorded for 300 s, which was enough to capture the peak stress. The selected range of shear rate was sufficient to analyse the effect of the applied shear rate on the stress growth behaviour.

STRESS RAMP-UP

The controlled stress mode of the rheometer is used to perform the stress ramp-up tests by linearly increasing the stress at a rate of 0.1 – 10 Pa. s^{-1}, depending upon the consistency of the sample, till the shear rate reaches 300 s^{-1} (Fig. 2.4a). The resultant rotation of geometry is recorded, and used to calculate the shear rate and apparent viscosity. The result is plotted either in the form of apparent viscosity as function of shear stress or strain vs shear stress. From the viscosity curve, the yield stress can be determined from the sharp decline in viscosity above the yield stress or by the sudden increase (non-linearity) in the slope of the strain curve. If the decline in viscosity or non-linearity in strain is not very sharp and clear, the point of intersection between the straight lines extending from the plateau where viscosity is more or less constant (structured state) and unstructured sample where everything is broken down (liquid-like state), can be used to determine the yield stress values (Zhu et al., 2001).

CLAEYS ET AL. PROTOCOL (CLAEYS ET AL., 2015)

First, a stress growth test is performed at a shear rate of 1 s^{-1} for 30 s followed by a pre-shearing step at a particular shear rate (300 s^{-1} for Couette and 150 s^{-1} in case of vane) for 15 s. The desired shear rate is then set for a period of 100 s to get the steady state value of stress, followed by a low shear rate step (0.001 s^{-1}) for 6 s. The same cycle is repeated for each selected shear rate from 100 to 0.01 s^{-1} by performing 11 cycles (Fig. 2.4b). The undrained shear strength of mud samples is obtained from the first step (i.e., stress growth) of the protocol while the dynamic yield stress is deduced from the equilibrium flow curve by applying any suitable rheological model (typically Bingham model).

EQUILIBRIUM FLOW CURVE (EFC) TEST

The increasing or decreasing equilibrium flow curves are performed by linearly increasing or decreasing the shear rates (within the range of 0.01 and 100 s^{-1}) after a time period of 100 s to get steady state stress values, without performing any pre-shearing, stress growth or low shear rate steps (Fig. 2.4c and 2.4d). The duration of 100 s was found to be enough to attain steady state values of stresses for the applied shear rates. The yield stress values are then obtained either by viscosity declines or by applying rheological models to the flow curves.

SHEAR RATE RAMP UP AND RAMP DOWN TEST (CSRT)

Controlled shear rate ramp up and ramp down (CSRT) tests consist of shear rate ramping up and down by linearly increasing the shear rate from 0.01 to 100 s^{-1} and then linearly decreasing from 100 to 0 s^{-1}. These experiments were performed without giving enough time to the system under investigation to attain steady state values. However, at lower shear rates (from 0.01 to 5 s^{-1}) a slower increasing or decreasing rate was used, as can be seen in Fig. 2.4e. At lower shear rates, significant changes in mud structure are typically observed and that is why slower sweep rate was performed, in order to capture these changes more effectively. These experiments were performed to determine both yield stresses and the thixotropic behaviour of mud samples.

PRE-SHEAR TEST

In this protocol, similar to Claeys et al. protocol, a pre-shearing step was performed at a shear rate of 100 s^{-1} for 100 s, followed by a linear shear rate ramp down step from 100 to 0.01 s^{-1}. The change from one shear rate to another during the ramp down was too short for the system to reach steady-state stress values. The pictorial representation of the protocol is presented in Fig. 2.4f. The yield stress values were determined from the flow curve of the mud sample.

2.4.2. METHODS FOR OSCILLATORY MEASUREMENTS

OSCILLATORY AMPLITUDE SWEEP

Oscillatory amplitude sweep experiments typically involve the application of a sinusoidal strain or stress at a particular frequency. The outcome of this method can be plotted in the form of storage modulus (G') and loss modulus (G'') curves as a function of either stress or strain. Several ways of determining yield stress from oscillatory experiments have been suggested in the literature such as: (1) cross-over point between

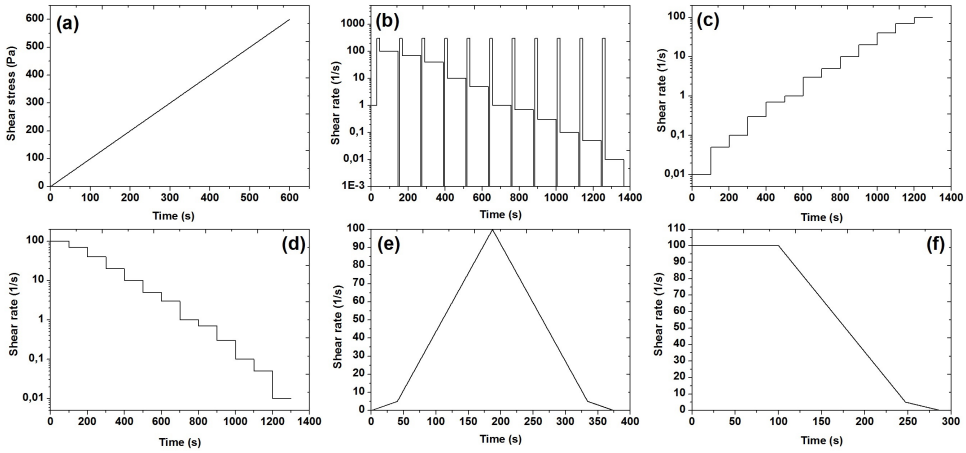

Figure 2.4: Pictorial representation of the protocols (a) stress ramp-up, (b) Claeys et al. protocol, (c) increasing EFC, (d) decreasing EFC, (e) shear rate ramp up and ramp down (CSRT) and (f) pre-shear test.

$G^{'}$ and $G^{''}$ (Renou et al., 2010, Kugge et al., 2011, Perge et al., 2014), (2) decline in storage modulus as a function of stress/strain, given by the point of intersection between the horizontal line representing the linear viscoelastic behaviour and a line representing the non-linear behaviour well above the yield point (Rouyer et al., 2005, De Graef et al., 2011), (3) by plotting the elastic stress as a function of stress/strain, where the elastic stress τ_E is defined by:

$$\tau_E = G^{'}\gamma \tag{2.1}$$

At very small stress/strain a linear behaviour is typically observed followed by a sharp decline in τ_E above yield point. The accuracy of these methods may depend on the applied frequency. Preliminary amplitude sweep tests at different frequencies were performed to analyze the suitable value of the frequency for amplitude sweep tests. In this thesis, the oscillatory stress amplitude was linearly increased at a constant frequency of 1 Hz. The material's response was obtained in terms of $G^{'}$ and $G^{''}$ as a function of the applied amplitude. This test also permitted to determine the linear viscoelastic (LVE) regime for the mud samples, which was required to perform frequency sweep tests.

OSCILLATORY FREQUENCY SWEEP

Frequency sweep tests are performed from 0.1 to 100 Hz within the linear viscoelastic (LVE) regime. The selected amplitude for frequency sweep tests is tuned for each mud sample based on the results of preliminary amplitude sweep tests. This test is conducted for studying the rheological properties of the mud without disturbing the structure of the material. $G^{'}$ and $G^{''}$ are recorded as a function of frequency. The complex modulus (G^*) and the phase angle (δ) can then be calculated as follows:

$$G^* = \sqrt{G'^2 + G''^2} \tag{2.2}$$

$$\delta = \tan^{-1} \frac{G''}{G'} \tag{2.3}$$

2.4.3. METHODS FOR STRUCTURAL RECOVERY

The structural recovery test for mud samples is performed using a three step protocol. In the first step of the experimental protocol, a resting time is imposed to each sample to ensure a reproducible state for each sample. During this resting period, the initial structure level of the samples before shearing is determined by oscillatory time sweep within linear viscoelastic (LVE) regime at 1 Hz. It was found that the resting time was long enough for all the samples to attain the constant storage modulus values (i.e., plateau). Since the continuous phase (i.e., water) of the samples is Newtonian, the elastic character comes from the presence of particles and flocs. Therefore, the storage modulus is an appropriate parameter to assess the structural level in the suspensions. Furthermore, it should be noted that the small amplitude time sweep experiments are non-destructive and thus the evolution of the structure can be recorded in the absence of shear forces (i.e., almost at rest conditions).

A steady shearing step (second step in the protocol) is then performed to destroy the structure of the system under investigation. Preliminary studies were performed to investigate the effect of two different shearing modes (oscillating and steady) on the structural breakdown and recovery in mud sediments. The higher structural breakdown was found in the case of steady shearing. The pre-shear rate values can have a significant effect on the structural evolution, thus, different pre-shear rates, ranging from 5 to 100 s^{-1}, were chosen to study the recovery of the structure as function of these shear rates. These shear rates were selected to have lower, intermediate and higher shearing action, based on a preliminary analysis. The shearing step was performed for 800 s. It was observed that this time was long enough for the viscosity (measured during this same period) to reach a constant value. This implies that the system has reached a steady-state structure. Apart from pre-shear rate, it is also useful to investigate the effect of pre-shear duration on the structural regrowth of the mud sediments. Shearing steps were performed at two different pre-shearing rates (10 s^{-1} and 30 s^{-1}) by varying the pre-shearing duration from 10 to 800 s. The pre-shearing rates were selected to analyze the effect of pre-shearing time for two specific cases: (i) 10 s^{-1}, for which $G'_\infty/G'_0 > 1$ and (ii) 30 s^{-1}, for which $G'_\infty/G'_0 < 1$.

The third step of the protocol is the study of the structural recovery of sediments, after the shearing step. An oscillatory time sweep experiment is performed within the LVE regime during which the structure is left to recover with minimal disturbance. The amplitude of the oscillations, to remain in the LVE regime, was determined by performing amplitude sweep experiments immediately after the shearing step. Preliminary studies were also performed to select the suitable frequency of oscillation for the recovery step. The results showed that a frequency of 1 Hz is the most suited for the considered mud sediments. The pictorial representation of the experimental protocol is shown in Fig. 2.5.

To quantify the structural recovery parameters, a stretched exponential function, adapted

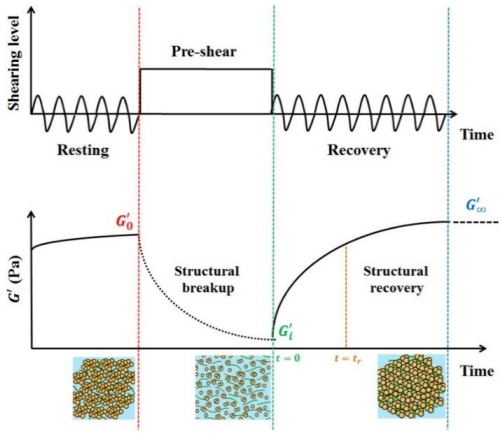

Figure 2.5: Schematics of the experimental protocol employed for the structural breakup and recovery in mud samples.

from (Mobuchon et al., 2007, Mobuchon et al., 2009), was used:

$$\frac{G'(t)}{G'_0} = \frac{G'_i}{G'_0} + \left(\left(\frac{G'_\infty - G'_i}{G'_0}\right)\left(1 - \exp\left[-\left(\frac{t}{t_r}\right)^d\right]\right)\right) \tag{2.4}$$

where $G^{'}(t)$ is the time dependent storage modulus of suspensions recorded after shearing, $G^{'}_0$ is the storage modulus before structural breakup (i.e., the "undisturbed" sample), $G^{'}_i$ is the storage modulus right after the pre-shearing step (i.e., first value of the storage modulus obtained in the recovery step at $t \rightarrow 0$), $G^{'}_\infty$ is the equilibrium storage modulus as $t \rightarrow \infty$, t_r is the characteristic time of the material and denotes the rate of structural build-up (i.e., the time required for the system to attain 63% of its final value, $G^{'}_\infty$) and d is the stretching exponent which reflects the sensitivity of the storage modulus on time (smaller value of d means faster recovery of storage modulus initially and slower at the later period) and its value lies within the range [0; <1]. The fitting parameters in Eq. 2.4 are $G^{'}_\infty$, t_r and d. In order to link the structural parameter ($G^{'}/G^{'}_0$) with yield stresses, amplitude sweep tests at a constant frequency of 1 Hz were performed after the recovery steps of different duration in the range $G^{'}_i < G^{'} < G^{'}_\infty$. The effect of pre-shear rate and pre-shear time on the apparent viscosity was also analyzed by carrying out a shearing step followed by a stress ramp-up test at a rate of 1 Pa/s (without measuring steady state viscosity).

In order to study the influence of shear induced particles migration and/or sedimentation on the rheological properties of mud, structural recovery tests were performed to analyze the modulus of the samples before and after the shearing step. The outcome of these tests are shown in Fig. A.1 for the mud samples from SW location, which showed the existence of sand-sized particles (Fig. 2.3). These sand particles can settle during shearing action. In case of mud sample with lower bulk density and no yield stress, the

modulus of the sample showed a decrease as a function of time even before the shearing step, which became further enhanced after the shearing step (Fig. A.1a). This decrease in modulus comes from the concentration gradient of particles due to sedimentation. On the other hand, the mud sample from the same location (SW) but having higher bulk density and yield stress value displayed a significant increase in modulus as a function of time, particularly after the shearing step (Fig. A.1b). This increase in modulus represents the recovery in structure which became more or less equal to the initial structural level after certain time (i.e., negligible effect of sedimentation). The same result was also obtained for the mud sample from KH location. Hence, this result shows that the sedimentation of particles is extremely fast and it is almost impossible to eliminate the sedimentation effect during rheological analysis of mud samples with no yield stress. However, the existence of yield stress, even for small values, is enough to stabilize the mud sample for the time interval relevant for the rheological analysis. This stabilization of mud sample is mainly linked to the presence of organic matter (Table 2.1), in combination with a specific particle concentration. A network of organic matter - clay particles is hence formed which prevents the significant segregation and settling of particles.

2.5. RHEO-OPTICAL ANALYSIS

SEVERAL, optical techniques have been used in rheo-optical devices, depending on the material under investigation and the observation scale. Different shearing devices like a 4-roll mill (Hamberg et al., 2001), controlled strain rheometer (Mighri and Huneault, 2001) and parallel plate (Deyrail and Cassagnau, 2004, Grenard et al., 2011) have been used so far to perform deformation under controlled environment. Recently, a novel parallel plate rheo-optical device (RheOptiCAD®) was designed by CAD Instruments (Illiers-Combray, France) and reported by Boitte et al., 2013. With this device a video recording during shearing is obtained from which the structural changes in the samples can be studied. The device has primarily been designed to be mounted on an inverted microscope. Even though it can be used to visualize readily opaque structures (Didi et al., 2004), the device is not suited to analyze the optical behaviour of very concentrated clay suspensions (our topic of interest) as it makes use of transmitted light. Therefore, a modified version of RheOptiCAD® was proposed (Shakeel, van Kan, et al., 2019) for the structural analysis of mud flocs under shearing action.

This modified RheOptiCAD® version has an upright microscope instead of an inverted microscope, as shown in Fig. 2.6. The design of the top and bottom plate of the RheOptiCAD® was adapted for observation from above. An opening with an oval shape was made in the top plate, to accommodate the microscope objectives (18 mm × 8 mm = 144 mm^2), defining the dimensions of the observation window. In the modified design, with an upright microscope using epi-illumination and observation of reflected light, the displacement of the top plate is limited: the top plate can move with an amplitude of 12 mm, the bottom plate can travel as far as 20 mm. For the upright microscope in the setup, suitable components were chosen in the Olympus BXFM-BX3M modular microscopy/illuminator system. The selected camera was a USB 3.0 connected monochrome CMOS camera with a $1''$ target (12.5 × 10 mm) and a resolution of 2592 × 2048 pixels (UI-3180CP-M-GL Rev.2, IDS GmbH, D). Temperature could be controlled

within the range of 10 – 80 °C using a Peltier system TEC-1090 Controller/Peltier Driver (Meerstetter Engineering, CH) (30 mm × 30 mm) mounted on the bottom plate. The sample is typically placed on a rectangular microscopy cover slip (24 × 60 mm) attached to the bottom plate. To ensure the parallelism and planarity of microscopy glass slides, important for better observation and fine-tune controlling of deformation, the glass slides were bound to the aluminum plates (top and bottom) by creating vacuum between them. Before measurement, the bottom plate is raised until the sample is in contact with both plates. Table A4 summarizes some important details about the already reported rheo-optical systems, in comparison to our designed system.

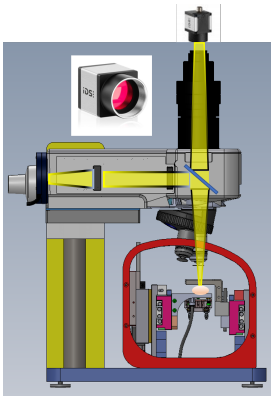

Figure 2.6: The optical layout of modified RheOptiCAD® device. A 1″ CMOS camera (see insert) is fitted on the epi-illumination module of the microscope. Further information regarding the device can be found in Shakeel, van Kan, et al., 2019.

For the structural analysis of mud flocs under shearing action, a 20× microscope objective was used. The mud samples were diluted with tap water, to permit a clear observation of the flocs under the microscope. In all experiments, the mud flocs were deformed instead of displaced, due to the perfect contact of flocs with both upper and lower plates. The videos or images (2592 × 2048 pixels) were recorded in the x-y plane with an LED light as illumination. Oscillatory experiments were performed using a frequency f of 1 Hz and amplitudes A between 0.1 and 0.2 mm, for the bottom plate. Continuous strain experiments were conducted by placing the mud flocs between the upper and lower plates and setting the movement of both plates in same direction at a rate of 0.003 mm/s and 0.17 mm/s for top and bottom plate, respectively. The gap between the upper and lower plate was maintained between 10 µm and 100 µm. All experiments were performed at a constant temperature of 20 °C.

2.6. FLOC SETTLING ANALYSIS

To analyze the size, shape, and settling velocity of mud flocs, video of settling experiments were performed using an home-made apparatus (FLOCCAM) similar to the one described in Ye et al., 2020. A schematic representation of the apparatus is shown in Fig. 2.7. The mud samples were diluted with tap water, drawn up with a wide-mouth

pipette, then gently introduced to the water column to permit images of freely settling flocs to be recorded. An open-source package Safas (Sedimentation and Floc Analysis Software, (MacIver, 2021)) is used to select flocs and determine their settling velocity from the videos. Individual flocs are re-segmented using WEKA, a machine learning-based image segmentation tool, to obtain high quality shape and size information.

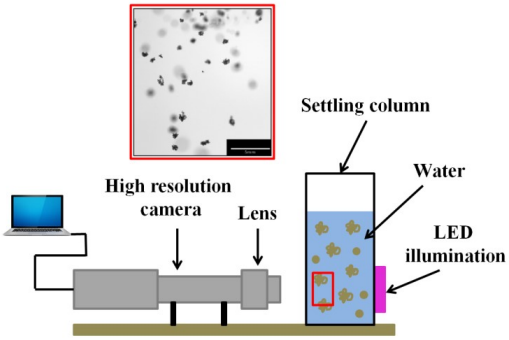

Figure 2.7: Schematics of the settling column apparatus (FLOCCAM) used for the floc analysis.

The following parameters were estimated from the videos for the mud flocs:

2.6.1. MEAN DIAMETER

Mean diameter, d_m [µm], was calculated from the diameter of major axis (d_{major}) and minor axis (d_{minor}) of the object in an image according to Ye et al., 2020:

$$d_m = \sqrt{d_{major} \times d_{minor}} \tag{2.5}$$

2.6.2. ASPECT RATIO

The aspect ratio (AR) of the flocs was estimated by using their major axis (d_{major}) and minor axis (d_{minor}) as follows:

$$\text{Aspect ratio} = \frac{d_{\text{major}}}{d_{\text{minor}}} \tag{2.6}$$

2.6.3. EFFECTIVE DENSITY OF MUD FLOCS

The density of a mud floc, ρ_f, is:

$$\rho_f = \rho_w + \frac{9\eta v}{2R_f^2 g} \tag{2.7}$$

where ρ_f and ρ_w are the floc and water density, respectively, η is the dynamic viscosity of water, v is the floc settling velocity, g is the acceleration due to gravity and R_f is the radius of the floc. The mean density of flocs can be estimated by averaging the density for each size.

2.6.4. FRACTAL DIMENSION

Assuming that the flocs are fractal objects and composed of primary particles of size a, the volume fraction of solids ϕ_s inside a floc is given by:

$$\phi_s = \frac{N \cdot a^3}{R_f^3} = \left(\frac{R_f}{a}\right)^{D-3} \tag{2.8}$$

where N is the number of solid particles in a floc and D is the fractal dimension of flocs. The density of flocs is linked to the volume fraction by:

$$\frac{\rho_f - \rho_w}{\rho_s} = \frac{\phi_s(\rho_s - \rho_w)}{\rho_s} \tag{2.9}$$

where ρ_s is the solid (clay) density. Combining Eq. 2.8 and Eq. 2.9 gives:

$$\rho_f - \rho_w = (\rho_s - \rho_w)\left(\frac{R_f}{a}\right)^{D-3} \tag{2.10}$$

By fitting the function $(\rho_f - \rho_w)$ as a function of R_f, the fractal dimension D can be determined (Manning and Dyer, 1999, Guo et al., 2021). In the case of natural flocs, as found in ports and estuaries, objects are not fractal and it is therefore more appropriate to speak of pseudo-fractal dimension (Malarkey et al., 2015).

2.7. IN-SITU ANALYSIS USING RHEOTUNE

THE Rheotune (from Stema Systems, see Fig. 2.8) records the amplitudes which are triggered by mechanical vibrations at the frequency range of 500 – 800 Hz. The recordings can then be used to get the information about the (Bingham) yield stress and density of mud layers (Fonseca et al., 2019).

2.8. ORGANIC MATTER DEGRADATION EXPERIMENTS

The organic matter content (i.e., total organic carbon = TOC) of the mud samples was determined using an ISO standard (ISO:10694, 1995) and the TOC values for different locations are presented in Table 2.1. Organic matter degradation was assessed by measuring carbon release over time upon incubation of the samples in the laboratory in closed glass bottles sealed with butyl rubbers topers under anaerobic (CH_4 and CO_2) and aerobic (CO_2) conditions as described in detail in Zander et al., 2020. To analyse organic matter degradation under anaerobic conditions, the bottle headspace was perfused with N_2 and samples thereafter incubated at 36 °C in the dark. Carbon release was calculated from the increase in headspace pressure in combination with gas chromatographic analyses of headspace composition and is reported as the sum of CH_4-C and CO_2-C measured in the gas phase and the share of CO_2-C dissolved in the aqueous phase. Aerobic organic matter degradation was quantified by flushing the bottle headspace with atmospheric air and incubating the samples at 20 °C in the dark. Carbon release was calculated from

Figure 2.8: In situ device for measuring the yield stress (Rheotune).

the increase in the concentration of headspace CO_2, measured by gas chromatography, considering CO_2 dissolution.

Table 2.1: Total organic carbon (TOC) of mud samples from different locations. The standard deviation covers the variability of TOC values in different mud layers and different sampling campaigns.

Locations ID	TOC content (% TS*)
RV	6.2±0.7
RT	4.1±0.3
SC	4.1±0.3
SH	4.2±0.4
KB	3.4±0.7
VH	3.8±0.3
PK	3.8±0.5
KH	3.8±0.3
SW	2.6±1.0

*This TOC value is based on the dry mass of the solids

3

YIELD STRESS AND RHEO-OPTICAL ANALYSIS

Among different rheological properties, yield stress is the most important characteristic of mud particularly for maintenance operations in ports and waterways. Yield stresses are dependent on the material (shear) history and composition, which implies that robust protocols should be developed to study the yield stress dependence on a given parameter. The associated measurements, performed in the laboratory, should give a rheological fingerprint which is representative for the in-situ behaviour of the mud. Therefore, the main aim of this chapter is to find the rheological geometry and measurement protocols which are best adapted to study natural mud samples. The constraints are that (i) the measurement should be reasonably fast with good repeatability and (ii) the major changes in sample structure (i.e., two-step yielding) should be recorded. Various conventional and unconventional rheological protocols were performed and compared using different geometries. The "best" protocol is derived from this study. Furthermore, the structural analysis of mud flocs during shearing, leading to the two-step yielding, is discussed.

Parts of this chapter have been published in Marine Geology **427**, 106247 (2020) (Shakeel et al., 2020d), Estuarine, Coastal and Shelf Science **257**, 107407 (2021) (Shakeel, Kirichek, Talmon, et al., 2021), Colloids and Surfaces A: Physicochemical and Engineering Aspects **624**, 126827 (2021) (Shakeel, MacIver, et al., 2021).

3.1. INTRODUCTION

YIELD stress is typically defined as a critical stress below which the materials behave like an elastic solid whereas they tend to flow above that critical value of stress. Yield stress has been found to be an important parameter to define navigable fluid mud layers for ports and waterways (Kirichek et al., 2018, Møller et al., 2006, Q. Nguyen and Boger, 1992). Recently, it has been found that, instead of a single yielding response, a prominent two-step yielding behaviour can be observed for different soft materials including fine-grained sediments (Nie et al., 2020). From the last two decades, a huge interest in yield stress materials has led to the development of several experimental techniques for estimating yield stress values. Conventional methods to measure yield stresses typically include steady stress/shear rate sweep, oscillatory amplitude sweep, creep and stress growth experiments (Coussot, 2014, Dinkgreve et al., 2016, Q. Nguyen and Boger, 1992). In addition to these conventional methods, there are some unconventional rheological protocols particularly reported for mud samples such as Claeys et al. protocol (Claeys et al., 2015). Apart from different rheological methods, several geometries including concentric cylinder (Couette), parallel plate, cone plate and vane type, are available to perform rheological measurements. Each geometry has its own merits and limitations, which makes it suitable for wide range of complex systems. Despite the numerous studies on the rheological properties of natural mud samples (see Table 1.2, Chapter 1), a systematic comparison between all available geometries and methods as a function of the properties (composition) of the mud samples is still missing.

In literature, the rheological analysis of mud samples showed a two-step yielding phenomenon (Mehta et al., 2014, Nie et al., 2020). However, the open question that remains to be answered is whether the mud flocs/clusters formed after the first yield point have specific characteristics, linked to the sample composition and shear history. Up to now, the origin of two-step yielding in mud samples is not well understood. In this chapter, the main aim is to find the suitable rheological method and geometry that will ensure a fast and reliable measurement of the changes in sample structure and their corresponding yield stresses. First, a comparison between different conventional methods for yield stress analysis using different geometries is presented. Then, the unconventional rheological methods are compared with the selected conventional protocol and geometry, in order to choose the suitable combination of geometry and method for yield stress analysis of mud. In the end, the origin of the two-step yielding behaviour in mud samples is investigated with the help of rheo-optical analysis.

3.2. YIELD STRESS ANALYSIS OF MUD

3.2.1. DIFFERENT CONVENTIONAL METHODS FOR YIELD STRESS

STRESS RAMP-UP

The rheological analysis of concentrated suspensions using rheological geometries such as Couette and parallel plate may encounter the problem of wall slip, particularly at low shear rate/shear stress (Barnes, 1995). The wall slip effect presents itself as a difference in viscosity values for geometries with different sizes and the existence of a two-step yielding instead of a single step. The existence of wall slip can be easily recognized, for

example, for the parallel plate geometry by using different gaps and comparing the results (Yoshimura and Prud'homme, 1988). This wall slip effect can also be identified by comparing the results of smooth and roughened/serrated geometries. In this study, both approaches have been used to identify any possible wall slip effect. In the case of parallel plates, stress ramp-up experiments were performed with variable gaps. For Couette geometry, grooved geometry was used to compare the obtained results of stress ramp-up with the smooth geometry. Both these approaches showed the absence of wall slip, as the results were similar, for the investigated fluid mud sample (see Fig. B1 in Appendix B). Similar results, i.e., absence of wall slip, were also observed for other two samples (pre-consolidated and consolidated samples).

Stress ramp-up tests (defined in Chapter 2) were used to determine the yield stress of mud samples because of their wide applicability for yield stress measurements of suspensions. Although the stress ramp-up method can provide reproducible results, yet it was found that this method depends on the type of geometry used for the measurements. The apparent viscosity of the fluid mud (FM) layer as a function of shear stress for different geometries is shown in Fig. 3.1a. From the viscosity curve, two-step yielding was identified from the decline in viscosity, for all three geometries. Pre-consolidated (PS) and consolidated (CS) mud layers displayed similar trends of apparent viscosity as a function of shear stress for different geometries, as shown in Appendix B (Fig. B2). Cone and plate geometry was discarded for further experimentation because the response of the material was very scattered due to the presence of large particles within the small gap of cone and plate. In order to compare the yield stress values of different samples, the approach reported by Zhu et al., 2001 was used to obtain the yield stress values by extrapolation. The stress values associated with these two yield points are referred to as static yield stress, τ_s (first decline) and fluidic yield stress, τ_f (second decline) (see Fig. 3.1a).

A similar two-step yielding is reported in literature for different systems such as colloidal glasses (Pham et al., 2008), carbopol microgel (Shao et al., 2013), colloidal gel (Chan and Mohraz, 2012), magneto-rheological systems (Segovia-Gutiérrez et al., 2012) and muscovite dispersions (Nosrati et al., 2011). For example, Potanin, 2019 reported the effect of two different polymers (xanthan gum and carboxymethyl cellulose (CMC)) on the two-step yielding behaviour of silica dispersions. The results showed the convergence of two-step yielding into a single step by adding xanthan gum into silica dispersions while the two-step yielding phenomenon retained by the incorporation of CMC into the dispersion. The disappearance of two-step yielding in case of xanthan gum was attributed to the integration of silica particles into the uniform network of xanthan gum. The system investigated in the current study, i.e., fine-grained sediments, is primarily composed of clay particles and organic matter/biopolymer. On the basis of the existence of a two-step yielding in mud samples, it can be stated that the organic matter/biopolymer in mud samples act in the same way as CMC in silica dispersions, i.e., as a thickening agent without forming a polymeric network. The origin of this two-step yielding behaviour in mud samples is discussed in more details in Sec. 3.3.

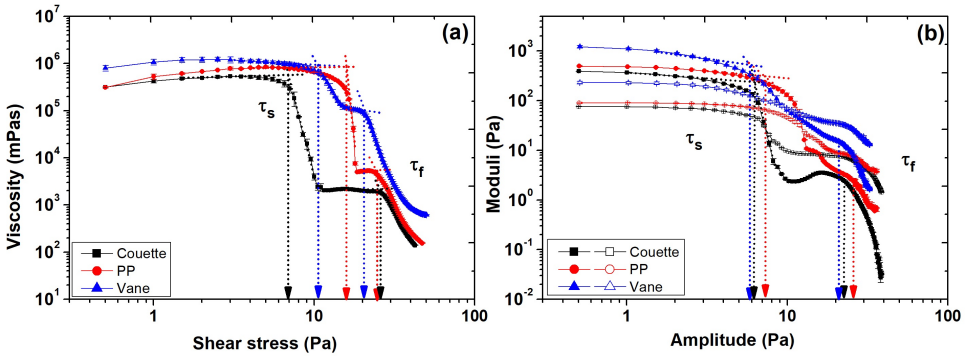

Figure 3.1: (a) Apparent viscosity as a function of shear stress for fluid mud layer (1134 kg. m^{-3}) from KH location using different geometries, (b) storage modulus (filled symbols) and loss modulus (empty symbols) as a function of amplitude for fluid mud layer (1134 kg. m^{-3}) from KH location using different geometries at 1 Hz. Bars represent standard deviation.

OSCILLATORY AMPLITUDE SWEEP

Preliminary oscillatory amplitude sweep tests were performed at different frequencies to determine the suitable frequency for a particular geometry. It was observed that at higher frequencies there was no cross-over between $G^{'}$ and $G^{''}$. This implies that the system retains its solid-like characteristics even at high amplitudes. This is, however, due to the fact that at these high frequencies the observation time was not long enough and, therefore, higher amplitudes would be required to destroy the structure of the system, i.e., to impart fluidization. A suitable frequency for all the geometries and mud layers was found to be 1 Hz. Similar results for oscillatory strain sweeps as a function of different frequencies for natural mud samples (Yueqing Bay, China) were also reported in the literature (Yang and Yu, 2018). They showed that the cross-over amplitude (i.e., δ = 45°) shifted towards higher values with the increase in frequency.

As already discussed in Sec. 2.4.2, different criteria can be used to determine yield stress values from the output of amplitude sweep tests such as a sharp decline in storage modulus, cross-over between $G^{'}$ and $G^{''}$, and a decline in elastic stress. The storage and loss moduli of the fluid mud layer as a function of oscillation amplitude at a frequency of 1 Hz for different geometries is displayed in Fig. 3.1b. The static (first yield point) and fluidic (second yield point) yield stress values from this plot can be determined by the intersection of a line representing $G^{'}$ behaviour below the yield points with the line demonstrating the behaviour of $G^{'}$ above the yield points. This approach was previously reported to determine the yield stress values of foams, carbopol gels, emulsions and commercial lubricating greases (Cyriac et al., 2015, Dinkgreve et al., 2016, Rouyer et al., 2005).

Two-step yielding was also observed in oscillatory amplitude sweep tests for all three considered geometries. Similar two-step yielding in oscillatory amplitude sweep tests was also reported in literature for silica dispersions (Potanin, 2019), capillary suspensions (Ahuja and Gamonpilas, 2017) and surfactant pastes (Shukla et al., 2015). For example, for CoNi nanoplatelet based magneto-rheological fluids (MRFs), two-step yield-

ing was observed in amplitude sweep tests which was attributed to the inter-cluster bond breaking (first yield point) and the cluster breaking (second yield point) (Arief and Mukhopadhyay, 2019). A strain hardening phenomenon was also observed for these MR fluids (increase in G' or G'' after the first yield point) (Arief and Mukhopadhyay, 2019). A similar increase in storage modulus, after the first yield point, was also observed for the mud samples, particularly for pre-consolidated and consolidated sediments (see Fig. B3 in Appendix B), which suggested the existence of strain hardening/jamming phenomenon in the mud samples.

STRESS GROWTH

Stress growth experiments were carried out at shear rates ranging from 0.01 to 10 s^{-1} using different geometries for mud samples. The results for fluid mud layer in terms of stress evolution as a function of time is shown in Fig. 3.2. As already explained in Sec. 2.4.1, different criteria can be used to determine the yield stress values from this method. In this study, peak stress value was chosen to represent the yield stress as it was easy to define. In the cases where the peak stress was not observed, the equilibrium value of stress was used as a yield stress value (i.e., at higher shear rate). It can clearly be seen from Fig. 3.2a that at lower shear rates for Couette geometry, the peak stress corresponded to the static yield stress (first yield point) while the response at higher shear rate (10 s^{-1}) resulted in peak stress value similar to the fluidic yield stress (second yield point), as obtained through stress and amplitude sweep tests.

Similarly, at lower shear rates for parallel plate geometry (Fig. 3.2b), the peak stress values were closer to the first yield point whereas for higher shear rates, the equilibrium stress value was considered and it was similar to the fluid yield stress (second yield point). In contrast, for vane geometry (Fig. 3.2c), two-step yielding was evident for lower shear rates (0.01 – 0.10 s^{-1}) with two peak stress values. However, for higher shear rates, one or no peak stress was observed due to the destruction of structure at such higher shear rates. The selection of the appropriate shear rate is critical for obtaining the desired yield stress from this method, as already explained in the literature (Rogers et al., 2010, Stokes and Telford, 2004, Q. Yuan et al., 2017). Stress growth experiments were also reported in the literature to investigate the two-step yielding in colloidal glasses (Pham et al., 2008) and two peak yield stresses were observed as a function of applied strain. Similar results for stress growth tests were observed for pre-consolidated and consolidated mud layers, as shown in Appendix B (Fig. B4 and B5).

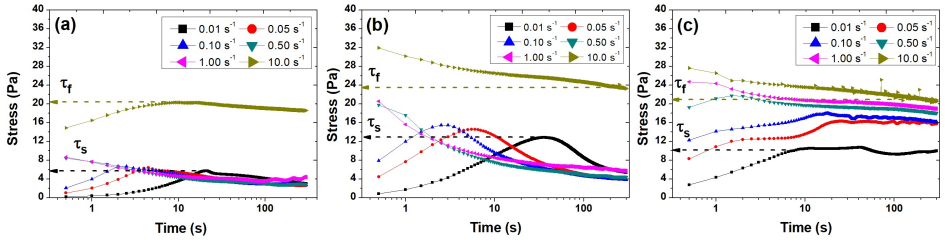

Figure 3.2: Stress evolution as a function of time for (a) Couette, (b) parallel plate and (c) vane geometries at various shear rates for fluid mud layer (1134 kg. m^{-3}) from KH location.

CREEP

The creep tests were performed with the stress values taken from the following four regions of apparent viscosity curves obtained through the stress ramp-up tests: (i) stress below first yield point (first plateau), (ii) stress above first yield point, (iii) stress below second yield point (second plateau), and (iv) stress above second yield point. The resultant strain as a function of experimental time for fluid mud layer using different geometries is shown in Fig. 3.3 It is evident from Fig. 3.3 that the creep responses of fluid mud sample for the selected stresses are significantly different for all three geometries. In short, below the static yield stress (first yield point), the values of strain are small and not so dependent on experimental time. A sudden increase in strain is observed above the static yield stress which becomes again linear after 30 s, as a function of experimental time. The initial increase in strain can be attributed to the breakdown of inter-connected flocs while the linear behaviour after 30 s can be linked to the existence of individual flocs, which resist the applied stress.

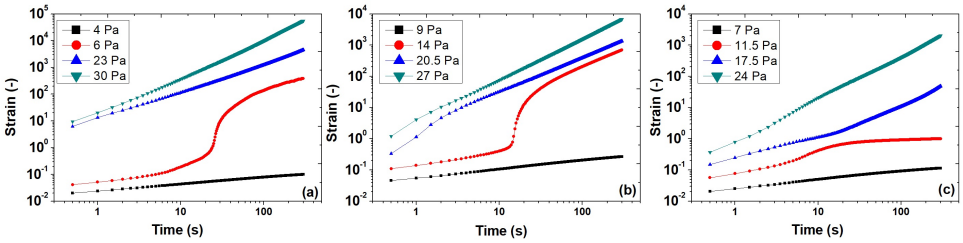

Figure 3.3: Strain as a function of time for fluid mud layer (1134 kg. m^{-3}) from KH location using (a) Couette (b) parallel plate and (c) vane geometries at various applied stresses.

A linear increase in strain, with higher values, is observed for the stresses below the second yield point which is also evident for the stresses higher than the second yield point but with different slopes. This difference in slopes can be associated with the breakage/reorganization of flocs, as explained in Sec. 3.3. Hence, this approach also confirmed the existence of two-step yielding in mud sediments by having different levels of structural breakdown in creep tests. The creep method has been reported to successfully measure the yield stress values of fresh cement pastes, polymeric gels and emulsions using cone and plate and Couette geometries (Dinkgreve et al., 2016, Qian and Kawashima, 2016). Creep tests have also been used in the literature to study the two-step yielding in dilute colloidal gels of poly methyl methacrylate (PMMA) microspheres (Chan and Mohraz, 2012). They also found different material's response at different applied stresses, due to the existence of two-step yielding in the investigated samples. Pre-consolidated and consolidated mud samples also displayed a similar response for creep test (see Fig. B6 and B7 in Appendix B).

COMPARISON OF YIELD STRESS VALUES

The comparison of static and fluidic yield stress values, obtained from different geometries, using various conventional rheological methods for fluid mud layer is shown in Fig. 3.4. It is clear from the figure that both static and fluidic yield stress values, obtained through different geometries and rheological methods, are of the same order of

magnitude. Furthermore, it can be seen that the static yield values are comparatively lowest (i.e., 5.8 – 7.1 Pa) for the Couette geometry while the fluidic yield stress values are smallest (i.e., 20.5 – 22.5 Pa) for the vane geometry. These results show that the Couette geometry is more effective in breaking the network of flocs/aggregates (first yield point) while vane geometry is most efficient for the breaking of reorganized flocs into smaller flocs (second yield point), see Sec. 3.3. The effective structural breaking of a sample using vane geometry led to the fact that vanes are used as mixers for preparing polymeric blends with enhanced mechanical and structural properties (Qu et al., 2013, Xiaochun et al., 2015).

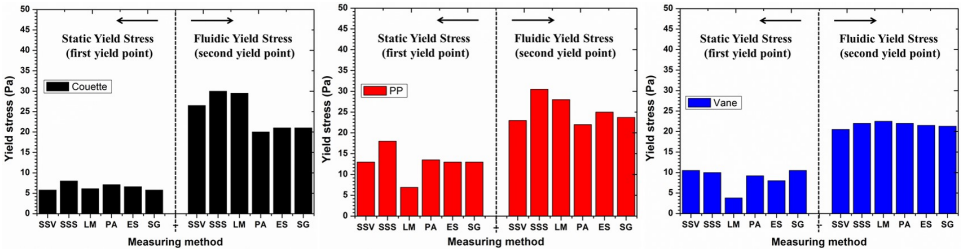

Figure 3.4: Comparison of static and fluidic yield stress values of fluid mud layer (1134 kg. m^{-3}) from KH location using different geometries; SSV = viscosity decline from stress ramp-up, SSS = deformation slopes from stress ramp-up, LM = loss modulus decline from oscillatory amplitude sweep, PA = phase angle from oscillatory amplitude sweep, ES = elastic stress from oscillatory amplitude sweep, SG = stress growth.

Static yield stress values are higher for parallel plate geometry (i.e., 6.9 – 18 Pa) than Couette geometry (i.e., 5.8 – 7.1 Pa). This may be due to the fact that parallel plate geometry offers less disturbance to the samples when the top plate is put into position. When the bob is put into place in the case of Couette geometry, the sample is more disturbed. The influence of this disturbance on the fluidic yield stress values was negligible as similar values were observed for both geometries. Similar trends in static and fluidic yield stress values, obtained from different geometries using several conventional rheological methods, were also observed for the other two mud layers (see Fig. B8 and B9 in Appendix B). Stress ramp-up tests with Couette geometry were proven to be practical and time efficient tests for measuring all structural breakdowns within the mud samples associated to static and fluidic yield stresses (two-step yielding).

3.2.2. DIFFERENT UNCONVENTIONAL METHODS FOR YIELD STRESS

Different protocols are available to measure the rheology (particularly the flow curve) of mud sediments, as presented in Fig. 2.4. In order to compare these different rheological protocols, pre-consolidated mud sample was selected. The two representations of the flow curves (shear stress vs shear rate and apparent viscosity vs shear stress) for mud sample are shown in Fig. 3.5a and 3.5b, using different unconventional protocols with Couette geometry. The static and fluidic yield stress values were estimated from the viscosity declines in Fig. 3.5b. Due to the curvature of the shear stress behaviour, yield stress ranges are given in Table 3.1, where necessary. It is clear from this table that large differences are observed in both static and fluidic yield stresses. This suggests that the mud samples, even though in their partially disturbed state, still have some structure

depending on their shear history (i.e., depending on the protocol used).

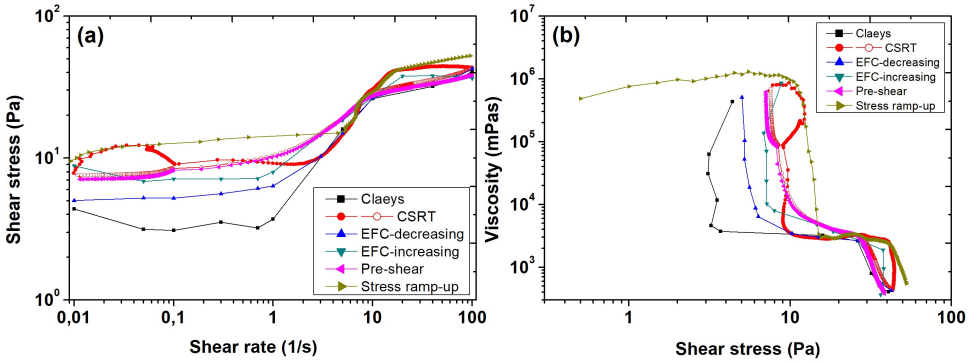

Figure 3.5: (a) Shear stress as a function of shear rate and (b) apparent viscosity as a function of shear stress for pre-consolidated mud sample (1151 kg. m^{-3}) from KB location using Couette geometry; solid symbols in CSRT protocol represent the ramp-up and the empty symbols represent the ramp-down.

From Fig. 3.5b and Table 3.1 it can be seen that "CSRT-ramp up", "EFC-increasing" and "stress ramp-up" display higher static and fluidic yield stress values as compared to the rest of the methods. All these methods start with a low shearing action. This implies that the samples are in a less disturbed state and this results in higher yield stress values. For the characterization of mud for harbour applications, it is important that the measurements are done in conditions reproducing in-situ situations. This implies that a method should be favored in which the sample undergoes a transition from an undisturbed state to an unstructured state. All three methods cited above ("CSRT-ramp up", "EFC-increasing" and "stress ramp-up") correspond to this requirement, and as can be seen in Table 3.1, the values found for the fluidic yield stress are very close and in the range of 38 – 40 Pa.

The fluidic yield stress is of importance for harbour applications, as it corresponds to the structural state most encountered in harbours. The authorities of Port of Emden for example used 50 − 100 Pa of yield point as a criterion for their nautical bottom (Wurpts and Torn, 2005), which corresponds to the definition of fluidic yield stress. These three methods are, therefore, suitable to estimate the fluidic yield stress of mud for harbour applications. However, the EFC-increasing protocol is a time-consuming test and from CSRT-ramp up the determination of the static yield stress is not very straightforward. Therefore, the stress ramp-up protocol was chosen for further analysis and empirical data fitting.

The fluidic yield stress values found for the other methods are also very similar, i.e., in the range of 26 – 29 Pa. These values are lower than the ones found from the protocols mentioned above, as the samples were in a less structured state. The static yield stress values are different from one another and lie in the range of 3.7 – 11 Pa. The lowest value was obtained by using Claeys et al. protocol (Claeys et al., 2015), which is due to the fact that with this protocol, the structure of the sample readily broken during measurement. The comparison of the different protocols was also performed for mud sample using vane

Table 3.1: Static and fluidic yield stress values of pre-consolidated mud sample (1151 kg. m^{-3}) from KB location obtained from viscosity declines with Couette geometry for different protocols.

Method	Static Yield Stress (Pa)	Fluidic Yield Stress (Pa)
Claeys et al. protocol	3.1 – 4.4	26
CSRT-ramp up	9.0 – 12.3	40
CSRT-ramp down	7.6	29
EFC-decreasing	5.2	26
EFC-increasing	7.1	38
Pre-shear	7.1	27
Stress ramp-up	11	40

geometry, as the Claeys et al. protocol was proposed with the vane type geometry. The results of different protocols for pre-consolidated mud sample, using vane geometry, are displayed in Fig. B10a (Appendix B). For Claeys et al. protocol, the conventional yield stress values are also reported in Table B1, in the form of an "undrained shear strength" obtained from the first step in the protocol (see Fig. B10b in Appendix B) and Bingham yield stress. The "Bingham yield stress" was determined from the extrapolation of shear stress vs shear rate curve for shear rate approaching to zero.

In stress ramp-up test, an undisturbed mud sample is sheared and at the first viscosity decline the structure is partially broken (or disturbed). The sample is nearly completely broken/disturbed above second yield point. On the other hand, in Claeys et al. protocol, the first step of applying shear rate of 1 s^{-1} gives the peak stress of about 46.7 Pa (Table B1), which represents the fluidization or structural breakup for undisturbed mud sample. Therefore, this value corresponds to the fluidic yield stress (i.e., 40 Pa) in Couette, which also shows the structural breakup for undisturbed mud sample (blue dashed arrow in Fig. 3.6a). Furthermore Bingham yield stress (i.e., estimated by extrapolating the flow curve to zero shear rate, as shown by the orange dashed line in Fig. 3.6b) for Claeys et al. protocol represents the stress required to break the residual structure of the mud sample (i.e., 26.5 Pa) or the minimum stress required to keep the material in flow condition. This value, therefore, corresponds to the difference between fluidic yield stress and the point where the static part is completely disturbed (i.e., 40 – 15 = 25 Pa), as shown by the orange dashed arrow in Fig. 3.6a. Note that the undrained shear strength value is highly dependent on the applied shear rate, which is another limitation of the Claeys et al. protocol. The difference in undrained shear strength values between Couette and vane geometry is also striking. This illustrates the importance of the measuring geometry to get information on this type of systems.

In order to further verify the correlation between static and fluidic yield stresses with conventional yield stresses (i.e., undrained shear strength and Bingham yield stress), stress ramp-up test followed by a constant high shear test (at 300 s^{-1} for 500 s) and then stress ramp-down test was performed for mud samples having two different densities (1151 and 1256 kg. m^{-3}) obtained from PK location. Claeys et al. protocol was also carried out for the same samples to get conventional yield stresses. It was found that the

undrained shear strength corresponds to the fluidic yield stress and the Bingham yield stress matches with the difference between the fluidic yield point and the static yield point (see Fig. B11 and B12; Table B2 and B3). The fluidic yield stress obtained from stress ramp-down step also resembles the Bingham yield stress, due to the fact that the sample was extensively sheared during the constant shear rate step performed before the stress ramp-down step. However, this fact needs to be verified by systematic investigation of a larger range of sub-samples from Port of Hamburg and mud samples from other sources. The correspondence between these terminologies of yield stresses (static and fluidic) and the terminologies used in literature is presented in Table 3.2.

Table 3.2: Correspondence between our yield stress terminologies and the terminologies used in literature.

Toorman, 1994	**Toorman, 1997**	**Wurpts and Torn, 2005**	**Claeys et al., 2015**	**This study**
	Static yield stress	Criterion for navigation	Undrained shear strength	Fluidic yield stress
Bingham yield stress	Dynamic yield stress		Bingham yield stress	*ΔYS = Fluidic – Static
(True) yield stress		Yield stress		Static yield stress

*In case of non-thixotropic system (i.e., very small static yield stress), fluidic yield stress approaches Bingham yield stress.

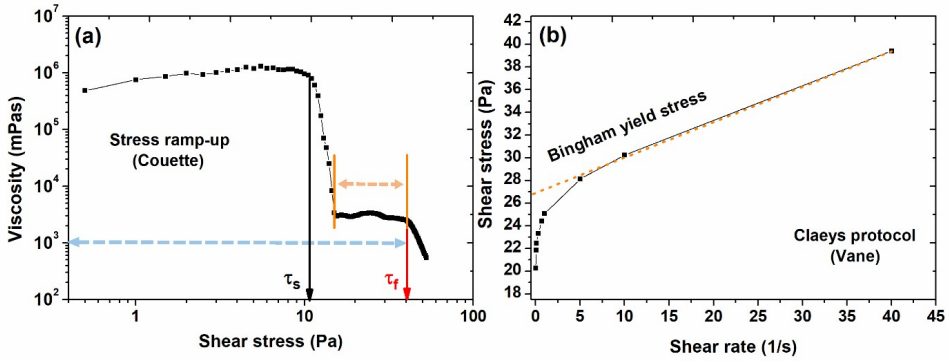

Figure 3.6: (a) Apparent viscosity as a function of shear stress for pre-consolidated mud sample (1151 kg. m^{-3}) from KB location using stress-ramp up test with Couette geometry; (b) shear stress as a function of shear rate for pre-consolidated mud sample (1151 kg. m^{-3}) from KB location using Claeys et al. protocol with vane geometry. Blue dashed arrow represents the structural breakdown of undisturbed mud sample (i.e., fluidic yield point), orange dashed arrow represents the difference between the fluidic yield point and the point where the static part is completely disturbed, orange dashed line represents the extrapolation of flow curve to obtain the Bingham yield stress.

3.2.3. OPTIMIZATION OF STRESS RAMP-UP TEST

In order to optimize the experimental time of the stress ramp-up protocol for mud samples of different consistencies/densities, stress ramp-up tests with varying sweep rates (0.1 – 10 Pa/s) were performed for different mud layers from KB location using Couette geometry. The results are shown in Figs. 3.7a-c. It can be seen from Fig. 3.7a that for the sample with lower densities (i.e., fluid mud), slower sweep rates (0.1 – 0.2 Pa/s) were more appropriate to obtain both viscosity declines, since the static yield stress transition

lies in the very low shear stress range. For the consolidated mud sample (with higher density), higher stress ramp-up rates (3 – 10 Pa/s) were possible to determine the static and fluidic yield stress values (Fig. 3.7c). The preferred stress ramp-up rates for different mud layers along with their approximate experimental times are presented in Table B4 (Appendix B). Based on this analysis, it can be concluded that stress ramp-up test is fast, reliable and robust for measuring the yield stresses (both static and fluidic) of mud samples.

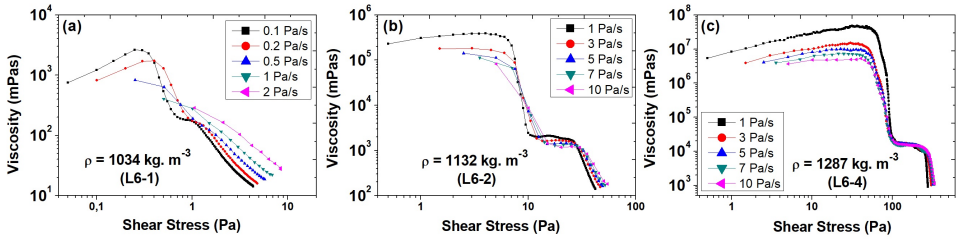

Figure 3.7: Apparent viscosity as a function of shear stress using varying sweep rates with stress ramp-up test for mud samples with varying densities from KB location.

3.3. RHEO-OPTICAL ANALYSIS OF MUD

IN the literature, the two-step yielding phenomenon has been observed in diverse systems, including carbopol microgel (Shao et al., 2013), colloidal glasses (Pham et al., 2008), capillary suspensions (Ahuja and Gamonpilas, 2017), silica dispersions (Potanin, 2019), surfactant pastes (Shukla et al., 2015), magneto-rheological systems (Segovia-Gutiérrez et al., 2012) and muscovite dispersions (Nosrati et al., 2011). Typically, this two-step yielding has been explained by the breakage of inter-connected network of flocs/clusters (i.e., first yield, named "static yield" in the present article) followed by the disruption of individual flocs/clusters (i.e., second yield or "fluidic yield")(Arief and Mukhopadhyay, 2019). A more in-depth study of the structure of the mud samples was performed by rheo-optical analysis after first and second yield points.

The RheOptiCAD® oscillatory shearing test (see Sec. 2.5) was performed by placing the diluted mud sample between two plates, at a frequency of 1 Hz. The extracted images from the recorded video are shown in Fig. 3.8 for a mud sample from RV location. At the onset of shearing (Fig. 3.8a), an inter-connected network of mud flocs was observed, which is responsible for the high moduli values within LVE (Fig. 3.1b). After further shearing, this floc network started to collapse, which represents the first (static) yield point in the amplitude sweep and stress ramp-up tests. After breakage of the continuous floc network, continued shearing resulted in the formation of hollow cylinder-like structures (Fig. 3.8b-c), which resisted the application of shear. Therefore, the plateau behaviour after the first decline in amplitude sweep and stress ramp-up tests (in between the first and second yield step, Fig. 3.1) was attributed to these cylinder-like structures. These structures were also observed in mud samples from RT, KH and SW locations (see Fig. B13 in Appendix B), although the mud flocs from SW location were irregularly shaped, likely due to the presence of larger silt/sand particles, which may have

hindered the re-orientation of organic matter to create the structures observed in other samples. It is important to note that this analysis was performed on diluted mud samples and, therefore, sand/silt particles settled down and find sediment was picked and dropped in between the plates. Therefore, this two-step yielding mechanism may be relevant for find sediment and the presence of sand particles can effect the formation of cylinder-like structures (as observed for SW) and the breakage of floc network.

The formation of similar cylinder-like structures (referred to as log-rolling flocs in (Varga et al., 2019)), by shearing between parallel plates or in a Couette cell, has been reported in literature for different weakly attractive suspensions (e.g., carbon black particles in mineral oil, polyamide particles in water or water/glycerine mixture and hollow glass spheres in mineral oil)(Varga et al., 2019). Varga et al., 2019 attributed the formation of these structures to the hydrodynamic coupling between the confining geometry and flocs, which was verified by experiments and simulations. Furthermore, the authors have also studied the influence of strain on the formation of log-rolling flocs and the influence of the gap between the plates on the stability of the flocs, as a function of the ratio between gap size and mean particle radius. Likewise, the development of log-rolling structures as a function of shearing action along with the existence of two-step yielding at higher solid content, in oscillatory amplitude sweep tests, has been reported in literature for silica rod suspensions (Das et al., 2021).

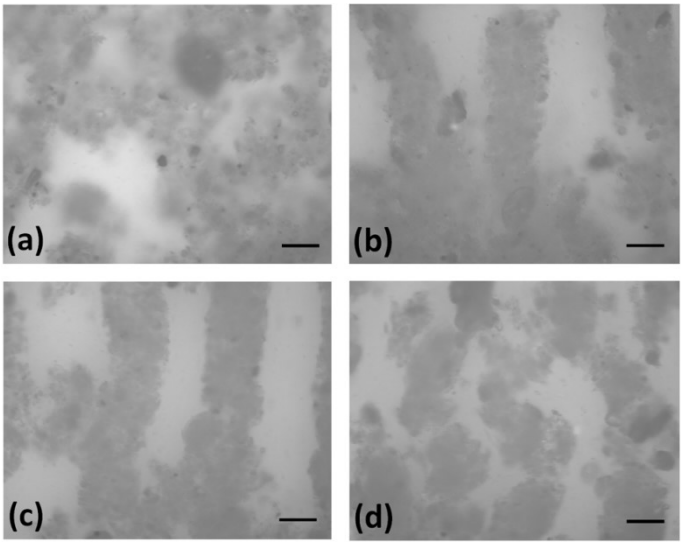

Figure 3.8: The snapshots from the recorded video at (a) t = 2 s, (b) t = 30 s, (c) t = 50 s and (d) t = 100 s for mud sample from RV location, oscillatory sheared at a frequency of 1 Hz and amplitude of 0.1 mm with the gap between the plates of 20 µm. The scale bar represents 70 µm.

These cylinder-like structures break down into smaller flocs on continuous shearing (Fig. 3.8d), which is associated to the second yield point observed in the rheological tests. Therefore, the mechanism for two-step yielding in mud suspensions is the breakage of inter-connected network of flocs (static yield) followed by the formation of cylinder-like

structures (plateau after first decline) and then the collapse of individual flocs into particles or smaller flocs (fluidic yield). The complete mechanism of two-step yielding is pictorially presented in Fig. 3.9. It is important to note that the existence of two-step yielding is mainly due to the presence of a narrow gap between the measuring instrument (bob) and the cup, which allows the re-organization of flocs. In contrary, in in-situ conditions, the static yield point may not be observed and, therefore, the fluidic yield stress value is an important parameter to define a limit for the nautical bottom in ports and waterways. Fluidic yield stress was linked with the complete structural breakdown in fluid mud which is needed for controllability and manoeuvrability of vessels. Furthermore, this static yield point can still provide a useful understanding about the stresses required to disturb the interconnected network of mud flocs and the difference between the fluidic and static yield stresses can give an idea about the dynamic or Bingham yield stress of remoulded sample.

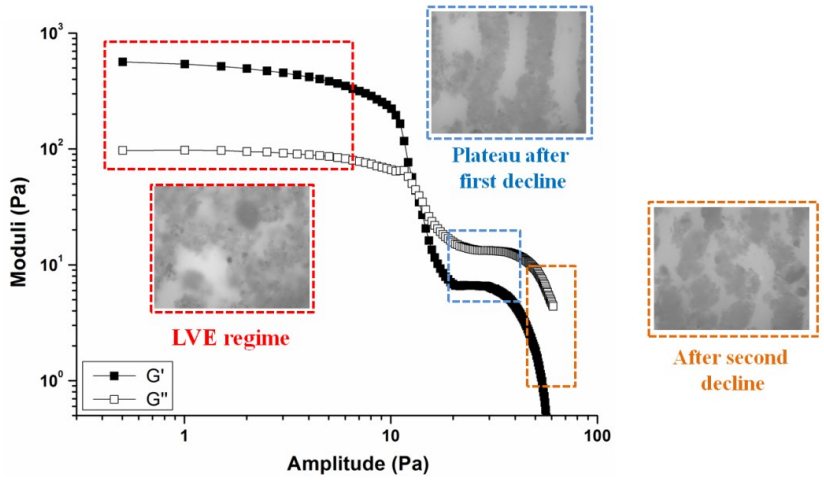

Figure 3.9: Schematics of the two-step yielding observed by amplitude sweep tests for mud samples.

3.4. CONCLUSIONS

FAST and easily repeatable measurements of yield stresses are important for practical applications. Therefore, different conventional and unconventional rheological protocols using different geometries were compared to obtain the flow curves and yield stress values. Three mud layers were chosen for comparative analysis having densities ranging from 1034 – 1287 kg. m^{-3}, by using different measuring geometries. Concentric cylinder (Couette), parallel plate, and vane geometries, were used to perform rheological experiments. Couette geometry is a suitable option for fluid mud samples because of the linear velocity profile within the gap. Vane geometry is to be used in case of consolidated systems (solid-like), where Couette geometry cannot be used because the bob can get stuck during the experiment. Parallel plate geometry is not a suitable option for investigating liquid-like samples because the sample can spread out of the gap during the shearing action. Parallel plate geometry can, however, be a good option to measure the

absolute values of yield stresses because it offers less disturbance in the sample structure when the top plate is set into place prior the experiment. Cone and plate geometry are not designed for mud sediments having large particles because of the very narrow gap between the cone and plate. This study showed that Couette and parallel plate geometries are the most suitable geometries for analysing all the structural break-downs of the mud samples.

Among conventional rheological protocols, creep test is not a straightforward method for analyzing the yield stress values of samples as in particular one must have a prior knowledge of the stress range in which the yielding occurs. On the other hand, amplitude sweep and stress growth tests involve different criterion for defining the yield stresses, which make them difficult to interpret and analyze. Stress ramp-up tests with Couette geometry were proven to be practical and time efficient tests for measuring all structural breakdowns within the mud samples associated to static and fluidic yield stresses (two-step yielding). This combination of rheological protocol and geometry was also compared with some unconventional rheological protocols typically employed for mud samples. The results showed that "CSRT-ramp up", "EFC-increasing" and "stress ramp-up" displayed higher static and fluidic yield stress values as compared to the rest of the methods. All these methods started with a low shearing action, implying starting from an undisturbed state of the sample, which resulted in higher values of the stresses. These methods are, therefore, suited to measure the yield stresses of mud sediments for harbour applications, where mud sediments usually exist in undisturbed state (i.e., structured state). However, the EFC-increasing protocol is still a longer test and from CSRT-ramp up the determination of static yield stress is not very straightforward. Therefore, the stress ramp-up protocol is the most suited and fastest method to analyze the yield stresses of mud sediments for harbour applications. Furthermore, the yield stress values from stress ramp-up test corresponds well with the conventional yield stress values obtained from Claeys et al. protocol, i.e., the fluidic yield stress corresponded to the undrained shear strength while the difference between fluidic and static yield stresses corresponded to the Bingham yield stress. The optimization of stress ramp-up test enabled to reduce the experimental time for different mud layers (~10 – 200 s), which is approximately 4 times faster than the conventional Claeys et al. protocol.

To understand the origin of two-step yielding behaviour in mud samples, the structural organization upon shearing of mud samples was examined by using a modified form of the RheOptiCAD® device. The RheOptiCAD® analysis showed the formation of cylinder-like structures in mud suspensions upon shearing action. Therefore, the first decline in viscosity or moduli (i.e. static yield) is linked to the breakage of interconnected network of flocs, the second plateau in viscosity or moduli behaviour is attributed to the formation of cylinder-like structures while the second decline (i.e. fluidic yield) is associated to the breakage of cylinder-like structures, formed upon further shearing. In future, a systematic investigation is needed to verify the correlation between Bingham yield stress and static and fluidic yield stresses of a larger range of sub-samples from Port of Hamburg and mud samples from other sources.

4

VARIABILITY IN RHEOLOGICAL PROPERTIES OF MUD

In literature, the rheological properties of harbour mud have been shown to vary significantly as a function of density but a systematic investigation of the rheological characteristics of mud from the Port of Hamburg is still missing. In this chapter, the variation in the rheological properties of mud are investigated as a function of sediment density and sampling location within the port. The properties of samples with different densities obtained from different layers at a given location are compared with the properties of samples of same densities obtained by diluting the densest mud sample collected from that location. Finally, the rheological results are related to an in-depth analysis of the sample composition, where parameters such as floc size, floc density and organic matter content are presented.

Parts of this chapter have been published in Geo-Marine Letters **39**, 427 (2019) (Shakeel, Kirichek, and Chassagne, 2019), Journal of Soils and Sediments **20**, 2553 (2020) (Shakeel et al., 2020b), Journal of Soils and Sediments **20**, 2546 (2020) (Kirichek et al., 2020), Journal of Non-Newtonian Fluid Mechanics **286**, 104434 (2020) (Shakeel et al., 2020c), Colloids and Surfaces A: Physicochemical and Engineering Aspects **624**, 126827 (2021) (Shakeel, MacIver, et al., 2021).

4.1. INTRODUCTION

DIFFERENT mud layers, with varying density, can be observed at each location in the port, corresponding to mud at different stages of consolidation. All these layers can vary in thickness and (rheological) properties like viscoelasticity, shear-thinning, thixotropy and yield stresses. In addition to the influence of geometry and protocol on the yield stresses of mud, the composition of these different naturally occurring mud layers can significantly affect the yield stresses. In literature, the rheological behaviour (i.e., yield stresses) is typically investigated as a function of mud density using step-by-step dilution of a high density consolidated mud (Fonseca et al., 2019, Huang and Aode, 2009, Soltanpour and Samsami, 2011). However, it is expected that the in-situ mud layers have significantly different composition, in addition to different water content for a given location, in particular in terms of organic matter content. To study the heterogeneity of mud layers, a comparative analysis of rheological properties of natural and diluted mud layers is performed in this chapter.

In literature, it has already been shown that rheological properties of mud are dependent on the mud density and that the presence of small amounts of organic matter/biopolymer is affecting the cohesion and rheological behaviour significantly (Malarkey et al., 2015, Parsons et al., 2016, Paterson et al., 1990, Paterson and Hagerthey, 2001, Schindler et al., 2015, Tolhurst et al., 2002, Wurpts and Torn, 2005). This organic matter content can vary along the port, which can result in totally different rheological fingerprint of mud samples. However, a systematic analysis of the influence of organic matter on the rheological properties of mud samples and a quantification thereof is still missing.

Floc size and floc density are dependent on their composition, their rheological (shear) history and the strength of the bonds within the floc (Coussot, 1997). For sediments in the marine environment, floc growth and shear-dependent restructuring also depends on solid concentration (related to water turbidity) of the water column (Manning and Dyer, 1999) as well as organic matter content. The correlation between flocs properties (i.e., floc size and floc density) and the bulk rheological properties of mud is not well explained yet in literature.

Traditionally, the surveying in ports is conducted using multibeam echo-sounders. However, the multibeam echo-sounding techniques are particularly adapted to water bodies with sharp interfaces like the one existing between a water phase and a sediment bed. Fluid mud layers, on the other hand, are layers with large vertical density gradients and multibeam echo-sounding techniques are, therefore, less adapted to detect them. The early developed measuring tools (such as radioactive probes) were typically designed to measure mud densities, where mud density was used as a criterion for defining the nautical bottom (e.g., the Port of Rotterdam and the Port of Zeebrugge) (McAnally et al., 2007). Since the early days of fluid mud research, it was recognised that the density is not the only parameter that should be accounted for to assess the nautical bottom and yield stress could also be used (Wurpts and Torn, 2005, PIANC, 1997, Kirichek et al., 2018). The in situ strength measurements of deposited and fluid mud only became possible in the last decade. One of the tools that provides yield stress is Rheotune. The working principle of the Rheotune is similar to the one of a tuning fork. Rheotune gives vertical

profiles of (Bingham) yield stress and density as output. However, this device needs to be calibrated for the in-situ samples. Moreover, the correlation between the yield stress measured in lab and in-situ needs to be investigated for mud samples from Port of Hamburg.

To summarize, the following research questions are being addressed in this chapter: What is the relation between rheological properties and density of mud (i.e., depth variability)? What are the differences between the rheological properties of natural and diluted mud layers? What is the influence of varying organic matter content along the port on the rheological characteristics of mud (i.e., spatial variability)? Is there a correlation between the flocs properties and bulk rheological properties of mud from different locations (i.e., varying organic matter content)? Is there any correlation between the yield stresses measured in laboratory using Rheometer and in-situ using Rheotune?

4.2. DEPTH VARIABILITY

IN addition to the naturally occurring mud layers, the diluted mud layers were prepared by diluting the dense mud sample (CS layer) from PK location using the water from the same location and gently mixed by hand, in order to test the mud samples having same composition but different density or water content. The obtained rheological properties for natural and diluted mud layers are compared in the following sections.

4.2.1. YIELD STRESS

In order to analyse the effect of density on the yield stress of mud sediments, stress ramp-up tests were performed to determine the yield stress values of natural and diluted mud layers. Figure 4.1a-b shows the outcome of these stress ramp-up tests, for natural and diluted mud layers from PK location, in the form of apparent viscosity as a function of shear stress. From these stress-viscosity curves, the two yield stress values were determined from the two sharp declines in viscosity (i.e., two-step yielding) (Shakeel et al., 2020d). A transition from two-step yielding to one-step yielding or no-yielding is found at low densities due to the liquid-like nature of the samples. A similar transition from two-step yielding to single-step yielding, as a function of volume fraction of solids, has also been reported in literature for magneto-rheological suspensions (Fernández-Toledano et al., 2014).

The fluidic yield stress values of natural and diluted mud layers as a function of density are presented in Fig. 4.2. Both natural and diluted mud layers display an exponential increase in yield stress as a function of density. A similar exponential increase in yield stresses as a function of density has been reported in literature for different mud sediments (Faas and Wartel, 2006, Huang and Aode, 2009, O'Brien and Julien, 1988). It is in particular found that the dependency of yield stress on density is significantly different for diluted mud samples as compared to natural mud samples. For all density values, diluted mud samples showed lower yield stress values as compared to natural mud samples. The same results were obtained for the static yield stress values (Fig. C1). The experimental data of yield stress values as a function of density was fitted with an empirical exponential relation. The difference in yield stress behaviour as a function of density

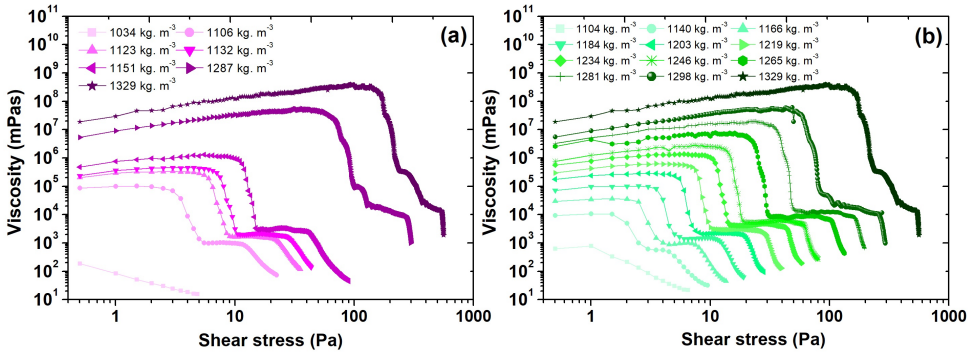

Figure 4.1: Apparent viscosity as a function of stress for (a) natural mud layers and (b) diluted mud layers from PK location. The colour intensity of symbols increases with the density.

for natural and diluted mud samples was also evident by comparing different values of the model parameters (Table C1 in Appendix C).

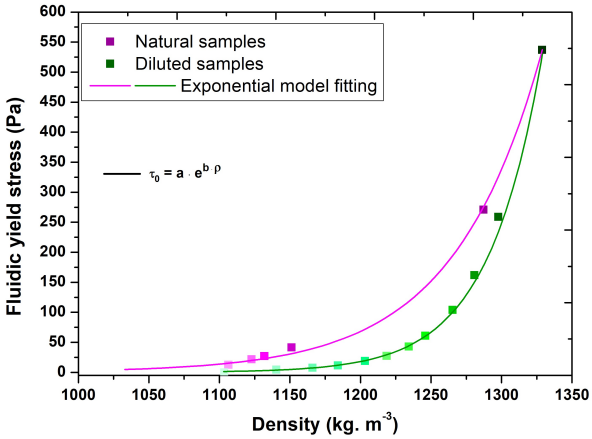

Figure 4.2: Fluidic yield stress values as a function of density for natural and diluted mud layers from PK location. Solid lines represent the model fitting. The colour intensity of symbols increases with the density.

4.2.2. MODULI

Apart from yield stress measurements, frequency sweep tests were performed within linear viscoelastic regime to determine the effect of density on the moduli of natural and diluted mud layers. Preliminary amplitude sweep tests were performed to find the linear viscoelastic regime for all the samples. Figure 4.3a-b shows the results of frequency sweep tests in the form of complex modulus as a function of frequency for natural and diluted mud layers. This test is typically conducted for studying the mechanical properties of the system without disturbing the structure of the material. It can be seen that the complex modulus of all the mud samples, except the ones with lower densities, was more

or less frequency independent, which confirmed the solid-like behaviour of the samples over the complete range of studied frequencies. An analogous solid-like behaviour (frequency independent modulus) of mud sediments as a function of frequency within LVE regime is described in literature (Soltanpour and Samsami, 2011, Van Kessel and Blom, 1998, J. Xu and Huhe, 2016). At higher frequencies, an increase in complex modulus was observed, which was not attributed to the system behaviour but rather to the inertial problems within the instrumentation at such high frequencies (data removed from the graphs). The mud samples with lower densities displayed a significant frequency dependency of complex modulus. In this case, the inertial problems were very prominent, even at frequencies as low as 2 Hz, triggered by the liquid-like nature of these samples.

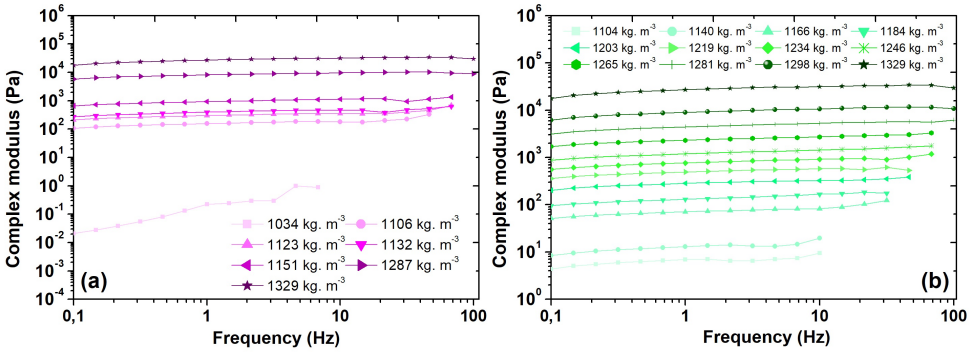

Figure 4.3: Complex modulus as a function of frequency for (a) natural mud layers and (b) diluted mud layers from PK location. The colour intensity of symbols increases with the density.

The complex modulus at 1 Hz is plotted as a function of density for natural and diluted mud layers (see Fig. 4.4a). An exponential increase in the complex modulus as a function of density is found for both natural and diluted mud layers. A similar increase in modulus of mud sediments as a function of volume fraction is also reported in literature (Huang and Aode, 2009). The relationship between complex modulus and density is different for diluted and natural mud samples. For all density values, lower complex modulus values are found for diluted mud as compared to natural mud. An empirical exponential relation was used in both cases to fit the experimental data of complex modulus as a function of density. The difference in complex modulus behaviour as a function of density for natural and diluted mud samples is thus also found by comparing the values of the model parameters (Table C2). Furthermore, the mud samples (natural or diluted) display a solid-like behaviour as confirmed by the small phase angle values (Fig. 4.4b). The samples having lowest densities even show a cross-over in frequency sweep test (i.e., $\delta = 45°$) which is due to their liquid-like behaviour, as already depicted by yield stress analysis. The differences in rheological properties of mud layers can be linked to several parameters i.e., mud composition, type and content of organic matter, ionic concentration and particle size distribution (Zander et al., 2020). The structural recovery behaviour of these natural and diluted mud layers is presented in Chapter 6.

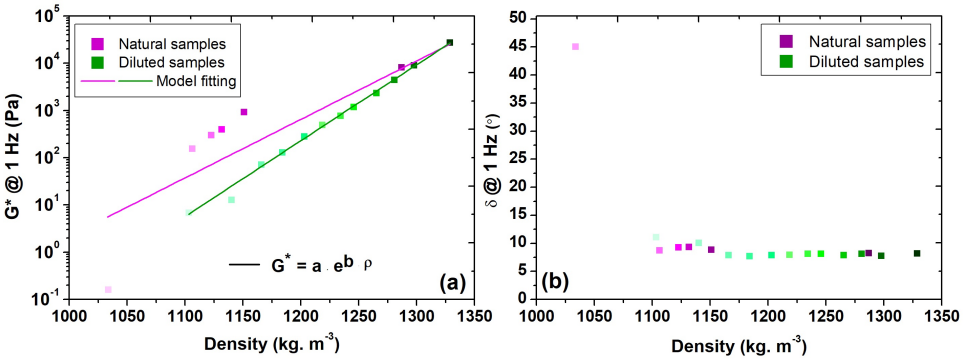

Figure 4.4: (a) Complex modulus (G^*) values and (b) phase angle (δ) values at 1 Hz as a function of density for natural and diluted mud layers from PK location. Solid lines represent the model fitting. The colour intensity of symbols increases with the density.

4.3. SPATIAL VARIABILITY

4.3.1. EFFECT OF SEDIMENT LOCATION

In order to investigate the influence of spatial variation on the yield stress of mud sediments, stress ramp-up tests were performed for the mud samples collected from different locations. Fig. 4.5a shows the outcome of stress ramp-up tests for the PS mud layer. Two yield stresses were determined from the sharp declines in viscosity. The comparison of static and fluidic yield stresses, TOC and density of the PS mud layer for all locations are presented in Fig. 4.5b. Both static and fluidic yield stresses follow the trends of density: higher densities lead to higher yield stresses and vice-versa. As expected, the organic matter content decreases in the seawards direction. However, the influence of organic matter content on the yield stresses is not evident because both density and organic matter content are varying for each sample.

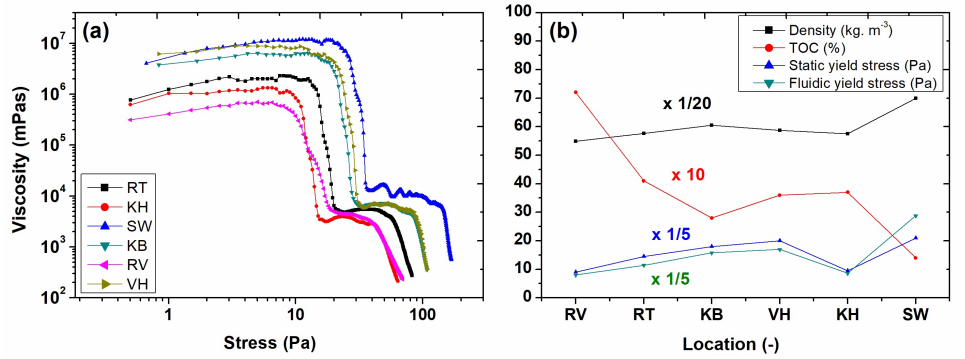

Figure 4.5: (a) Apparent viscosity as a function of stress for the PS mud layer of different locations, (b) evolution of density, TOC, static and fluidic yield stresses for different locations in the harbour for PS mud layer. Right side of figure represents upstream of the river and left side represents downstream. To plot all the parameters in one figure, some of them were multiplied with different factors indicated close to the curves in figure.

4.3.2. EFFECT OF ORGANIC MATTER CONTENT

YIELD STRESS

In order to clearly observe the effect of organic matter content on the rheological properties, mud samples were obtained from different locations of Port of Hamburg having similar densities but varying organic matter content. Fig. 4.6a and 4.6b presents the results of stress ramp-up tests for sediments having similar densities in the form of apparent viscosity as a function of stress. From these viscosity curves, two yield stresses were identified from the decline in viscosity and the values of static and fluidic yield stresses are presented in Table C3. The mud samples with similar densities displayed markedly different static and fluidic yield stress values. The mud samples from RV and RT locations reveal higher yield stress values, both static (9 Pa and 60 Pa) and fluidic (40 Pa and 312 Pa), as compared to the static (0.8 Pa and 18 Pa) and fluidic (2.44 Pa and 79 Pa) yield stress values of mud samples from locations VH and KB. Higher yield stresses, at a given density, can be linked with higher organic matter content.

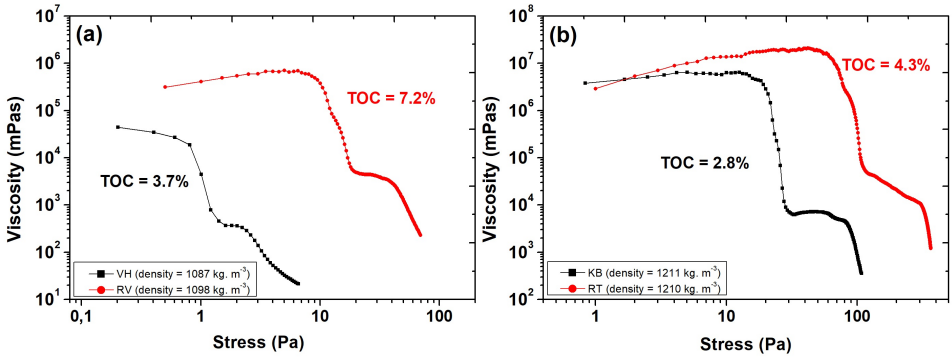

Figure 4.6: Apparent viscosity as a function of stress for mud sediments having (a) similar lower and (b) similar higher densities from different locations.

MODULI

The results of frequency sweep tests within linear regime are shown in Fig. 4.7a-d. It is observed that the complex modulus of all the samples display a very weak frequency dependency. Furthermore, the phase angle values are very small (no cross-over), which confirms the solid-like behaviour of the samples over the entire range of investigated frequencies. The complex modulus values are considerably different for the mud samples with similar densities, whereas the phase angle values are not markedly different from each other (see Table C3). Mud samples having higher organic matter content (RV and RT) have a higher complex modulus (417 Pa and 7909 Pa) than the ones with lower organic matter content (13 Pa and 1774 Pa), for a given density. The complex modulus is a measure of the consistency of the system, while the phase angle is representative of the degree of structuration (Lupi et al., 2016). The results show that the consistency of the mud samples can be varied by changing the TOC content whereas the degree of structuration remains the same for all the samples. This also means that the density of all investigated samples was higher than the one required to form a structured system.

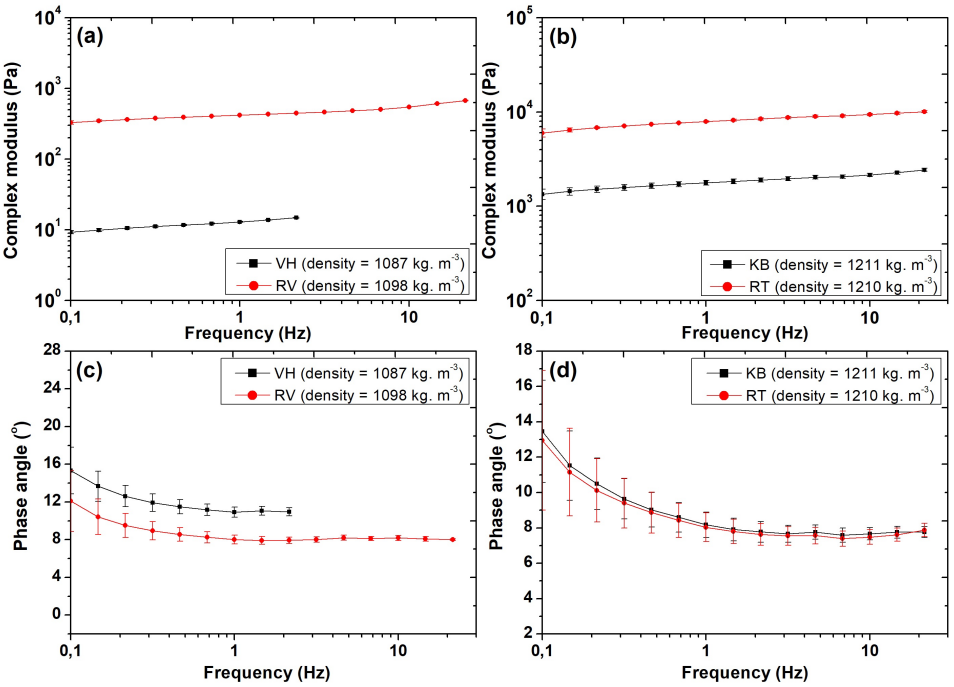

Figure 4.7: (a), (b) Complex modulus and (c), (d) phase angle as a function of frequency for mud sediments having (a), (c) similar lower and (b), (d) similar higher densities from different locations. Bars represent standard deviation. Solid line is a guide for the eye.

THIXOTROPY

The thixotropic behaviour of mud samples was studied by increasing and decreasing the shear rate between 0 and 100 s^{-1}. The shape of the hysteresis loop depends upon various factors including the nature of the material, shear history prior to the analysis, level and rate of shearing. Comprehensive reviews have been made on thixotropy by Barnes, 1997 and Mewis and Wagner, 2009. Fig. 4.8a and 4.8b shows the results of thixotropic experiments for the sediments having similar densities. Mud samples from RV and RT locations displayed a typical thixotropic behaviour (decrease in viscosity with shearing action), whereas an anti-thixotropy or negative thixotropy behaviour is found at lower shear rates for the sediments collected from VH and KB locations.

The similar combination of thixotropy and anti-thixotropy was also reported by (Nosrati et al., 2011) for muscovite dispersions. This peculiar combination of thixotropy and anti-thixotropy could be linked with a shear thickening phenomenon, which was observed for these samples in stress ramp-up tests at higher stresses. However, it could also be due to the fact that higher shearing action resulted in extensive structural breakdown, which ultimately resulted in better structural rearrangements and stronger structure at lower shear rate. The mud samples from RV location show a typical thixotropic behaviour for the entire investigated shear rate range by having lower stresses in the ramp down curve.

This behaviour may again be associated with their high organic content: a large number of flocs have been disrupted which require longer times to rearrange. The absence of anti-thixotropic character was also observed for the mud samples having higher densities. These results confirmed that the thixotropic behaviour of natural sediments is a strong function of both density and organic matter content.

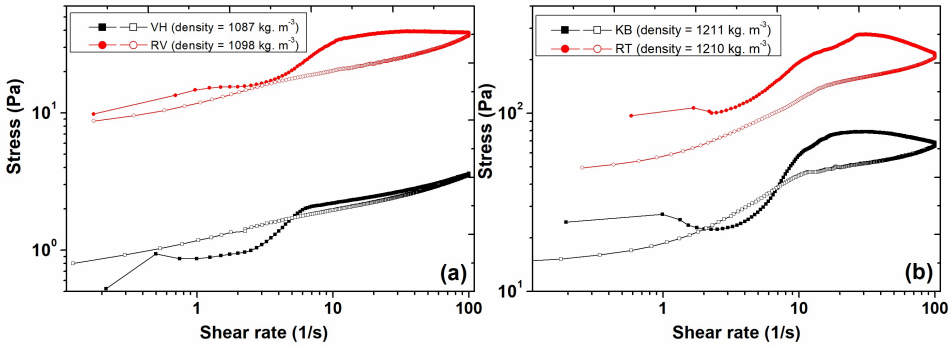

Figure 4.8: Stress as a function of shear rate for mud sediments having (a) similar lower and (b) similar higher densities from different locations. Filled symbols represent the shear rate ramp up and the empty symbols represent the shear rate ramp down experiment

4.4. SETTLING ANALYSIS OF MUD FLOCS

THE particle (floc) shape and density was investigated during settling to determine whether a correlation could be found between the floc properties and the bulk rheological properties. To analyse the mud floc size, settling velocity and to derive their density, settling experiments were performed with the experimental setup presented in Fig. 2.7. In Fig. 4.9, floc settling velocity is plotted against floc size (mean diameter) for mud samples obtained from different locations. A similar correlation between the settling velocity and the size of flocs has also been observed in literature (Dyer and Manning, 1999). Effective floc density was calculated with Stokes Law according to Eq. 2.7. These results show that the spread in effective density was in line with the trend in the organic matter content (TOC), i.e., RV > RT > KH > SW (see Table 2.1). The mud sample from RV location displays a relatively consistent effective density and a linear relationship between log(settling velocity) and log(floc size) whereas the mud sample from SW location, with the lowest organic matter content, shows a much larger spread in effective density values. For example, in case of the mud sample from RV location, the flocs appear to fall along the 30 kg. m^{-3} iso-line, while for mud sample from SW location, there is a wide spread in excess density values from below 10 kg. m^{-3} to above 800 kg. m^{-3}. Based on the effective density relation, this is equivalent to an effective density between 1.01 and 1.8 kg. m^{-3}.

In Fig. C2, the perimeter-based fractal dimension is calculated for the flocs as two times the slope of the log-log plot of perimeter versus area. This method for calculating the fractal dimension has been used in many studies (Fan et al., 2017, Wei et al., 2009, Wyatt et al., 2013, W. Xu et al., 2011, Zhao, 2004, Zheng et al., 2011), therefore, it provides

a convenient means of comparing the structural characteristics of flocs between different studies. From the plot of perimeter-based fractal dimension, it was found that SW sample has the smallest value of D_p, which is an indication of tightly packed, less open, or less porous mud flocs – having, hence, a larger density. The mud samples from other locations (RV, RT and KH) displayed similar values of D_p, within the range of 1.32 – 1.34.

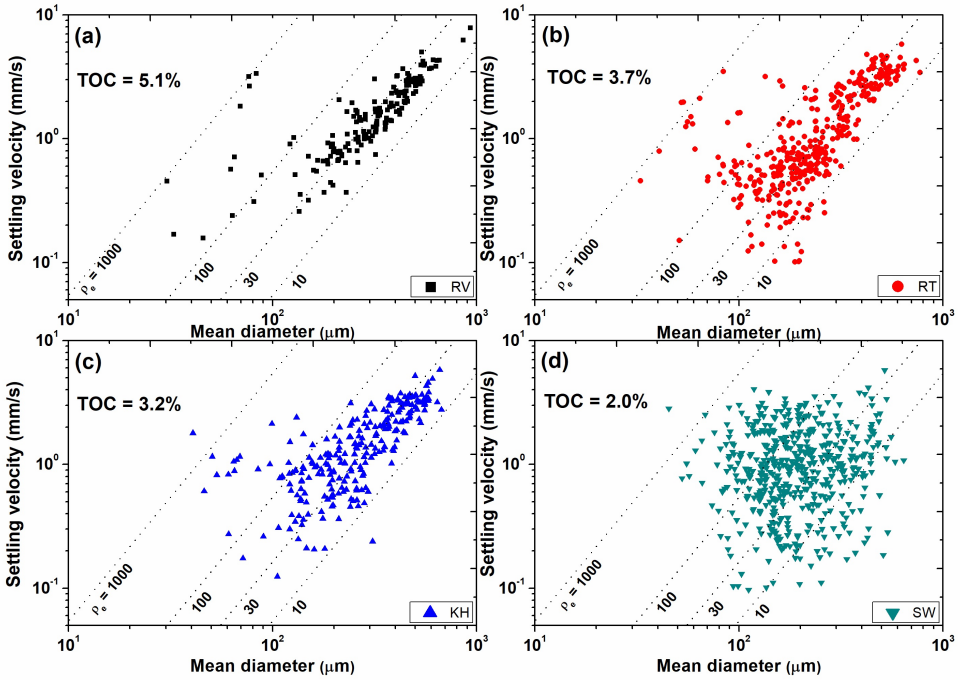

Figure 4.9: Settling velocity as a function of mean diameter for mud flocs from (a) RV location, (b) RT location, (c) KH location and (d) SW location. Dashed lines represent the iso-lines derived from Eq. 2.7.

The correlation between the settling velocity and the aspect ratio (obtained from Eq. 2.6) of the flocs for different locations is shown in Fig. C3. The result shows that the flocs with higher aspect ratio displayed lower settling velocity, for locations RV and RT. For KH and SW locations, there is no trend between aspect ratio and settling velocity. This result is in line with the TOC of these samples: larger amounts of organic matter tend to produce organic matter-rich flocs, which are highly cohesive and lead to the formation of elongated flocs by macro-aggregation of two flocs. The effective density of flocs is presented as a function of size of flocs in Fig. C4, which displays an exponential decay in floc density (i.e., straight line in a log-log plot), as is usually found in literature (Dyer and Manning, 1999). In Fig. 4.10, a histogram is presented representing the number of particles of a given mean diameter. The mean floc size was calculated as the simple mean of the measured values. The mean floc size was found to decrease in the following order: RV > KH > RT > SW. This result confirms that the floc size is largest for the mud sample from RV location (having highest organic matter content) and smallest for mud sample from SW

location (with lowest organic matter content). The presence of larger organic matter-rich flocs in RV sample also justifies the higher values of rheological parameters such as yield stresses and modulus. Furthermore, the low amount of organic matter in SW sample resulted in higher average effective density, smaller floc size, and higher settling rates of the flocs.

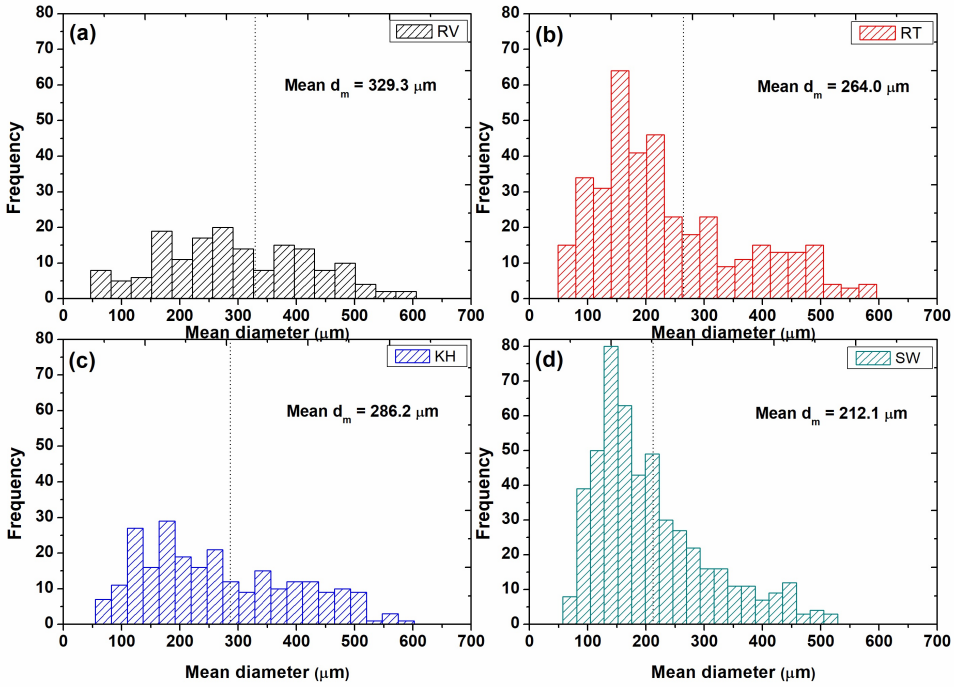

Figure 4.10: Floc size distribution for mud flocs from (a) RV location, (b) RT location, (c) KH location and (d) SW location with mean value of diameter marked with a vertical dashed line and the value is shown at the top right of each plot.

4.5. CORRELATION BETWEEN LAB AND IN-SITU MEASUREMENTS

TWO different locations at the Port of Hamburg were used to test the Rheotune and to compare the results with laboratory measurements: Vorhafen (VH) and Köhlfleet mit Köhlfleethafen (KH). Fig. 4.11 shows the yield stresses measured in situ and in laboratory as a function of density for two different locations of the Port of Hamburg. The in situ measurements match well with the laboratory experiments. This result shows that the Rheotune can be effectively used to monitor the in-situ yield stress values for defining navigable mud layer. Moreover, Port of Hamburg also analyzed the correlation between the fluidic yield stress obtained from rheometer and the Bingham yield stress obtained from in-situ Rheotune for KH location. They observed higher values of Bingham yield stress (around 40%) as compared to the fluidic yield stress. This was linked to the definition of both yield stresses, second decline in viscosity was termed as fluidic

yield stress while the extrapolation of flow curve from higher shear rate was defined as Bingham yield stress. However, in future, port of Hamburg will calibrate the Rheotune for fluidic yield stress, instead of Bingham yield stress.

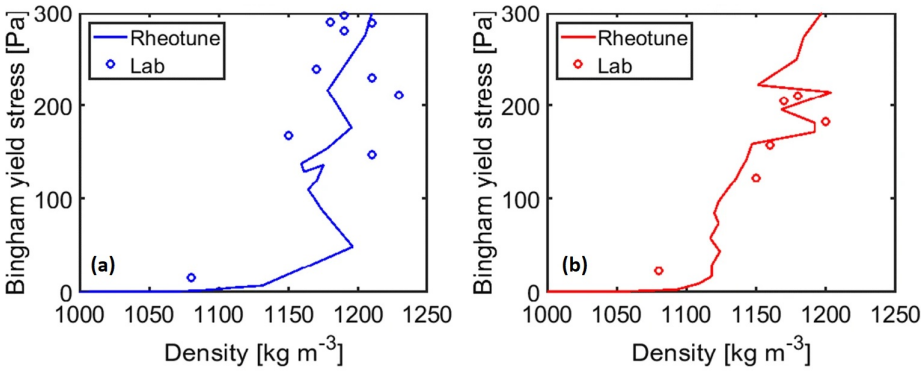

Figure 4.11: Comparison of densities and yield stresses measured in situ using the Rheotune and in laboratory using the Couette rheometer for (a) Vorhafen (VH) and Köhlfleet mit Köhlfleethafen (KH) locations in Port of Hamburg.

4.6. CONCLUSIONS

A detailed rheological analysis was performed on the mud samples collected from different locations of the Port of Hamburg, Germany representing different layers within the sediment bed. Stress ramp-up tests, frequency sweep tests and thixotropic tests were performed to assess the rheological fingerprint of the considered mud sediments. The yield stress analysis of the mud samples of a given location displayed an increase in the yield stress values by going deeper into the sediment bed which is attributed to the increase in density of these samples.

Mud samples having similar densities were significantly rheologically dissimilar from each other due to the presence of organic matter. From stress ramp-up and frequency sweep tests, it was shown that the yield stresses and complex modulus of samples with higher organic matter content (RV and RT) display higher values than the samples with lower organic matter content, for a given density. The comparison between natural and diluted mud layers showed significantly different rheological properties particularly yield stresses, which was attributed to the differences in the composition of mud layers. Extensive mixing (i.e., by ultrasonic shaking and high-speed shearing) of mud samples after dilution can provide homogeneous systems but the floc network and the clay fabric will then be totally different from the ones found in in-situ conditions. The thixotropic studies revealed that all the sediments, except from RV location, exhibit a combination of thixotropic and anti-thixotropic behaviours. The sediments from RV location display only thixotropic behaviour for the entire shear rate range, which was linked to the their high organic matter content.

In the final part, a detailed analysis of mud flocs was performed with the help of a floc-camera settling setup, to obtain the floc size, density and settling velocity. The floc anal-

ysis confirmed the formation of larger flocs with higher aspect ratio (open and porous structure) for the samples with higher organic matter content, which explains the higher rheological properties for these samples. For SW location, the scattered behaviour of settling velocity as a function of floc size is due to the presence of silt/sand sized particles, as confirmed by PSD analysis (see Fig. 2.3a) from laser diffraction technique. In the end, the yield stress values obtained from laboratory and in-situ measurements were compared and the results showed good agreement between them.

5

RHEOLOGICAL MODELLING

For numerical modelling purposes, it is essential to have an empirical or semi-empirical model that can capture the rheological fingerprint (i.e., flow curve) of mud. In literature, there are several rheological models which can be used to fit the flow curve of mud. However, mud samples exhibiting two-step yielding cannot be fitted by existing models as they are meant for one-step yielding. Therefore, the main objective of this chapter is to propose an empirical or semi-empirical rheological model, which can effectively capture the two-step yielding behaviour of mud. The existing rheological models are first discussed and used to fit the rheological data of mud samples, in order to analyse their efficiency for fitting the two-step yielding behaviour of mud. Afterwards, an empirical model is proposed to fit the flow curve of mud samples from different locations and depths of Port of Hamburg. This rheological modelling also helps in analysing the influence of different parameters such as density and organic matter content on different rheological properties including static and fluidic yield stresses and infinite viscosity.

Parts of this chapter have been published in Estuarine, Coastal and Shelf Science **257**, 107407 (2021) (Shakeel, Kirichek, Talmon, et al., 2021)

5.1. INTRODUCTION

DIFFERENT empirical rheological models have been used in literature for the cohesive mud sediments (Van Kessel and Blom, 1998, Babatope et al., 2008, Bai et al., 2002, Coussot, 1997, Huang and Aode, 2009). Van Kessel and Blom, 1998 used a thixotropic model developed by Toorman, 1997, which is an extension of the Moore model (Moore, 1959) for characterizing the rheological behaviour of estuarine mud. Fonseca et al., 2019 analysed the rheological properties of mud sediments from Port of Santos, the Port of Rio Grande, the Port of Itajaí and the Amazon south navigation channel in Brazil, by fitting the data with a Bingham model. Yang, Yu, et al., 2014 investigated the rheological behaviour of mud sediments from shoal of the Hangzhou Bay, Yangtze River and Yangcheng Lake, China with the help of the Herschel-Bulkley model. Huang and Aode, 2009 used a Dual-Bingham model and Worrall-Tuliani model (Worrall and Tuliani, 1964) to fit the rheological data of mud samples obtained from two different locations of Hangzhou Bay, China. Similarly, J. Xu and Huhe, 2016 used a Dual Herschel-Bulkley model to examine the rheological data of estuarine mud obtained from Lianyungang, China. All these reported empirical models are usually effective for single-step yielding in the sample. However, no empirical/theoretical model is yet available in literature to capture the behaviour of two-step yielding in mud. Therefore, in this study, an empirical model is proposed to capture the dual yielding behaviour in mud samples.

5.2. EXISTING RHEOLOGICAL MODELS FOR FLOW CURVE

SEVERAL rheological models have been reported in the literature to fit the flow curves of the yield stress materials such as Bingham model (Bingham, 1922), Dual-Bingham plastic model (Huang and Aode, 2009), Papanastasiou model (Papanastasiou, 1987), Herschel-Bulkley model (Herschel and Bulkley, 1926), Worrall-Tuliani model (Worrall and Tuliani, 1964), Toorman model (Toorman, 1997) to name a few. Bingham, Herschel-Bulkley and Worrall-Tuliani models have been found in the literature to well describe the flow curves of different types of sediment. These models are given by:

Bingham model:

$$\tau = \tau_B + K\dot{\gamma} \tag{5.1}$$

Herschel-Bulkley model:

$$\tau = \tau_0 + K\dot{\gamma}^n \tag{5.2}$$

Worrall-Tuliani model:

$$\tau = \tau_0 + \mu_\infty\dot{\gamma} + \frac{\Delta\mu\dot{\gamma}}{1+\beta\dot{\gamma}} \tag{5.3}$$

Where K is the consistency index ($K = \mu_\infty$ when $n = 1$), n is the flow behaviour index, μ_∞ is the viscosity at higher shear rate, τ_0 is the yield stress and τ_B is the Bingham yield stress. It is noted that at high shear, Eq. 5.3 reduces to:

$$\tau(\dot{\gamma} \to \infty) = \tau_0 + \frac{\Delta\mu}{\beta} + \mu_\infty\dot{\gamma} \tag{5.4}$$

By comparing Eq. 5.1 and Eq. 5.4 one deduces that:

$$\Delta\mu = \beta(\tau_B - \tau_0) \tag{5.5}$$

5.2.1. EMPIRICAL FITTING OF FLOW CURVES WITH EXISTING RHEOLOGICAL MODELS

The approach used by Huang and Aode, 2009 was applied to fit the shear rate/shear stress function displaying a two-step yielding. Bingham and Herschel-Bulkley models were applied in each of two shear rate regimes defined by a critical shear rate ($\dot{\gamma}_c$). This critical shear rate was obtained from the cross-over between the two straight lines extrapolated from the lower and higher shear regions (Fig. 5.1). The value of this critical shear rate was observed to be about 20 s^{-1}. The Worrall-Tuliani model was applied on the whole shear rate regime because it can describe the flow curve both at lower and higher shear rates (Toorman, 1994).

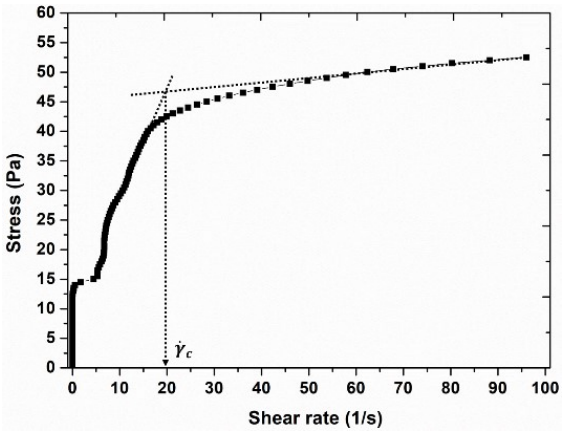

Figure 5.1: Shear stress as a function of shear rate for PS mud layer from KB location (1151 kg. m^{-3}) using stress ramp-up protocol with Couette geometry. The dashed lines represent the extrapolation of lower and higher shear regions to define the critical shear rate, $\dot{\gamma}_c$.

The values of the fitting parameters for all three models are given in Table 5.1 along with the static and fluidic yield stress values obtained from viscosity decline approach (VD). The yield stress (τ_0) value attained from the Worrall-Tuliani (WT) model was in close agreement with the static yield stress (τ_s) of the sample obtained from viscosity decline. Moreover, there was a complete agreement between the yield stress (τ_0) values obtained from the Bingham and Herschel-Bulkley (HB) models (both for lower shear regime and higher shear region) and from the viscosity declines. This result confirms that the viscosity decline approach of stress ramp-up protocol provides a reliable and fast way of determining the yield stresses (static and fluidic) of the mud samples. Furthermore, the Dual Bingham model or Dual Herschel-Bulkley model can capture the characteristic features of two-step yielding by fitting the basic model (i.e., Bingham or Herschel-Bulkley) to two different regions of the same flow curve. However, this fitting method requires

Table 5.1: Values of the model parameters (Eq. 5.1 – 5.3) along with the static and fluidic yield stresses obtained from viscosity decline approach (VD).

Model/ Approach	Shear rate (s^{-1})	τ_S (Pa)	τ_f (Pa)	τ_0 or τ_B (Pa)	μ_∞ or K (Pa.s or Pa.s^n)	n (-)	$\Delta\mu$ (Pa.s)	β (s)	R^2 (-)
VD	0 – 100	11	40	–	–	–	–	–	–
WT	0 – 100	–	–	11.10	0.06	–	3.68	0.09	0.96
Bingham	0.01 – 20	–	–	10.25	1.82	–	–	–	0.96
Bingham	20 – 100	–	–	41.57	0.13	–	–	–	0.95
HB	0.01 – 20	–	–	11.01	1.38	1.00	–	–	0.96
HB	20 – 100	–	–	33.08	2.79	0.43	–	–	0.99

VD = Viscosity decline approach; WT = Worrall-Tuliani model; HB = Herschel-Bulkley model

to define a critical shear rate which delimit each of the yielding regions. Therefore, for practical purpose, it is useful to develop a model that can capture both yielding steps in a single equation.

5.3. PROPOSED RHEOLOGICAL MODEL FOR TWO-STEP YIELDING

FROM rheological evidence, see Chapter 3, it appeared that the mud samples collected from the Port of Hamburg exhibited a two-step yielding behaviour. This two-step yielding is associated with two characteristic shear stresses termed as static yield stress (τ_s) and fluidic yield stress (τ_f), as defined in Sec. 3.2.1 of Chapter 3. The shear stress $\tau(\dot{\gamma})$ is, at lower shear rate ($\dot{\gamma}$), depending on τ_s and can be fitted by the function $\tau_{stat}(\tau_s, \dot{\gamma})$ and, at higher shear rate ($\dot{\gamma}$), depending on τ_f and fitted by the function $\tau_{fluid}(\tau_f, \dot{\gamma}_0, \dot{\gamma})$, where the transition between the two functions occurs at a shear rate defined as $\dot{\gamma}_0$. The following equation is proposed to fit $\tau(\dot{\gamma})$ over the whole range of shear rates:

$$\tau = \alpha\tau_{\text{stat}} + (1-\alpha)\tau_{\text{fluid}} \tag{5.6}$$

where the step function α is given by:

$$\alpha = 1 - \frac{1}{1+\exp\left(-k\left(\dot{\gamma}-\dot{\gamma}_0\right)\right)} \tag{5.7}$$

This function gives $\alpha(\dot{\gamma} < \dot{\gamma}_0) = 1$ and $\alpha(\dot{\gamma} > \dot{\gamma}_0) = 0$ with a transition at $\dot{\gamma} = \dot{\gamma}_0$, with a sharpness that depends on the value of k. Different values of k (i.e., 1, 10 and 100) were tested for the experimental data fitting of mud sediments. The best fitting was achieved by using $k = 10$ s, which was then used for fitting the complete data set. The function τ_{stat} is given by:

$$\tau_{\text{stat}} = \frac{\tau_s}{1+\dot{\gamma}_s/\dot{\gamma}} = \frac{\left(\tau_s/\dot{\gamma}_s\right)\dot{\gamma}}{\dot{\gamma}/\dot{\gamma}_s+1} \tag{5.8}$$

This function can be seen as an adaptation of the Worrall-Tuliani model, whereby $\tau_s/\dot{\gamma}_s$ can be identified as $\Delta\mu$ and $1/\dot{\gamma}_s$ as β, see Eq. 5.3. The Worrall-Tuliani model includes an initial shear stress τ_0 which does not appear in Eq. 5.8. From the analysis of this function, we find that:

$$\tau_{\text{stat}}\left(\dot{\gamma}_s \ll \dot{\gamma}_0\right) = \tau_s \tag{5.9}$$

$$\tau_{\text{stat}}\left(\dot{\gamma} = \dot{\gamma}_s\right) = \frac{\tau_s}{2} \tag{5.10}$$

The shear rate $\dot{\gamma}_s$ represents the shear rate for which the stress, τ_s is half of its value. The curvature of the first function can be changed by varying $\dot{\gamma}_s$. The Worrall-Tuliani model assumes that $\tau(\dot{\gamma} \to \infty) = \tau_\infty + \mu_\infty \dot{\gamma}$ and, hence, reduces to a Bingham model. This part has been left out in our model, since for higher shear rate, the stress does not follow a Bingham behaviour but display a second yield behaviour. This second step in yielding behaviour is captured by the function τ_{fluid} given by:

$$\tau_{\text{fluid}} = \tau_s + \frac{\tau_f}{1 + \left(\left(\dot{\gamma}_f - \dot{\gamma}_0\right) / \left(\dot{\gamma} - \dot{\gamma}_0\right)\right)^d} + \mu_\infty\left(\dot{\gamma} - \dot{\gamma}_0\right) \tag{5.11}$$

This model is an adaptation of the Worrall-Tuliani model, whereby the coefficient d enables to tune the "sharpness" of the curvature. For mud sediments, $d = 1$ was used, and hence the function can be seen as a Worrall-Tuliani model with origin $\dot{\gamma} = \dot{\gamma}_0$, which can be written:

$$\tau_{\text{fluid}} = \tau_s + \mu_\infty\left(\dot{\gamma} - \dot{\gamma}_0\right) + \frac{\tau_f\left(\dot{\gamma} - \dot{\gamma}_0\right) / \left(\dot{\gamma}_f - \dot{\gamma}_0\right)}{\left(\dot{\gamma} - \dot{\gamma}_0\right) / \left(\dot{\gamma}_f - \dot{\gamma}_0\right) + 1} \tag{5.12}$$

From Eq. 5.3, one can see that it is possible to identify τ_0 as τ_s, $\Delta\mu$ as $\tau_f / \left(\dot{\gamma}_f - \dot{\gamma}_0\right)$ and β as $1 / \left(\dot{\gamma}_f - \dot{\gamma}_0\right)$. This function τ_{fluid} does include a Bingham part, since:

$$\tau_{\text{fluid}}\left(\dot{\gamma} \to \infty\right) = \tau_s + \tau_f + \mu_\infty\left(\dot{\gamma} - \dot{\gamma}_0\right) \tag{5.13}$$

where $\tau_s + \tau_f$ can be seen as a (pseudo) Bingham yield stress for $\dot{\gamma} = \dot{\gamma}_0$. Furthermore, it is observed that:

$$\tau_{\text{fluid}}\left(\dot{\gamma} = \dot{\gamma}_0\right) = \tau_s \tag{5.14}$$

where τ_s is the "true" yield stress at $\dot{\gamma} = \dot{\gamma}_0$. It is also found that:

$$\tau_{\text{fluid}}\left(\dot{\gamma} = \dot{\gamma}_f\right) = \tau_s + \frac{\tau_f}{2} + \mu_\infty\left(\dot{\gamma}_f - \dot{\gamma}_0\right) \tag{5.15}$$

where $\tau_s + \frac{\tau_f}{2}$ can be seen as a (pseudo) Bingham yield stress for $\dot{\gamma} = \dot{\gamma}_f$.

In short, the two-step yielding model contains six fitting parameters: $\dot{\gamma}_0$, τ_s, $\dot{\gamma}_s$, τ_f, $\dot{\gamma}_f$ and μ_∞ (see Fig. 5.2). Two parameters, τ_s (static yield stress) and τ_f (fluidic yield stress) are important for practical applications.

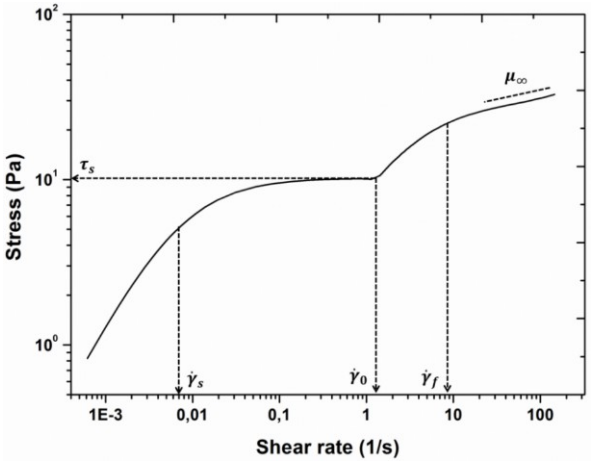

Figure 5.2: Theoretical representation of proposed empirical model along with the fitting parameters.

5

5.4. RHEOLOGICAL PARAMETRIZATION FOR POH MUD

THOUGH the Dual-Bingham and Dual-Herschel-Bulkley models can be adapted to fit each of the two yielding regions of flow curves, the selection of the critical shear rate which delimits these regions is difficult and time consuming to find, particularly in case of significant amount of experimental data-set. Therefore, an empirical model was derived which can be used to fit the data over the whole range of shear rates.

The experimental data of stress ramp-up tests, performed for the mud samples obtained from different locations/depths within the port (Fig. 2.1), were fitted with the proposed model, as shown in Fig. 5.3a for one sample. The model displays a good agreement with the experimental data and the values of the fitting parameters are also shown in Fig. 5.3a for that sample. It is known that the mud samples obtained from different locations of the port have different rheological fingerprints due to the variation in organic matter content. Therefore, after fitting all the experimental data with the model, the fitting parameters were correlated with the density and organic matter content (TOC), in order to generalize the model for the whole port.

Fig. 5.3b shows the fluidic yield stress (τ_f) as a function of density for the samples from all locations. The experimental data above the excess density ($\rho - \rho_w$) of 200 kg. m^{-3} shows deviation from the linear behaviour found at lower densities on a semi-log scale. Above 200 kg. m^{-3} the yield stress becomes independent of density (within the large experimental scatter). Mud with density above 200 kg. m^{-3} is not relevant for defining nautical bottom in ports and waterways. Consequently, the data above this density value was not considered further for the correlation between fitting parameters and density/TOC.

The experimental data of fluidic yield stress (τ_f) as a function of excess density ($\rho - \rho_w$) for different locations was fitted with a power law model, given as:

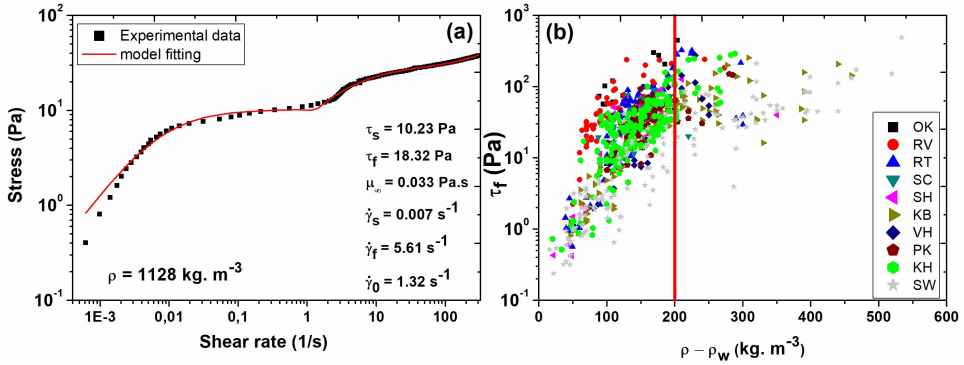

Figure 5.3: (a) Stress as a function of shear rate for mud sample from KB location obtained by performing stress ramp-up test using Couette geometry. The solid line represents the model fitting; (b) fluidic yield stress (τ_f), obtained from proposed model, as a function of excess density ($\rho - \rho_w$) for different locations. OK is an extra location in upstream direction (see Table A2).

5

$$\tau_f = a \cdot \left(\left(\rho - \rho_w \right) / \rho_w \right)^b \tag{5.16}$$

where 'a' and 'b' are two fitting parameters. It is evident that the parameter 'b' of different curves is similar while the other parameter ('a') is significantly different for different locations, as shown in Fig. 5.4a and 5.4b. It can also be seen that the organic matter content (TOC) shows a decreasing trend from location OK to SW (from the river side to the sea side). As the parameter 'b' was not varying significantly, a fixed value of 2.4 was used for parameter 'b'. The power law fitting was again performed with just one fitting parameter 'a', as shown in Fig. 5.4c. This fixed value of the fitting parameter 'b' is slightly lower than the one reported in literature for mud samples by Nie et al., 2020 who claimed 'b' to be within the range of $5.2 - 5.8$. The difference is most probably due to the higher density of their mud samples.

A similar approach was also used for the correlation between the static yield stress (τ_s) and excess density (see Fig. D1 in Appendix D). The correlation between fitting parameter 'a' (both static and fluidic) and TOC for different locations is shown in Fig. 5.4d. It is found that a strong correlation exists between the fitting parameter 'a' and the TOC for different locations. A similar approach is used for the correlation between infinite viscosity (μ_∞) and TOC where the fixed value of parameter 'b' was 1. The corresponding values for parameter 'a' is given in Fig. 5.5b. The correlation of the static shear rate $\dot{\gamma}_s$ with excess density for location RT is shown in Fig. 5.5a. For $\dot{\gamma}_s$, it can be seen that the parameter shows a decreasing trend with the excess density, except at very small densities, where a cluster of data is observed. This cluster of data was not included in the fitting because such low densities samples either behave like a Newtonian fluid (i.e., have no yield stress) or exhibit single-step yielding, and therefore, fitting with the proposed two-step yielding model can produce inaccurate parameters values.

Discarding this data, a power law fitting was applied for this parameter ($\dot{\gamma}_s$) as well, by

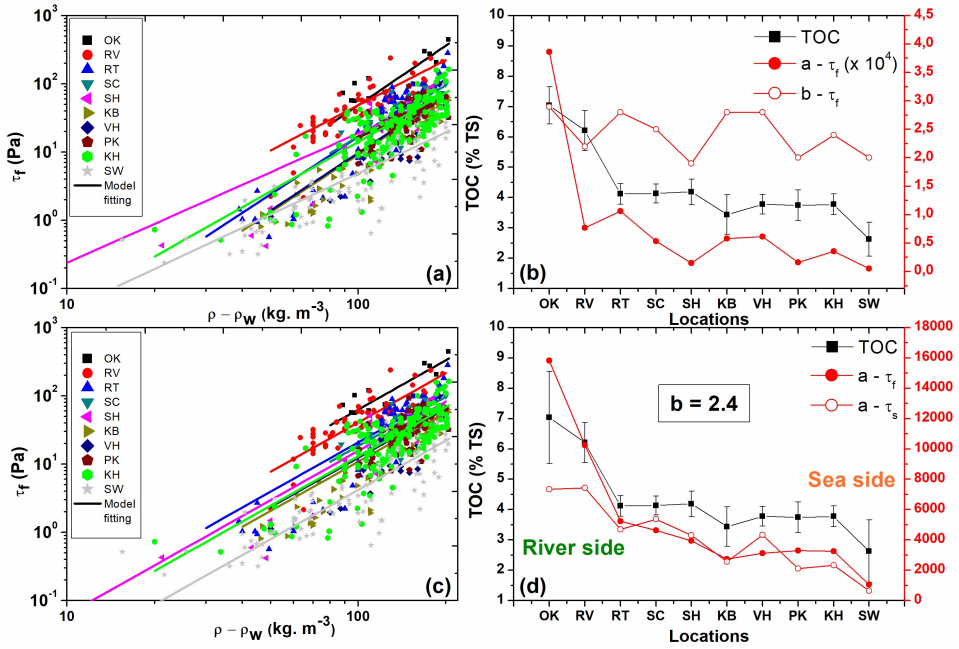

Figure 5.4: (a) Fluidic yield stress (τ_f) as a function of excess density ($\rho - \rho_w$) for different locations. The solid lines represent the power law fitting (Eq. 5.16) with two fitting parameters. ρ_w represents the density of water. (b) fitting parameters ('a' and 'b') of Eq. 5.16 for fluidic yield stress and TOC as a function of different locations. (c) fluidic yield stress (τ_f) as a function of excess density for different locations. The solid lines represent the power law fitting (Eq. 5.16) with one fitting parameter 'a' and the fixed value of parameter 'b'. (d) fitting parameter 'a' (both static and fluidic) and TOC as a function of different locations.

fixing the value of parameter 'b' equal to −2.4 (Fig. 5.5a). Fig. 5.5b shows a strong correlation between the fitting parameter 'a' for different model parameters and the TOC for different locations. The remaining two model parameters, $\dot{\gamma}_f$ and $\dot{\gamma}_0$ showed no correlation with the density of the samples. These parameters were observed to vary within the range of $2 - 22\ s^{-1}$ for $\dot{\gamma}_f$ and $0.1 - 13\ s^{-1}$ in case of $\dot{\gamma}_0$ for all the studied locations. However, the values of these parameters may depend on the stress ramp-up rate and type of TOC, which needs further investigation.

The upper and lower limits of the parameter 'a' for different model parameters were also estimated for all the locations, in order to cover the scatter of the data for each location (see Table D1 in Appendix D). These limits of parameter 'a' were estimated by fitting the higher and lower values of yield stresses with the same power law. Fig. 5.6 shows the power law fitting line (black line) along with the upper and lower limit lines (red lines) for KB location in case of fluidic yield stress. The samples having excess densities higher than 200 kg. m^{-3} are also plotted in Fig. 5.6, but these samples were not included in the fit. These samples are also within the upper and lower limits. However, some of these samples show a clear deviation from the predicted increase.

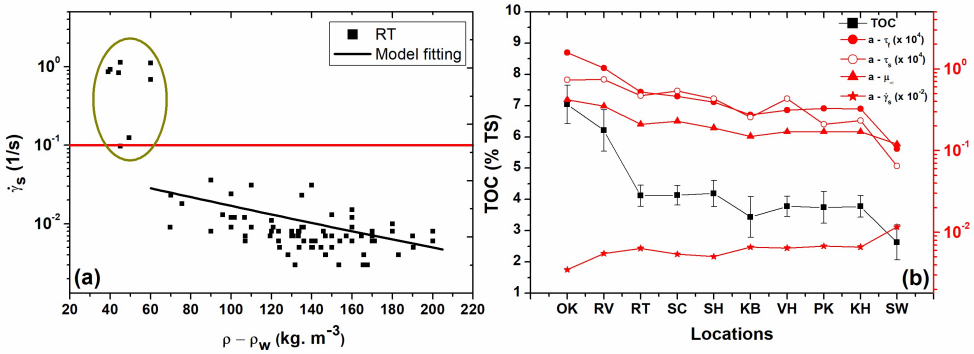

Figure 5.5: (a) $\dot{\gamma}_s$ as a function of excess density for RT location. The black solid line represents the power law fitting (Eq. 5.16) with one fitting parameter. (b) fitting parameter 'a' for different model parameters and TOC as a function of different locations.

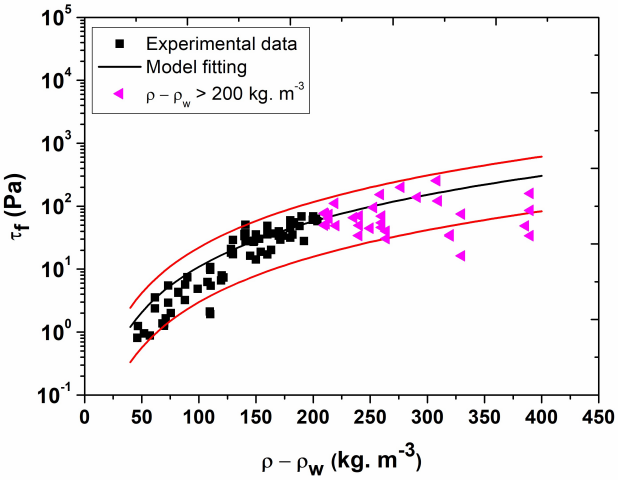

Figure 5.6: Fluidic yield stress (τ_f) as a function of excess density for KB location. The black line represents the power law fitting (Eq. 5.16) while the red lines represent the upper and lower limits of the parameter 'a' with the fixed value of b (i.e., 2.4).

5.5. CONCLUSIONS

In literature, there are several rheological models such as Bingham, Herschel-Bulkley and Worrall-Tuliani, which can be used to fit the flow curve data of mud. The yield stress obtained by fitting the rheological data of mud using Worrall-Tuliani model corresponded well with the static yield stress obtained from viscosity decline. However, in case of Bingham or Herschel-Bulkley mode, two regions of shear rate are identified with the help of a critical shear rate ($\dot{\gamma}_c$). These models are then applied in these two shear rate regions, which eventually resulted in two yield stress values. These yield stress values presented a good correlation with the static and fluidic yield stress values. However,

the estimation of this critical shear rate can become tedious, particularly for large number of flow curves.

In order to overcome this problem, an empirical model is proposed which is based on a step function. The proposed model is, therefore, not suited where two-step yielding is not observed. For those protocols, simple Bingham model or Worrall-Tuliani model can be used to fit the experimental data. This proposed model is accurate in capturing the two-step yielding behaviour of mud samples from Port of Hamburg, within the density range of 1050 − 1200 kg. m^{-3}. The rheological properties particularly the yield stresses showed a significant dependence on the organic matter content, as already described in previous chapter. The applicability of stress ramp-up protocol and the proposed empirical model need further investigation for the mud sediments from different ports.

6

STRUCTURAL RECOVERY

Apart from yield stress and flow curve analysis, the information regarding the structural recovery of mud after extensive shearing is critical for defining sediment management strategies. The structural recovery behaviour of synthetic suspensions has extensively been studied in literature, however, the structural evolution of mud sediments has not been investigated in detail. Therefore, in this chapter, the extent and rate of structural recovery of mud sediments are presented by measuring the storage modulus as a function of time using small amplitude oscillatory tests after a destructive steady shearing. This linear viscoelastic response of the sediments is further described as a function of several parameters including pre-shear rate, pre-shear time, mud density and organic matter content. The equilibrium storage modulus ($G^{'}_{\infty}$) and the characteristic time (t_r) for the structural recovery of mud are estimated by fitting the experimental data to a stretched exponential function. The normalized storage modulus, $G^{'}/G^{'}_{0}$ (i.e., so-called structural parameter) is related to the yield stresses of mud sediments. This study provides an extensive knowledge about the structural recovery in mud sediments under different shearing conditions, which can be useful for sediment management.

Parts of this chapter have been published in Journal of Non-Newtonian Fluid Mechanics **286**, 104434 (2020) (Shakeel et al., 2020c), Marine and Petroleum Geology **116**, 104338 (2020) (Shakeel et al., 2020a).

6.1. INTRODUCTION

THIXOTROPY is one of the very frequently observed complex rheological behaviours of the colloidal suspensions, in which the properties of the material are both time and shear rate dependent. There are several methods to study the thixotropic behaviour of a system. Mewis and co-workers have determined the inherent drawbacks of using steady shearing methods to analyse the structural recovery of the system because in these methods the material's structure has to be disturbed in order to be probed during the recovery phase (Schoukens and Mewis, 1978). Mewis and de Bleyser, 1972 have shown that one can study the structural recovery of a polyamide gel in linseed oil by performing oscillatory measurements (i.e., non-destructive) within the linear viscoelastic regime of the material. This linear viscoelastic method has, henceforth, been used to analyse the rate and extent of structural recovery after steady or large amplitude oscillatory shearing for a variety of materials such as polymeric solutions (Janssens et al., 2017), pickering emulsions (Whitby and Garcia, 2014), slurries (Phuoc et al., 2014), cement pastes (Roussel et al., 2012), nanocomposite systems (Mobuchon et al., 2007), emulsion gels (Sun and Zhang, 2015) and synthetic colloidal dispersions (Mobuchon et al., 2009). The rate and extent of this structural recovery can be expressed in terms of thixotropy at a given kinematical condition (Mewis and de Bleyser, 1972).

From literature overview, it appears that even though the thixotropic behaviour of synthetic suspensions (i.e., well-characterized clay in the presence of flocculating agents) has extensively been studied, the structural evolution of natural sediments has not been investigated. This probed to investigate the structural breakup and recovery of mud sediments using small deformation rheology as a function of several parameters including pre-shear time, pre-shear rate, sediment density, organic matter content and geometry of rheometer. The effect of these pre-shearing and recovery parameters on the yield stresses of mud sediments was further studied.

6.2. ONE SEDIMENT LOCATION

THE structural recovery in mud, after the structural breakdown caused by high shearing was analysed by performing time sweep oscillatory experiments at very small amplitudes and recording the storage modulus of the suspensions as a function of time, as detailed in the experimental Section 2.4.3. The recovery step was performed for an interval of 500 s, which was long enough to capture the significant part of the structural recovery in mud sediments (see Sec. E.1 in Appendix E). The influence of temperature on the structural recovery was also studied by performing measurements at 5 and 25 °C. The results showed a higher structural recovery at the temperature of 25 °C (see Sec. E.2 in Appendix E) and, therefore, this temperature was selected for the detailed analysis of structural recovery. Pre-consolidated mud samples (PS layer) from RT location were used for the detailed structural recovery analysis because of their average density (compared to all locations) and minimum sedimentation problem (i.e., stable sample).

6.2.1. EFFECT OF PRE-SHEAR RATE

The structural evolution in terms of normalized storage modulus (i.e., with respect to the initial storage modulus $G_0^{'}$) as a function of time is shown in Fig. 6.1a for different

pre-shearing rates. An oscillating modulus response was obtained in some cases (Fig. 6.1a) in particular for concentrated sediments which have been sheared at low shear rates. However, the normalized loss modulus ($G^{''}/G_0^{''}$), showed the reduction in oscillating behaviour with time (see Fig. E3a in Appendix E). The same type of oscillations have also been observed in the literature for polymeric solutions and synthetic suspensions, at the beginning of creep experiments, due to the elasticity of material (i.e., creep ringing). These oscillations also tend to disappear/minimize at longer experimental times (Goudoulas and Germann, 2016, Joshi et al., 2007). Therefore, the observed oscillations may be due to the elastic nature of the investigated samples.

It can be seen from the Fig. 6.1a that for low shear rates, a better recovery is obtained. Eq. 2.4 was used to fit the data. The fitting parameters are presented in Table E3. Two important parameters, $G_\infty^{'}/G_0^{'}$ and t_r are plotted as a function of pre-shear rate in Fig. 6.1b. It is interesting to note that both parameters display a decreasing trend with increasing shear rate till the shear rate of 35 s^{-1}, followed by an increase in both parameters for higher shear rates. This peculiar behaviour of parameters as a function of pre-shear rate was also observed in literature for synthetic suspensions of fumed silica and ferric-oxide (Kanai and Amari, 1993, Raghavan and Khan, 1995).

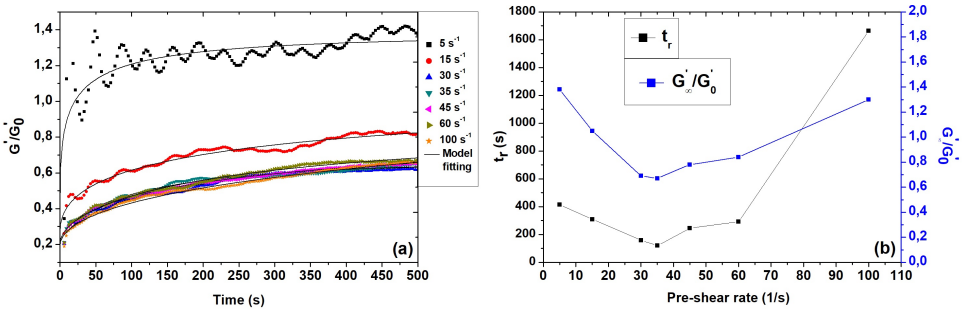

Figure 6.1: (a) Normalized storage modulus ($G^{'}/G_0^{'}$) as a function of time for different pre-shear rates using RT sediments, solid line represents model fitting, (b) model parameters ($G_\infty^{'}/G_0^{'}$ and t_r) as a function of pre-shear rate, the solid line is just a guide for the eye.

A possible explanation for this peculiar behaviour is presented in Fig. 6.2. The initial structure (Fig. 6.2a) is composed of an interconnected network of sediment-rich flocs along with polymer chains (i.e., organic matter). The bonds most prone to fail at shearing will be at the junction points between flocs. Therefore, at low pre-shear rates, it is believed that these bonds will break leading to an alignment of the polymer chains or reorganization of flocs (Fig. 6.2b). After shearing, it is assumed that the flocs will form a weaker interconnected network (with more open spaces) and have less junction points (Fig. 6.2c). With time, some strength will be recovered as a result of the reformation of the organic matter-flocs bonds. Nonetheless, the floc structure remains less interconnected as at the start, implying $G_\infty^{'}/G_0^{'} < 1$.

At very higher shear rates, in addition to the breakdown of the interconnected network of flocs, it is thought that the breaking or recoiling of individual flocs into smaller flocs

along with the scission and/or re-conformation of polymer chains could also occur (Fig. 6.2b). After shearing, it is expected that these smaller entities (flocs, particles and polymer chains) are able to interact in such a way that a better interconnected network is created (Fig. 6.2c). For the largest shear rate of 100 s^{-1}, the equilibrium structural parameter (G'_∞/G'_0) was then even larger than one (Table E3). This hypothesis of a densification of the network after shearing, when the interconnected structure has been broken in small entities, has in fact been predicted and experimentally observed in literature (Van Den Tempel, 1979).

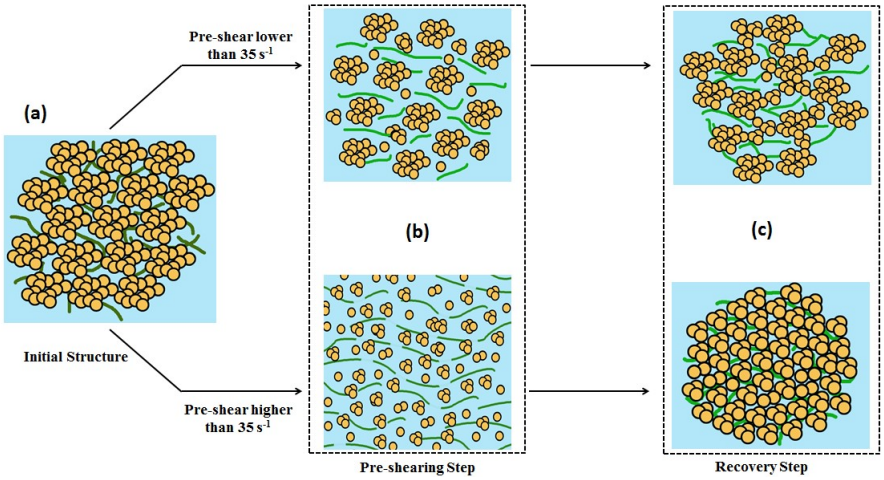

Figure 6.2: Schematic illustration of structural breakup and recovery at lower (< 35 s^{-1}) and higher (> 35 s^{-1}) pre-shear rate (a) initial structure, structural changes during the (b) pre-shearing step, and (c) recovery step

The time to reach 63% of G'_∞ (i.e., t_r) is shown in Fig. 6.1b as a function of pre-shear rate. As the equilibrium structural parameter (G'_∞/G'_0) decreases, at low pre-shear rates (< 35 s^{-1}), a decrease in recovery time (t_r) with increasing shear rate was also observed whereas a significant increase at higher shear rates was found. By applying smaller shear rates, as already explained previously (Fig. 6.2), the breakage of individual flocs is supposed not to be significant which is in accordance with smaller recovery times. As increasing the shear rate (below 35 s^{-1}) led to a lesser recovery, the recovery rate (see Fig. E3b in Appendix E) is increasing as function of shear rate. At high shear rates (above 35 s^{-1}), the breakdown of flocs is thought to be more pronounced with increasing shear rate which corresponded to a higher recovery time, a better recovery ($G'_\infty/G'_0 > 1$) and consequently a lower recovery rate. The same increase in characteristic time as a function of increasing pre-shearing rate is also observed for multi-walled carbon nanotubes (MWCNTs) based suspension in epoxy, by recording storage modulus as a function of time after pre-shearing and fitting the data to an exponential function (Khalkhal et al., 2011).

6.2.2. EFFECT OF PRE-SHEAR TIME

The evolution of the structural parameter ($G^{'}/G_0^{'}$) as a function of time for different pre-shearing duration and for two different pre-shear rates (10 and 30 s^{-1}) is shown in Fig. 6.3a and E4a. It is found that the influence of shearing duration on the structural evolution of the samples, for both shearing rates, was not very significant. As can be seen from Fig. E4b, the viscosity behaviour was, however, significantly different for these two cases. The model parameter of Eq. 2.4, presented in Tables E4 and E5, is also plotted as a function of pre-shearing time (Fig. 6.3b). For the lowest pre-shear rate (10 s^{-1}), the equilibrium structural parameter ($G_\infty^{'}/G_0^{'}$) was fluctuating as a function of pre-shearing time in the range (0.82 − 0.90) whereas for the highest pre-shear rate (30 s^{-1}), a decrease of $G_\infty^{'}/G_0^{'}$ as a function of pre-shearing time was found from 0.94 (t = 10 s) to 0.82 (t = 800 s). These findings are in line with the schematic illustration shown in Fig. 6.2.

Yüce and Willenbacher, 2017 investigated the effect of pre-shearing rate and time on the structural recovery of silver pastes. Their results revealed a strong dependency of the structural recovery on the pre-shear amplitude (i.e., lower recovery with higher pre-shear rate) whereas the recovery was not significantly affected by the pre-shear time. Similar results, i.e., structural recovery dependence on pre-shear rate and fairly independence of pre-shearing time was also observed for fumed silica suspensions and non-polar polymer/clay nanocomposites (Mobuchon et al., 2007, Raghavan and Khan, 1995).

At low pre-shear rate (10 s^{-1}), the viscosity displays an increase and then remained in good approximation constant as a function of time (Fig. E4b). However, at higher pre-shearing (30 s^{-1}), a continuous decrease in viscosity is observed. The observed overshoot in viscosity is related to the viscoelasticity of the material and it depends on the Deborah number (i.e., the ratio of relaxation time to experimental time). At low Deborah number (De), a typical increase in transient viscosity is usually observed. By increasing De (i.e. increasing the shear rate), the overshoot moves towards lower times. At very high De values, the overshoot cannot be observed as the experimental time is too fast. A monotonous decrease in viscosity is then observed.

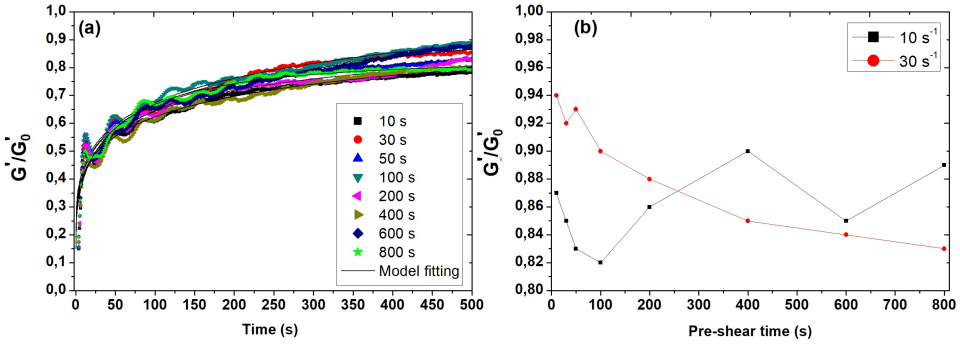

Figure 6.3: (a) Normalized storage modulus ($G^{'}/G_0^{'}$) as a function of time for different pre-shearing times using RT sediments pre-sheared at 30 s^{-1}; (b) equilibrium structural parameter ($G_\infty^{'}/G_0^{'}$) as a function of pre-shear time for different pre-shear rates.

6.2.3. EFFECT OF PRE-SHEAR RATE AND PRE-SHEAR TIME ON YIELD STRESSES

In addition to structural recovery, the influence of pre-shearing on the yield stresses of mud sediments was also investigated. The stress ramp-up experiments were performed immediately after the shearing step without the execution of any recovery step. Fig E5a and E5b show the results of stress ramp-up tests in terms of apparent viscosity as a function of stress for different pre-shearing rates and pre-shearing times, respectively. Two yield stresses, static and fluidic, were estimated from the two viscosity declines.

The correlation between the yield stresses and pre-shear rate or pre-shear time is shown in Fig. 6.4a and 6.4b, respectively. The yield stress values display a decrease with increasing shear rate up to a certain level and after which the values remain in good approximation constant (Fig. 6.4a). This behaviour may be attributed to the fact that when the structure was fully broken, the initial recovery of both micro and macro structures was faster than the experimental time of the stress ramp-up test. The yield stress values showed a decreasing trend as a function of pre-shear time as well (Fig. 6.4b). This reflects the extensive structural breakdown as a function of increasing shear time, as was already shown in Fig. 6.3b. Shear jamming was observed in the stress ramp-up experiments. This jamming occurred at high stresses and decreased as a function of pre-shear rate (see inset of Fig. E5a). The jamming remains the same for different pre-shearing times at 30 s^{-1} (see inset of Fig. E5b).

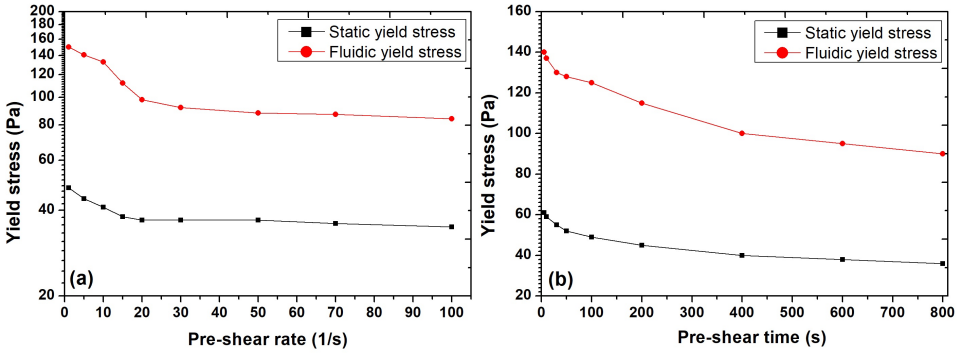

Figure 6.4: Correlation between the yield stresses, obtained from stress ramp-up tests, and the (a) pre-shearing rate and (b) pre-shearing time using RT sediments; the solid line is just a guide for the eye.

6.2.4. EFFECT OF STRUCTURAL RECOVERY TIME ON YIELD STRESSES

In natural environments, shear rates are time-dependent, and it is often so that the systems are not at full recovery. During the recovery phase, inter-particle forces will lead to the development of strength within the material structure. These natural systems, therefore, have time dependent yield stress and viscoelastic properties (Barnes, 1999). This time dependence was investigated by correlating the structural parameter ($G^{'}/G_0^{'}$), at a specific recovery time 't' chosen during the structural recovery step (Fig. E6), with its corresponding yield stresses. The pre-shear rate was taken to be 30 s^{-1} and was applied for 800 s. Fig. 6.5a displays the outcome of the amplitude sweep tests performed at different recovery times, i.e., for different $G^{'}/G_0^{'}$ values. The value, $G^{'}/G_0^{'}$ = 1, corresponds

to an experiment whereby the amplitude sweep test was performed right after the resting time (no pre-shear was applied). Two distinct declines (i.e., two-step yielding) in the storage modulus values were observed, associated to “static” and “fluidic” yield stresses. One can see that regardless of the recovery time, two yield stresses (i.e., two-step yielding) were always observed. This implies that even at very small recovery times (i.e. just after pre-shearing) the structure reforms at a macro-scale.

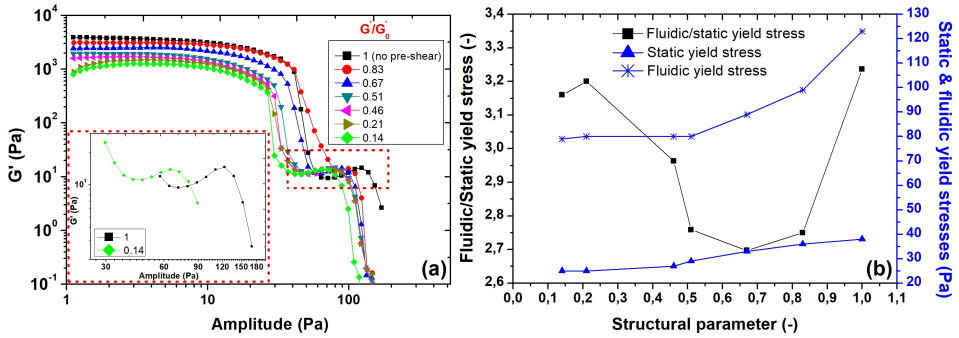

Figure 6.5: (a) Storage modulus as a function of amplitude for different values of structural parameter ($G^{'}/G^{'}_{0}$) using RT sediments, inset shows the plot of the dotted region at higher amplitudes, in order to clearly see the jamming phenomenon; (b) correlation between structural parameter and static, fluidic and fluidic/static yield stress values of RT sediments, the solid line is just a guide for the eye.

The correlation between the structural parameter ($G^{'}/G^{'}_{0}$) and the yield stresses is shown in Fig. 6.5b. It is found from the figure that the yield stresses show a sharp decline with decreasing structural parameter up to $G^{'}/G^{'}_{0} = 0.5$ and the yield stress values remained constant for $G^{'}/G^{'}_{0} < 0.5$. For $G^{'}/G^{'}_{0} < 0.5$, i.e. at small recovery times, both yield stresses were independent of the recovery time which implies that the restructuring within the sample at micro- and macro-scale was faster than the experimental time of the amplitude sweep (150 − 170 s). The values of the yield stresses were lower, implying that the micro and macro structures have not fully recovered. For higher recovery times, both static and fluidic yield stresses increased as function of the structural parameter, indicating that the stronger the micro-structure, the stronger the macro-structure. This is also in line with the conceptual representation displayed in Fig. 6.2 for high pre-shear rates. It can be noted from Fig. 6.5b that the ratio of fluidic to static yield stress showed a decline with increasing structural parameter for $G^{'}/G^{'}_{0} < 0.7$ and then a sudden increase for higher values of $G^{'}/G^{'}_{0}$. This may be linked with the fact that below the recovery time associated to $G^{'}/G^{'}_{0} = 0.7$, smaller or individual flocs remained the same (i.e., same fluidic yield stress) while the interconnected network of individual flocs (which gives rise to the static yield stress) was changing. On a side note, the existence of a jamming phenomenon was observed in the outcome of the amplitude sweep tests, in terms of an increase in storage modulus values at higher stress amplitudes (see inset of Fig. 6.5a). Such type of shear thickening/jamming behaviour in oscillatory amplitude sweep tests was also observed for fumed silica and Aeorsil nanoparticles-based suspensions (Fischer et al., 2007, Galindo-Rosales et al., 2009).

6.2.5. EFFECT OF SEDIMENT DENSITY

The effect of sediment density on the structural recovery was investigated by analysing different sediment layers collected from same location, in order to have similar organic matter content. The results for different sediment layers from RT location are presented in Fig. 6.6. The results display a decrease in recovered modulus values with the depth at which the samples were collected. This result was strongly correlated to the fact that the deeper the sediment, the higher the density. A high density leads to a higher structured network, which can be extensively disturbed by the shearing action. This also leads to lower structural recoveries in the sediments after the shearing step for higher sediment densities (i.e., smaller values of G'_∞/G'_0, see Table E6).

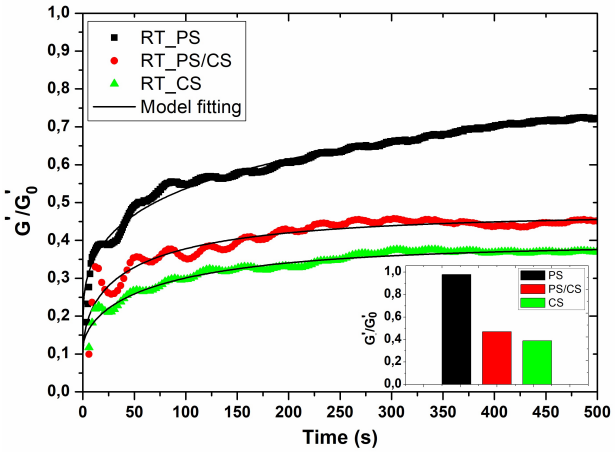

Figure 6.6: Normalized storage modulus (G'/G'_0) as a function of time for different mud layers collected from RT location pre-sheared at 100 s^{-1} using Couette geometry. Inset shows the equilibrium structural recovery (G'_∞/G'_0) for different mud layers.

6.2.6. EFFECT OF DILUTION

In addition to the natural density gradient (i.e., naturally existing mud layers), different mud densities were obtained in the laboratory by adding the water from the same location in the dense mud sample, as already discussed in Chapter 4. The structural recovery after pre-shearing in natural and diluted mud samples was then analysed. The structural growth in terms of normalized storage modulus as a function of time is shown in Fig. E7a and E7b for natural and diluted mud samples, respectively, obtained from location PK. It was found that the structural recovery, G'/G'_0 in natural mud samples decreased with increasing density, as already explained in previous section. However, the diluted mud samples displayed completely different behaviour (Fig. E7b). The values of the model parameters, Eq. 2.4 are presented in Table E7. The equilibrium structural recovery (G'_∞/G'_0) is plotted as a function of density for natural and diluted mud samples (Fig. 6.7). The natural samples displayed a decrease in structural recovery as a function of density while the diluted samples exhibited a significantly different behaviour with a maxima in the structural recovery curve. By diluting the initial dense mud sample, the

extent of structural recovery (G'_∞/G'_0) was first observed to increase and then decrease.

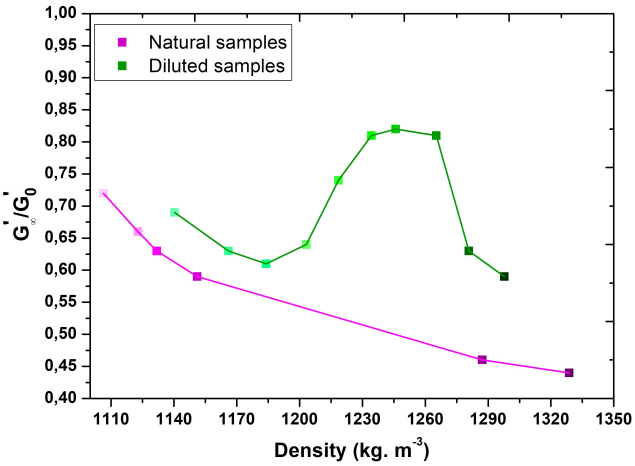

Figure 6.7: Equilibrium structural recovery (G'_∞/G'_0) as a function of density for natural and diluted mud layers from PK location. Solid lines are just the guide for the eye. The colour intensity of symbols increases with the density.

The possible explanation for the observed differences in structural recovery as a function of density between natural and diluted mud samples is the formation of heterogeneous micro-structures obtained by diluting the mud samples. These heterogeneous structures are likely to be created as hand mixing was used to prepare the diluted samples. This gentle mixing method was preferred to keep the mud as undisturbed as possible. Therefore, it is hypothesized that by diluting a mud suspension using hand mixing, the resulting system will be composed of large aggregates which will interconnect at rest with each other to form a space filling network (Fig. 6.8). This floc network may then break down into smaller flocs or individual particles during the pre-shear step of the structural recovery protocol. During the structural recovery step, a more homogeneous and stronger aggregate network is subsequently formed, which displays a better structural recovery. However, after a critical dilution, further dilution of the mud samples results in a network structure of smaller aggregates as it becomes easier to break the original flocs by hand mixing. The pre-shearing step for these samples was, therefore, not able to extensively disturb the structure and the resulting structural recovery is observed to decrease. This behaviour is also evident from the viscosity evolution as a function of time during pre-shear step (Fig. E8). The pre-shearing step extensively disturbed the dense mud samples (1265 – 1298 kg. m^{-3}) as can be seen from the significant decrease in viscosity even after 300 s. However, for lower density samples, a slight decrease in viscosity was observed initially. The viscosity remained constant after that initial decrease. This behaviour shows that the size of the aggregates, formed after dilution, is significantly dependent on both the degree of mixing and the concentration/density of the mud samples.

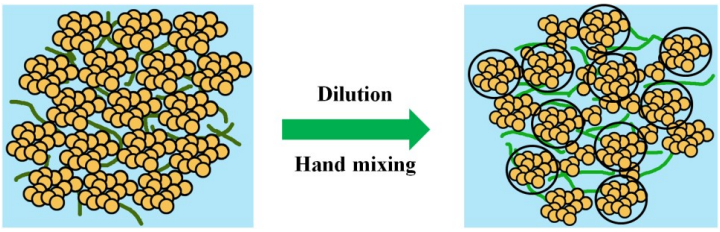

Figure 6.8: Schematic representation of structural rearrangements in mud sample after dilution via hand mixing. Yellow circles represent clay particles, green lines represent organic matter and black circles represent the clay aggregates.

6.3. DIFFERENT SEDIMENT LOCATIONS: EFFECT OF TOC CONTENT

THE effect of organic matter content on the structural recovery in mud sediments was investigated. Several samples were collected from different locations of Port of Hamburg with varying organic matter content. Fig. 6.9 shows the structural regrowth in mud sediments as a function of time for different samples pre-sheared at 100 s^{-1} using Couette geometry. Fig. 6.9 clearly shows that the sample with lowest organic matter content (SW) displays a higher recovery than the samples having higher organic matter (ZS, OK, DE and RV). Furthermore, in the case of sediments from SW location, the equilibrium structural recovery (G'_∞/G'_0) was higher than 1 (Table E8), which may be linked to the presence of higher amount of sand, (see particle size distribution of the sample from SW location in Fig. 2.3a). The shearing action is known to facilitate the settling of sand particles (Coussot, 1997). Because of the settling, a structure consisting of a majority of clay particles might be formed with a higher elasticity than the initial sediment sample (see Fig. 6.10). The settling of sand particles in sand-clay mixtures during flow and the resultant increase in yield stress values were reported in the literature (Ilstad et al., 2004). The extensive shearing of the samples having higher amount of organic content may cause severe destruction/re-conformation of the polymeric chains which are not able to regain their initial state after cessation of shearing (i.e., smaller values of G'_∞/G'_0, Table E8). Therefore, a large amount of polymers in a suspension is not beneficial for the structural recovery phenomenon, as also reported in literature for flocculated bentonite suspensions (Hammadi et al., 2014) and kaolinite suspensions flocculated with aluminium sulfate hydrate (Yu et al., 2011).

Fig. E9 shows higher structural recoveries for the sediments pre-sheared using vane geometry. The equilibrium structural parameter (G'_∞/G'_0) of the sediments pre-sheared by vane geometry is much higher than the one observed with Couette (see Table E9). This may be attributed to the fact that vane geometry is very effective in disturbing the macroscopic/bulk structure of the sample. During the recovery step, this bulk material can regrow to a stronger structure. This efficiency of the vane geometry to form highly structured samples has led to its utilization as a mixer for preparing polymeric blends with enhanced mechanical and structural properties (Qu et al., 2013, Xiaochun et al., 2015). As far as the characteristic time t_r is concerned, the effect of organic matter was

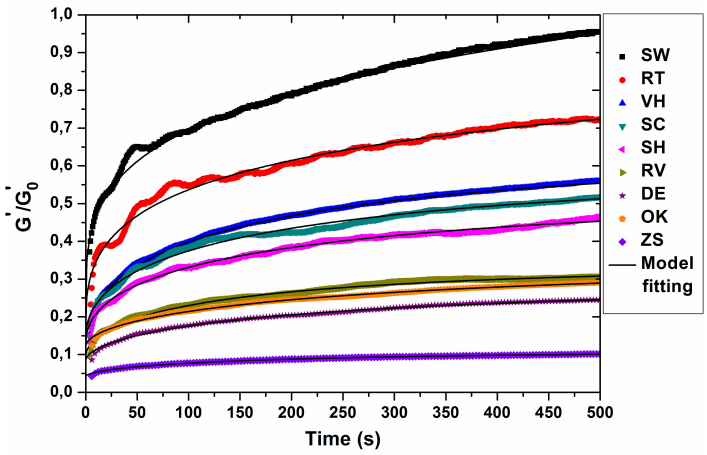

Figure 6.9: Normalized storage modulus ($G^{'}/G^{'}_{0}$) as a function of time for different pre-consolidated (PS) sediment samples pre-sheared at 100 s^{-1} using Couette geometry.

not very significant on its value for both Couette and vane geometries. This implies that the vane geometry was useful in attaining stronger equilibrium structures of the sediments without affecting their characteristic recovery time (t_r).

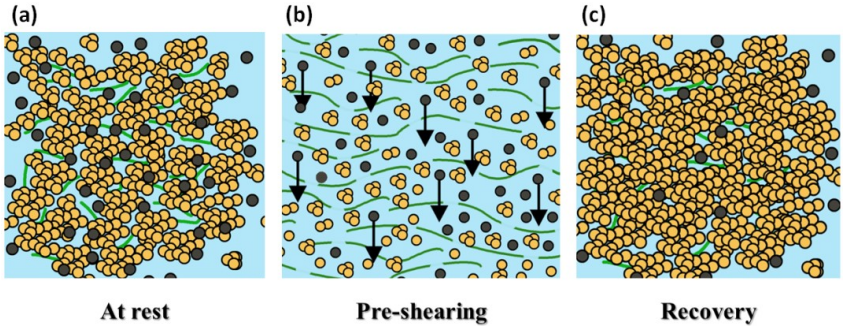

Figure 6.10: Schematic illustration of structural breakdown and recovery in sediments from SW location (a) initial sample, (yellow circles represent clay particles), (b) structural changes during the pre-shearing step, black arrows represent the settling of sand particles (shown as black circles) during shearing action, (c) structural changes during recovery step.

This study was focused on the structural recovery in mud sediments after a steady pre-shearing action, which is different from the concept of thixotropy (i.e., continuous decrease in viscosity with shearing action and the subsequent recovery of viscosity in time when the applied shear is removed). However, both these approaches provide similar outcome regarding the thixotropic character of the sample. From this study, it was found that the mud layer with lowest density displayed faster structural recovery than the one with highest density. Likewise, for similar mud samples, the area of thixotropic loop (upward and downward viscosity/stress curve) was very small for the mud sample with

lowest density (see Fig. 4.8). This behaviour can be related to a very fast structural recovery in lower density mud samples. The area of thixotropic loop for dense mud layers, on the other hand, was significant implying a slower recovery. The insight into the rheological behaviour of natural muddy sediments, in particular the effect of pre-shearing on structural recovery is very important. This has wide implications for a marine environment as this rheological behaviour will influence the mud re-suspension behaviour, bed stability, erosion, sediment mixing, turbulence damping and also the ability to define navigable mud layers.

6.4. CONCLUSIONS

IN this chapter, the structural recovery of mud sediments was investigated by varying different pre-shearing conditions. The structural recovery behaviour of mud samples from one location (RT) was first thoroughly studied. The equilibrium structural recovery ($G^{'}_{\infty}/G^{'}_{0}$) of the sediments obtained from the RT location displays an interesting behaviour as a function of pre-shearing rate with a minimum value at 35 s^{-1} and an increase in structural parameter after this pre-shear rate. This behaviour is linked with the existence of two structure levels (i.e., two-step yielding). The structural parameter ($G^{'}/G^{'}_{0}$) is observed to be strongly correlated to the yield stress values up to a certain value ($G^{'}/G^{'}_{0}$ = 0.5). Below this value of structural parameter, it is found that the structural recovery is faster than the time required to perform the dynamic amplitude sweep tests.

The equilibrium structural recovery ($G^{'}_{\infty}/G^{'}_{0}$) is independent of shearing time but a higher structural recovery was obtained with vane geometry as compared to the Couette geometry. The highest values for equilibrium structural recovery ($G^{'}_{\infty}/G^{'}_{0}$) are found for the sediments having the lowest density and lowest organic matter content. The characteristic time of recovery (t_r) is found to be significantly affected by the pre-shear rate. This study provides an extensive knowledge about the structural recovery in mud sediments as a function of different pre-shearing conditions. This knowledge is especially important for a proper modelling of mud dynamics in in-situ conditions, as it highlights the relevant timescales and system behaviour associated to the changes in shear stresses.

7

ORGANIC MATTER DEGRADATION

The presence of organic matter in cohesive sediment results in the formation of clay-organic matter flocs, which leads to complex rheological behaviour including shear-thinning, viscoelasticity, thixotropy and two-step yielding in mud. In this chapter, the influence of the microbial degradation of sediment organic matter on the rheological properties of mud samples was studied. This study provides a thorough understanding of the influence of organic matter degradation on the rheological properties of mud, which can be used to optimize sediment management strategies in ports and waterways.

Parts of this chapter have been published in Journal of Soils and Sediments (Zander, Shakeel, et al., 2022, Shakeel et al., 2022).

7.1. INTRODUCTION

ORGANIC matter (OM) in water-sediment systems originates from (i) natural sources including plant litter, eroded topsoils, pelagic and planktonic biomass, or (ii) anthropogenic sources such as surface runoff and urban sewage, as listed in Zander et al., 2020. Organic matter can be either suspended in the water phase, as pure organic matter or bound to fine and still suspended mineral particles, or be bound to the already settled sediment. In suspensions, organic matter can interact with clay particles either by creating bridges between the particles or by charge neutralization (Lagaly and Dékány, 2013), forming a flocculated system. The presence of these clay-organic flocs typically results in a complex rheological fingerprint of mud, including shear thinning, viscoelasticity, thixotropic behaviour and two-step yielding (Coussot, 1997, Van Kessel and Blom, 1998, Shakeel et al., 2020b, Shakeel et al., 2020d). For instance, a significant increase in rheological properties (i.e., yield stresses, moduli and thixotropy) was observed for mud samples having a high organic matter content, which may be attributed to the formation of a strong network of clay-organic flocs (Shakeel, Kirichek, and Chassagne, 2019).

Under anaerobic conditions, the microbial degradation of sediment organic matter results in the formation of carbon dioxide (CO_2) and methane (CH_4). These greenhouse gases are either released through the water column or remain entrapped in the mud layers. Entrapped gas bubbles sample are found to affect the rheological properties and the density of mud and to be responsible for delayed consolidation. Given the role of clay-organic flocs for the rheological and cohesive properties of mud (Tolhurst et al., 2002, Wurpts and Torn, 2005, Malarkey et al., 2015, Schindler et al., 2015, Parsons et al., 2016, Shakeel, Kirichek, and Chassagne, 2019), degradation of organic matter can be expected to significantly influence the rheological fingerprint of mud. For the investigation area, Zander, Groengroeft, et al., 2022 have shown that the organic matter present in the sediment can be separated into differently degradable pools based on their degradation kinetics and corresponding half-lives (Zander, Groengroeft, et al., 2022). However, a systematic analysis of the hypothesized effect of organic matter degradation on the rheological properties of mud is still missing.

The main aim of this chapter was, therefore, to investigate whether the microbial degradation of organic matter resulted in any significant effect on the rheological properties of fine-grained sediments. To this end, the rheological properties of freshly sampled and thereafter further microbially degraded mud of similar densities, collected from different locations of the Port of Hamburg, Germany, are analyzed. In the first part of study, the rheological analysis of fresh samples and samples degraded for 250 days is compared, while in the second part, the effect of degradation time on the rheological properties is studied. In the end, the microbial degradation of organic matter under both anaerobic and aerobic conditions is compared and discussed.

7.2. ANAEROBIC DEGRADATION

7.2.1. FIXED DEGRADATION TIME

The rheological analysis of fresh samples thereafter degraded for 250 days was performed for the PS mud layer collected from three different locations of Port of Hamburg (RV, RT

and KH). The differences between rheological properties for these samples are reported in this subsection.

BULK DENSITY

The excess bulk density ($\rho - \rho_w$) of a fresh sample, where ρ_w is the density of water, was plotted as a function of the change in excess bulk density obtained by the difference between excess bulk density of degraded and fresh mud samples (Fig. F1). It is found that the change in bulk density occurring during the long-term (250 days) incubation period was lower than 5% of its original value. It was, therefore, assumed that changes in rheological properties between fresh and degraded samples reported in the following subsections were not related to the change in density.

YIELD STRESS

In order to investigate the influence of organic matter degradation on the yield stress of mud, stress ramp-up tests were performed. Fig. F2 shows the behaviour of apparent viscosity as a function of shear stress for fresh mud samples and mud samples that have been degraded for 250 days. A two-step yielding behaviour was clearly identified from the two declines in viscosity. The example given in Fig. F2 shows that degraded mud has lower yield stress values than fresh mud. It is hypothesized that the decrease in yield stresses upon microbial decay has a biological and a physical origin. Microbial breakdown of organic bridging between particles reduces particle-particle interactions (biological origin). The presence of gas resulting from anaerobic decay causes a decrease in bulk density, leading to further decline in yield stress (physical origin – triggered by biochemical factors). The later was supported by Jommi et al., 2019 who found that the presence of gas must be accounted for when studying the reduction in shear stresses by organic matter decay. A decrease in yield stress values by removing the organic matter content was also reported in literature for fine-grained sediments (Faas and Wartel, 2006).

In order to further quantify the effect of organic matter degradation on the yield stress of mud samples from different locations, the change in static and fluidic yield stresses (degraded – fresh) was plotted as a function of yield stress of fresh samples in Fig. 7.1. A decrease in yield stress values is observed as a consequence of the degradation of organic matter, for all the investigated locations. Moreover, this decrease in yield stresses was found to be strongly correlated to the yield stress values of the original, freshly sampled mud, i.e., the higher the original yield stress, the higher its reduction as a result of organic matter degradation (resulting in a negative slope). This shows that the effect of organic matter degradation on the yield stresses was more pronounced for the mud samples having higher yield stress values before degradation. The higher yield stress values of mud samples are typically associated to either higher density or higher organic matter content (Van Kessel and Blom, 1998, Soltanpour and Samsami, 2011, J. Xu and Huhe, 2016). In order to compare the effect of organic matter degradation on different rheological properties (i.e., yield stress, moduli and structural recovery), the following empirical equation was used to fit the experimental data of change in rheological property (degraded – fresh) as a function of the same rheological property before degradation, for all the locations:

$$y = a + bx \tag{7.1}$$

where a and b represent the intercept and slope of the line, respectively. For instance, the values of a and b were observed to be 0.99 and −0.37 for static yield stress and 1.73 and −0.28 for fluidic yield stress. The values of the slope clearly indicate that the yield stresses (static and fluidic) were reduced by 1/3 of its original value due to the degradation of organic matter.

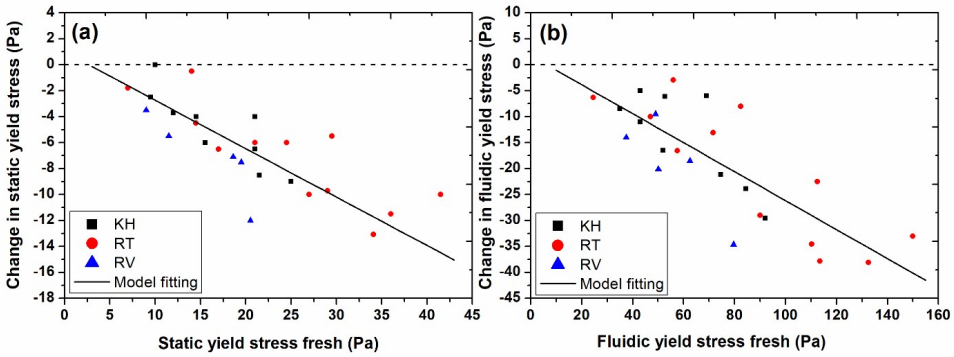

Figure 7.1: (a) Change in static yield stress (degraded – fresh) as a function of static yield stress of fresh mud sample from different locations, and (b) change in fluidic yield stress (degraded – fresh) as a function of fluidic yield stress of fresh mud sample from different locations. The dashed line represents the value where the degraded and fresh mud samples have same yield stresses. The solid line represents the empirical fitting using Eq. 7.1.

7

CROSS-OVER AMPLITUDE

In addition to the yield stress of mud samples, the solid-liquid transition (a crossover between $G^{'}$ and $G^{''}$) was studied by performing oscillatory amplitude sweep tests at 1 Hz. Fig. 7.2a presents the storage and loss moduli as a function of oscillatory amplitude for fresh mud sample and mud sample degraded for 250 days. The results confirmed the existence of a two-step yielding behaviour (i.e., two declines in moduli) in mud samples. A linear viscoelastic (LVE) regime was identified from an independent behaviour of moduli at smaller amplitudes, which also provided essential information to perform frequency sweep tests within LVE regime. Apart from LVE regime, the solid-liquid transition was estimated from the crossover between $G^{'}$ and $G^{''}$ and the corresponding amplitude was stated as crossover amplitude. Fig. 7.2a clearly depicts a decrease in crossover stress by the degradation of organic matter, which is in accordance with the yield stress analysis. Change in crossover amplitude (degraded – fresh) is plotted as a function of crossover amplitude of fresh mud sample for different locations (see Fig. 7.2b). The results again show the significant effect of organic matter degradation on the crossover amplitude for the mud samples having higher crossover amplitude before degradation. This experimental data was also fitted with Eq. 7.1 and the values of a and b were found to be 0.49 and −0.35, respectively.

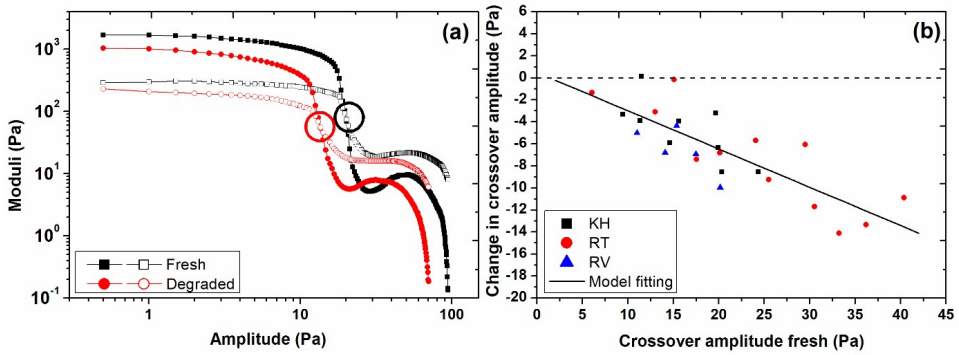

Figure 7.2: (a) Storage (filled symbols) and loss (empty symbols) moduli as a function of oscillatory amplitude for fresh mud sample and mud sample degraded for 250 days, collected from KH location. The circles represent the crossover amplitude. (b) change in crossover amplitude (degraded – fresh) as a function of crossover amplitude of fresh mud sample from different locations. The dashed line represents the value where the degraded and fresh mud samples have the same crossover amplitude. The solid line represents the empirical fitting using Eq. 7.1

MODULI

In order to analyze the strength of mud samples before and after degradation of organic matter, frequency sweep tests were performed within LVE regime (i.e., without affecting their structure) from 0.1 to 100 Hz. The outcome of frequency sweep tests is shown in terms of complex modulus and phase angle as a function of frequency for fresh mud sample and mud sample degraded for 250 days, see Fig. F3a and F3b. Both fresh and degraded mud samples showed solid-like character, i.e., an almost independence of complex modulus on frequency and significantly smaller values of phase angle (Lupi et al., 2016). However, a weaker system (with lower complex modulus and higher phase angle values) was observed after the degradation of organic matter as compared to the fresh mud sample. The values of complex modulus and phase angle at 1 Hz were selected to investigate the effect of organic matter degradation on the strength of mud samples from different locations. Fig. 7.3a shows the correlation between the change in complex modulus (degraded – fresh) and the values of complex modulus of fresh mud samples for different locations. A decrease in complex modulus was observed due to the degradation of organic matter, which became more pronounced for the fresh samples having higher complex modulus, which may again be linked to the higher density of the samples. The empirical fitting of the experimental data of complex modulus using Eq. 7.1 resulted in the values of 92.9 and −0.49 for a and b, respectively. The correlation between the change in phase angle (degraded – fresh) and the values of phase angle of fresh mud samples, for different locations, was not very prominent (Fig. 7.3b). However, the degraded samples exhibited slightly higher values of the phase angle as compared to the fresh mud samples (i.e., positive values of change in phase angle), which indicated a weaker system, as already observed from other results.

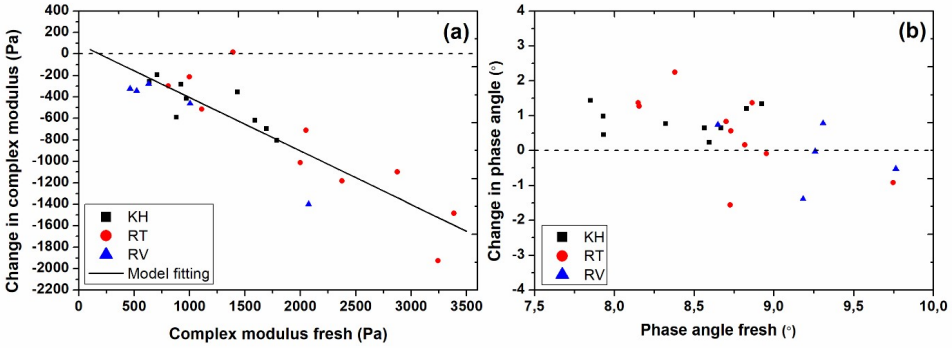

Figure 7.3: (a) Change in complex modulus (degraded – fresh) at 1 Hz as a function of complex modulus at 1 Hz of fresh mud sample from different locations. The solid line represents the empirical fitting using Eq. 7.1, (b) change in phase angle (degraded – fresh) at 1 Hz as a function of phase angle at 1 Hz of fresh mud sample from different locations. The dashed line represents the value where the degraded and fresh mud samples have same complex modulus or phase angle at 1 Hz.

THIXOTROPY

The thixotropic behaviour of fresh and degraded mud samples was analyzed by performing shear rate controlled ramp-up and ramp-down experiments from 0 to 100 s^{-1}. The outcome of shear rate ramp-up and ramp-down experiments display the existence of a typical thixotropic character (clockwise loop) at higher shear rates for both fresh mud sample and mud sample degraded for 250 days (Fig. 7.4a). However, at lower shear rates, an anti-thixotropic character (counterclockwise loop) was observed, which may be attributed to a shear thickening phenomenon or the structural reorganization due to the shearing action. A similar combination of thixotropy and anti-thixotropy as a function of shear rate has been reported in literature for fine-grained sediments (Yang, Yu, et al., 2014). Furthermore, the values of shear stress as a function of shear rate was significantly lower for the degraded mud sample as compared to the fresh mud sample, which is again in line with the previous results. The hysteresis area between the clockwise loop (i.e., typical thixotropic character) of the ramp-up and ramp down curves was estimated in order to investigate the effect of organic matter degradation on the thixotropic character of mud samples. The change in hysteresis area (degraded – fresh) as a function of the values of hysteresis area of fresh mud samples, for different locations, is presented in Fig. 7.4b. A similar influence of organic matter degradation was observed on hysteresis area (i.e., thixotropy) as already observed for other rheological properties including yield stresses and moduli. The empirical fitting of Eq. 7.1 for thixotropic data resulted in the values of 39.84 and −0.29 for a and b, respectively. This decrease in hysteresis area also indicate that the degraded mud sample behave closer to the mineral suspension as the hysteresis comes mainly from the organic matter.

It is interesting to note that the value of parameter b (i.e., slope) is similar, within the range of 0.28 to −0.49, for different rheological properties. This behaviour suggests that the overall influence of organic matter degradation is similar on different rheological properties, i.e., the extent of decrease in rheological properties as a function of organic

matter degradation is similar. This similar effect on different rheological properties is linked to the fact that these properties represent either the structure of mud samples at "rest" or the destruction of structure from an undisturbed state.

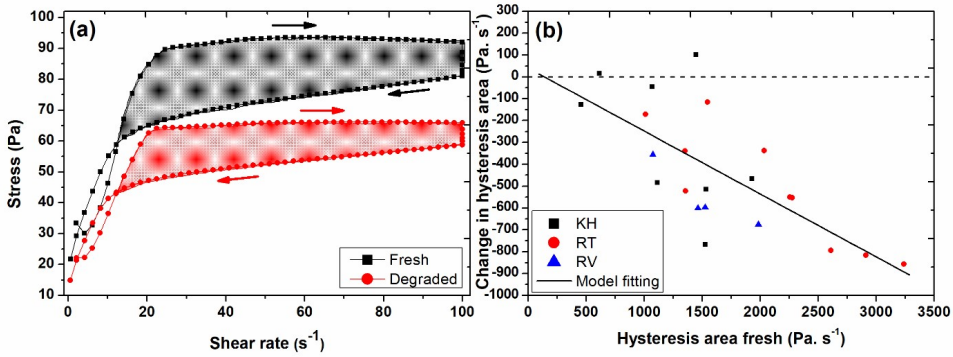

Figure 7.4: (a) Shear stress as a function of shear rate obtained by performing shear rate controlled ramp-up and ramp-down experiments for fresh mud sample and mud sample degraded for 250 days, collected from KH location. The direction of arrows represent the ramp-up or ramp-down curve. The filled region represent the hysteresis area, (b) change in hysteresis area (degraded – fresh) as a function of hysteresis area of fresh mud sample from different locations. The dashed line represents the value where the degraded and fresh mud samples have same hysteresis area. The solid line represents the empirical fitting using Eq. 7.1.

STRUCTURAL RECOVERY

In addition to the thixotropic character of fresh and degraded mud samples, the structural recovery after intensive pre-shearing was investigated using a three step protocol explained in Sec. 2.4.3. The normalized time dependent storage modulus (G'/G'_0) as a function of time for fresh mud sample and mud sample degraded for 250 days is presented in Fig. F4. The results show higher normalized modulus values, at any particular time, for the degraded mud samples as compared to the fresh mud samples.

In order to further quantify the structural recovery behaviour of fresh and degraded mud samples, Eq. 2.4 was used to fit the experimental data of third step of structural recovery protocol. The change in normalized equilibrium storage modulus, G'_∞/G'_0 (degraded – fresh) as a function of the values of normalized equilibrium storage modulus of fresh mud samples is plotted in Fig. 7.5a for different locations. It can be seen that the values of normalized equilibrium storage modulus (G'_∞/G'_0) are higher for the degraded mud samples (i.e., positive values of change in normalized equilibrium storage modulus) than for the fresh mud samples. This may be attributed to the fact that the degradation of organic matter result in a weaker system, behaving as a purely mineral suspension without the bridging effect provided by organic matter, which eventually has a better structural recovery (i.e., higher values of modulus, higher strength) after pre-shearing.

Furthermore, Fig. 7.5b shows a strong correlation between the change in characteristic time, t_r (degraded – fresh) and the values of characteristic time of fresh mud samples, for different locations, as already observed for other rheological properties. In this case, the values of the fitting parameters, a and b, were observed to be 206.7 and −1.06, re-

spectively. It is clear that the slope (b) of the fitting line (Eq. 7.1) of the change of characteristic time over characteristic time found for the fresh sample is significantly different from the value of slope for the change of other investigated rheological properties. This is due to the fact that other rheological properties (i.e., yield stresses and moduli) represented the strength of mud samples before any disturbance while the characteristic time showed the recovery behaviour of structure/strength in mud after complete breakdown. Moreover, it is interesting to note that below a certain characteristic time for the fresh mud sample (i.e., ~200 s), the value for characteristic time of degraded mud samples was higher than for the fresh samples while above this critical value of time, the characteristic time of degraded mud samples showed a decrease as compared to the fresh mud samples. This behaviour may again be linked to the variable density of the mud samples, in addition to the organic matter degradation.

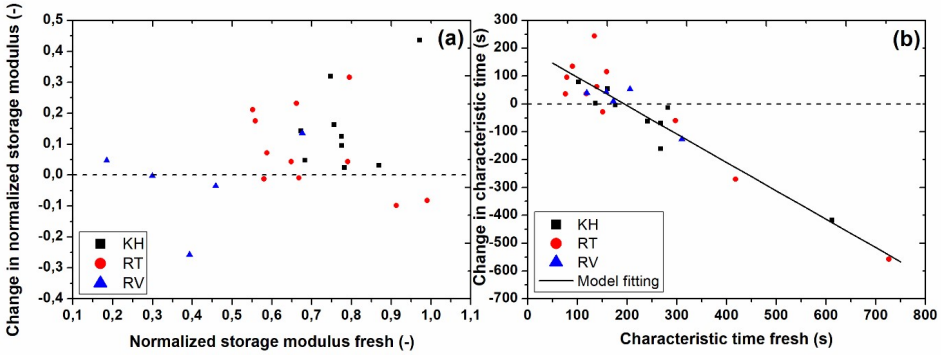

Figure 7.5: (a) Change in normalized equilibrium storage modulus, G'_{∞}/G'_0 (degraded – fresh) as a function of normalized equilibrium storage modulus, G'_{∞}/G'_0 of fresh mud sample from different locations, and (b) change in characteristic time, t_r (degraded – fresh) as a function of characteristic time, t_r of fresh mud sample from different locations. The dashed line represents the value where the degraded and fresh mud samples have same normalized equilibrium storage modulus or characteristic time. The solid line represents the empirical fitting using Eq. 7.1.

7.2.2. EFFECT OF DEGRADATION TIME

The rheological analysis of degraded mud, discussed so far, was performed for the samples degraded for 250 days. The change in different rheological properties is plotted as a function of degradation time, see Fig. 7.6. For instance, the change in yield stresses (static and fluidic), crossover amplitude and complex modulus (degraded – fresh) as a function of degradation time showed two critical values of degradation time after which the change in rheological properties was significant (Fig. 7.6a and 7.6b). Initially, after 3 days of degradation, a significant decrease in above mentioned rheological properties was observed, which became constant until 150 days, and after that a further decrease in rheological properties was evident. This behaviour may be attributed to the presence of differently degradable organic matter pools which have also been identified by analysis of degradation kinetics (Zander, Groengroeft, et al., 2022), which dominated degradation at different incubation time. Further detailed analysis of the influence of short term

degradation on the rheological properties of mud samples is reported in Zander, Shakeel, et al., 2022.

The extent of structural recovery after pre-shearing, represented by the normalized equilibrium storage modulus (G'_∞/G'_0), was higher for the degraded mud sample as compared to the fresh mud sample, for all the investigated degradation time intervals (Fig. 7.6c). This behaviour again suggested the better structural recovery in degraded mud due to the weaker system that upon degradation of bridging organic matter behaves like a purely mineral system, even after 3 days of degradation. The change in characteristic time (t_r), however, displayed a significant increase as a function of degradation time (Fig. 7.6d). This may be attributed to the fact that the characteristic recovery time of fresh mud sample was lower than 200 s, which resulted in longer characteristic time of degraded mud sample, as already explained in Fig. 7.5b.

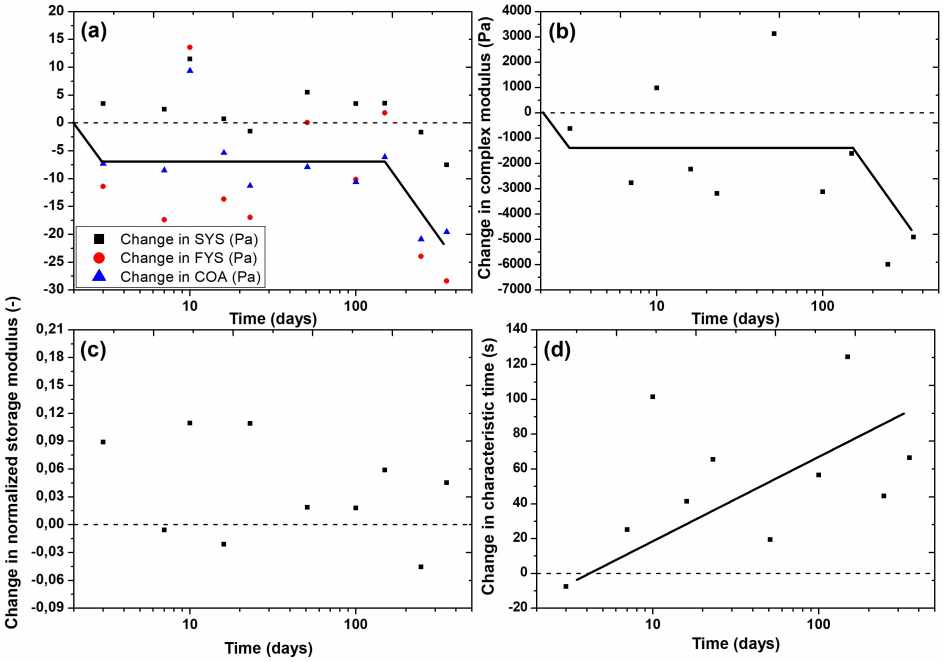

Figure 7.6: (a) Change in static yield stress (SYS), fluidic yield stress (FYS) and crossover amplitude (COA) as a function of degradation time, (b) change in complex modulus at 1 Hz as a function of degradation time, (c) change in normalized equilibrium storage modulus, G'_∞/G'_0 as a function of degradation time, and (b) change in characteristic time, t_r as a function of degradation time for the mud sample collected from RT location. The dashed line represents the value where the degraded and fresh mud samples have same rheological property. The solid line is a guide for the eye.

7.2.3. EFFECT OF BULK DENSITY AND TOC CONTENT

In addition to the PS mud layer from certain locations, the influence of bulk density and TOC content on the degradation of organic matter and the resultant rheological properties was investigated by considering different mud layers (i.e., FM, PS and CS) from dif-

ferent locations of Port of Hamburg. The change in fluidic yield stress (degraded – fresh) as a function of fluidic yield stress of fresh mud samples is plotted in Fig. 7.7a for different mud layers from KH location. The result shows the clear differences for the change in fluidic yield stress between the fluid mud (FM), pre-consolidated (PS) and consolidated (CS) mud layers. The largest absolute change of fluidic yield stress was observed for the denser, i.e. deeper and more consolidated layer (CS). On average, the change in fluidic yield stresses were about threefold larger than the change in static yield stresses. Due to the fact that the absolute change in yield stress was the largest for CS layer, data from these layers were then used to investigate a possible spatial trend in more detail. The change of fluidic yield stress showed clear decrease from upstream to downstream locations for anaerobic organic matter decay (see Fig. 7.7b).

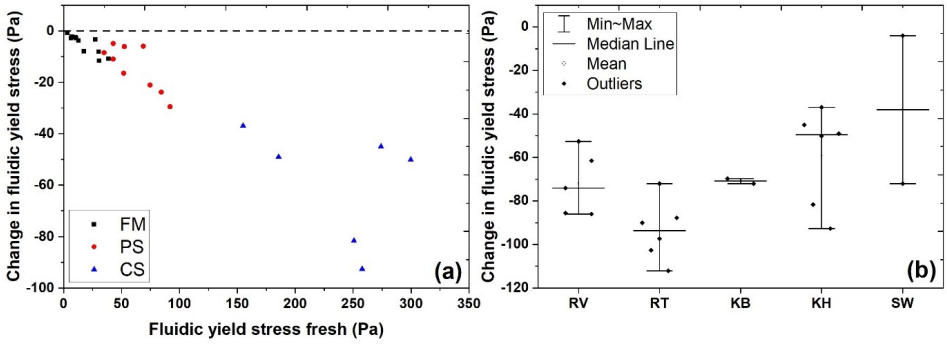

Figure 7.7: (a) Change in fluidic yield stress (degraded – fresh) as a function of fluidic yield stress of fresh mud samples representing different mud layers from KH location. The dashed line represents the value where the degraded and fresh mud samples have same yield stresses, (b) change in fluidic yield stress for consolidated (CS) mud layer from different locations. (RV = 6.2% TOC, RT = 4.1% TOC, KB = 3.4% TOC, KH = 3.8% TOC, SW = 2.6% TOC).

The top fluidic sediment layers (FM) show the lowest absolute yield stress change. These FM layers contain the highest share of organic carbon in the light density fraction, SOM degradability and SOM pools (Zander et al., 2020, Zander, Groengroeft, et al., 2022), corroborating the relevance of easily degradable organic matter for the effects of SOM decay on the rheological behaviour of sediments. The more dense layers (i.e. CS layer) showed the largest change between the initial and the decayed yield stress (Fig. 7.7a). This appears plausible as more consolidated sediments have more mass and hence more degradable carbon per unit volume than less consolidated or fluidic sediments, leading to a higher absolute reduction of yield stresses. Jommi et al., 2019 described that gas in peat layers led to a dramatic reduction of the mobilised (load below maximum) shear strength, although the ultimate (maximum) shear strength was hardly affected. The spatial trends of the yield stress change (Fig. 7.7b) coincide with the known stratification of organic matter content and its degradability, with higher microbial mass and its degradability in upstream locations and lower microbial mass and its degradability in downstream samples. Upstream locations (RV and RT) showed the greatest absolute changes in yield stress for consolidated layers, reflecting the higher share of easily available organic matter and the largest amount of degradable carbon at these sites (Zander, Sha-

keel, et al., 2022). Moreover, the yield stress–density correlation for degraded mud shows similar slope (parameter b) while lower intercept value (parameter a) as compared to the fresh mud for power law fitting (see Fig. F5). This result verifies the correlation between parameter a and TOC, as discussed in Chapter 5.

7.3. ANAEROBIC VERSUS AEROBIC DEGRADATION

In addition to the anaerobic degradation, the mud samples were also degraded under aerobic conditions, as explained in Sec. 2.8. The change of fluidic yield stress shows a decrease in yield stress after anaerobic SOM decay (i.e., negative values), which is attributed to the biological mechanism (breakdown of bridging between organic matter and clay particles) and physical mechanism (entrapment of gas bubbles). However, a partial increase in yield stress values is observed after aerobic decay with a large scatter (see Fig. 7.8). This behaviour may be attributed to the fact that mud samples naturally occur under anaerobic conditions and the metallic ions (i.e., Fe) typically present in adsorbed state under these conditions. However, by putting these samples under aerobic conditions, the liberation of these metallic ions can be facilitated (Zhang et al., 2014) and produce binding effect with clay particles or make metal complexes, which in turn compensate the decrease in yield stresses due to the organic matter degradation. Under in-situ conditions, FM layer is typically degraded under aerobic conditions, however, due to their lower density, the influence of organic matter degradation on the rheological properties is not very evident for this mud layer. This result clearly indicate that the degradation of organic matter under different conditions can totally change the rheological properties of mud samples. However, the influence of aerobic degradation of organic matter on the rheological properties of mud needs further investigation.

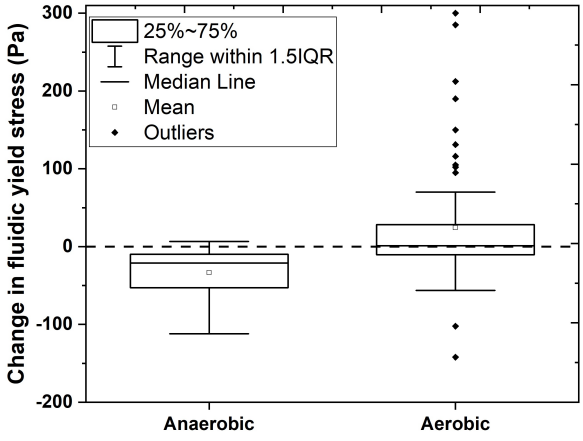

Figure 7.8: Change in fluidic yield stress (degraded – fresh) of mud samples from different mud layers and from different locations (RV, RT, KB, KH and SW) under anaerobic and aerobic degradation conditions. The dashed line represents the value where the degraded and fresh mud samples have same yield stresses. 1.5IQR = factor 1.5 of the interquartile range (25% – 75%).

7.4. CONCLUSIONS

The presence of organic matter in cohesive sediments results in the formation of clay-organic flocs, which eventually leads to complex rheological behaviour including shear-thinning, viscoelasticity, thixotropy and two-step yielding in mud. However, this organic matter undergoes microbial degradation under in-situ conditions and produces CO_2 and CH_4. Apart from producing greenhouse gases, organic matter degradation can significantly affect the rheological properties of mud by diminishing organic bridges between mineral particles and hence changing the clay-organic floc structures. Therefore, in this study, the influence of organic matter degradation on the rheological properties of mud samples was examined. The mud samples were collected from different depths and locations of the Port of Hamburg, Germany, in order to have varying bulk density and organic matter content.

The results show a significant decrease in rheological properties including yield stresses (static and fluidic), crossover amplitude, complex modulus and thixotropic hysteresis area for degraded mud samples as compared to the fresh mud samples. The slopes (b) of the lines, correlating the change (degraded – fresh) in above mentioned rheological properties as a function of the same rheological property of the fresh mud, are similar and vary within the range of –0.28 to –0.49. This behaviour shows that the influence of organic matter degradation is similar for all the rheological properties representing the strength of mud samples. Moreover, the fact that organic matter degradation results in a decrease in rheological properties of mud is an indirect proof of a concept that the organic matter interacts (either by bridging or charge neutralization) with the clay particles to form clay-organic flocs. The structural recovery tests displayed a higher extent of recovery in mud after pre-shearing for the degraded mud than for the fresh mud, which suggests the existence of a pure clay-dominated, OM-depleted system after organic matter degradation. The behaviour of the characteristic recovery time (t_r) shows that below a certain value for fresh mud sample (i.e., ~200 s), the characteristic time of degraded mud samples is higher than the fresh samples while above this critical value of time, the characteristic time of degraded mud samples show a decrease as compared to the fresh mud samples. The effect of degradation time on the rheological properties of mud samples display two critical time periods (3 days and 150 days) after which a significant change in rheological properties of mud samples is observed, which may be attributed to the presence of two differently degradable pools of organic matter in the considered mud sample. The influence of microbial degradation on the rheological properties is more pronounced for CS mud layers and also for the samples collected from upstream locations, due to the higher organic matter content or its higher degradability. The observed decrease in rheological properties of mud under anaerobic conditions is not clearly observed for aerobic degradation, which is attributed to the release of adsorbed metallic ions and the resultant binding between clay particles and metallic ions. Hence, this study provided a useful understanding about the influence of organic matter degradation on the rheological properties of mud, which can be used to optimize the sediment management strategies in ports and waterways.

8

CONCLUSIONS AND FUTURE DIRECTIONS

This chapter summarises the outcomes of the dissertation in the form of answers to the sub-questions and the main research question presented in Chapter 1. The main findings of the research are given, along with critical comments. Finally, recommendations for further research are presented.

8.1. ANSWERS TO THE KEY RESEARCH QUESTIONS

Safe navigation in ports and waterways is ensured by maintaining a desired nautical bottom, i.e., the level based on which Under-Keel Clearance (UKC) is defined. Most of the port authorities choose bulk density as a criterion for nautical bottom as, for instance, Port of Rotterdam. As navigability is strongly linked to the flow properties of the water-mud medium, rheological properties like viscosity and yield stress (i.e., stress required to initiate the flow of mud) are more suitable physical parameters for the nautical bottom. The relation between density and yield stress can be significantly influenced by several parameters including type and content of organic matter, clay type, particle size distribution (PSD) and salinity. Hence, it is difficult and impractical to choose a critical value of the density for the whole port that has varying above mentioned parameters in different port areas. Therefore, a rheological property (i.e., yield stress) is a more appropriate parameter to define the nautical bottom. This leads to the main research question of the present study: "How are the rheological properties of mud influenced by different parameters including organic matter content, bulk density and sampling locations"? However, in order to answer the main research question, several key research questions are to be answered first.

Which rheological geometry and rheological protocol are appropriate to analyse the yield stresses of harbour mud?

Couette geometry is an adapted geometry to analyse mud samples in this study because the average particle size of all investigated samples was much smaller than the gap between bob and cup. Vane geometry is to be used in case of consolidated systems (solid-like), where Couette geometry cannot be used because the bob can get stuck during the experiment and wall slip could occur. Parallel plate geometry is not a suitable option for investigating diluted liquid-like samples because the sample can spread out of the gap during the shearing action. Parallel plate geometry can, however, be a good option to measure the absolute values of yield stresses because it offers less disturbance in the sample structure when the top plate is set into place prior the experiment. Cone and plate geometry is not designed for mud sediments having large particles because of the very narrow gap between the cone and plate. This study showed that Couette and parallel plate geometries are the most suitable geometries for analysing all the structural break-downs of the samples.

Among conventional rheological protocols, creep test is not a straightforward method for analysing the yield stress values of samples as in particular one must have a prior knowledge of the stress range in which the yielding occurs. On the other hand, amplitude sweep and stress growth tests involve different criterion for defining the yield stresses, which make them difficult to interpret and analyse. Stress ramp-up tests with Couette geometry were proven to be practical and time efficient tests (Chapter 3) for measuring all structural breakdowns within the mud samples associated to static and fluidic yield stresses (two-step yielding). This combination of rheological protocol and geometry was also compared with some unconventional rheological protocols typically employed for mud samples. The results showed that "CSRT-ramp up", "EFC-increasing" and "stress ramp-up" displayed higher static and fluidic yield stress values as compared

to the rest of the methods. All these methods started with a low shearing action, implying starting from an undisturbed state of the sample, which resulted in higher values of the stresses. These methods are, therefore, suited to measure the yield stresses of mud sediments for harbour applications, where mud sediments usually exist in undisturbed state (i.e., structured state). However, the EFC-increasing protocol is a long test and from CSRT-ramp up the determination of static yield stress is not very straightforward. Therefore, the stress ramp-up protocol is the most suited and fastest method to analyse the yield stresses of mud sediments for harbour applications. Furthermore, the yield stress values from stress ramp-up test correspond well with the conventional yield stress values obtained from Claeys et al. protocol. The optimization of stress ramp-up test enabled to reduce the experimental time for different mud layers (the experimental time for stress ramp-up being ~10 – 200 s), which is approximately 4 times faster than the conventional Claeys et al. protocol.

What is the spatial and depth variability of the rheological properties of mud?

The rheological properties (yield stress and moduli) of the mud samples of a given location display an increase as a function of the depth into the sediment bed (Chapter 4). This increase is attributed to the increase in density of the samples. The relation between yield stress and density could be fitted with a universal power law, for all locations in the port. Mud samples having similar densities but varying organic matter content show significantly different rheological fingerprint (Chapter 4). For instance, the values of yield stresses and moduli are higher for samples with higher organic matter content (RV and RT locations) than samples with lower organic matter content, for a given density. As the amount of organic matter (represented by Total Organic Carbon, TOC) is varying from location to location, a spatial variability in the yield stresses of mud is observed. The yield stresses decreases from upstream (high TOC) to downstream (low TOC).

The thixotropic studies revealed that all the samples, except from RV location, exhibit a combination of thixotropic and anti-thixotropic behaviours. The samples from RV location display only thixotropic behaviour for the entire shear rate range, which was linked to their high organic matter content. The floc settling analysis confirmed the formation of large flocs with high aspect ratio (open and porous structure) for the samples with higher organic matter content, which explained the higher strength for these samples (Chapter 4). For SW location, the scattered behaviour of the settling velocity as a function of floc size revealed the presence of silt/sand sized particles, as confirmed by PSD analysis from laser diffraction technique.

How much different are the rheological properties of natural and artificially made mud layers?

The yield stresses, moduli and structural recovery of the natural and artificially made mud layers were significantly dissimilar from each other (Chapter 4). Despite having the same PSD, natural and diluted mud samples had nonetheless a significantly different exponential dependency of rheological properties on density. This behaviour can be attributed to a difference in organic matter composition (and particularly the state of oxidation) between the layers as a function of depth. The very peculiar behaviour of the extent of structural recovery as a function of density for the artificially made mud sam-

ples was attributed to the structural heterogeneity caused by the preparation of these samples by hand mixing. Extensive mixing (i.e., by ultrasonic shaking and high-speed shearing) of mud samples after dilution can provide homogeneous systems but the floc network and the clay fabric will then be totally different from the ones found in in-situ conditions.

Which rheological model(s) is suited to fit the experimental data of mud?

In literature, there are several rheological models such as Bingham, Herschel-Bulkley and Worrall-Tuliani, which can be used to fit the flow curve data of mud. The yield stress obtained by fitting the rheological data of mud using Worrall−Tuliani model corresponded well with the static yield stress obtained from viscosity decline. In the case of Bingham or Herschel−Bulkley models, two regions of shear rate were identified with the help of a critical shear rate ($\dot{\gamma}_c$). These models were then applied in these two shear rate regions, from which two yield stress values were obtained for each model. However, the estimation of the critical shear rate $\dot{\gamma}_c$ is tedious when a large number of flow curves are analysed.

In order to overcome this problem, an empirical model was proposed which is based on a step function (Chapter 5). This proposed model was accurate in capturing the two-step yielding behaviour of mud samples from Port of Hamburg, within the density range of $1050 - 1200$ kg. m^{-3}. Furthermore, the important result from the empirical fitting was that the fluidic yield stress correspond to the undrained shear strength and the difference between fluidic and static yield stresses is close to the Bingham yield stress. However, the latter needs further investigation.

How much and how fast the structure (or strength) of mud recovers itself after the disturbances (i.e., pre-shear)?

Extensive studies were performed on pre-consolidated sediment (PS) samples from RT location due to their average density (compared to all locations) and minimum sedimentation problem. The equilibrium structural recovery (G'_∞/G'_0) of the sediments obtained from the RT location displays an interesting behaviour as a function of pre-shearing rate with a minimum value at 35 s^{-1} and an increase in structural parameter after this pre-shear rate (Chapter 6). This behaviour is linked with the existence of two structure levels (i.e., two-step yielding). The structural parameter (G'/G'_0) is observed to be strongly correlated to the yield stress values up to a certain value ($G'/G'_0 = 0.5$). Below this value of structural parameter, it is found that the structural recovery is faster than the time required to perform the dynamic amplitude sweep tests.

The equilibrium structural recovery (G'_∞/G'_0) is independent of shearing time but a higher structural recovery was obtained with vane geometry as compared to the Couette geometry. The highest values for structural recovery (G'_∞/G'_0) are found for the sediments having the lowest density and lowest organic matter content (Chapter 6). This shows that there is a strong spatial and depth variability in structural recovery behaviour as well, in addition to the yield stresses. The characteristic time of recovery (t_r) was found to be significantly affected by the pre-shear rate and organic matter content.

What is the effect of degradation of organic matter, present in mud, on the rheological

characteristics of mud?

The presence of organic matter in cohesive sediments results in the formation of clay-organic flocs, which eventually imparts complex rheological behaviour to mud. However, this organic matter undergoes microbial degradation under in-situ conditions and produces CO_2 and CH_4. Organic matter degradation can significantly affect the rheological properties of mud by diminishing organic bridges between mineral particles and by creating gas bubbles which both weakens the clay-organic floc structures.

The results show a significant decrease in rheological properties including yield stresses (static and fluidic), crossover amplitude, complex modulus and thixotropic hysteresis area for degraded mud samples as compared to the fresh mud samples, by keeping the density constant (Chapter 7). The slopes of the lines, correlating the change (degraded – fresh) in above mentioned rheological properties as a function of the same rheological property of the fresh mud, were similar and vary within the range of –0.28 to –0.49. This behaviour shows that the influence of organic matter degradation is similar for all the rheological properties representing the strength of mud samples. The structural recovery tests show a higher recovery in mud after pre-shearing for the degraded mud than for the fresh mud, which is also in line with the fact that the elastic properties of organic matter are lost upon degradation and, hence, the system acts more like a colloidal suspension of hard particles. The effect of degradation time on the rheological properties of mud samples displayed two critical time periods (3 days and 150 days) after which a significant change in rheological properties of mud samples was observed, which may be attributed to the presence of two differently degradable pools of organic matter in the considered mud sample. The influence of microbial degradation on the rheological properties is more pronounced for CS mud layers and also for the samples collected from upstream locations, due to the higher organic matter content or its higher degradability. The observed decrease in rheological properties of mud under anaerobic conditions is not clearly observed for aerobic degradation, which is attributed to the release of adsorbed metallic ions and the resultant binding between clay particles and metallic ions.

8.2. MAIN OUTPUT OF THIS RESEARCH

It was found that the mud samples exhibited two yield stresses (static and fluidic), which were attributed to the structural reorganization due to shearing action (see Sec. 3.3). It was, therefore, important to first identify which yield stress (static or fluidic) is more appropriate to use as a criterion for nautical bottom. As explained in Sec 3.3, the first yield point (static) represents the breakage of interconnected network of flocs while the plateau behaviour of viscosity/moduli after the first decline shows the formation of cylinder like structures. Hence, it is important to note that the existence of two-step yielding is mainly due the narrow gap between bob and cup, which allows the re-organization of flocs. In in-situ conditions, even though both partial destruction/rearrangement of the network (static yield stress) and complete destruction of the structure (fluidic yield stress) can occur, it was accepted, during discussions with HPA representatives, that the fluidic yield stress is the one to be considered as a safe threshold for controllability and maneuverability of vessels.

In order to provide a suitable value of yield stress as a starting point for future pilot experiments in port, the fluidic yield stress values are plotted as a function of excess density for key locations in Port of Hamburg, Germany (Fig. 8.1a). It was found that 50 Pa can be used as a criterion for navigable mud layer for all these locations, with a corresponding critical bulk density of 1150 kg. m^{-3}. This value of fluidic yield stress (50 Pa) is selected, as a safe number for practical use, on the basis of liquid-like nature of the mud samples below this critical value. Moreover, this value is in accordance with the critical yield stress value reported in literature for Port of Emden (50 – 100 Pa) (Wurpts and Torn, 2005). However, this value will be verified by another PhD student, who is doing CFD simulations of a ship navigating through fluid mud using rheological parameters from the present study, for the definition of fluid mud. These simulations are also validated, in a first step, using large-scale experiments in a water-soil flume where a plate has been dragged in fluid mud (Lovato et al., 2021). Moreover, this definition of navigable mud layer based on yield stress (50 Pa) and bulk density is currently being adopted in one of the key locations (KH) of the Port of Hamburg for pilot experiments, where ships penetrate in moored condition in fluid mud during low tide phase. The sinking test (i.e., immersion of stationary ship into the fluid mud at berth) with hopper dredger showed that the ship floated in the fluid mud at all times and which verifies the fulfilment of Archimedes' buoyancy principle. This result verifies that the yield stress value of 50 Pa can be used as a criterion for mooring ships. In the next step, pilot experiments will be performed to investigate the critical value of yield stress for sailing through fluid mud, which is expected to be lower than 50 Pa.

It is important to highlight that for RT location the corresponding density is about 1120 kg. m^{-3} for 50 Pa, slightly lower than the other locations. This lower value of critical density is mainly related to the higher organic matter content of mud samples. Moreover, the critical densities corresponding to 50 Pa for the far upstream (RV) and far downstream (SW) locations are 1085 and 1215 kg. m^{-3}, respectively (Fig. 8.1b). The lower critical density for RV location is mainly linked to the higher organic matter content while the higher critical density for SW location is associated to the lower organic matter content and the higher sand content, which eventually lead towards an increase in bulk density and a decrease in yield stresses due to the presence of non-cohesive sand particles. This behaviour proves that bulk density is not a suitable parameter for defining the nautical bottom in Port of Hamburg, as it varies from 1085 to 1215 kg. m^{-3} for a certain yield stress value. This also justifies the selection of yield stress for defining navigable mud layer. This density-yield stress correlation for different locations of port of Hamburg will be used to calibrate the in-situ measurement device (Rheotune).

In summary, the approach undertaken in this thesis, i.e., the systematic study of all parameters of the system, geometries, protocols, sample types, degradation and seasonality has shown that this type of approach is essential for a proper system knowledge. The full behaviour of the mud samples has been mapped, and this enables to find (see Fig. 8.1) the suitable value of yield stress as a starting point for future pilot experiments. The fluid mud layer, in all the locations it was observed, exhibited relatively small yield stress values and weak thixotropic behaviour. This confirms that despite the fact that rheology of fluid mud is complex, this layer can be navigable due to its liquid-like na-

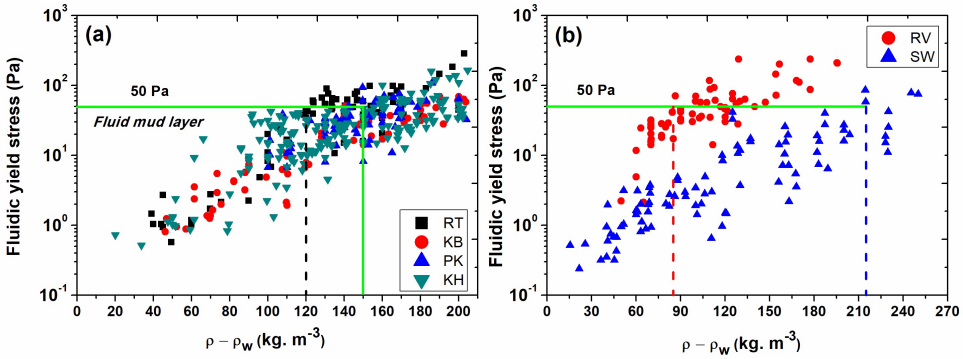

Figure 8.1: Fluidic yield stress as a function of excess density ($\rho - \rho_w$) for (a) key locations, (b) far upstream (RV) and far downstream (SW) locations in Port of Hamburg, Germany. Green solid line represents the critical value of yield stress (50 Pa) and density (1150 kg. m^{-3}). Dashed lines represent the critical density value for RT, RV and SW locations corresponding to 50 Pa.

ture. Furthermore, this study clearly demonstrated that even small amounts of organic matter can significantly change the rheological behaviour of mud. This research further verified the existence of two-step yielding behaviour for mud with the help of rheological and floc analysis. This two-step yielding behaviour of mud was further captured by using an empirical model, which provided key rheological parameters for CFD simulations.

8.3. DISCUSSION, LIMITATIONS AND FUTURE DIRECTIONS

In literature, yield stress has been used to define the nautical bottom, for instance, Port of Emden used a yield stress of 50 − 100 Pa as a criterion to define navigable mud layer (Wurpts and Torn, 2005). However, this value is higher than the value suggested in this study (i.e., 50 Pa) as a starting point for pilot experiments for mud from Port of Hamburg. This difference in values can be associated to the difference in composition of mud (clay content and organic matter content), state of organic matter (fresh or degraded) and criterion of estimating the yield stresses.

In addition to the yield stress, thixotropy or structural recovery is one of the very frequently observed complex rheological behaviours of the mud. This peculiar property can significantly influence the yield stress values (lower yield stress values for disturbed sample/higher yield stress values for undisturbed sample) and, hence, its correlation with the yield stress values is critical. The correlation between fluidic yield stress and hysteresis area (obtained from the thixotropy loop test) for mud from different locations of Port of Hamburg is presented in Fig. 8.2a. It can be clearly seen that there is a strong correlation between both parameters, even for the locations which represent boundary conditions (i.e., RV and SW). Moreover, the critical value of hysteresis area corresponding to the suggested yield stress value of 50 Pa is around 1400 Pa. s^{-1}. This confirms that the mud samples having fluidic yield stress below 50 Pa exhibits weak thixotropic behaviour (i.e., small hysteresis area), which verifies that the selected yield stress value (50 Pa) will not be significantly influenced by the thixotropic character of mud. Moreover,

the correlation between the structural recovery (i.e., in terms of G'_{∞}/G'_0) and fluidic yield stress of mud from different locations is shown in Fig. 8.2b. It is clear that the samples having fluidic yield stress lower than 50 Pa shows structural recovery upto 70 − 100%, which shows that the structure fully recovers itself (within about 500 – 700 s) and verifies the lower thixotropic character of mud. For mud samples with fluidic yield stress higher than 50 Pa, the structural recovery is around 30 − 70%, i.e., strong thixotropic behaviour. However, this correlation is not very strong as compared to the correlation between fluidic yield stress and hysteresis area, which shows that the thixotropic loop test is a fast and reliable method to determine the thixotropic character of mud.

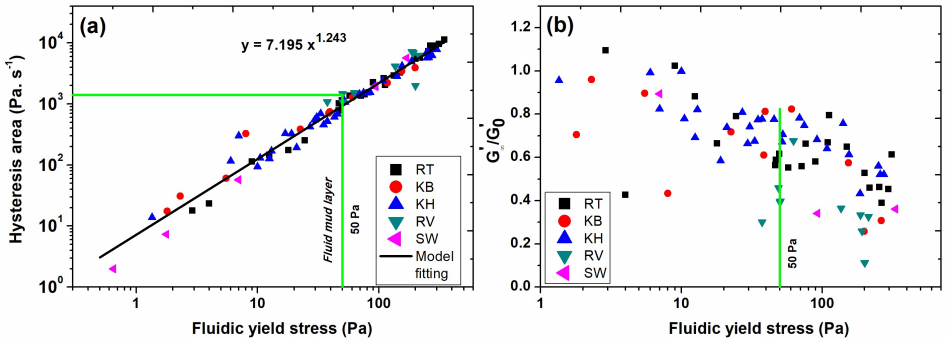

Figure 8.2: (a) Hysteresis area (obtained from the thixotropy loop test) as a function of fluidic yield stress for different locations, (b) equilibrium structural parameter (G'_{∞}/G'_0) as a function of fluidic yield stress for different locations. Green solid line represents the critical value of fluidic yield stress (50 Pa) and hysteresis area (1400 Pa. s^{-1}).

The correlation between fluidic yield stress and bulk density for natural mud samples, artificially made mud samples (diluted) and anaerobically degraded mud samples is presented in Fig. 8.3. It is found that the degraded mud samples show intermediate behaviour of fluidic yield stress as compared to the other two types of samples. This result shows that the dilution of mud samples causes a significant decrease in yield stresses, which is attributed to the mixing effect imposed during the dilution, as discussed in Chapter 4. On the other hand, the reduction in yield stresses due to the degradation of organic matter is lower than the one observed for diluted samples. This information is very important for both laboratory studies where mud dilution is typically performed to investigate the density−yield stress correlation and also for in-situ studies where microbial degradation occurs as a function of time.

In order to identify the fluid mud layers on the vessel during sampling campaigns, funnel test was performed. This is a simple test to understand the flow behaviour of slurries/suspensions by measuring the volumetric flow rate of the sample coming out of the funnel. The correlation between fluidic yield stress and the volumetric flow rate obtained from the funnel test is shown in Fig. 8.4. It is found that for low fluidic yield stresses, the volumetric flow rate is high. At a certain critical value of fluidic yield stress (40 Pa), the volumetric flow rate is almost zero and remains constant for higher fluidic yield stress values. This critical value of fluidic yield stress shows the transition between

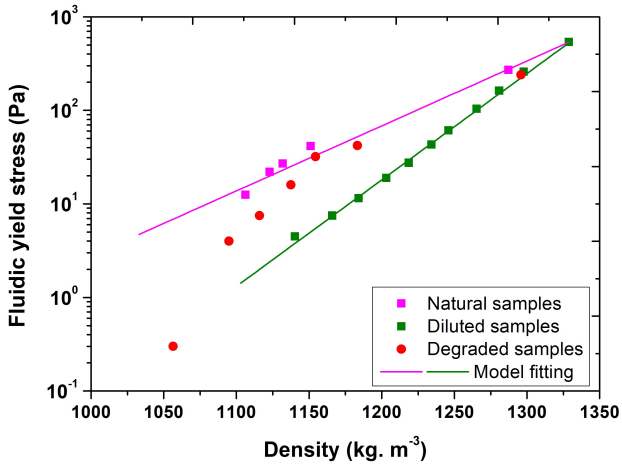

Figure 8.3: Fluidic yield stress as a function of bulk density of natural mud samples, artificially made samples (diluted) and anaerobically degraded mud samples collected from PK location. The solid lines represent the simple exponential model fitting, as discussed in Chapter 4.

fully flowing material (fluid mud) and pre-consolidated material. It is also found that this critical fluidic yield stress value is lower than the suggested yield stress value (50 Pa), which is mainly due to the fact that a funnel test is based on the bulk flow of material, which requires lower yield stress values, as gravity is the main driver for flow. Furthermore, the presence of larger fibres and sand particles in mud can significantly affect its flowing behaviour. In the future, this correlation needs further understanding by performing more funnel tests on-site along with rheological analysis. Note that the two-step yielding model has been implemented in the software of Rheotune for Port of Hamburg, where the fluidic yield stress will be measured in-situ for nautical bottom application. In the end, the influence of yield stress of mud on the ship navigation needs to be investigated through numerical simulations and in-situ pilot experiments, in order to define the critical yield stress value for sailing through fluid mud.

The present study is mainly focused on the analysis of natural mud samples collected from Port of Hamburg, Germany. However, the same understanding and developed knowledge (rheological protocol, rheological two-step yielding model and yield stress limit for navigability) could be applied to various ports. Experiments with different clay type, ionic strength, pH and PSD could be conducted to study the influence of each parameter on the rheological fingerprint (yield stress, moduli and structural recovery) of mud samples. Mineral clay systems with selected biopolymers could be used to mimic in-situ mud samples and to investigate the degradation of samples as a function of biopolymer type and content. The two-step yielding model could be refined by analysing the effect of above mentioned parameters on the rheological behaviour of mud and by incorporating them in the model.

The comparative analysis of yield stresses presented in this study can also be of use to the researchers in different fields. The applicability of studied geometries and rheolog-

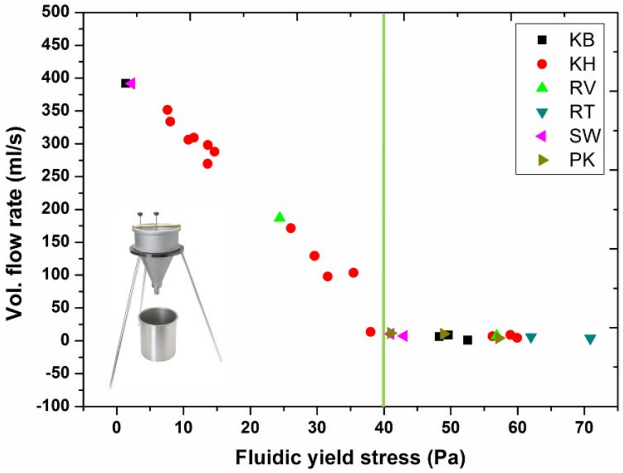

Figure 8.4: Volumetric flow rate (obtained from funnel test) as a function of fluidic yield stress for mud samples from different locations. Green solid line represents the critical value of fluidic yield stress (40 Pa) where the volumetric flow rate is almost zero.

ical methods can be generalized to any kind of suspension, emulsion or gel. In view of recent developments in rheology, the two-step yielding behaviour of these systems is of particular interest. The correlation between static and fluidic yield stresses as pointed out in the thesis is an open field of study. One can wonder whether it is possible to estimate the fluidic yield stress from the static yield stress. The correlation between yield stresses and modulus can in particular be helpful to study the link between the seismic measurements and rheology (Ma et al., 2021).

ACKNOWLEDGEMENTS

This research work would not have been possible without the help and support of many people during my four years of PhD and, therefore, I want to acknowledge all of them.

First of all, I am extremely grateful to my daily supervisor and promotor Claire Chassagne for giving me the opportunity to pursue my PhD studies under her guidance. You taught me how to be critical, how to work independently and be more structured. Your constant help, support and guidance gave me the energy to perform my research with so much passion. Our discussions taught me a lot about critical thinking and expressing my ideas in a structured way. You were always there when I had problems and thought along with me to find solutions. Also, the never ending jokes during the meetings and at the lunch table were the icing on the cake. I feel grateful for having the chance to work with you. I found more a friend in you rather than a supervisor, who always stand for her students. I will never forget our memorable conference (particularly in Cambridge) and Hamburg trips (particularly my first experience on vessel for collecting mud). I hope I will get a chance to work with you or people like you in the future as well. I really could not have done it without you!

To my second supervisor, Alex Kirichek, Thank you for believing in me and guiding me for effective coordination and communication with Port of Hamburg. Your constant efforts and contacts with other ports make this research even more interesting. Your caring attitude, inspiring ideas and constructive feedback really helped me to a lot to perform this research. Moreover, your sense of humour made the process pretty enjoyable. Thank you for giving me a friendly environment. To my another promotor, Julie Pietrzak, I really appreciate the support you provided for making my whole PhD journey easy and smooth for me.

I would like to thank and acknowledge Hamburg Port Authority for providing financial support for this research work. Moreover, I would also like to thank people from Hamburg Port Authority particularly Nino, Jasper and Ulrich, for their enormous efforts during sampling campaigns for collecting mud samples and for their hospitality during our visits to Hamburg.

I would also really like to acknowledge all the MUDNET team members for providing the knowledge and insights from different perspectives on mud particularly, Julia, Florian, Stefano, Menno and Xu. I had a great time with all of you during the meetings, discussions and parties. I am thankful for giving me the opportunity for some interdisciplinary research which broadens my point of view about mud.

As I spent whole duration of my PhD in Deltares, I could not complete this acknowledgement by acknowledging Deltares for providing their facilities throughout my research and the people who provided critical comments on my research, special thanks to Arno.

I had many discussions with him which actually sometimes give me the opportunity to understand things in a better way. I am also really thankful to Saskia, Floris and other colleagues from Deltares for providing their assistance whenever I need. Your help is much appreciated. I would also like to thank our section secretary Otti for making life much easier by handling the paperwork and providing support whenever needed.

I am very thankful for my colleagues and friends particularly Waqas. I really value the time we spent together and the fun we had during watching cricket matches. Waqas, friend to a brother, I had a great time with you on personal and professional level and will always remember your help and kindness. Looking for many family trips together in future. I also want to thank my Master student, Jan-Willem for your hard work during your Master's project. It was a pleasure to supervise you and discuss different approaches to the problems you faced. I also want to thank people with whom I work in collaboration particularly Paul, Zeinab, Ryan, Gosia and Atha. At the end of this section, I want to say special thanks from the bottom of my heart to Claire, Alex and Julia for being there as friends. As most of the time I was in Deltares and could not get more opportunity to have other PhD colleagues as friends, Alex and Claire filled this gap for me.

I would also like to thank my colleagues in Pakistan from UET KSK Campus. A special thanks to Dr. Tanveer and Dr. Saima for your continuous support from the beginning. Thank you to all my Pakistani friends (Imran, Hussam, Noman, Saad, Aftab, Mohsan, Qasim, Tanveer, Osama) in Delft and their families for all the Eid gatherings, BBQ's and volleyball matches. I never felt away from home.

A big thanks to my parents and sisters for supporting me throughout the years. Their lifetime hard work and prayers made me capable enough to own this degree. I am also thankful to my in-laws for their constant love, encouragement and faith in me.

My final word of appreciation is for my wife, Ujala, who has stood by me through all my struggles. She gave me support and help, discussed ideas and prevented several wrong decisions. I thank you for your understanding and cooperation along with cooking delicious dishes, especially during the busy times of your own PhD process. I could not be able to finish this work without your support. Insiya (my lovely daughter), thank you so much for bringing joy and happiness in our lives and making this dissertation writing even more challenging.

Ahmad Shakeel
Delft, April 2022

A

APPENDIX A

Table A1: Characteristics of the sampling locations at the Port of Hamburg.

Locations ID	Distance from Elbe River (km)	Coordinates (WGS 84)	
		°N	°E
RV	616	53.477625	9.984925
RT	619	53.511615	9.949098
SC	620	53.538433	10.000369
SH	621	53.516918	9.935416
KB	623	53.529945	9.938585
VH	624	53.538188	9.949979
PK	627	53.533910	9.905856
KH	629	53.538894	9.881215
SW	643	53.567833	9.679490

Table A2: Characteristics of the extra sampling locations at the upstream (river side) of Port of Hamburg.

Locations ID	TOC content (% TS)	Distance from Elbe River (km)	Coordinates (WGS 84)	
			°N	°E
ZS	4.7±1.8	599	53.398950	10.186919
OK	7.0±1.5	607	53.447645	10.096688
DE	3.9±0.3	615	53.505052	10.060279

A

Table A3: Sampling dates of the monitoring campaigns conducted to collect mud samples from Port of Hamburg.

Campaign #	Sampling date(s)
1	05-06-2018 – 07-06-2018
2	26-06-2018 – 28-06-2018
3	07-08-2018 – 09-08-2018
4	18-09-2018 – 20-09-2018
5	06-11-2018 – 08-11-2018
6	18-03-2019 – 19-03-2019
7	06-05-2019 – 08-05-2019
8	04-06-2019 – 06-06-2019
9	02-07-2019 – 04-07-2019
10	14-08-2019
11	24-09-2019 – 26-09-2019
12	05-11-2019 – 05-11-2019
13	28-04-2020
14	12-05-2020
15	26-05-2020 – 27-05-2020
16	09-06-2020
17	22-06-2020 – 23-06-2020
18	11-08-2020 – 12-08-2020
19	08-09-2020
20	28-09-2020
21	03-11-2020

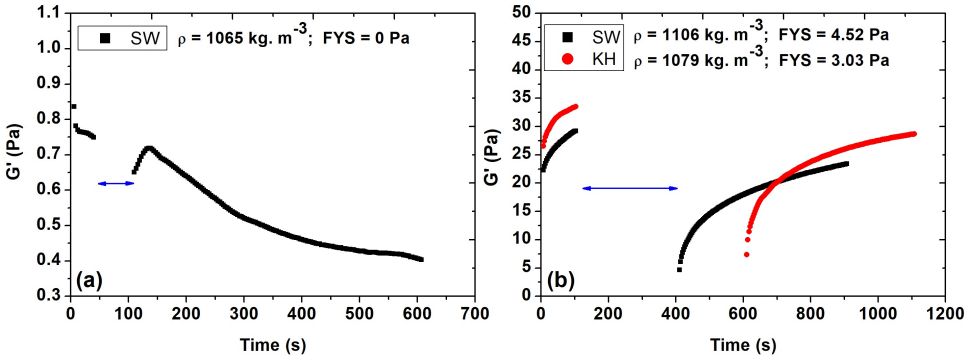

Figure A.1: Storage modulus as a function of time, before and after the shearing step performed at 300 s^{-1} represented by blue arrrows for (a) mud sample with no yield stress and (b) mud samples with small yield stress values.

A

Table A4: Key characteristics of some of the already reported rheo-optical systems.

Rheometer/Shearing Cell	Microscope/Camera	Advantages	Limitations	Ref.
IR-200 Rheometer without transducer, Quartz Cone & Plate/Plate-plate geometry	Upright Optical microscope, CCD camera, halogen white lamp	Rotation can be reversed, mechanism for temperature control	Largest image size 640 × 480 pixels, not suitable at high shear rates	Kume et al., 1995
Custom made parallel plate shear cell	Inverted confocal scanning laser microscope	Higher accuracy from mechanical point of view	Lengthy process for sample preparation, requirement of pair of cassettes for every analysis, difficulty in reproducibility, absence of temperature control mechanism	Wu et al., 2007
Custom made parallel plate shear cell; Anton-Paar MCR 301 Rheometer, Cone and plate/plate-plate geometry	Upright microscope objective with CCD camera, LED backlight source; Inverted microscope objective with CCD camera	Allows to shear a very large surface of sample (~70 cm^2); Measurement of stress	Control of gap variation between the plates was difficult, stress measurement was not possible, possible movement of only bottom plate, no mechanism for temperature control; Not suitable for suspensions due to inverted microscope	Grenard et al., 2011
Custom made parallel plate shear cell	Confocal scanning laser microscope, CCD camera	Temperature controlling mechanism	Fixed gap, movement of only one plate	Tamborini et al., 2014
Custom made cone and plate shear cell	Inverted confocal scanning laser microscope, green He–Ne laser	Movement of both plates, imaging of planes parallel as well as perpendicular to glass plate	Fixed position of microscope objective in cell, variation in gap width caused by a slight wobbling of the glass plate, not suitable for higher shear rates, no temperature controlling mechanism	Didi et al., 2004
Stress-controlled Bohlin Gemini Rheometer, Cone and Plate geometry	Inverted confocal scanning laser microscope	A wide range of shear strain, up to 50% amplitude	Fixed position of microscope objective in cell, no recording of images (absence of camera)	Basu et al., 2011
Linear parallel-plate shear cell	Inverted fast confocal microscope	Wall slip prevention by coating the slides with disordered layers of colloid, solvent trap to minimize evaporation	Possible movement of only top plate, no temperature controlling mechanism	Koumakis et al., 2012, Besseling et al., 2007
Custom made parallel plate shear cell	Inverted fast-scanning confocal microscope	Teflon sheets to minimize evaporation, synchronization of image acquisition and shearing action	Possible movement of only bottom plate, image size 512 × 512 pixels	Zausch et al., 2008
Custom made parallel plate shear cell	Inverted microscope, CCD camera	Roughened plates to minimize wall slip, movement of both plates	Image size 1024 × 1024 pixels, only oscillatory mode of shearing	Knowlton et al., 2014
Anton-Paar MCR 301 Rheometer, Cone and Plate geometry	Inverted confocal scanning laser microscope	Sandblasted plates to minimize wall slip, solvent trap to minimize evaporation	Image size 512 × 512 pixels, fixed gap width between cone and plate	Sentjabrskaja et al., 2015
Velocity-controlled Couette rheometer	Inverted fluorescent microscope, CCD camera	Allows to access local velocities up to 1 m/s	Not suitable for suspensions due to inverted microscope	Goyon et al., 2008
Stress-controlled rheometer AR2000, Cone and Plate/Plate-plate geometry	Inverted confocal scanning laser microscope	Roughened plates to minimize wall slip, solvent trap to minimize evaporation	Not suitable for suspensions due to inverted microscope	Besseling et al., 2009
Custom made parallel plate shear cell	Inverted confocal scanning laser microscope	Temperature controlling mechanism, vacuum joining of glass coverslip with the plate, movement of both plates	No stress measurement, not suitable for suspensions due to inverted microscope	Boitte et al., 2013
Custom built constant stress shear cell, Cone and Plate geometry	Inverted fast-scanning confocal microscope	Solvent trap to minimize evaporation, cost-effective, availability of range and resolution of applied stresses through selection of transfer fluid	Absence of temperature controlling mechanism, not suitable for suspensions due to inverted microscope	Chan and Mohraz, 2013
Custom made parallel plate shear cell	Inverted confocal scanning laser microscope	Stress measurement, Solvent trap to minimize evaporation, possibility of biaxial shear experiments	Absence of temperature controlling mechanism, gluing of cover slip with the plate, not suitable for suspensions due to inverted microscope	Lin et al., 2014
Anton-Paar MCR 301 Rheometer, Cone and Plate/Plate-plate geometry	Inverted laser scanning confocal microscope	Wide range of applied torque, presence of normal force sensor	Not suitable for suspensions due to inverted microscope, image size 256 × 256 pixels	Dutta et al., 2013
Rotational rheometer HAAKE MARS III, Cone and Plate/Plate-plate geometry	Inverted polarized reflected light microscope, CCD camera	Temperature controlling mechanism, in addition to light microscopy, RAMAN spectroscopy measurements also available	Not suitable for suspensions due to inverted microscope setup	Kotula et al., 2016
Custom made parallel plate shear cell	Upright optical microscope, CCD camera	Temperature controlling mechanism	Possible movement of only bottom plate, suitable for small amplitude deformation	Mackley et al., 1999
Custom made parallel plate shear cell	Upright optical microscope, CMOS camera, LED light	Suitable for suspensions due to upright microscope, temperature controlling mechanism, vacuum joining of glass coverslip with the plate, movement of both plates, gap variation between two plates is possible from 0 − 5 mm, CMOS camera instead of CCD which provides reduced blooming and smearing, image size 2592 × 2048 pixels with square pixels for undistorted image, fluorescent marker is not required, microscope objective with large working distance	No mechanism for stress measurement	Shakeel, van Kan, et al., 2019

B

APPENDIX B

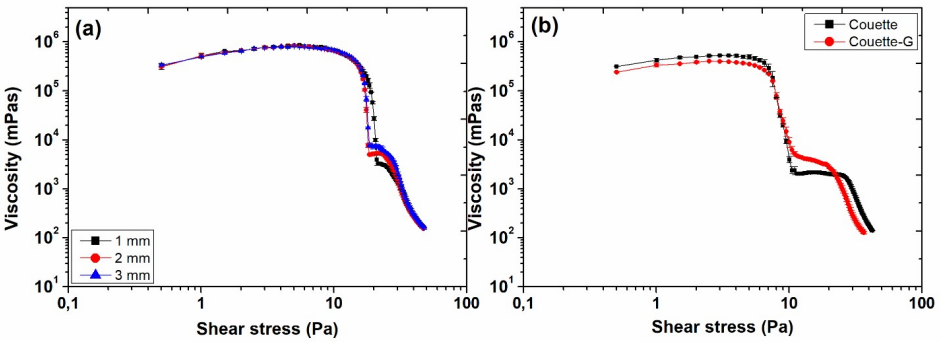

Figure B1: Apparent viscosity as a function of shear stress for (a) parallel plate geometry with variable gap and (b) smooth and grooved Couette geometries for fluid mud layer (1134 kg. m^{-3}) from KH location. Bars represent standard deviation.

Table B1: Values of undrained shear strength and Bingham yield stress obtained from Claeys protocol for different geometries.

Geometry	Undrained Shear Strength (Pa)	Bingham Yield Stress (Pa)
Couette	20.1	25
Vane	46.7	26.5

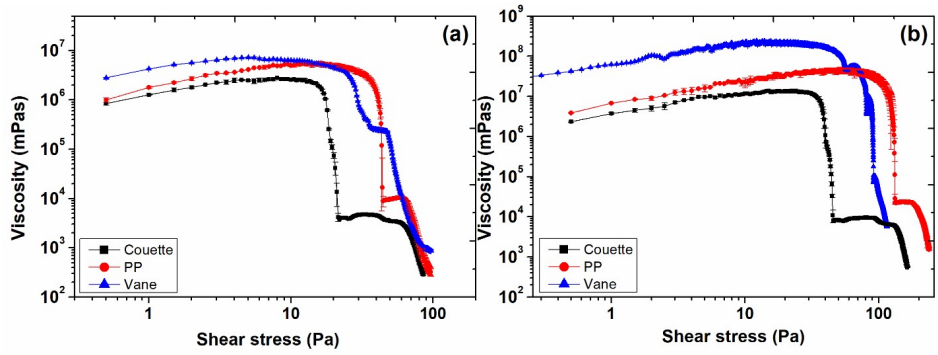

Figure B2: Apparent viscosity as a function of shear stress for (a) pre-consolidated (1158 kg. m^{-3}) and (b) consolidated (1186 kg. m^{-3}) mud layers from KH location using different geometries. Bars represent the standard deviation.

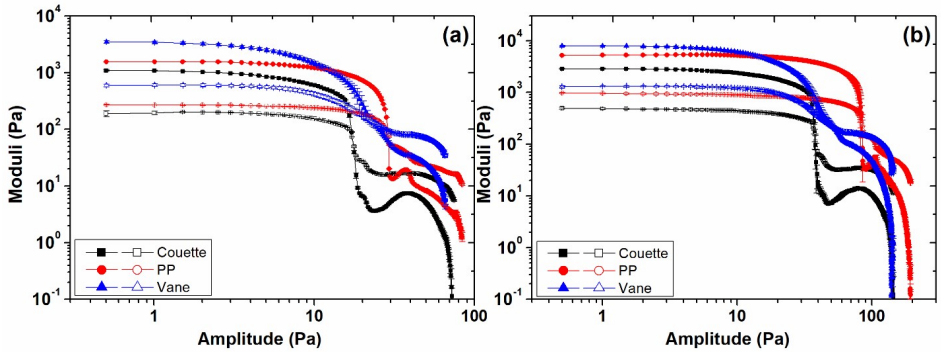

Figure B3: Storage modulus (filled symbols) and loss modulus (empty symbols) as a function of amplitude for (a) pre-consolidated (1158 kg. m^{-3}) and (b) consolidated (1186 kg. m^{-3}) mud layers from KH location using different geometries at 1 Hz. Bars represent standard deviation.

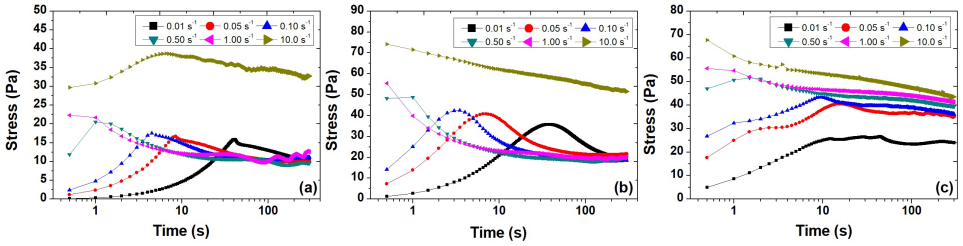

Figure B4: Stress evolution as a function of time for (a) Couette, (b) parallel plate and (c) vane geometries at various shear rates for pre-consolidated mud layer (1158 kg. m^{-3}) from KH location.

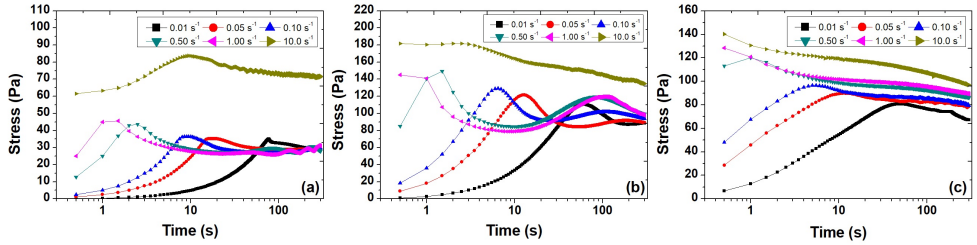

Figure B5: Stress evolution as a function of time for (a) Couette, (b) parallel plate and (c) vane geometries at various shear rates for consolidated mud layer (1186 kg. m^{-3}) from KH location.

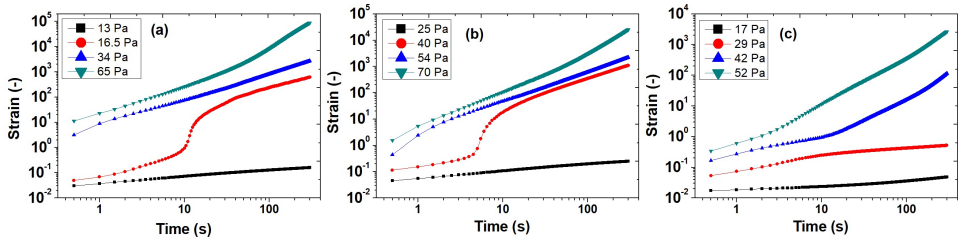

Figure B6: Strain as a function of time for pre-consolidated mud layer (1158 kg. m^{-3}) from KH location using (a) Couette (b) parallel plate and (c) vane geometries at various applied stresses.

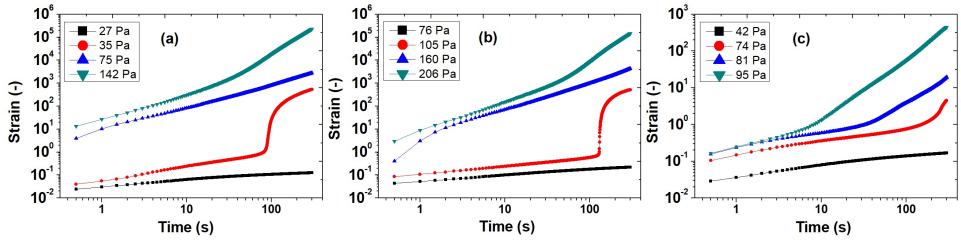

Figure B7: Strain as a function of time for consolidated mud layer (1186 kg. m^{-3}) from KH location using (a) Couette (b) parallel plate and (c) vane geometries at various applied stresses.

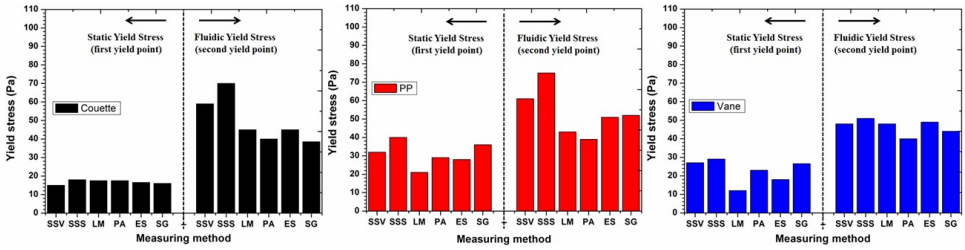

Figure B8: Comparison of static and fluidic yield stress values of pre-consolidated mud layer (1158 kg. m^{-3}) from KH location using different geometries; SSV = viscosity decline from stress sweep, SSS = deformation slopes from stress sweep, LM = loss modulus decline from oscillatory amplitude sweep, PA = phase angle from oscillatory amplitude sweep, ES = elastic stress from oscillatory amplitude sweep, SG = stress growth.

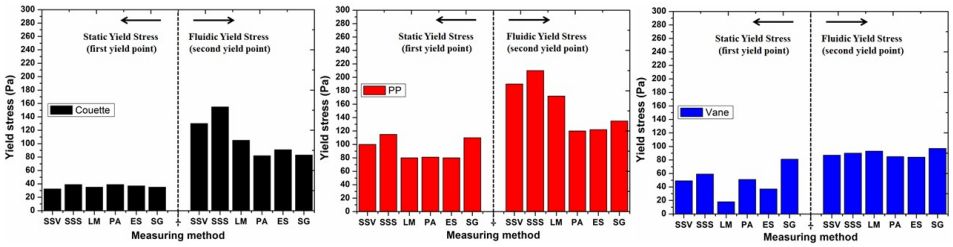

Figure B9: Comparison of static and fluidic yield stress values of consolidated mud layer (1186 kg. m^{-3}) from KH location using different geometries; SSV = viscosity decline from stress sweep, SSS = deformation slopes from stress sweep, LM = loss modulus decline from oscillatory amplitude sweep, PA = phase angle from oscillatory amplitude sweep, ES = elastic stress from oscillatory amplitude sweep, SG = stress growth.

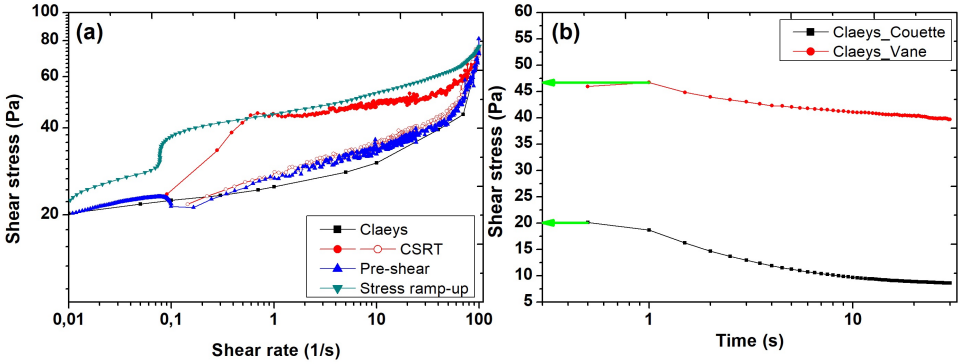

Figure B10: (a) Shear stress as a function of shear rate for pre-consolidated mud sample (1151 kg. m^{-3}) from KB location using vane geometry; solid symbols in CSRT protocol represent the ramp-up and the empty symbols represent the ramp-down; (b) shear stress as a function of time obtained for a shear rate of 1 s^{-1} (first step in Claeys protocol) for pre-consolidated mud sample (1151 kg. m^{-3}) from KB location using different geometries. The green arrows represent the undrained shear strength.

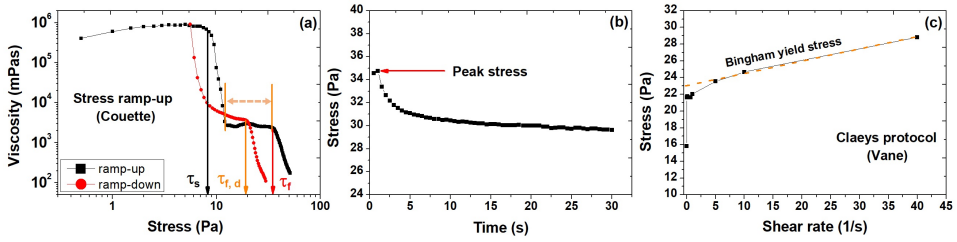

Figure B11: (a) Apparent viscosity as a function of shear stress for ramp-up and ramp-down tests at 1 Pa/s; a constant shear rate test at 300 s^{-1} was performed for 500 s after the ramp-up (b) shear stress as a function of time for 1 s^{-1} shear rate (first step in Claeys protocol) and (c) shear stress as a function of shear rate for mud sample obtained from PK location. Bulk density of the sample is 1151 kg. m^{-3}.

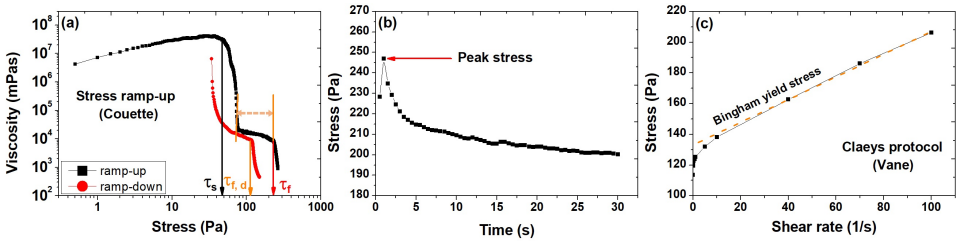

Figure B12: (a) Apparent viscosity as a function of shear stress for ramp-up and ramp-down tests at 1 Pa/s, a constant shear rate test at 300 s^{-1} was performed for 500 s after the ramp-up (b) shear stress as a function of time for 1 s^{-1} shear rate (first step in Claeys protocol) and (c) shear stress as a function of shear rate for mud sample obtained from PK location. Bulk density of the sample is 1256 kg. m^{-3}.

Table B2: Yield stress values of the mud sample obtained from PK location with density 1151 kg. m^{-3} (Figure B11).

Parameter	Value (Pa)
Undrained shear strength (peak stress)	34.7
Bingham yield stress	23
Fluidic yield stress (ramp-up), τ_f	37
Fluidic yield stress (ramp-down), $\tau_{f,d}$	20
Difference between fluidic and static yield point	25

Table B3: Yield stress values of the mud sample obtained from PK location with density 1256 kg. m^{-3} (Figure B12).

Parameter	Value (Pa)
Undrained shear strength (peak stress)	246
Bingham yield stress	132
Fluidic yield stress (ramp-up), τ_f	230
Fluidic yield stress (ramp-down), $\tau_{f,d}$	120
Difference between fluidic and static yield point	153

Table B4: Preferred stress ramp-up rates and approximate experimental times for different mud layers.

Mud Layer	Fluidic Yield Stress Range (Pa)	Preferred Stress Ramp-up Rate (Pa/s)	Approximate Experimental Time (s)
Fluid mud	1 – 9	0.1	10 – 90
Pre-consolidated	10 – 99	1	10 – 99
Consolidated	100 – 1000	5	20 – 200

B

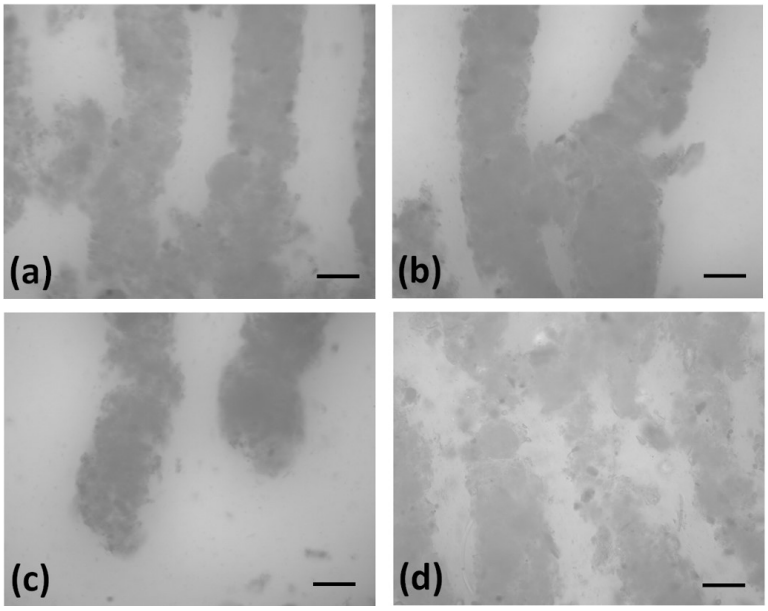

Figure B13: The snapshots from the recorded video at t = 50 s for (a) diluted mud sample from RV location, (b) diluted mud sample from RT location, (c) diluted mud sample from KH location and (d) diluted mud sample from SW location, oscillatory sheared at a frequency of 1 Hz and amplitude of 0.1 − 0.2 mm with the gap between the plates of 10 − 100 μm. The scale bar represents 70 μm.

C

APPENDIX C

Table C1: Values of the model parameters for yield stresses of natural and diluted mud layers.

Mud Layers	a (Pa)	Std. Error	b ($m^3.\ kg^{-1}$)	Std. Error	R^2
Natural	3.6×10^{-7}	2.1×10^{-7}	0.016	0.0004	0.99
Diluted	5.5×10^{-12}	3.9×10^{-12}	0.024	0.0005	0.99

Table C2: Values of the model parameters for complex modulus of natural and diluted mud layers.

Mud Layers	a (Pa)	Std. Error	b ($m^3.\ kg^{-1}$)	Std. Error	R^2
Natural	9.1×10^{-13}	1.4×10^{-12}	0.029	0.0012	0.99
Diluted	2.1×10^{-15}	3.7×10^{-15}	0.033	0.0012	0.99

Table C3: Characteristics of the investigated mud samples with similar higher densities and similar lower densities.

Sample Location	Bulk Density (kg. m^{-3})	TOC (% TS)	Static yield stress (Pa)	Fluidic yield stress (Pa)	Complex modulus @ 1 Hz (Pa)	Phase angle @ 1 Hz (°)
VH	1087	3.7	0.8	2.44	13±0.2	11±0.5
RV	1098	7.2	9	40	417±0.3	8±0.5
KB	1211	2.8	18	79	1774±102	8±0.7
RT	1210	4.3	60	312	7909±137	8±0.8

C

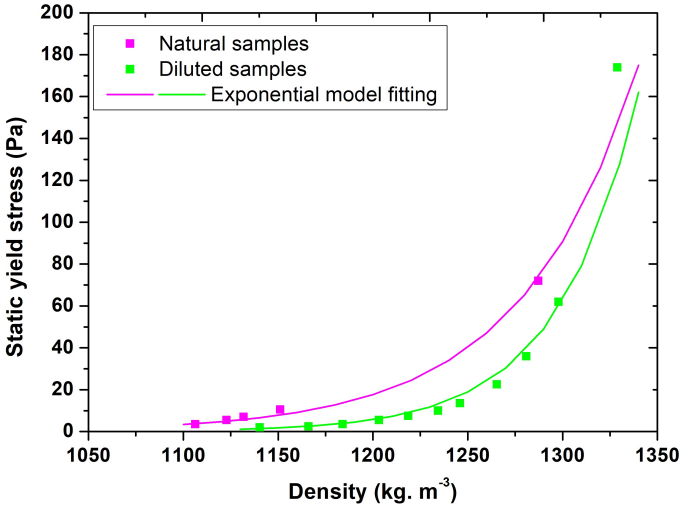

Figure C1: Static yield stress values as a function of density for natural and diluted mud layers from PK location. Solid lines represent the exponential model fitting.

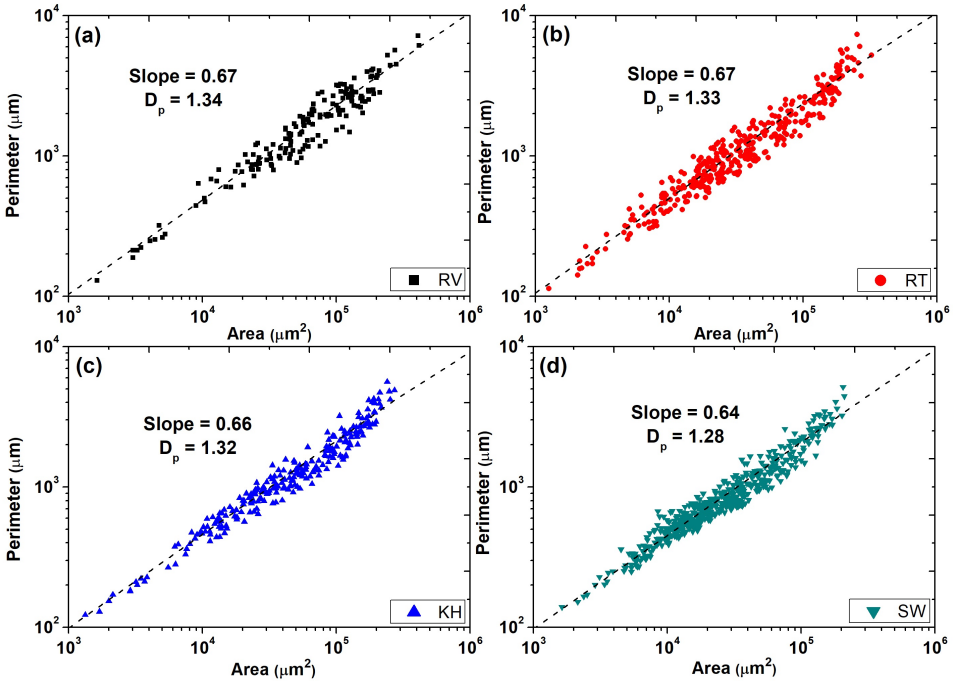

Figure C2: Perimeter-based fractal dimension (D_p) calculated from the log-log plot of perimeter versus area for mud flocs from (a) RV location, (b) RT location, (c) KH location and (d) SW location. Dashed line represents the linear fit of the data.

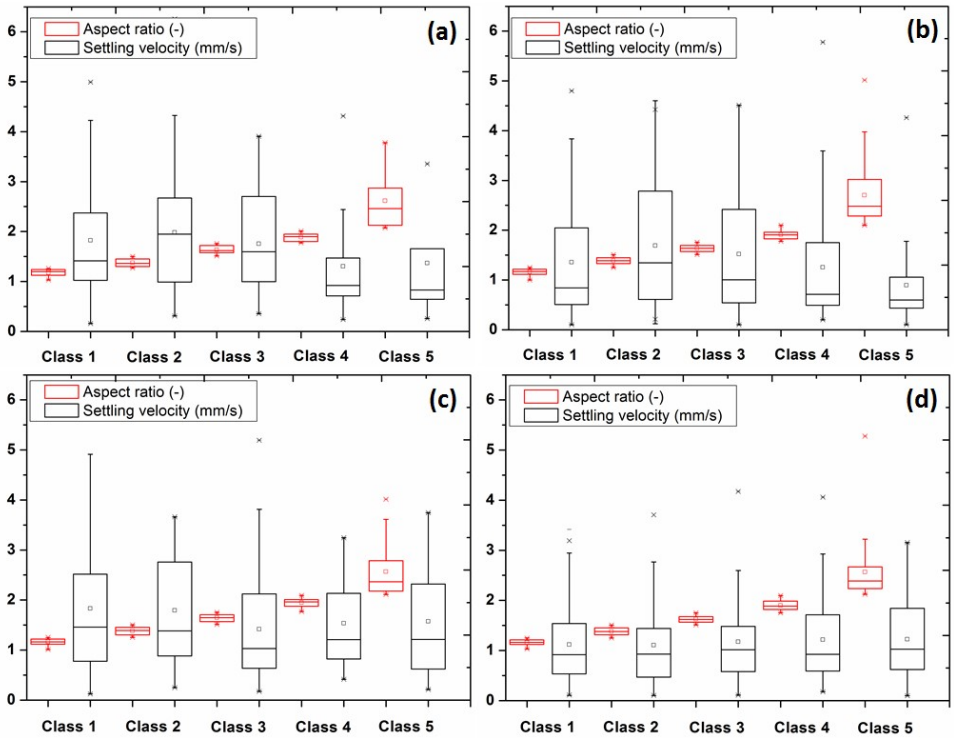

Figure C3: Aspect ratio (AR) and the corresponding settling velocity for 5 different classes of flocs for (a) RV location, (b) RT location, (c) KH location and (d) SW location. AR of Class 1 = 1 − 1.25, AR of Class 2 = 1.25 − 1.5, AR of Class 3 = 1.5 − 1.75, AR of Class 4 = 1.75 − 2, and AR of Class 5 = 2 − 5.

C

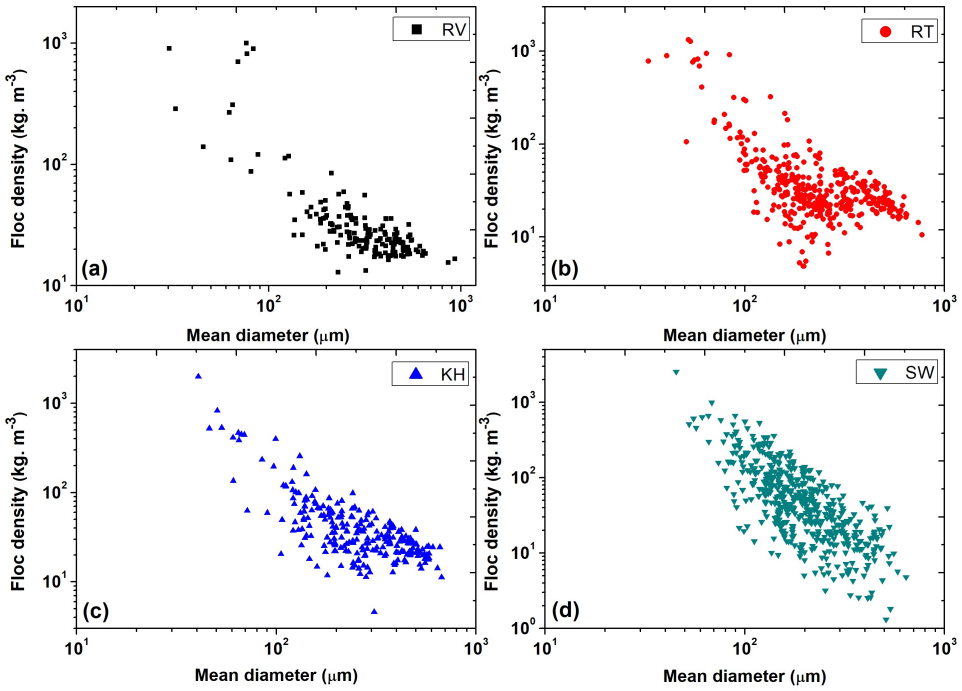

Figure C4: Effective floc density as a function of mean diameter for mud flocs from (a) RV location, (b) RT location, (c) KH location and (d) SW location.

D

APPENDIX D

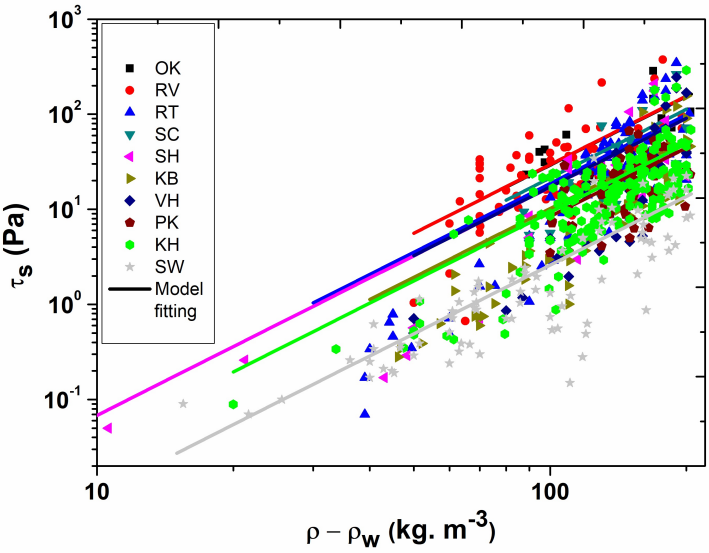

Figure D1: Static yield stress (τ_s) as a function of excess density ($\rho - \rho_w$) for different locations. The solid lines represent the power law fitting (Eq. 5.16) with one fitting parameter 'a' and fixed value of parameter 'b'. ρ_w represents the density of water.

D

Table D1: Values of the power law fitting (Eq. 5.16), upper limit and lower limit of parameter 'a' for static and fluidic yield stresses at a fixed value of parameter 'b' (i.e., 2.4) for different locations.

Location	Parameter 'a' (Static)			Parameter 'a' (Fluidic)		
	Upper limit	Model fitting	Lower limit	Upper limit	Model fitting	Lower limit
OK	12700	7336	3150	27200	15826	6950
RV	28800	7421	1510	32252	10252	2730
RT	14700	4688	340	12200	5229	720
SC	12800	5367	890	10300	4630	1280
SH	12300	4310	330	10200	3934	630
KB	8560	2564	230	5530	2731	750
VH	10120	4323	370	5240	3118	690
PK	6300	2111	480	8920	3289	790
KH	7300	2339	300	11900	3264	590
SW	1600	652	130	5050	1053	125

E

APPENDIX E

E.1. EFFECT OF RECOVERY TIME

After the shearing step, time sweep experiments were performed for 500 s. This time was long enough for the storage modulus to reach an almost constant value, as can be seen from Fig. E1 where two experiments with smaller and longer recovery times are presented. Furthermore, the values of the fitting parameters for Eq. 2.4 were also in close agreement with each other (Table E1), which implies that 500 s is enough to assess a steady-state recovery. Each experiment was performed twice and the reproducibility of the results was quite good (experimental error < 2%), as can be seen from Fig. E1 and Table E1.

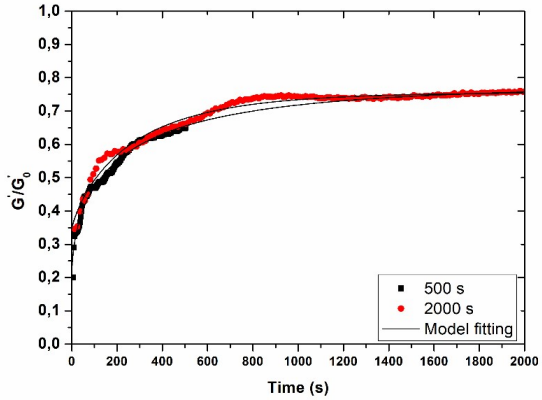

Figure E1: Structural recovery for different recovery times after pre-shearing at 30 s^{-1} using mud sample from RT location.

Table E1: Values of the model parameters (Eq. 2.4) for different recovery times.

Build-up Time (s)	G'_∞ (Pa)	G'_∞/G'_0	t_r (s)	d (-)	R^2 (-)
500	2462	0.82	62	0.55	0.99
2000 (fitting for 500 s)	2412	0.80	65	0.61	0.99
Average	2437	0.81	63.5	0.58	0.99
Std. deviation	35	0.01	2.1	0.04	0
2000	2391	0.80	71	0.72	0.98

E.2. EFFECT OF TEMPERATURE

To investigate the influence of temperature on the structural regrowth, the experiments were carried out at a pre-shear rate of 100 s^{-1} and at the temperatures of 5 and 25 °C. The same temperature was maintained during the pre-shearing and the structural recovery steps. Figure E2a and E2b present the normalized structural recovery (G'/G'_0) for the mud samples from RT and SW locations, respectively. The results showed an increase in structural recovery and equilibrium structural parameter (G'_∞/G'_0) when the temperature was changed from 5 to 25 °C for both types of sediments. This result was attributed to the enhanced inter-particle interactions at higher temperatures. Similar results were also reported for the structural recovery of MWCNTs suspensions in epoxy where the structural parameter was increasing with temperature (Khalkhal et al., 2011). However, in contrary to the results of Khalkhal et al., 2011, it was also found that the values for the characteristic time and stretching exponent also increased with temperature (Table E2). This behaviour may be associated with the presence of polymer/organic matter in the investigated sediment suspensions. The reorganization/breaking of polymeric chains during shearing is probably facilitated at higher temperatures which then results in a slower recovery of the structure associated with higher values of the characteristic time.

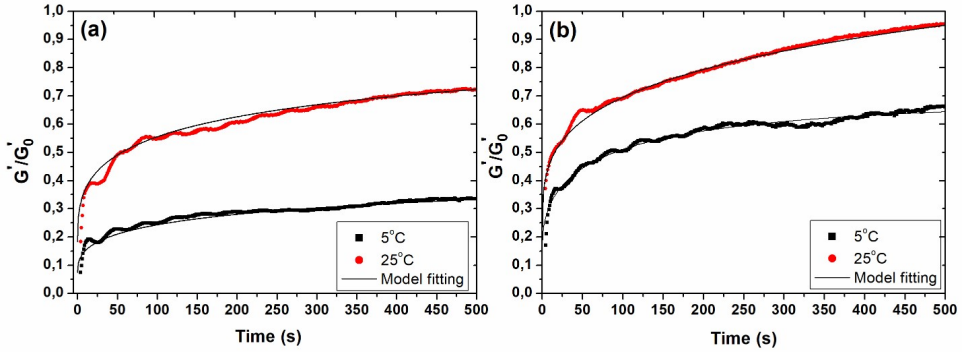

Figure E2: Normalized storage modulus (G'/G'_0) as a function of time for different temperatures using the mud samples from (a) RT location and (b) SW location, pre-sheared at 100 s^{-1}.

Table E2: Values of the model parameters (Eq. 2.4) for different temperatures of mud sediments.

Sample ID	Temperature (°C)	G'_∞ (Pa)	G'_∞/G'_0	t_r (s)	d (-)	R^2 (-)
RT	25	3145	0.98	369	0.41	0.98
RT	5	3103	0.45	329	0.37	0.97
SW	25	2380	1.13	343	0.75	0.99
SW	5	1607	0.69	89	0.51	0.98

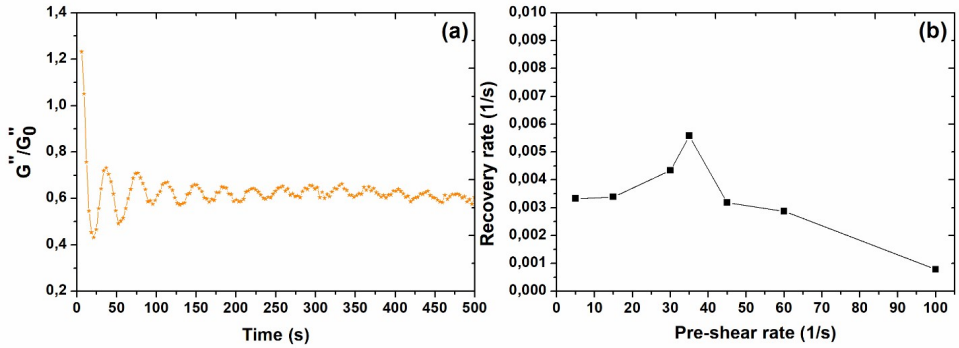

Figure E3: (a) Normalized loss modulus (G''/G''_0) as a function time for pre-shearing at 100 s^{-1} using RT sediments, (b) recovery rate ($(G'_\infty/G'_0)/t_r$) as a function of pre-shear rate for RT sediments, the solid line is just a guide for the eye.

Table E3: Values of the model parameters (Eq. 2.4) for different pre-shearing rates.

Pre-shear rate (s^{-1})	G'_∞ (Pa)	G'_∞/G'_0	t_r (s)	d (-)	R^2 (-)
5	3255	1.38	415	0.37	0.57
15	2068	1.05	310	0.46	0.96
30	1527	0.69	159	0.67	0.99
35	1388	0.67	120	0.67	0.99
45	1606	0.78	245	0.58	0.99
60	1646	0.84	292	0.59	0.99
100	2644	1.30	1664	0.50	0.99

Table E4: Values of the model parameters (Eq. 2.4) for different shearing times at 10 s^{-1}.

Pre-shear time (s)	G'_∞ (Pa)	G'_∞/G'_0	t_r (s)	d (-)	R^2 (-)
10	2803	0.87	47	0.91	0.81
30	3030	0.85	145	0.72	0.94
50	2754	0.83	70	0.75	0.85
100	2947	0.82	90	0.57	0.82
200	3294	0.86	126	0.58	0.89
400	3371	0.90	160	0.62	0.90
600	2979	0.85	65	0.77	0.81
800	3270	0.89	131	0.66	0.94

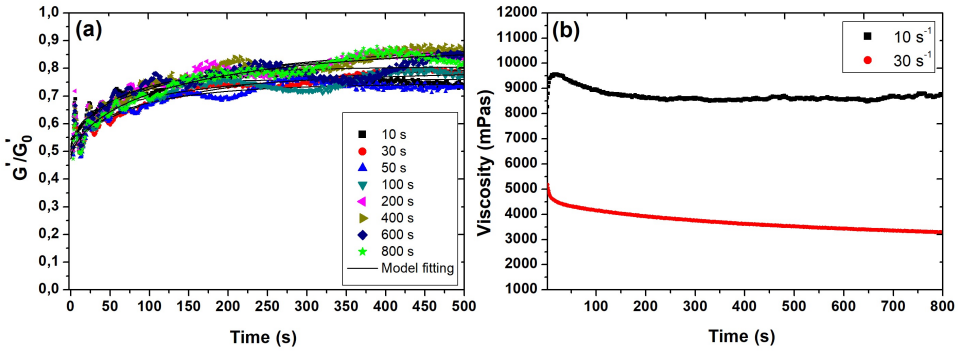

Figure E4: (a) Normalized storage modulus ($G^{'}/G_0^{'}$) as a function of time for different pre-shearing times using RT sediments pre-sheared at 10 s^{-1}; (b) viscosity as a function of time for different pre-shear rates during the shearing step.

E

Table E5: Values of the model parameters (Eq. 2.4) for different shearing times at 30 s^{-1}.

Pre-shear time (s)	$G_\infty^{'}$ (Pa)	$G_\infty^{'}/G_0^{'}$	t_r (s)	d (-)	R^2 (-)
10	2810	0.94	115	0.37	0.96
30	3349	0.92	262	0.34	0.96
50	2790	0.93	90	0.39	0.96
100	3919	0.90	460	0.32	0.96
200	2776	0.88	100	0.40	0.96
400	3283	0.85	254	0.34	0.98
600	3479	0.84	399	0.38	0.98
800	2470	0.83	54	0.54	0.97

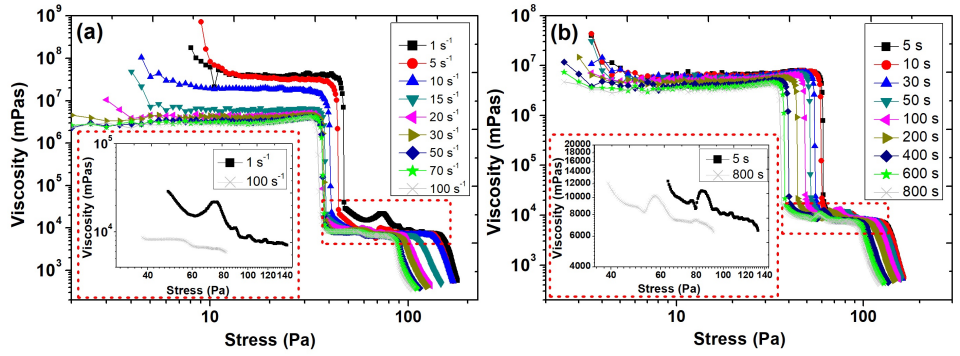

Figure E5: Apparent viscosity as a function of stress using RT sediments for different (a) pre-shearing rates and (b) pre-shearing times. Inset shows the plot of the dotted region at higher shear stresses, in order to clearly see the jamming phenomenon.

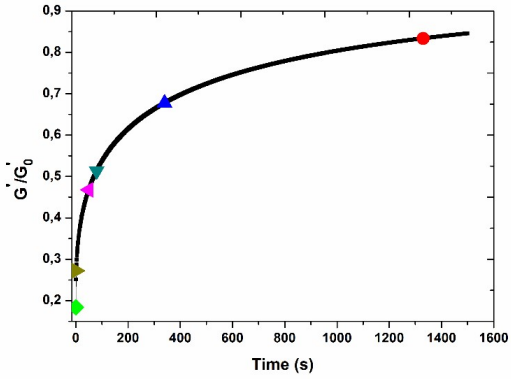

Figure E6: Schematic representation of structural recovery step having different values of structural parameter, different colored points represent the selected recovery times to perform amplitude sweep tests.

Table E6: Values of the model parameters (Eq. 2.4) for different sediment layers collected from RT location.

Mud layer	Density (kg. m^{-3})	G'_{∞} (Pa)	G'_{∞}/G'_0	t_r (s)	d (-)	R^2 (-)
RT_PS	1228	3145	0.98	369	0.41	0.98
RT_PS/CS	1258	5539	0.47	53	0.53	0.90
RT_CS	1282	12670	0.39	82	0.62	0.97

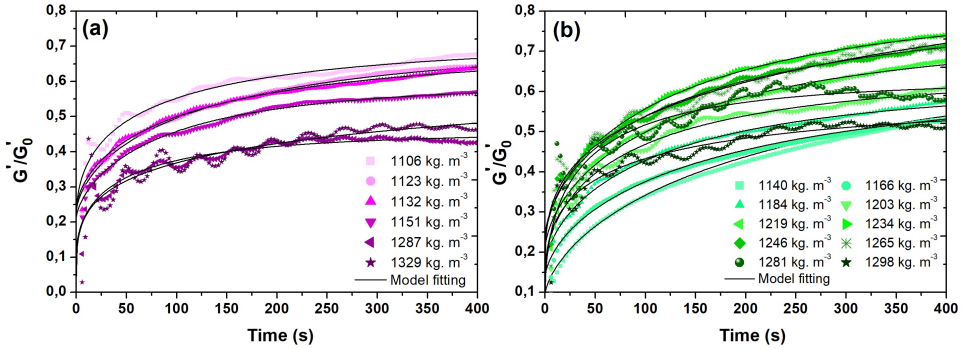

Figure E7: Normalized storage modulus ($G^{'}/G^{'}_0$) as a function of time for (a) natural mud layers and (b) diluted mud layers obtained from PK location.

Table E7: Values of the model parameters (Eq. 2.4) for natural and diluted mud layers from PK location.

Sample ID	G'_∞ (Pa)	Std. Error	t_r (s)	Std. Error	d (-)	Std. Error	R^2 (-)	G'_∞/G'_0
Samples from PK location								
PK1	1.13×10^2	2.3	80	9	0.52	0.03	0.96	0.72
PK2	2.02×10^2	2.1	135	6	0.65	0.01	0.99	0.66
PK3	2.80×10^2	3.5	121	7	0.62	0.02	0.99	0.63
PK4	5.03×10^2	3.5	94	3	0.71	0.02	0.99	0.59
PK5	3.83×10^3	63.9	51	4	0.56	0.04	0.92	0.46
PK6	1.6×10^4	7177	47	4	0.41	0.07	0.80	0.44
Diluted Samples of PK6								
PK6D2	2.20×10^1	0.5	248	17	0.68	0.01	0.99	0.69
PK6D3	5.00×10^1	0.9	185	12	0.65	0.01	0.99	0.63
PK6D4	8.9×10^1	1.1	121	6	0.66	0.02	0.99	0.61
PK6D5	1.74×10^2	3.2	96	8	0.60	0.02	0.98	0.64
PK6D6	3.26×10^2	4.1	145	7	0.66	0.01	0.99	0.74
PK6D7	6.04×10^2	7.1	151	7	0.66	0.01	0.99	0.81
PK6D8	9.9×10^2	23.9	164	17	0.58	0.02	0.99	0.82
PK6D9	2.53×10^3	55.8	195	15	0.38	0.04	0.96	0.81
PK6D10	2.77×10^3	63.9	81	6	0.54	0.05	0.85	0.63
PK6D11	4.8×10^3	232.4	43	9	0.45	0.04	0.90	0.59

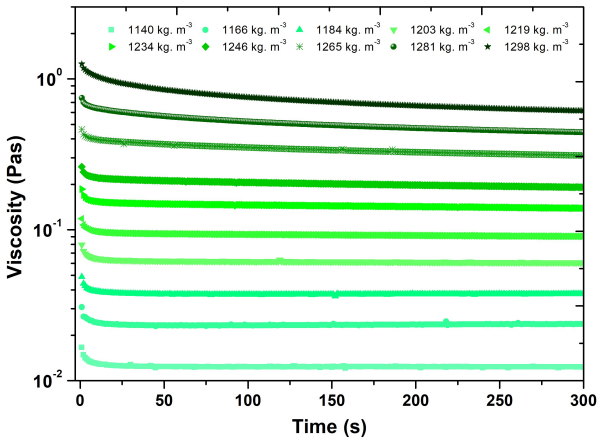

Figure E8: Apparent viscosity as a function of time at a shear rate of 300 s^{-1} during pre-shear step for diluted mud samples from PK location.

Table E8: Values of the model parameters (Eq. 2.4) for different mud samples with Couette geometry.

Location	Density (kg. m^{-3})	G'_{∞} (Pa)	G'_{∞}/G'_0	t_r (s)	d (-)	R^2 (-)
SW	1393	2380	1.13	343	0.75	0.99
RT	1228	3145	0.98	369	0.41	0.98
VH	1180	517	0.63	178	0.58	0.99
SC	1248	891	0.61	211	0.52	0.99
SH	1227	1177	0.55	229	0.51	0.99
RV	1148	533	0.34	147	0.59	0.99
DE	1193	273	0.29	235	0.61	0.99
OK	1151	237	0.35	313	0.59	0.99
ZS	1235	359	0.11	177	0.62	0.99

Table E9: Values of the model parameters (Eq. 2.4) for different mud samples with Vane geometry.

Location	Density (kg. m^{-3})	G'_{∞} (Pa)	G'_{∞}/G'_0	t_r (s)	d (-)	R^2 (-)
SW	1393	7753	1.25	240	0.45	0.99
RT	1228	9506	1.09	192	0.43	0.98
VH	1180	2185	1.02	216	0.53	0.99
SC	1248	3937	1.13	323	0.46	0.99
SH	1227	4698	1.11	253	0.43	0.99
RV	1148	2467	0.74	245	0.49	0.99
DE	1193	1186	0.53	189	0.61	0.99
OK	1151	801	0.28	207	0.61	0.99
ZS	1235	1408	0.25	168	0.61	0.99

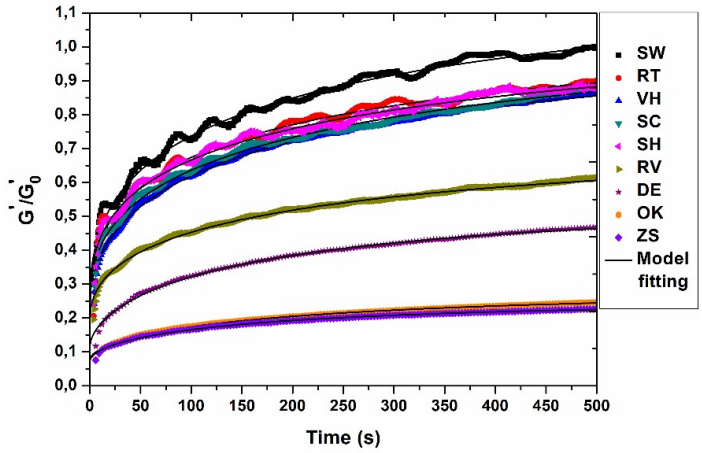

Figure E9: Normalized storage modulus (G'/G'_0) as a function of time for different pre-consolidated (PS) sediment samples pre-sheared at 100 s^{-1} using vane geometry.

F

APPENDIX F

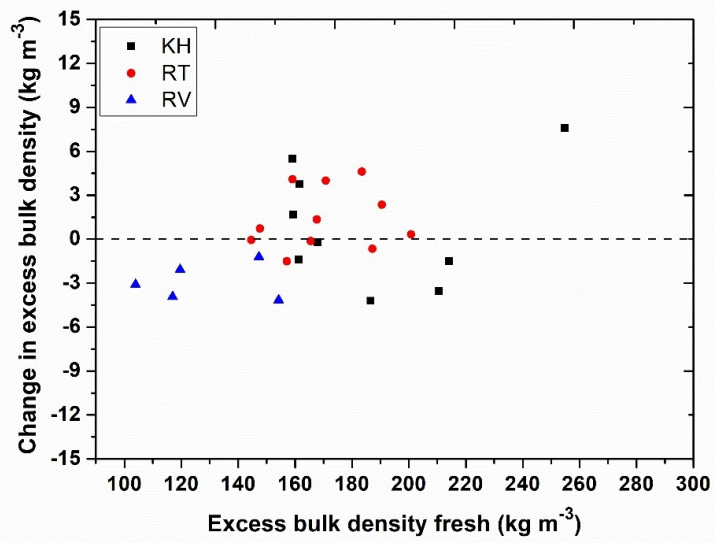

Figure F1: Change in excess bulk density (degraded – fresh) as a function of excess bulk density of fresh PS mud sample from different locations. The dashed line represents the value where the degraded and fresh mud samples have the same bulk densities.

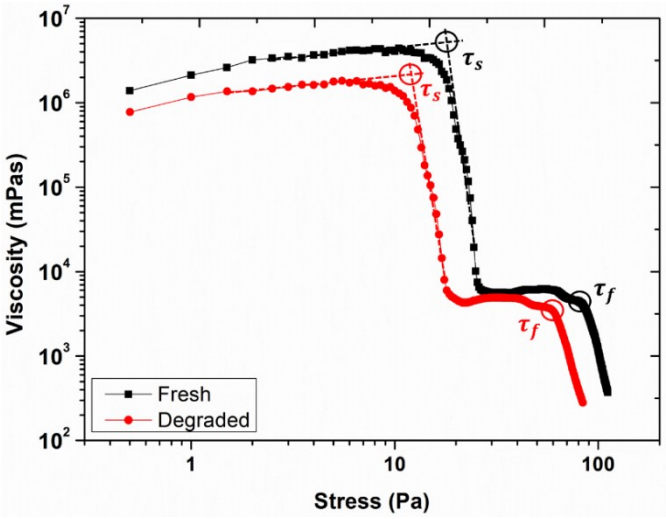

Figure F2: Apparent viscosity as a function of shear stress for fresh mud sample and mud sample degraded for 250 days, collected from KH location. The circles represent the static (τ_s) and fluidic (τ_f) yield stresses.

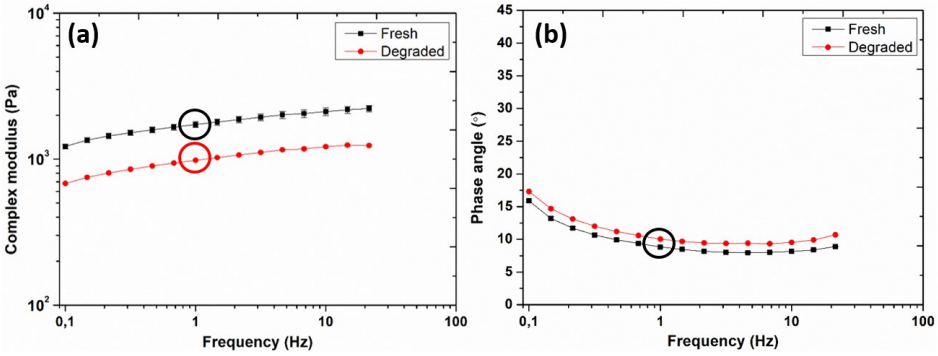

Figure F3: (a) Complex modulus and (b) phase angle as a function of frequency for fresh mud sample and mud sample degraded for 250 days, collected from KH location. The circles represent the complex modulus and phase angle at 1 Hz.

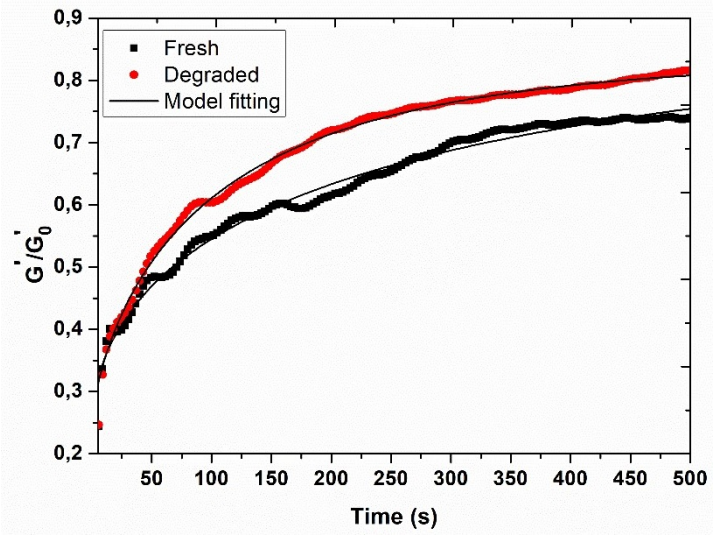

Figure F4: Normalized storage modulus, G'/G'_0 as a function of time obtained from the structural recovery step for fresh mud sample and mud sample degraded for 250 days, collected from KH location. The solid line represents the empirical fitting using Eq. 2.4.

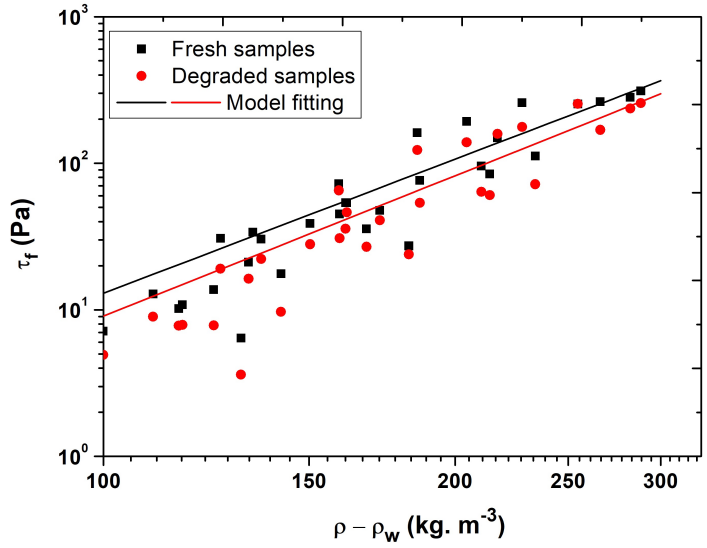

Figure F5: Fluidic yield stress (τ_f) as a function of excess density ($\rho - \rho_w$) for fresh and anaerobically degraded mud samples from KH location. The solid lines represent the power law fitting (Eq. 5.16) with two fitting parameters of values a = 14218 Pa, b = 3.04 for fresh samples and a = 13711, b = 3.18 for degraded samples.

REFERENCES

Ahuja, A., & Gamonpilas, C. (2017). Dual yielding in capillary suspensions. *Rheologica Acta*, *56*(10), 801–810. https://doi.org/10.1007/s00397-017-1040-1

Ahuja, A., Potanin, A., & Joshi, Y. M. (2020). Two step yielding in soft materials. *Advances in Colloid and Interface Science*, *282*, 102179. https://doi.org/10.1016/j.cis.2020.102179

Arief, I., & Mukhopadhyay, P. K. (2019). Magnetorheology in coni nanoplatelet-based mrfs: Effect of platelet orientation and oscillatory shear. *Journal of Magnetism and Magnetic Materials*, *479*, 326–331. https://doi.org/10.1016/j.jmmm.2019.02.055

Aubry, T., Razafinimaro, T., Jacinto, R. S., & Bassoulet, P. (2003). Rheological properties of a natural estuarine mud. *Applied Rheology*, *13*(3), 142–149. https://doi.org/10.1515/arh-2003-0010

Babatope, B., Williams, P. R., & Williams, D. J. A. (2008). Cohesive sediment characterization by combined sedimentation and rheological measurements. *Journal of Hydraulic Engineering*, *134*(9), 1333–1336. https://doi.org/10.1061/(ASCE)0733-9429(2008)134:9(1333)

Babatope, B., Williams, P., & Williams, D. (2006). In situ rheometry of cohesive sediments under water wave pressure. *Continental shelf research*, *26*(4), 488–498. https://doi.org/10.1016/j.csr.2005.12.007

Bai, Y. C., Ng, C. O., Shen, H. T., & Wang, S. Y. (2002). Rheological properties and incipient motion of cohesive sediment in the haihe estuary of china. *China Ocean Engineering*, *16*(4), 483–498.

Barnes, H. A. (1995). A review of the slip (wall depletion) of polymer solutions, emulsions and particle suspensions in viscometers: Its cause, character, and cure. *Journal of Non-Newtonian Fluid Mechanics*, *56*(3), 221–251. https://doi.org/10.1016/0377-0257(94)01282-M

Barnes, H. A. (1997). Thixotropy—a review. *Journal of Non-Newtonian fluid mechanics*, *70*(1-2), 1–33. https://doi.org/10.1016/S0377-0257(97)00004-9

Barnes, H. A. (1999). The yield stress—a review or ‘ ’—everything flows? *Journal of Non-Newtonian Fluid Mechanics*, *81*(1-2), 133–178. https://doi.org/10.1016/S0377-0257(98)00094-9

Barnes, H. A., & Nguyen, Q. D. (2001). Rotating vane rheometry—a review. *Journal of non-Newtonian fluid mechanics*, *98*(1), 1–14. https://doi.org/10.1016/S0377-0257(01)00095-7

Basu, A., Wen, Q., Mao, X., Lubensky, T., Janmey, P. A., & Yodh, A. (2011). Nonaffine displacements in flexible polymer networks. *Macromolecules*, *44*(6), 1671–1679. https://doi.org/10.1021/ma1026803

Benamar, A., Anne, P., Brasselet, S., & Bourdin, F. (2015). Rheological behaviour of marine sediments for assessing nautical depth, 107–110. https://doi.org/10.5150/cmcm.2015.022

Besseling, R., Weeks, E. R., Schofield, A., & Poon, W. (2007). Three-dimensional imaging of colloidal glasses under steady shear. *Physical review letters*, *99*(2), 028301. https://doi.org/10.1103/PhysRevLett.99.028301

Besseling, R., Isa, L., Weeks, E. R., & Poon, W. C. (2009). Quantitative imaging of colloidal flows. *Advances in colloid and interface science*, *146*(1-2), 1–17. https://doi.org/10.1016/j.cis.2008.09.008

Bingham, E. C. (1922). *Fluidity and plasticity* (Vol. 2). McGraw-Hill.

Bird, R. B., Dai, G., & Yarusso, B. J. (1983). The rheology and flow of viscoplastic materials. *Reviews in Chemical Engineering*, *1*(1), 1–70. https://doi.org/10.1515/revce-1983-0102

Boitte, J.-B., Vizcaïno, C., Benyahia, L., Herry, J.-M., Michon, C., & Hayert, M. (2013). A novel rheo-optical device for studying complex fluids in a double shear plate geometry. *Review of Scientific Instruments*, *84*(1), 013709. https://doi.org/10.1063/1.4774395

Bougouin, A., Benamar, A., Jarno, A., Marin, F., & Pantet, A. (2022). Rheological behaviour of pure clay and coarse-grained clay suspensions using an inclined blade vane-in-cup. *Journal of Non-Newtonian Fluid Mechanics*, *300*, 104714. https://doi.org/10.1016/j.jnnfm.2021.104714

Carneiro, J. C., Fonseca, D. L., Vinzon, S. B., & Gallo, M. N. (2017). Strategies for measuring fluid mud layers and their rheological properties in ports. *Journal of Waterway, Port, Coastal, and Ocean Engineering*, *143*(4), 04017008. https://doi.org/10.1061/(ASCE)WW.1943-5460.0000396

Chan, H. K., & Mohraz, A. (2012). Two-step yielding and directional strain-induced strengthening in dilute colloidal gels. *Physical Review E*, *85*(4), 041403. https://doi.org/10.1103/PhysRevE.85.041403

Chan, H. K., & Mohraz, A. (2013). A simple shear cell for the direct visualization of step-stress deformation in soft materials. *Rheologica Acta*, *52*(5), 383–394. https://doi.org/10.1007/s00397-013-0679-5

Cheng, D. C. (1986). Yield stress: A time-dependent property and how to measure it. *Rheologica Acta*, *25*(5), 542–554. https://doi.org/10.1007/BF01774406

Cheng, D. C.-H. (1987). Thixotropy. *International Journal of Cosmetic Science*, *9*(4), 151–191. https://doi.org/10.1111/j.1467-2494.1987.tb00472.x

Christopoulou, C., Petekidis, G., Erwin, B., Cloitre, M., & Vlassopoulos, D. (2009). Ageing and yield behaviour in model soft colloidal glasses. *Philosophical Transactions of the Royal Society of London A: Mathematical, Physical and Engineering Sciences*, *367*(1909), 5051–5071. https://doi.org/10.1098/rsta.2009.0166

Claeys, S., Staelens, P., Vanlede, J., Heredia, M., Van Hoestenberghe, T., Van Oyen, T., & Toorman, E. (2015). A rheological lab measurement protocol for cohesive sediment. *INTERCOH2015. Book of Abstracts*.

Clayton, S., Grice, T., & Boger, D. (2003). Analysis of the slump test for on-site yield stress measurement of mineral suspensions. *International journal of mineral processing*, *70*(1-4), 3–21. https://doi.org/10.1016/S0301-7516(02)00148-5

Coussot, P. (2007). Rheophysics of pastes: A review of microscopic modelling approaches. *Soft Matter*, *3*(5), 528–540. https://doi.org/10.1039/B611021P

Coussot, P. (2014). Yield stress fluid flows: A review of experimental data. *Journal of Non-Newtonian Fluid Mechanics*, *211*, 31–49. https://doi.org/10.1016/j.jnnfm.2014.05.006

Coussot, P., & Piau, J. M. (1994). On the behavior of fine mud suspensions. *Rheologica Acta*, *33*(3), 175–184. https://doi.org/10.1007/BF00437302

Coussot, P., Tabuteau, H., Chateau, X., Tocquer, L., & Ovarlez, G. (2006). Aging and solid or liquid behavior in pastes. *Journal of Rheology*, *50*(6), 975–994. https://doi.org/10.1122/1.2337259

Coussot, P. (1997). *Mudflow rheology and dynamics*. CRC Press.

Cyriac, F., Lugt, P. M., & Bosman, R. (2015). On a new method to determine the yield stress in lubricating grease. *Tribology Transactions*, *58*(6), 1021–1030. https://doi.org/10.1080/10402004.2015.1035414

Dagois-Bohy, S., Somfai, E., Tighe, B. P., & van Hecke, M. (2017). Softening and yielding of soft glassy materials. *Soft Matter*, *13*(47), 9036–9045. https://doi.org/10.1039/C7SM01846K

Das, M., Chambon, L., Varga, Z., Vamvakaki, M., Swan, J. W., & Petekidis, G. (2021). Shear driven vorticity aligned flocs in a suspension of attractive rigid rods. *Soft Matter*. https://doi.org/10.1039/D0SM01576H

De Graef, V., Depypere, F., Minnaert, M., & Dewettinck, K. (2011). Chocolate yield stress as measured by oscillatory rheology. *Food Research International*, *44*(9), 2660–2665. https://doi.org/10.1016/j.foodres.2011.05.009

Derec, C., Ducouret, G., Ajdari, A., & Lequeux, F. (2003). Aging and nonlinear rheology in suspensions of polyethylene oxide–protected silica particles. *Physical Review E*, *67*(6), 061403. https://doi.org/10.1103/PhysRevE.67.061403

Deyrail, Y., & Cassagnau, P. (2004). Phase deformation under shear in an immiscible polymer blend: Influence of strong permanent elastic properties. *Journal of Rheology*, *48*(3), 505–524. https://doi.org/10.1122/1.1718582

Didi, D., Hans, W., Alfons van, B., & Arnout, I. (2004). Confocal microscopy of colloidal dispersions in shear flow using a counter-rotating cone–plate shear cell. *Journal of Physics: Condensed Matter*, *16*(38), S3917–S3927. https://doi.org/10.1088/0953-8984/16/38/010

Dinkgreve, M., Paredes, J., Denn, M. M., & Bonn, D. (2016). On different ways of measuring "the" yield stress. *Journal of Non-Newtonian Fluid Mechanics*, *238*, 233–241. https://doi.org/10.1016/j.jnnfm.2016.11.001

Dutta, S., Mbi, A., Arevalo, R. C., & Blair, D. L. (2013). Development of a confocal rheometer for soft and biological materials. *Review of scientific instruments*, *84*(6), 063702. https://doi.org/10.1063/1.4810015

Dyer, K. R., & Manning, A. J. (1999). Observation of the size, settling velocity and effective density of flocs, and their fractal dimensions. *Journal of Sea Research*, *41*(1), 87–95. https://doi.org/10.1016/S1385-1101(98)00036-7

Faas, R. W., & Wartel, S. I. (2006). Rheological properties of sediment suspensions from eckernforde and kieler forde bays, western baltic sea. *International Journal of Sediment Research*, *21*(1), 24–41.

Faas, R. W., & Reed, A. H. (2010). Comparative analysis of two techniques for determining the rheological properties of fluid mud suspensions. *Marine Georesources Geotechnology*, *28*(4), 345–362. https://doi.org/10.1080/1064119X.2010.514251

Fan, H., Liu, X., Wang, H., Han, Y., Qi, L., & Wang, H. (2017). Oxygen transfer dynamics and activated sludge floc structure under different sludge retention times at low dissolved oxygen concentrations. *Chemosphere*, *169*, 586–595. https://doi.org/10.1016/j.chemosphere.2016.10.137

Fernández-Toledano, J. C., Rodríguez-López, J., Shahrivar, K., Hidalgo-Álvarez, R., Elvira, L., Espinosa, F. M. d., & Vicente, J. d. (2014). Two-step yielding in magnetorheology. *Journal of Rheology*, *58*(5), 1507–1534. https://doi.org/10.1122/1.4880675

Fischer, C., Plummer, C. J. G., Michaud, V., Bourban, P.-E., & Månson, J.-A. E. (2007). Pre- and post-transition behavior of shear-thickening fluids in oscillating shear. *Rheologica Acta*, *46*(8), 1099–1108. https://doi.org/10.1007/s00397-007-0202-y

Fonseca, D. L., Marroig, P. C., Carneiro, J. C., Gallo, M. N., & Vinzón, S. B. (2019). Assessing rheological properties of fluid mud samples through tuning fork data. *Ocean Dynamics*, *69*(1), 51–57. https://doi.org/10.1007/s10236-018-1226-9

Fontein, W., & Wal, J. (n.d.). Assessing nautical depth efficiently in terms of rheological characteristics.

Galindo-Rosales, F. J., Rubio-Hernández, F. J., & Velázquez-Navarro, J. F. (2009). Shear-thickening behavior of aerosil® r816 nanoparticles suspensions in polar organic liquids. *Rheologica Acta*, *48*(6), 699–708. https://doi.org/10.1007/s00397-009-0367-7

Gordon, R. B. (1974). Dispersion of dredge spoil dumped in near-shore waters. *Estuarine and Coastal Marine Science*, *2*(4), 349–358. https://doi.org/10.1016/0302-3524(74)90004-8

Goudoulas, T. B., & Germann, N. (2016). Viscoelastic properties of polyacrylamide solutions from creep ringing data. *Journal of Rheology*, *60*(3), 491–502. https://doi.org/10.1122/1.4945819

Goyon, J., Colin, A., Ovarlez, G., Ajdari, A., & Bocquet, L. (2008). Spatial cooperativity in soft glassy flows. *Nature*, *454*(7200), 84–87. https://doi.org/10.1038/nature07026

Grenard, V., Taberlet, N., & Manneville, S. (2011). Shear-induced structuration of confined carbon black gels: Steady-state features of vorticity-aligned flocs. *Soft Matter*, *7*(8), 3920–3928. https://doi.org/10.1039/C0SM01515F

Guo, C., Manning, A. J., Bass, S., Guo, L., & He, Q. (2021). A quantitative lab examination of floc fractal property considering influences of turbulence, salinity and sediment concentration. *Journal of Hydrology*, *601*, 126574. https://doi.org/10.1016/j.jhydrol.2021.126574

Hamberg, L., Walkenström, P., Stading, M., & Hermansson, A.-M. (2001). Aggregation, viscosity measurements and direct observation of protein coated latex particles under shear. *Food Hydrocolloids*, *15*(2), 139–151. https://doi.org/10.1016/S0268-005X(00)00060-6

Hammadi, L., Boudjenane, N., & Belhadri, M. (2014). Effect of polyethylene oxide (peo) and shear rate on rheological properties of bentonite clay. *Applied Clay Science*, *99*, 306–311. https://doi.org/10.1016/j.clay.2014.07.016

Harrison, W., & Wass, M. L. (1965). Frequencies of infaunal invertebrates related to water content of chesapeake bay sediments. *Southeastern Geology*, *6*(4), 177–186.

He, W., Nan, J., Li, H., & Li, S. (2012). Characteristic analysis on temporal evolution of floc size and structure in low-shear flow. *Water Research*, *46*(2), 509–520. https://doi.org/10.1016/j.watres.2011.11.040

Herschel, W. H., & Bulkley, R. (1926). Proc. 29th ann. *26*, 621–630.

Huang, Z., & Aode, H. (2009). A laboratory study of rheological properties of mudflows in hangzhou bay, china. *International Journal of Sediment Research*, *24*(4), 410–424. https://doi.org/10.1016/S1001-6279(10)60014-5

Ibanez Sanz, M. (2018). *Flocculation and consolidation of cohesive sediments under the influence of coagulant and flocculant* (Thesis). https://doi.org/10.4233/uuid:6e96db66-1df0-4ed1-b343-92939d58d864

Ilstad, T., Elverhøi, A., Issler, D., & Marr, J. G. (2004). Subaqueous debris flow behaviour and its dependence on the sand/clay ratio: A laboratory study using particle tracking. *Marine Geology*, *213*(1), 415–438. https://doi.org/10.1016/j.margeo.2004.10.017

Inglis, C., & Allen, F. (1957). The regimen of the thames estuary as affected by currents, salinities, and river flow. *Proceedings of the Institution of Civil Engineers*, *7*(4), 827–868. https://doi.org/10.1680/iicep.1957.2705

ISO:10694. (1995). Soil quality — determination of organic and total carbon after dry combustion (elementary analysis).

ISO:17892-3. (2015). Geotechnical investigation and testing — laboratory testing of soil — part 3: Determination of particle density.

James, A., Williams, D., & Williams, P. (1987). Direct measurement of static yield properties of cohesive suspensions. *Rheologica Acta*, *26*(5), 437–446. https://doi.org/10.1007/BF01333844

Janssens, W., Goderis, B., & Van Puyvelde, P. (2017). The effect of shear history on urea containing gliadin solutions. *Journal of Polymer Engineering*, *37*(9), 861–867. https://doi.org/10.1515/polyeng-2016-0188

Jeong, S. W., & Park, S.-S. (2016). On the viscous resistance of marine sediments for estimating their strength and flow characteristics. *Geosciences Journal*, *20*(2), 149–155. https://doi.org/10.1007/s12303-015-0032-3

Jia, D., Hollingsworth, J. V., Zhou, Z., Cheng, H., & Han, C. C. (2015). Coupling of gelation and glass transition in a biphasic colloidal mixture—from gel-to-defective gel-to-glass. *Soft matter*, *11*(45), 8818–8826. https://doi.org/10.1039/C5SM01531F

Jiang, F., & Mehta, A. J. (1995). Mudbanks of the southwest coast of india iv: Mud viscoelastic properties. *Journal of Coastal Research*, *11*(3), 918–926. http://www.jstor.org/stable/4298392

Jommi, C., Muraro, S., Trivellato, E., & Zwanenburg, C. (2019). Experimental results on the influence of gas on the mechanical response of peats. *Géotechnique*, *69*(9), 753–766. https://doi.org/10.1680/jgeot.17.P.148

Joshi, Y. M., Reddy, G. R. K., Kulkarni, A. L., Kumar, N., & Chhabra, R. P. (2007). Rheological behaviour of aqueous suspensions of laponite: New insights into the ageing phenomena. *Proceedings of the Royal Society A: Mathematical, Physical and Engineering Sciences*, *464*(2090), 469–489. https://doi.org/10.1098/rspa.2007.0250

Kanai, H., & Amari, T. (1993). Strain-thickening transition in ferric-oxide suspensions under oscillatory shear. *Rheologica acta*, *32*(6), 539–549. https://doi.org/10.1007/BF00369070

Kanai, H., Navarrete, R., Macosko, C., & Scriven, L. (1992). Fragile networks and rheology of concentrated suspensions. *Rheologica acta*, *31*(4), 333–344. https://doi.org/10.1007/BF00418330

Khalkhal, F., Carreau, P. J., & Ausias, G. (2011). Effect of flow history on linear viscoelastic properties and the evolution of the structure of multiwalled carbon nanotube suspensions in an epoxy. *Journal of Rheology*, *55*(1), 153–175. https://doi.org/10.1122/1.3523628

Kinloch, I. A., Roberts, S. A., & Windle, A. H. (2002). A rheological study of concentrated aqueous nanotube dispersions. *Polymer*, *43*(26), 7483–7491. https://doi.org/10.1016/S0032-3861(02)00664-X

Kirichek, A., Chassagne, C., Winterwerp, H., & Vellinga, T. (2018). How navigable are fluid mud layers? *Terra et Aqua*, *151*, 6–18.

Kirichek, A., & Rutgers, R. (2020). Monitoring of settling and consolidation of mud after water injection dredging in the calandkanaal. *Terra et Aqua*, *160*, 16–26.

Kirichek, A., Shakeel, A., & Chassagne, C. (2020). Using in situ density and strength measurements for sediment maintenance in ports and waterways. *Journal of Soils and Sediments*, *20*(6), 2546–2552. https://doi.org/10.1007/s11368-020-02581-8

Knappe, E., Manga, M., Le Friant, A., & scientists, I. 3. (2020). Rheology of natural sediments and its influence on the settling of dropstones in hemipelagic marine sediment. *Earth and Space Science*, *7*(3), e2019EA000876. https://doi.org/10.1029/2019EA000876

Knoch, D., & Malcherek, A. (2011). A numerical model for simulation of fluid mud with different rheological behaviors. *Ocean Dynamics*, *61*(2-3), 245–256. https://doi.org/10.1007/s10236-010-0327-x

Knowlton, E. D., Pine, D. J., & Cipelletti, L. (2014). A microscopic view of the yielding transition in concentrated emulsions. *Soft Matter*, *10*(36), 6931–6940. https://doi.org/10.1039/C4SM00531G

Kotula, A. P., Meyer, M. W., De Vito, F., Plog, J., Hight Walker, A. R., & Migler, K. B. (2016). The rheo-raman microscope: Simultaneous chemical, conformational, mechanical, and microstructural measures of soft materials. *Review of Scientific Instruments*, *87*(10), 105105. https://doi.org/10.1063/1.4963746

Koumakis, N., Laurati, M., Egelhaaf, S., Brady, J., & Petekidis, G. (2012). Yielding of hard-sphere glasses during start-up shear. *Physical review letters*, *108*(9), 098303. https://doi.org/10.1103/PhysRevLett.108.098303

Koumakis, N., & Petekidis, G. (2011). Two step yielding in attractive colloids: Transition from gels to attractive glasses. *Soft Matter*, *7*(6), 2456–2470. https://doi.org/10.1039/C0SM00957A

Kramb, R. C., & Zukoski, C. F. (2010). Yielding in dense suspensions: Cage, bond, and rotational confinements. *Journal of Physics: Condensed Matter*, *23*(3), 035102. https://doi.org/10.1088/0953-8984/23/3/035102

Krieger, I. M., & Maron, S. H. (1954). Direct determination of the flow curves of non-newtonian fluids. iii. standardized treatment of viscometric data. *Journal of Applied Physics, 25*(1), 72–75. https://doi.org/10.1063/1.1721523

Kugge, C., Vanderhoek, N., & Bousfield, D. (2011). Oscillatory shear response of moisture barrier coatings containing clay of different shape factor. *Journal of colloid and interface science, 358*(1), 25–31. https://doi.org/10.1016/j.jcis.2011.02.051

Kume, T., Asakawa, K., Moses, E., Matsuzaka, K., & Hashimoto, T. (1995). A new apparatus for simultaneous observation of optical microscopy and small-angle light scattering measurements of polymers under shear flow. *Acta polymerica, 46*(1), 79–85. https://doi.org/10.1002/actp.1995.010460112

Lagaly, G., & Dékány, I. (2013). Colloid clay science. *Developments in clay science* (pp. 243–345). Elsevier. https://doi.org/10.1016/B978-0-08-098258-8.00010-9

Lin, N. Y., McCoy, J. H., Cheng, X., Leahy, B., Israelachvili, J. N., & Cohen, I. (2014). A multi-axis confocal rheoscope for studying shear flow of structured fluids. *Review of Scientific Instruments, 85*(3), 033905. https://doi.org/10.1063/1.4868688

Lovato, S., Kirichek, A., Toxopeus, S., Settels, J. W., Talmon, A., & Keetels, G. (2021). The resistance of a plate moving through mud: Experiments and simulations. *Nutts 2021: 23rd Numerical Towing Tank Symposium*.

Lupi, F. R., Shakeel, A., Greco, V., Oliviero Rossi, C., Baldino, N., & Gabriele, D. (2016). A rheological and microstructural characterisation of bigels for cosmetic and pharmaceutical uses. *Materials Science and Engineering: C, 69*, 358–365. https://doi.org/10.1016/j.msec.2016.06.098

Ma, X., Kirichek, A., Shakeel, A., Heller, K., & Draganov, D. (2021). Laboratory seismic measurements for layer-specific description of fluid mud and for linking seismic velocities to rheological properties. *The Journal of the Acoustical Society of America, 149*(6), 3862–3877. https://doi.org/10.1121/10.0005039

MacIver, M. (2021). Safas: Sedimentation and floc analysis software. https://doi.org/10.5281/zenodo.225144034

Mackley, M., Wannaborwon, S., Gao, P., & Zhao, D. (1999). The optical microscopy of sheared liquids using a newly developed optical stage. *Microscopy and analysis*.

Malarkey, J., Baas, J. H., Hope, J. A., Aspden, R. J., Parsons, D. R., Peakall, J., Paterson, D. M., Schindler, R. J., Ye, L., Lichtman, I. D., Bass, S. J., Davies, A. G., Manning, A. J., & Thorne, P. D. (2015). The pervasive role of biological cohesion in bedform development. *Nature Communications, 6*, 6257. https://doi.org/10.1038/ncomms7257

Manning, A. J., & Dyer, K. R. (1999). A laboratory examination of floc characteristics with regard to turbulent shearing. *Marine Geology, 160*(1), 147–170. https://doi.org/10.1016/S0025-3227(99)00013-4

May, E. B. (1973). *Environmental effects of hydraulic dredging in estuaries*. Alabama Marine Resources Laboratory.

McAnally, W. H., Friedrichs, C., Hamilton, D., Hayter, E., Shrestha, P., Rodriguez, H., Sheremet, A., & Teeter, A. (2007). Management of fluid mud in estuaries, bays, and lakes. i: Present state of understanding on character and behavior. *Journal of Hydraulic Engineering, 133*(1), 9–22. https://doi.org/10.1061/(ASCE)0733-9429(2007)133:1(9)

McAnally, W. H., Kirby, R., Hodge, S. H., Welp, T. L., Greiser, N., Shrestha, P., McGowan, D., & Turnipseed, P. (2016). Nautical depth for us navigable waterways: A review. *Journal of Waterway, Port, Coastal, and Ocean Engineering*, *142*(2), 04015014. https://doi.org/10.1061/(ASCE)WW.1943-5460.0000301

McMinn, W. A. M., Keown, J., Allen, S. J., & Burnett, M. G. (2004). Effect of shear on concentrated hydrous ferric floc rheology. *Water Research*, *38*(7), 1873–1883. https://doi.org/10.1016/j.watres.2004.01.010

Mehta, A. J. (2013). *An introduction to hydraulics of fine sediment transport* (Vol. 38). World Scientific Publishing Company.

Mehta, A. J., Samsami, F., Khare, Y. P., & Sahin, C. (2014). Fluid mud properties in nautical depth estimation. *Journal of waterway, port, coastal, and ocean engineering*, *140*(2), 210–222. https://doi.org/10.1061/(ASCE)WW.1943-5460.0000228

Messaoudi, A., Bouzit, M., & Boualla, N. (2018). Physical and rheological properties of the chorfa dam mud: Dependency on solids concentration. *Applied Water Science*, *8*(6), 178. https://doi.org/10.1007/s13201-018-0805-8

Mewis, J. (1979). Thixotropy - a general review. *Journal of Non-Newtonian Fluid Mechanics*, *6*(1), 1–20. https://doi.org/10.1016/0377-0257(79)87001-9

Mewis, J., & de Bleyser, R. (1972). Dynamic behavior of thixotropic systems. *Journal of Colloid and Interface Science*, *40*(3), 360–369. https://doi.org/10.1016/0021-9797(72)90345-1

Mewis, J., & Wagner, N. J. (2009). Thixotropy. *Advances in Colloid and Interface Science*, *147*, 214–227. https://doi.org/10.1016/j.cis.2008.09.005

Mighri, F., & Huneault, M. A. (2001). Dispersion visualization of model fluids in a transparent couette flow cell. *Journal of Rheology*, *45*(3), 783–797. https://doi.org/10.1122/1.1357823

Mobuchon, C., Carreau, P. J., & Heuzey, M.-C. (2007). Effect of flow history on the structure of a non-polar polymer/clay nanocomposite model system. *Rheologica Acta*, *46*(8), 1045–1056. https://doi.org/10.1007/s00397-007-0188-5

Mobuchon, C., Carreau, P. J., & Heuzey, M.-C. (2009). Structural analysis of non-aqueous layered silicate suspensions subjected to shear flow. *Journal of Rheology*, *53*(5), 1025–1048. https://doi.org/10.1122/1.3193720

Møller, P. C., Mewis, J., & Bonn, D. (2006). Yield stress and thixotropy: On the difficulty of measuring yield stresses in practice. *Soft matter*, *2*(4), 274–283. https://doi.org/10.1039/B517840A

Moore, F. (1959). The rheology of ceramic slip and bodies. *Trans. Brit. Ceram. Soc.*, *58*, 470–492.

Nguyen, Q. D., Akroyd, T., De Kee, D. C., & Zhu, L. (2006). Yield stress measurements in suspensions: An inter-laboratory study. *Korea-Australia Rheology Journal*, *18*(1), 15–24.

Nguyen, Q., & Boger, D. (1992). Measuring the flow properties of yield stress fluids. *Annual Review of Fluid Mechanics*, *24*(1), 47–88. https://doi.org/10.1146/annurev.fl.24.010192.000403

Nie, S., Jiang, Q., Cui, L., & Zhang, C. (2020). Investigation on solid-liquid transition of soft mud under steady and oscillatory shear loads. *Sedimentary Geology*, *397*, 105570. https://doi.org/10.1016/j.sedgeo.2019.105570

Nosrati, A., Addai-Mensah, J., & Skinner, W. (2011). Rheology of aging aqueous muscovite clay dispersions. *Chemical Engineering Science*, *66*(2), 119–127. https://doi.org/10.1016/j.ces.2010.06.028

Oberrecht, D., & Wurpts, A. (2014). Investigations of rheological flow properties based on lab data of fluid mud samples and an extended model approach. *Die Küste, 81 Modelling*, (81), 455–462. https://hdl.handle.net/20.500.11970/101706

O'Brien, J. S., & Julien, P. Y. (1988). Laboratory analysis of mudflow properties. *Journal of hydraulic engineering*, *114*(8), 877–887. https://doi.org/10.1061/(ASCE)0733-9429(1988)114:8(877)

Papanastasiou, T. C. (1987). Flows of materials with yield. *Journal of Rheology*, *31*(5), 385–404. https://doi.org/10.1122/1.549926

Parker, W. R., & Kirby, R. (1982). Time dependent properties of cohesive sediment relevant to sedimentation management-european experience. *Estuarine comparisons* (pp. 573–589). Academic Press. https://doi.org/10.1016/B978-0-12-404070-0.50041-7

Parsons, D. R., Schindler, R. J., Hope, J. A., Malarkey, J., Baas, J. H., Peakall, J., Manning, A. J., Ye, L., Simmons, S., Paterson, D. M., Aspden, R. J., Bass, S. J., Davies, A. G., Lichtman, I. D., & Thorne, P. D. (2016). The role of biophysical cohesion on subaqueous bed form size. *Geophysical research letters*, *43*(4), 1566–1573. https://doi.org/10.1002/2016GL067667

Paterson, D. M., Crawford, R. M., & Little, C. (1990). Subaerial exposure and changes in the stability of intertidal estuarine sediments. *Estuarine, Coastal and Shelf Science*, *30*(6), 541–556. https://doi.org/10.1016/0272-7714(90)90091-5

Paterson, D. M., & Hagerthey, S. E. (2001). Microphytobenthos in constrasting coastal ecosystems: Biology and dynamics. In K. Reise (Ed.), *Ecological comparisons of sedimentary shores* (pp. 105–125). Springer Berlin Heidelberg. https://doi.org/10.1007/978-3-642-56557-1_6

Perge, C., Taberlet, N., Gibaud, T., & Manneville, S. (2014). Time dependence in large amplitude oscillatory shear: A rheo-ultrasonic study of fatigue dynamics in a colloidal gel. *Journal of Rheology*, *58*(5), 1331–1357. https://doi.org/10.1122/1.4887081

Pham, K. N., Petekidis, G., Vlassopoulos, D., Egelhaaf, S. U., Poon, W. C. K., & Pusey, P. N. (2008). Yielding behavior of repulsion- and attraction-dominated colloidal glasses. *Journal of Rheology*, *52*(2), 649–676. https://doi.org/10.1122/1.2838255

Phuoc, T. X., Wang, P., McIntyre, D., & Shadle, L. (2014). Synthesis and characterization of a thixotropic coal–water slurry for use as a liquid fuel. *Fuel Processing Technology*, *127*, 105–110. https://doi.org/10.1016/j.fuproc.2014.06.019

PIANC. (1997). Approach channels, a guide for design. *Supplement to Bulletin*, (95).

Potanin, A. (2019). Rheology of silica dispersions stabilized by polymers. *Colloids and Surfaces A: Physicochemical and Engineering Aspects*, *562*, 54–60. https://doi.org/10.1016/j.colsurfa.2018.11.020

Qian, Y., & Kawashima, S. (2016). Use of creep recovery protocol to measure static yield stress and structural rebuilding of fresh cement pastes. *Cement and Concrete Research*, *90*, 73–79. https://doi.org/10.1016/j.cemconres.2016.09.005

Qu, J.-P., Chen, H.-Z., Liu, S.-R., Tan, B., Liu, L.-M., Yin, X.-C., Liu, Q.-J., & Guo, R.-B. (2013). Morphology study of immiscible polymer blends in a vane extruder. *Journal of Applied Polymer Science*, *128*(6), 3576–3585. https://doi.org/10.1002/app.38573

Raghavan, S. R., & Khan, S. A. (1995). Shear-induced microstructural changes in flocculated suspensions of fumed silica. *Journal of Rheology*, *39*(6), 1311–1325. https://doi.org/10.1122/1.550638

Reed, A. H., Faas, R. W., Allison, M. A., Calliari, L. J., Holland, K. T., O'Reilly, S., Vaughan, W., & Alves, A. (2009). Characterization of a mud deposit offshore of the patos lagoon, southern brazil. *Continental Shelf Research*, *29*(3), 597–608. https://doi.org/10.1016/j.csr.2009.02.001

Renou, F., Stellbrink, J., & Petekidis, G. (2010). Yielding processes in a colloidal glass of soft star-like micelles under large amplitude oscillatory shear (laos). *Journal of Rheology*, *54*(6), 1219–1242. https://doi.org/10.1122/1.3483610

Rogers, S. A., Callaghan, P. T., Petekidis, G., & Vlassopoulos, D. (2010). Time-dependent rheology of colloidal star glasses. *Journal of Rheology*, *54*(1), 133–158. https://doi.org/10.1122/1.3270524

Ross, M. A., & Mehta, A. J. (1989). On the mechanics of lutoclines and fluid mud. *Journal of Coastal Research*, 51–62. http://www.jstor.org/stable/25735365

Roussel, N., Ovarlez, G., Garrault, S., & Brumaud, C. (2012). The origins of thixotropy of fresh cement pastes. *Cement and Concrete Research*, *42*(1), 148–157. https://doi.org/10.1016/j.cemconres.2011.09.004

Rouyer, F., Cohen-Addad, S., & Höhler, R. (2005). Is the yield stress of aqueous foam a well-defined quantity? *Colloids and Surfaces A: Physicochemical and Engineering Aspects*, *263*(1-3), 111–116. https://doi.org/10.1016/j.colsurfa.2005.01.025

Samsami, F., Khare, Y. P., & Mehta, A. J. (2012). Rheometric characterization of the fluid mud forming potential of a bay mud. *8th International Symposium on Lowland Technology*, 917–921.

Schindler, R. J., Parsons, D. R., Ye, L., Hope, J. A., Baas, J. H., Peakall, J., Manning, A. J., Aspden, R. J., Malarkey, J., Simmons, S., Paterson, D. M., Lichtman, I. D., Davies, A. G., Thorne, P. D., & Bass, S. J. (2015). Sticky stuff: Redefining bedform prediction in modern and ancient environments. *Geology*, *43*(5), 399–402. https://doi.org/10.1130/G36262.1

Schoukens, G., & Mewis, J. (1978). Nonlinear rheological behaviour and shear-dependent structure in colloidal dispersions. *Journal of Rheology*, *22*(4), 381–394. https://doi.org/10.1122/1.549497

Segovia-Gutiérrez, J. P., Berli, C. L. A., & Vicente, J. d. (2012). Nonlinear viscoelasticity and two-step yielding in magnetorheology: A colloidal gel approach to understand the effect of particle concentration. *Journal of Rheology*, *56*(6), 1429–1448. https://doi.org/10.1122/1.4742186

Sentjabrskaja, T., Chaudhuri, P., Hermes, M., Poon, W., Horbach, J., Egelhaaf, S., & Laurati, M. (2015). Creep and flow of glasses: Strain response linked to the spatial distribution of dynamical heterogeneities. *Scientific reports*, *5*(1), 1–11. https://doi.org/10.1038/srep11884

Sentjabrskaja, T., Babaliari, E., Hendricks, J., Laurati, M., Petekidis, G., & Egelhaaf, S. U. (2013). Yielding of binary colloidal glasses. *Soft Matter*, *9*(17), 4524–4533. https://doi.org/10.1039/C3SM27903K

Shakeel, A., Kirichek, A., & Chassagne, C. (2019). Is density enough to predict the rheology of natural sediments? *Geo-Marine Letters*, *39*(5), 427–434. https://doi.org/10.1007/s00367-019-00601-2

Shakeel, A., Kirichek, A., & Chassagne, C. (2020a). Effect of pre-shearing on the steady and dynamic rheological properties of mud sediments. *Marine and Petroleum Geology*, *116*, 104338. https://doi.org/10.1016/j.marpetgeo.2020.104338

Shakeel, A., Kirichek, A., & Chassagne, C. (2020b). Rheological analysis of mud from port of hamburg, germany. *Journal of Soils and Sediments*, *20*, 2553–2562. https://doi.org/10.1007/s11368-019-02448-7

Shakeel, A., Kirichek, A., & Chassagne, C. (2020c). Rheological analysis of natural and diluted mud suspensions. *Journal of Non-Newtonian Fluid Mechanics*, *286*, 104434. https://doi.org/10.1016/j.jnnfm.2020.104434

Shakeel, A., Kirichek, A., & Chassagne, C. (2020d). Yield stress measurements of mud sediments using different rheological methods and geometries: An evidence of two-step yielding. *Marine Geology*, *427*, 106247. https://doi.org/10.1016/j.margeo.2020.106247

Shakeel, A., Kirichek, A., Talmon, A., & Chassagne, C. (2021). Rheological analysis and rheological modelling of mud sediments: What is the best protocol for maintenance of ports and waterways? *Estuarine, Coastal and Shelf Science*, *257*, 107407. https://doi.org/10.1016/j.ecss.2021.107407

Shakeel, A., MacIver, M. R., van Kan, P. J. M., Kirichek, A., & Chassagne, C. (2021). A rheological and microstructural study of two-step yielding in mud samples from a port area. *Colloids and Surfaces A: Physicochemical and Engineering Aspects*, *624*, 126827. https://doi.org/10.1016/j.colsurfa.2021.126827

Shakeel, A., van Kan, P. J. M., & Chassagne, C. (2019). Design of a parallel plate shearing device for visualization of concentrated suspensions. *Measurement*, *145*, 391–399. https://doi.org/10.1016/j.measurement.2019.05.101

Shakeel, A., Zander, F., de Klerk, J.-W., Kirichek, A., Gebert, J., & Chassagne, C. (2022). Effect of organic matter degradation in cohesive sediment: A detailed rheological analysis. *Journal of Soils and Sediments*. https://doi.org/10.1007/s11368-022-03156-5

Shao, Z., Negi, A. S., & Osuji, C. O. (2013). Role of interparticle attraction in the yielding response of microgel suspensions. *Soft Matter*, *9*(22), 5492–5500. https://doi.org/10.1039/C3SM50209K

Shukla, A., Arnipally, S., Dagaonkar, M., & Joshi, Y. M. (2015). Two-step yielding in surfactant suspension pastes. *Rheologica Acta*, *54*(5), 353–364. https://doi.org/10.1007/s00397-015-0845-z

Soltanpour, M., & Samsami, F. (2011). A comparative study on the rheology and wave dissipation of kaolinite and natural hendijan coast mud, the persian gulf. *Ocean Dynamics*, *61*(2), 295–309. https://doi.org/10.1007/s10236-011-0378-7

Steffe, J. F. (1996). *Rheological methods in food process engineering*. Freeman press.

Stokes, J. R., & Telford, J. H. (2004). Measuring the yield behaviour of structured fluids. *Journal of Non-Newtonian Fluid Mechanics, 124*(1), 137–146. https://doi.org/10.1016/j.jnnfm.2004.09.001

Sun, G., & Zhang, J. (2015). Structural breakdown and recovery of waxy crude oil emulsion gels. *Rheologica Acta, 54*(9), 817–829. https://doi.org/10.1007/s00397-015-0873-8

Tamborini, E., Cipelletti, L., & Ramos, L. (2014). Plasticity of a colloidal polycrystal under cyclic shear. *Physical review letters, 113*(7), 078301. https://doi.org/10.1103/PhysRevLett.113.078301

Tolhurst, T. J., Gust, G., & Paterson, D. M. (2002). The influence of an extracellular polymeric substance (eps) on cohesive sediment stability. In J. C. Winterwerp & C. Kranenburg (Eds.), *Proceedings in marine science* (pp. 409–425). Elsevier. https://doi.org/10.1016/S1568-2692(02)80030-4

Toorman, E. A. (1994). An analytical solution for the velocity and shear rate distribution of non-ideal bingham fluids in concentric cylinder viscometers. *Rheologica Acta, 33*(3), 193–202. https://doi.org/10.1007/BF00437304

Toorman, E. A. (1997). Modelling the thixotropic behaviour of dense cohesive sediment suspensions. *Rheologica Acta, 36*(1), 56–65. https://doi.org/10.1007/bf00366724

Uhlherr, P., Guo, J., Tiu, C., Zhang, X.-M., Zhou, J.-Q., & Fang, T.-N. (2005). The shear-induced solid–liquid transition in yield stress materials with chemically different structures. *Journal of Non-Newtonian Fluid Mechanics, 125*(2-3), 101–119. https://doi.org/10.1016/j.jnnfm.2004.09.009

Uliczka, K. (2005). Investigations of the baw to the nautical bottom. *Workshop Nautical Bottom, Flanders Hydraulics Research Ghent University*.

Van Den Tempel, M. (1979). Rheology of concentrated suspensions. *Journal of Colloid and Interface Science, 71*(1), 18–20. https://doi.org/10.1016/0021-9797(79)90216-9

Van Kessel, T., & Blom, C. (1998). Rheology of cohesive sediments: Comparison between a natural and an artificial mud. *Journal of Hydraulic Research, 36*(4), 591–612. https://doi.org/10.1080/00221689809498611

Vantorre, M., Laforce, E., & Delefortrie, G. (2006). A novel methodology for revision of the nautical bottom. *VLIZ Special Publication*.

Varga, Z., Grenard, V., Pecorario, S., Taberlet, N., Dolique, V., Manneville, S., Divoux, T., McKinley, G. H., & Swan, J. W. (2019). Hydrodynamics control shear-induced pattern formation in attractive suspensions. *Proceedings of the National Academy of Sciences, 116*(25), 12193–12198. https://doi.org/10.1073/pnas.1901370116

Wei, J., Gao, B., Yue, Q., Wang, Y., Li, W., & Zhu, X. (2009). Comparison of coagulation behavior and floc structure characteristic of different polyferric-cationic polymer dual-coagulants in humic acid solution. *Water research, 43*(3), 724–732. https://doi.org/10.1016/j.watres.2008.11.004

Whitby, C. P., & Garcia, P. C. (2014). Time-dependent rheology of clay particle-stabilised emulsions. *Applied Clay Science, 96*, 56–59. https://doi.org/10.1016/j.clay.2014.03.005

Whitehouse, R., Soulsby, R., Roberts, W., & Mitchener, H. (2000). *Dynamics of estuarine muds: A manual for practical applications*. Thomas Telford.

Worrall, W., & Tuliani, S. (1964). Viscosity changes during the ageing of clay-water suspensions. *Trans Brit Ceramic Soc*, *63*, 167–185.

Wu, Y. L., Brand, J. H., van Gemert, J. L., Verkerk, J., Wisman, H., van Blaaderen, A., & Imhof, A. (2007). A new parallel plate shear cell for in situ real-space measurements of complex fluids under shear flow. *Review of Scientific Instruments*, *78*(10), 103902. https://doi.org/10.1063/1.2794226

Wurpts, R., & Torn, P. (2005). 15 years experience with fluid mud: Definition of the nautical bottom with rheological parameters. *Terra et Aqua*, *99*, 22–32.

Wyatt, N. B., O'Hern, T. J., Shelden, B., Hughes, L. G., & Mondy, L. A. (2013). Size and structure of chlorella zofingiensis/fecl3 flocs in a shear flow. *Biotechnology and bioengineering*, *110*(12), 3156–3163. https://doi.org/10.1002/bit.24996

Xiaochun, Y., Zhongwei, Y., Guangjian, H., Zhitao, Y., & Baiping, X. (2015). The design and performance of a vane mixer based on extensional flow for polymer blends. *Journal of Applied Polymer Science*, *132*(9). https://doi.org/10.1002/app.41551

Xu, J., & Huhe, A. (2016). Rheological study of mudflows at lianyungang in china. *International Journal of Sediment Research*, *31*(1), 71–78. https://doi.org/10.1016/j.ijsrc.2014.06.002

Xu, W., Gao, B., Yue, Q., & Wang, Y. (2011). Effect of shear force and solution ph on flocs breakage and re-growth formed by nano-al13 polymer. *Water Research*, *44*(6), 1893–1899. https://doi.org/10.1016/j.watres.2009.11.029

Yang, W., Tan, S. K., Wang, H., & Yu, G. (2014). Rheological properties of bed sediments subjected to shear and vibration loads. *Journal of waterway, port, coastal, and ocean engineering*, *140*(1), 109–113. https://doi.org/10.1061/(ASCE)WW.1943-5460.0000211

Yang, W., & Yu, G. (2018). Rheological response of natural soft coastal mud under oscillatory shear loadings. *Journal of Waterway, Port, Coastal, and Ocean Engineering*, *144*(4), 05018005. https://doi.org/10.1061/(ASCE)WW.1943-5460.0000461

Yang, W., Yu, G.-l., Tan, S. k., & Wang, H.-k. (2014). Rheological properties of dense natural cohesive sediments subject to shear loadings. *International Journal of Sediment Research*, *29*(4), 454–470. https://doi.org/10.1016/S1001-6279(14)60059-7

Yang, W., Yu, M., & Yu, G. (2018). Stratification and rheological properties of near-bed cohesive sediments in west lake, hangzhou, china. *Journal of Coastal Research*, *34*(1), 185–192. https://doi.org/10.2112/JCOASTRES-D-16-00182.1

Ye, L., Manning, A. J., & Hsu, T.-J. (2020). Oil-mineral flocculation and settling velocity in saline water. *Water research*, *173*, 115569. https://doi.org/10.1016/j.watres.2020.115569

Yoshimura, A., & Prud'homme, R. K. (1988). Wall slip corrections for couette and parallel disk viscometers. *Journal of Rheology*, *32*(1), 53–67. https://doi.org/10.1122/1.549963

Yu, W.-z., Gregory, J., Campos, L., & Li, G. (2011). The role of mixing conditions on floc growth, breakage and re-growth. *Chemical Engineering Journal*, *171*(2), 425–430. https://doi.org/10.1016/j.cej.2011.03.098

Yuan, D. Q., Wang, Y. L., & Feng, J. (2014). Contribution of stratified extracellular polymeric substances to the gel-like and fractal structures of activated sludge. *Water Research*, *56*, 56–65. https://doi.org/10.1016/j.watres.2014.02.028

Yuan, Q., Zhou, D., Khayat, K. H., Feys, D., & Shi, C. (2017). On the measurement of evolution of structural build-up of cement paste with time by static yield stress test vs. small amplitude oscillatory shear test. *Cement and Concrete Research*, *99*, 183–189. https://doi.org/10.1016/j.cemconres.2017.05.014

Yüce, C., & Willenbacher, N. (2017). Challenges in rheological characterization of highly concentrated suspensions - a case study for screen-printing silver pastes. *JoVE*, (122), e55377. https://doi.org/10.3791/55377

Zander, F., Groengroeft, A., Eschenach, A., Heimovaara, T., & Gebert, J. (2022). Organic matter pools in sediments of the tidal elbe river. *Limnology and Oceanography*.

Zander, F., Heimovaara, T., & Gebert, J. (2020). Spatial variability of organic matter degradability in tidal elbe sediments. *Journal of Soils and Sediments*, *20*(6), 2573–2587. https://doi.org/10.1007/s11368-020-02569-4

Zander, F., Shakeel, A., Kirichek, A., Chassagne, C., & Gebert, J. (2022). Effect of organic matter degradation in cohesive sediment: A spatiotemporal analysis of yield stresses. *Journal of Soils and Sediments*. https://doi.org/10.1007/s11368-022-03155-6

Zausch, J., Horbach, J., Laurati, M., Egelhaaf, S. U., Brader, J. M., Voigtmann, T., & Fuchs, M. (2008). From equilibrium to steady state: The transient dynamics of colloidal liquids under shear. *Journal of Physics: Condensed Matter*, *20*(40), 404210. https://doi.org/10.1088/0953-8984/20/40/404210

Zhang, C., Yu, Z.-g., Zeng, G.-m., Jiang, M., Yang, Z.-z., Cui, F., Zhu, M.-y., Shen, L.-q., & Hu, L. (2014). Effects of sediment geochemical properties on heavy metal bioavailability. *Environment international*, *73*, 270–281. https://doi.org/10.1016/j.envint.2014.08.010

Zhao, Y. (2004). Settling behaviour of polymer flocculated water-treatment sludge ii: Effects of floc structure and floc packing. *Separation and purification technology*, *35*(3), 175–183. https://doi.org/10.1016/S1383-5866(03)00133-3

Zheng, H., Zhu, G., Jiang, S., Tshukudu, T., Xiang, X., Zhang, P., & He, Q. (2011). Investigations of coagulation–flocculation process by performance optimization, model prediction and fractal structure of flocs. *Desalination*, *269*(1-3), 148–156. https://doi.org/10.1016/j.desal.2010.10.054

Zhu, L., Sun, N., Papadopoulos, K., & De Kee, D. (2001). A slotted plate device for measuring static yield stress. *Journal of Rheology*, *45*(5), 1105–1122. https://doi.org/10.1122/1.1392299

LIST OF FIGURES

List of Tables

CURRICULUM VITÆ

Ahmad SHAKEEL

22-01-1991 Born in Lahore, Pakistan.

EDUCATION

2001–2006 Primary Education
Govt. Muslim High School Lahore, Pakistan

2006–2009 Secondary Education
Govt. Islamia College Civil Lines Lahore, Pakistan

2009–2013 B.Sc. in Chemical (Polymer) Engineering
University of Engineering and Technology Lahore, Pakistan

2013–2015 Erasmus Mundus European Masters in Engineering Rheology
KU Leuven, Belgium (2013–2014)
University of Minho, Portugal (2014–2015)
University of Calabria, Italy (2014–2015)

2018–2022 PhD. Delft University of Technology, The Netherlands
Thesis: Rheological Analysis of Mud
Promotor Dr. C. Chassagne

EXPERIENCE

2015–2018 Lecturer
University of Engineering and Technology Lahore, Pakistan

List of Publications

Journal publications related to this thesis

1. **A. Shakeel**, C. Chassagne, J. Bornholdt, N. Ohle, A. Kirichek *From fundamentals to implementation of yield stress for nautical bottom: Case study of the Port of Hamburg*, Ocean Engineering (Under Review).

2. **A. Shakeel**, W. Ali, C. Chassagne, A. Kirichek *The rheological properties of kaolinite suspensions in the presence of different biopolymers*, Colloids and Surfaces A: Physicochemical and Engineering Aspects (Under Review).

3. **A. Shakeel**, F. Zander, J. Gebert, C. Chassagne, A. Kirichek *Influence of anaerobic degradation of organic matter on the rheological properties of cohesive mud from different European ports*, Journal of Marine Science and Engineering **10**, 446 (2022).

4. **A. Shakeel**, F. Zander, J. de Klerk, A. Kirichek, J. Gebert, C. Chassagne *Effect of organic matter degradation in cohesive sediment: A detailed rheological analysis*, Journal of Soils and Sediments (2022).

5. F. Zander, **A. Shakeel**, A. Kirichek, C. Chassagne, J. Gebert, *Effects of organic matter degradation in cohesive sediment: Linking sediment rheology to spatio-temporal patterns of organic matter degradability*, Journal of Soils and Sediments (2022).

6. **A. Shakeel**, M.R. MacIver, P.J.M. van Kan, A. Kirichek, C. Chassagne *A rheological and microstructural study of two-step yielding in mud samples from a port area*, Colloids and Surfaces A: Physicochemical and Engineering Aspects **624**, 126827 (2021).

7. **A. Shakeel**, A. Kirichek, A. Talmon, C. Chassagne *Rheological analysis and rheological modelling of mud sediments: What is the best protocol for maintenance of ports and waterways?*, Estuarine, Coastal and Shelf Science **257**, 107407 (2021).

8. **A. Shakeel**, A. Kirichek, C. Chassagne *Rheology and yielding transitions in mixed kaolinite/bentonite suspensions*, Applied Clay Science **211**, 106206 (2021).

9. X. Ma, A. Kirichek, **A. Shakeel**, K. Heller, D. Draganov *Laboratory seismic measurements for layer-specific description of fluid mud and for linking seismic velocities to rheological properties*, The Journal of the Acoustical Society of America **149**, 3862 (2021).

10. **A. Shakeel**, A. Kirichek, C. Chassagne *Rheological analysis of mud from Port of Hamburg, Germany*, Journal of Soils and Sediments **20**, 2553 (2020).

11. **A. Shakeel**, A. Kirichek, C. Chassagne *Rheological analysis of natural and diluted mud suspensions*, Journal of Non-Newtonian Fluid Mechanics **286**, 104434 (2020).

12. **A. Shakeel**, A. Kirichek, C. Chassagne *Yield stress measurements of mud sediments using different rheological methods and geometries: An evidence of two-step yielding*, Marine Geology **427**, 106247 (2020).

13. **A. Shakeel**, A. Kirichek, C. Chassagne *Effect of pre-shearing on the steady and dynamic rheological properties of mud sediments*, Marine and Petroleum Geology **116**, 104338 (2020).

14. **A. Shakeel**, Z. Safar, M. Ibanez, L. van Paassen, C. Chassagne *Flocculation of Clay Suspensions by Anionic and Cationic Polyelectrolytes: A Systematic Analysis*, Minerals **10**, 999 (2020).

15. A. Kirichek, **A. Shakeel**, C. Chassagne *Using in situ density and strength measurements for sediment maintenance in ports and waterways*, Journal of Soils and Sediments **20**, 2546 (2020).

16. **A. Shakeel**, A. Kirichek, C. Chassagne *Is density enough to predict the rheology of natural sediments?*, Geo-Marine Letters **39**, 427 (2019).

17. **A. Shakeel**, P.J.M. van Kan, C. Chassagne *Design of a parallel plate shearing device for visualization of concentrated suspensions*, Measurement **145**, 391 (2019).

Book chapter related to this thesis

1. **A. Shakeel**, A. Kirichek, C. Chassagne. Rheology of Mud: An Overview for Ports and Waterways Applications. In *Sediment Transport - Recent Advances*, IntechOpen (2021).

Oral and Poster Presentations in Conferences

1. **A. Shakeel**, A. Kirichek, C. Chassagne. Spatial variability in the yield stress of mud at Port of Hamburg, Germany, **INTERCOH Conference**, Delft, the Netherlands, 13 – 17 September, 2021.

2. **A. Shakeel**, A. Kirichek, C. Chassagne. The origin of two-step yielding in natural mud: wall slip or structural reorganization?, **INTERCOH Conference**, Delft, the Netherlands, 13 – 17 September, 2021.

3. **A. Shakeel**, A. Kirichek, C. Chassagne. Rheological analysis of mud for ports and waterways applications: a way forward, **MudNet Conference**, 29 – 30 March, 2021 (Online).

4. **A. Shakeel**, R. MacIver, C. Chassagne, A.J. Manning. Rheological and structural analysis of mud from Port of Hamburg, Germany, **AGU Fall Meeting**, 1 – 17 December, 2020 (Online).

5. **A. Shakeel**, A. Kirichek, C. Chassagne. Stabilization of kaolinite suspensions using bentonite: a detailed rheological analysis, **18th International Congress on Rheology**, 13 – 18 December, 2020 (Online).

6. **A. Shakeel**, A. Kirichek, C. Chassagne, A.J. Manning. Effect of pre-shearing on the steady and dynamic rheological properties of marine sediments, **Ocean Sciences Meeting**, San Diego, California, 16 – 21 February, 2020.

7. **A. Shakeel**, A. Kirichek, C. Chassagne. Structural breakup and recovery in natural mud after steady pre-shearing, **Viscoplastic Fluids: from Theory to Application**, Cambridge, UK, 16 – 20 September, 2019.

8. **A. Shakeel**, A. Kirichek, C. Chassagne. Revising the definition of fluid mud by establishing new protocols for rheological measurements, **XVII European Conference on Soil Mechanics and Geotechnical Engineering**, Reykjavík, Iceland, 1 – 6 September, 2019.

9. F. Zander, **A. Shakeel**, A. Kirichek, C. Chassagne, J. Gebert. Biological activity affects rheological properties in surface water sediments, **11th InterPore Conference**, Valencia, Spain, 6 – 10 May, 2019.

10. **A. Shakeel**, F. Zander, J. Gebert, A. Kirichek, C. Chassagne. Rheological characterization of fluid mud in ports and waterways, **11th International SedNet Conference**, Dubrovnik, Croatia, 3 – 5 April, 2019.

11. **A. Shakeel**, C. Chassagne, A.J. Manning. Rheo-optical analysis of natural sediments under continuous and oscillating shearing action, **AGU Fall Meeting**, Washington, D.C., USA, 10 – 14 December, 2018.

Additional Journal Publications

1. **A. Shakeel**, K. Rizwan, U. Farooq, S. Iqbal, T. Iqbal, N.S. Awwad, H.A. Ibrahium *Polymer based nanocomposites: A strategic tool for detection of toxic pollutants in environmental matrices*, Chemosphere **303**, 134923 (2022).

2. **A. Shakeel**, K. Rizwan, U. Farooq, S. Iqbal, A.A. Altaf *Advanced polymeric/inorganic nanohybrids: An integrated platform for gas sensing applications*, Chemosphere **294**, 133772 (2022).

3. **A. Shakeel**, U. Farooq, D. Gabriele, A.G. Marangoni, F.R. Lupi *Bigels and multi-component organogels: An overview from rheological perspective*, Food Hydrocolloids **111**, 106190 (2021).

4. H. Mahmood, S. Mehmood, **A. Shakeel**, T. Iqbal, M.A. Kazmi, A.R. Khurram, M. Moniruzzaman *Glycerol assisted pretreatment of lignocellulose wheat straw materials as a promising approach for fabrication of sustainable fibrous filler for biocomposites*, Polymers **13**, 388 (2021).

5. U. Farooq, L. Upadhyaya, **A. Shakeel**, G. Martinez, M. Semsarilar *pH-responsive nano-structured membranes prepared from oppositely charged block copolymer nanoparticles and iron oxide nanoparticles*, Journal of Membrane Science **611**, 118181 (2020).

6. **A. Shakeel**, U. Farooq, C. Chassagne *Interfacial and bulk stabilization of oil/water system: a novel synergistic approach*, Nanomaterials **10**, 356 (2020).

7. **A. Shakeel**, H. Mahmood, U. Farooq, Z. Ullah, S. Yasin, T. Iqbal, C. Chassagne, M. Moniruzzaman *Rheology of pure ionic liquids and their complex fluids: a review*, ACS Sustainable Chemistry & Engineering **7**, 13586 (2019).

8. S. Yasin, **A. Shakeel**, T. Iqbal, F. Ahmad, H. Mahmood, P.F. Luckham, N. Ullah, *Effect of experimental conditions on nano-indentation response of low density polyethylene (LDPE)*, Journal of Macromolecular Science, Part A: Pure and Applied Chemistry **56**, 640 (2019).

9. **A. Shakeel**, U. Farooq, T. Iqbal, S. Yasin, F.R. Lupi, D. Gabriele, *Key characteristics and modelling of bigels systems: A review*, Materials Science and Engineering: C **97**, 932 (2019).

Additional Book Chapters

1. F.R. Lupi, **A. Shakeel**, U. Farooq, N. Baldino, D. Gabriele. Edible organogels produced with fatty alcohols: the use of policosanol as organogelator. In *Development of Trans-Free Lipid Systems and their Use in Food Products*, Royal Society of Chemistry (2022).

2. F.R. Lupi, **A. Shakeel**, N. Baldino, D. Gabriele. Rheology of food bigel system. In *Advances in Food Rheology and Its Applications*, Elsevier (2022).